Bulletin 43
(Part 3 of 4 Parts)

THE SHOCK AND VIBRATION BULLETIN

Part 3
Skylab, Vibration Testing and Analysis

JUNE 1973

A Publication of
THE SHOCK AND VIBRATION
INFORMATION CENTER
Naval Research Laboratory, Washington, D.C.

Office of
The Director of Defense
Research and Engineering

SYMPOSIUM MANAGEMENT

THE SHOCK AND VIBRATION INFORMATION CENTER

Robert O. Belsheim, Director
Henry C. Pusey, Coordinator
Edward H. Schell, Coordinator
Rudolph H. Volin, Coordinator

Bulletin Production

Graphic Arts Branch, Technical Information Division,
Naval Research Laboratory

Bulletin 43
(Part 3 of 4 Parts)

THE SHOCK AND VIBRATION BULLETIN

JUNE 1973

A Publication of
THE SHOCK AND VIBRATION
INFORMATION CENTER
Naval Research Laboratory, Washington, D.C.

The 43rd Symposium on Shock and Vibration was held at the Asilomar Conference Grounds, Pacific Grove, California, on 5-7 December 1972. The U.S. Army, Fort Ord, was host.

Office of
The Director of Defense
Research and Engineering

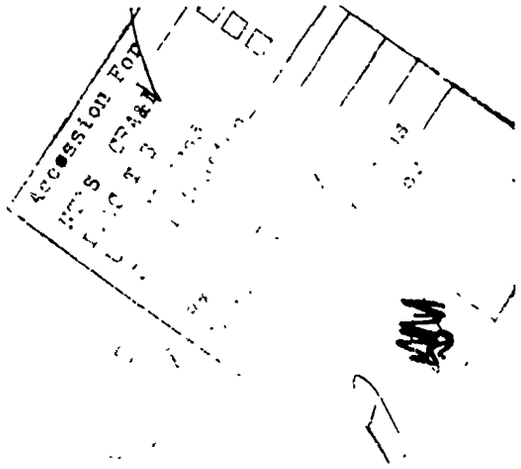

CONTENTS

PART 3

Skylab

Vibration Testing and Analysis

PAPERS APPEARING IN PART 1

REMARKS
Dr. Elias Klein, ret., Sarasota, Florida

Invited Papers

A QUARTER CENTURY OF PROGRESS
Mr Dwight C. Kennard, Consultant, Traverse City, Michigan

FORMER SHOCK
Dr. Donald E. Marlowe, Vice President for Administration, Catholic University, Washington, D. C.

THE ARMY'S BIG FIVE AND RDTE PROGRAM THRUSTS
Major General John R. Guthrie, Deputy Commanding General for Materiel Acquisition, Army Materiel Command Headquarters, Washington, D. C.

Submarine Shock Testing

UNDERWATER EXPLOSION TESTS WITH THE SWEDISH FULL-SCALE TEST SECTION "STÅLMYGGAN". PART I: TEST SECTION WITH OBJECTS AND MEASURING POINTS, ARRANGEMENTS AND DIMENSIONAL MEASUREMENTS
H. Nilsson, Kockums Mekaniska Verkstads AB, Naval Department, Malmö, Sweden

UNDERWATER EXPLOSION TESTS WITH THE SWEDISH FULL-SCALE SUBMARINE TEST SECTION "STÅLMYGGAN": RECORDING AND DATA REDUCTION SYSTEM
L. Westin and A. Hennngson, Military Electronics Laboratory, Stockholm, Sweden

Design Techniques

PAPERS APPEARING IN PART 4

Prediction and Experimental Techniques

Isolation and Damping

SKYLAB

SKYLAB VIBROACOUSTIC TESTING
AN OVERVIEW

G. M. Moseley
Teledyne Brown Engineering
Huntsville, Alabama

Skylab Orbital Workshop and Payload Assembly vibration and acoustic tests performed at Houston, Texas are discussed. Test article configurations, ground test objectives, testing constraints, tests systems, and the general program are described. Scope of additional papers to be presented in this series is discussed.

INTRODUCTION

The Skylab program is a manned orbital scientific space station to be launched in mid-1973 in a near-earth orbit up to 235 nautical miles. The 100-ton laboratory complex has multi-purpose scientific investigation capabilities. The three-man crew, brought to the orbiting laboratory by an Apollo spacecraft, will carry out more than fifty significant experiments in medicine, science, technology, earth resources, and operations. The first mission will last up to 28 days, and two subsequent missions will last up to 56 days each.

In support of the structural designs and qualifications of Skylab hardware, a ground test program was conducted at the Manned Spacecraft Center (MSC), Houston, Texas, Vibration and Acoustic Test Facility (VATF). These tests, from January 1971 to July 1972, were late enough in the design of Skylab to allow use of established structural configurations and was early enough in the program to precede most component qualifications.

A series of eight papers has been prepared covering the Skylab test program at Houston. This paper is first in the series and is structured to give an overview of the test program and will serve as an introduction to the remaining papers. Paper titles and authors are listed in Table I. These papers report work done under direction of NASA-Marshall Space Flight Center.

This paper discusses in the following paragraphs objectives of the ground tests, test configurations, testing constraints, the tests conducted, and the general scope of the other papers in the series.

OBJECTIVES OF GROUND TESTING

The Skylab major structural systems and components would require testing to verify structural integrity and satisfactory component functioning during the programmed life of the systems. This testing could be accomplished on an individual basis with a large number of small tests designed to impose predetermined environmental criteria on the specimens. A more efficient method of tests whereby all major structural systems and components are assembled as one unit and tested to prescribed environmental criteria could provide a less expensive method of achieving the desired goals. This latter method was chosen for the Skylab ground test program.

The test philosophy was to subject the Skylab system to a combined vibration and acoustic test environment that best simulated actual launch and flight conditions. The size of the available test facilities dictated the testing be accomplished in three major sections:

1. The orbital workshop
2. The payload assembly consisting of the airlock module, multiple docking adapter, apollo telescope mount, deployment assembly and shroud
3. The apollo service module.

The test objectives, as determined by the cognizant system contractor and NASA organizations, were to simulate the launch vehicle lift-off and boost, engine cut-off, vehicle separation environments and math model boundary conditions. These objectives were met during a related series of acoustic and vibration tests imposed on the major test articles.

Data acquired from these tests were used for verification of the orbital workshop, payload assembly and service module structural integrity and dynamic response characteristics. The data were also used to evaluate dynamic response criteria and for dynamic structural qualification of flight hardware components.

TEST CONFIGURATION

The test procedure followed in testing of the Orbital Workshop, Payload Assembly, and Service Module was to perform acoustic tests in the Manned Spacecraft Center Vibration and Acoustic Test Facility (MSC VATF) Spacecraft Acoustic Laboratory and then vibration tests in the MSC VATF Spacecraft Vibration Laboratory. The scope of this paper is limited to a description of the tests and test articles. Test details will be covered in other papers of this series as indicated in Table I.

A. Orbital Workshop

1. Acoustic Tests

The workshop was stacked in the Spacecraft Acoustic Laboratory with the S-IVB aft interstage and Instrument Unit SA-500D. Appropriate acoustic shields closed out both top and bottom of the stack. Figure 1 is a sketch depicting components in the stack and Figure 2 is a photograph of the stack in the Spacecraft Acoustic Laboratory.

2. Vibration Tests

For vibration testing the workshop was stacked in the Spacecraft Vibration Laboratory on a vibration test fixture. The S-IVB aft interstage and Instrument Unit SA-500D were not used in this test. Figure 3 is a photograph of the Orbital Workshop Spacecraft Vibration Laboratory stack.

B. Payload Assembly

1. Acoustic Tests

Acoustic test hardware for the launch configuration consisted of the S-IVB Forward Skirt with tank dome, Instrument Unit, Fixed Airlock Shroud, Airlock Module, Multiple Docking Adapter, Apollo Telescope Mount, ATM Deployment Assembly, and Payload Shroud. These components were stacked vertically in the Spacecraft Acoustic Laboratory reverberant chamber. The assembly rested on pneumatic casters and was acoustically sealed at the floor. Figures 4 and 5 are sketch and photograph depicting this configuration.

2. Vibration Tests

Stacking was identical for the Payload Assembly launch configuration vibration testing performed in the Spacecraft Vibration Laboratory. The assembly rested on a vibration test fixture used for suspension system attachment and for force input attach points. Figure 6 is a photograph of this configuration. For orbital configuration, the Payload Shroud was removed, the Apollo Telescope Mount was placed in the deployed position, and the Service Module was added to the stack. The Apollo Telescope Mount and Service Module were suspended on individual suspension systems. Figure 7 is a sketch depicting components in this stack. Figure 8 is a composite photograph of the stacked configuration.

C. Service Module

The Service Module was mated with a Command Module and subjected to both acoustic and vibration testing in the Spacecraft Vibration Laboratory (Figures 9 and 10). Since this testing was performed concurrently with installation of the reverberant chamber walls (the reverberant chamber was used for the first time to perform the Orbital Workshop test), the Service Module acoustic testing was conducted using special ducts to apply the acoustic energy using progressive wave mode of operation. A special fixture was used for supporting the Service Module during the acoustic testing, and a modified ground support ring mated to four air springs supported the Service Module for the vibration testing.

D. Component Tests

Component tests directly applicable to the Orbital Workshop/Payload Assembly Program were conducted in the MSC Spacecraft Acoustic Laboratory to resolve problems discovered during prior Payload Assembly acoustic testing:

1. The Instrument Unit-Flight Control Computer was installed in the Payload Assembly stacked in the reverberant chamber. Both mass simulated dummy and engineering models of the Flight Control Computer were tested to acoustical qualification criteria. A modal survey of the

Instrument Unit in the area of the Flight Control Computer was also made in this same configuration.

2. Apollo Telescope Mount/Control Moment Gyro acoustic tests were made to assist with Control Moment Gyro qualifications. A flight type Control Moment Gyro was mounted on the Apollo Telescope Mount which was stacked inside the Payload Shroud. The test article was subjected to adjusted acoustical qualification criteria for the prescribed time, after which it was to be functionally operated for its required life cycle time.

TEST SYSTEMS

A number of unique systems were assembled to meet the objectives and constraints of this program, the most significant of these systems are:

- Spacecraft Acoustic Laboratory (SAL)
- Automatic Acoustic Control System for the SAL
- Automatic Modal Tuning and Analysis System (AMTAS)
- Modal test air springs, ballast and isolation for high force shaker systems
- Transient Vibration Control System
- Acceleration exceedance detectors.

The Spacecraft Acoustic Laboratory reverberant room (47 ft, 4 in. wide, 45 ft, 4 in. deep and 75 ft high) has the capability to acoustically excite test vehicles up to 74 ft in height with high level energy over a wide frequency range. Approximately 250,000 watts of acoustic power can be provided by the 4500 horsepower laboratory compressor in conjunction with various horn combinations. Horns with 25, 50, 100, 250, and 630 Hz cut-off frequencies were used. High and low frequency WAS -3000 and EPT -200 air modulators were used to modulate the horns.

The automatic acoustic control system is a digital computer system that adjusts the acoustic level, seen by designated control microphones strategically spaced around the test article. The control computer displays this spectra along with the acceptable 1/3 octave band tolerances for immediate evaluation by test personnel.

The Automatic Modal Tuning and Analysis System (AMTAS) was specifically created for the Skylab modal testing program to give fast turn around to large quantities of structural data that otherwise could not be analyzed within the required time frame. This system performed highly interrelated control and data acquisition functions. A General Automation 18/30 digital computer was used for basic data acquisition and display.

AMTAS simultaneously controlled as many as twelve modal shakers each having a maximum sinusoidal force output of 150 lb. The data objective of the system was to provide normalized responses, mode shapes and orthogonality tabulation after each modal tuning run was completed. These data provided a high level of confidence in the validity and adequacy of the test results. AMTAS included a capability to protect the test vehicle from excessive force or motions. Additional details of the AMTAS and acoustic systems and other test systems are contained in additional papers in this series (See Table I).

TESTING CONSTRAINTS

A. Systems Limitations

Acoustics tests had no systems limitations. Tests were conducted with ample margin of power to obtain the required spectra.

Vibration testing high force sweeps were limited in force application due to reaching the limit of shaker capabilities. This resulted in lower instrumentation response levels and therefore resolution was not as good as would be desired.

Also, suspension system and shaker stinger characteristics combined in some cases to constrain testing. Where vibration sweep frequencies coincided with natural frequencies of shaker stingers and shaker suspension systems, the desired force levels for the sweeps could not be maintained for fear of failing some part of the system due to the large displacements encountered.

B. Structural Response and Loads

Flight type structural systems were included in the test articles and these systems were protected from overtest condition in both vibration and acoustic tests by automatic response and load limiting systems.

The vibration response limiting on certain components and structural systems was accomplished through use of properly calibrated accelerometers feeding a monitoring system that caused a shaker master control interrup when an established level was exceeded. The established level was usually 10 percent lower than the maximum do-no-exceed level. The load limiting system operated in much the same manner with strain gage devices feeding the monitoring system.

TEST PROGRAM

A chronology of the Skylab Vibro Acoustic Test Program is given to enable the reader to grasp somewhat the size of the program and the enormous amount of data collected. The Orbital Workshop was tested in the Spacecraft Acoustic Laboratory, in February 1971, to lift-off and boost condition acoustic levels of 151 dB and 149 dB overall sound pressure levels (OASPL), respectively. Vibration tests in three mutually perpendicular axes and modal survey testing were performed in the spacecraft vibration laboratory. Vibration exciters located strategically around the workshop were programmed to give proper loading for force controlled and motion controlled sine sweep tests. Frequencies of sweep tests were 5 to 60 Hz for longitudinal axis and 4 to 20 Hz for lateral axes. Modal dwell tests were run at 23 frequencies determined from the previous sweep tests. Mechanical impedance test data were acquired at selected locations for analytical purposes. Workshop test was completed in May 1971.

Payload Assembly testing began in the Spacecraft Acoustic Laboratory in August 1971. Lift-off and boost condition acoustic levels of 150 and 153 dB OASPL respectively, were imposed on the assembly. Launch configuration vibration tests in the longitudinal axis were performed in the Spacecraft Vibration Laboratory. Testing was performed in the same manner as workshop vibration tests. Modal dwell tests were run at 40 frequencies determined from previous sweep tests.

The Payload Assembly Orbital Configuration Vibration tests were completed in June 1972. Twelve sweep tests were made for the purpose of identifying frequencies of possible modes. Thirty-one separate modes were successfully acquired from the orbital configuration tests.

Two special component tests were run in the Spacecraft Acoustic Laboratory as a result of the previously conducted acoustic tests. The Instrument Unit/Flight Control Computer and the Apollo Telescope Mount/Control Moment Gyro received separate special acoustic qualification tests.

The Flight Control Computer tests were conducted in October 1971 at the Spacecraft Acoustic Laboratory in the Payload Assembly launch configuration. Engineering model and mass simulated Flight Control Computers were used to evaluate the proper specification levels for qualification testing of this component.

The Apollo Telescope Mount/Control Moment Gyro special qualification test was conducted April 1972 at the Spacecraft Acoustic Laboratory with the Apollo Telescope Mount, installed in the Payload Shroud including double angle nose cone. A live Control Moment Gyro was subjected to maximum flight acoustic environments to determine whether any bearing or operation problems would occur due to this environment.

Mechanical Impedance tests conducted on Payload Assembly components in July 1972 completed the Skylab Orbital Workshop/Payload Assembly testing at MSC.

OTHER PAPERS

A series of seven additional papers has been prepared to cover the details of development of unique testing equipment, facilities and computer software required for the extensive Skylab ground test program. Subjects discussed are:

- Skylab Vibration and Acoustic Structural Test Systems
- Orbital Workshop Vibroacoustic Test Program
- Skylab Payload Assembly Vibroacoustic Test Program
- Development of an Automatic Modal Tuning and Analysis System for Performing Skylab Modal Surveys
- Skylab Modal Survey Testing
- Use of Generalized Mass Contributions in Correlation of Test and Analytical Vibration Modes
- Vibration and Acoustic Tests of the Reconfigured Service Module Adapted for Skylab Missions.

Table I contains a list of the Skylab testing papers prepared for presentation to the

43rd Shock and Vibration Symposium. Also included in the table are author's names and company affiliations.

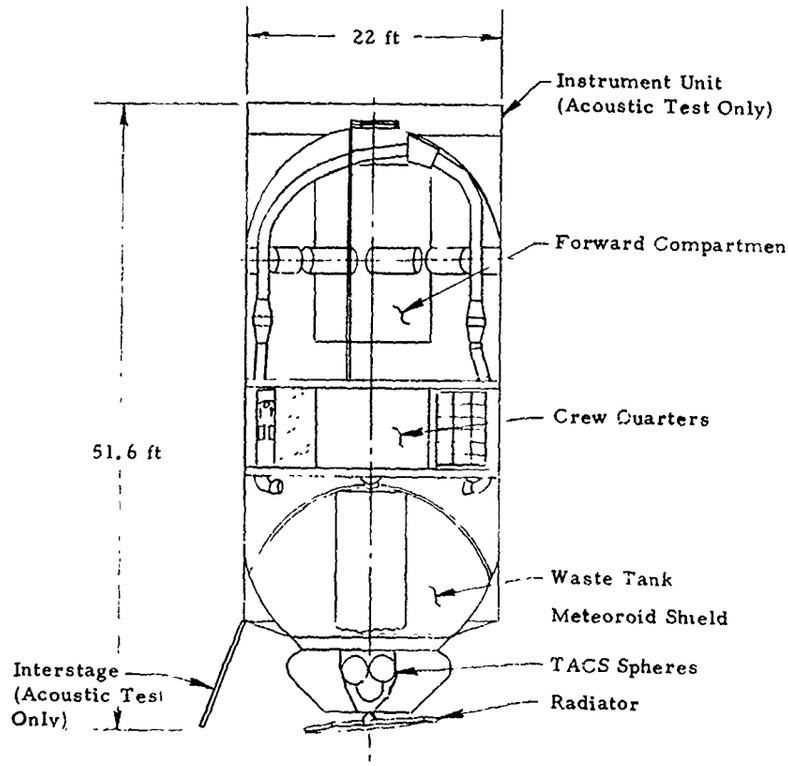

FIGURE 1. ORBITAL WORKSHOP VIBROACOUSTIC TEST ARTICLE

FIGURE 2. ORBITAL WORKSHOP STACK IN SPACECRAFT ACOUSTIC LABORATORY

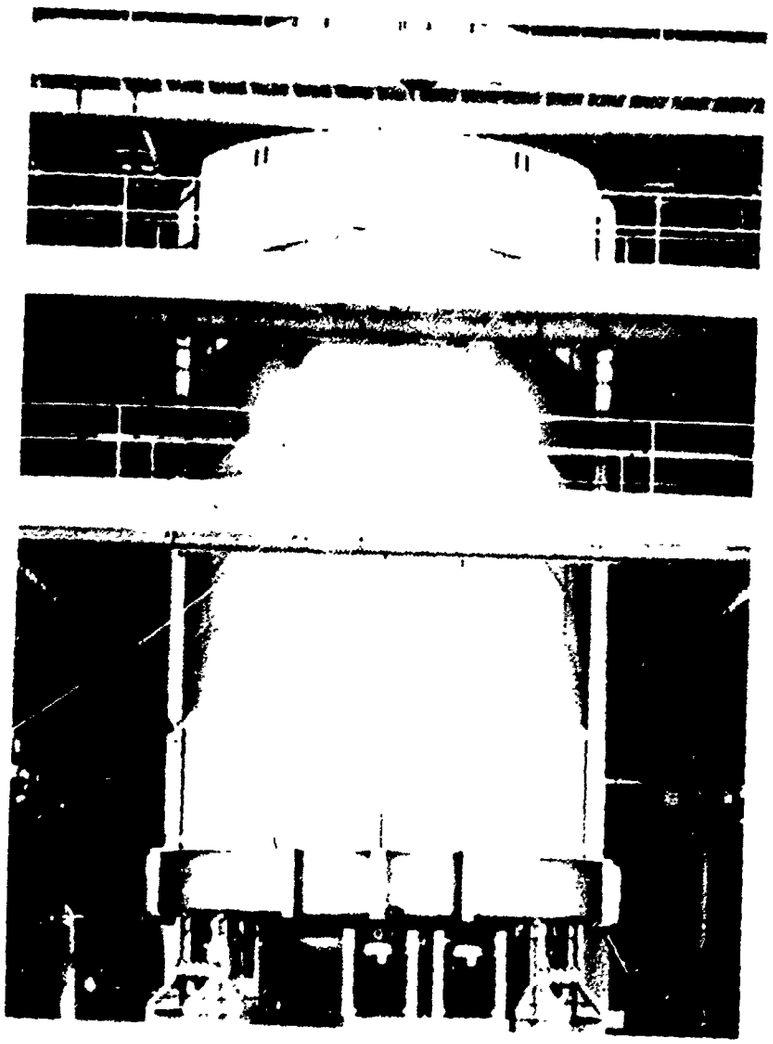

FIGURE 3. ORBITAL WORKSHOP STACK IN SPACECRAFT VIBRATION LABORATORY

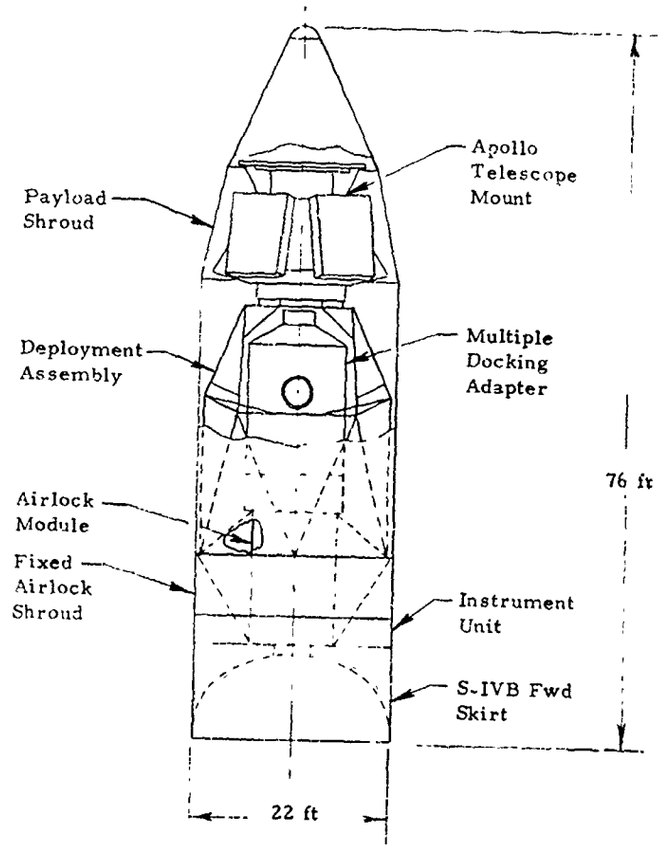

FIGURE 4. PAYLOAD ASSEMBLY LAUNCH CONFIGURATION IN SPACECRAFT ACOUSTIC LABORATORY

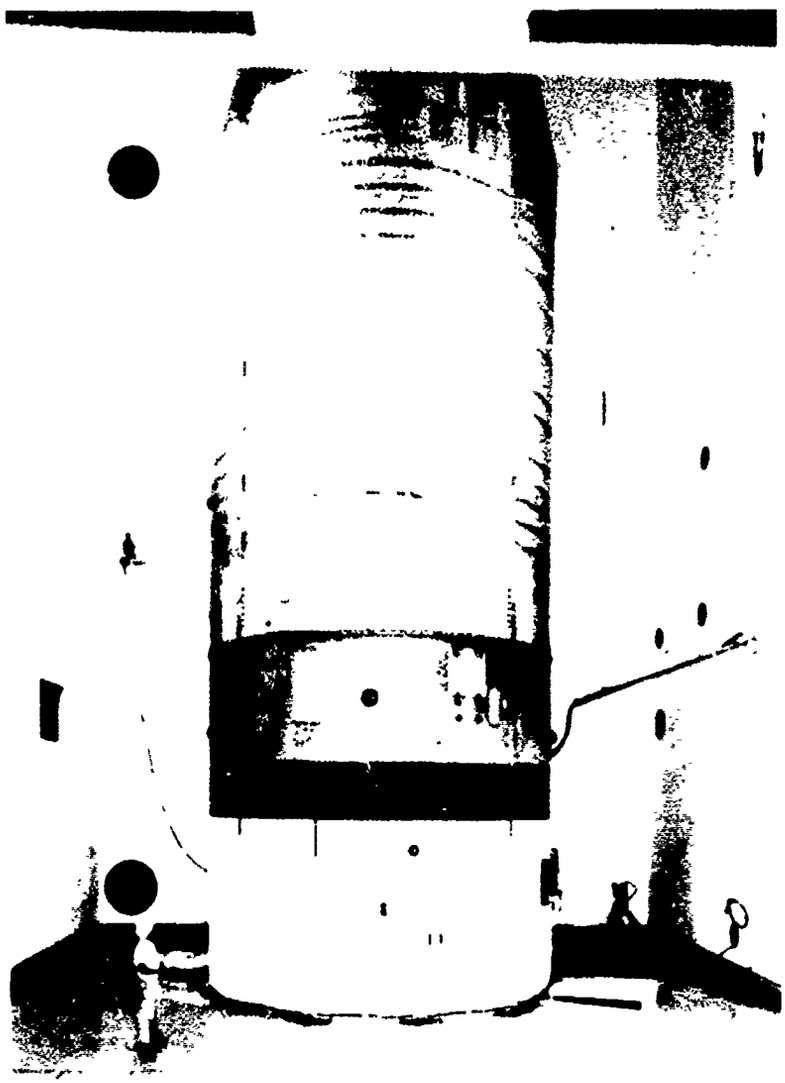

FIGURE 5. PAYLOAD ASSEMBLY STACKED IN SPACECRAFT ACOUSTIC LABORATORY

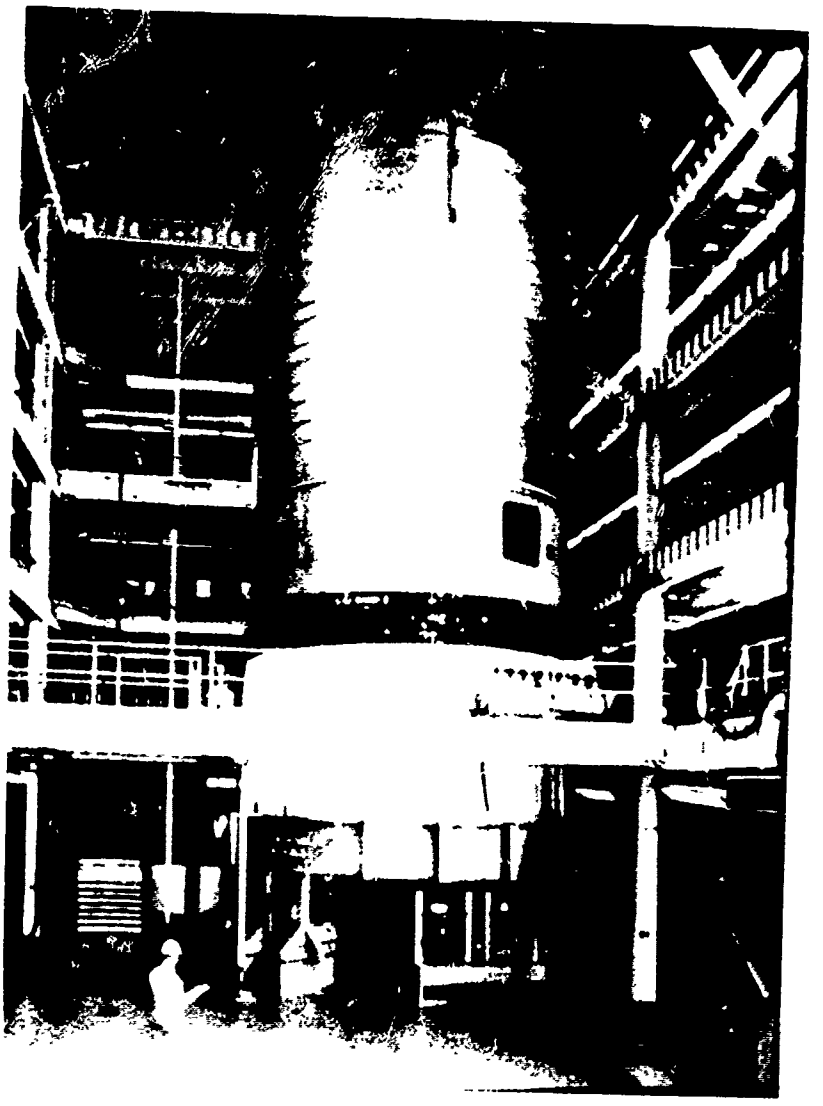

FIGURE 6. PAYLOAD ASSEMBLY STACK IN SPACECRAFT VIBRATION LABORATORY

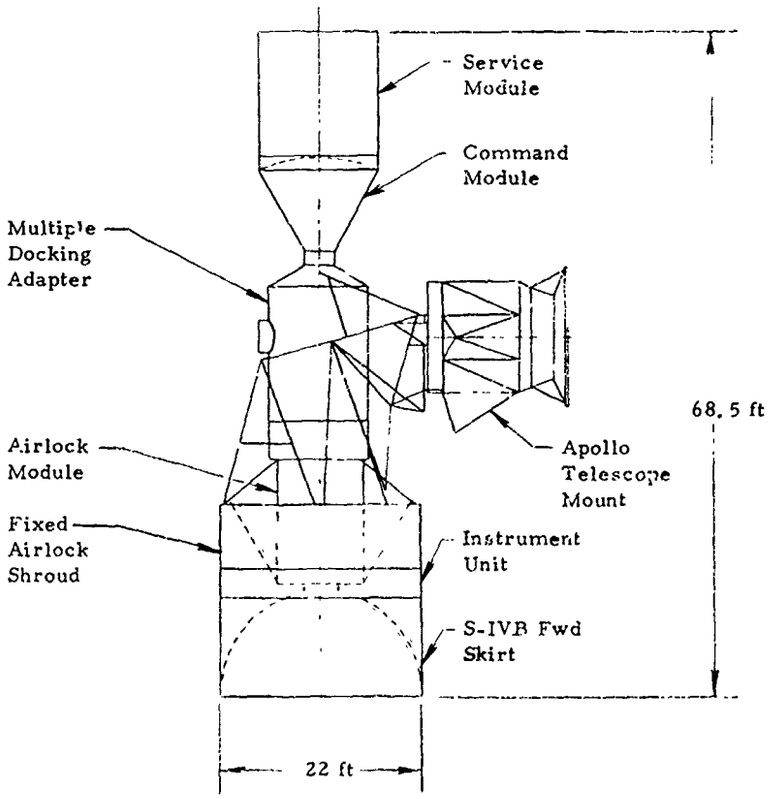

FIGURE 7. PAYLOAD ASSEMBLY ORBITAL CONFIGURATION IN SPACECRAFT VIBRATION LABORATORY

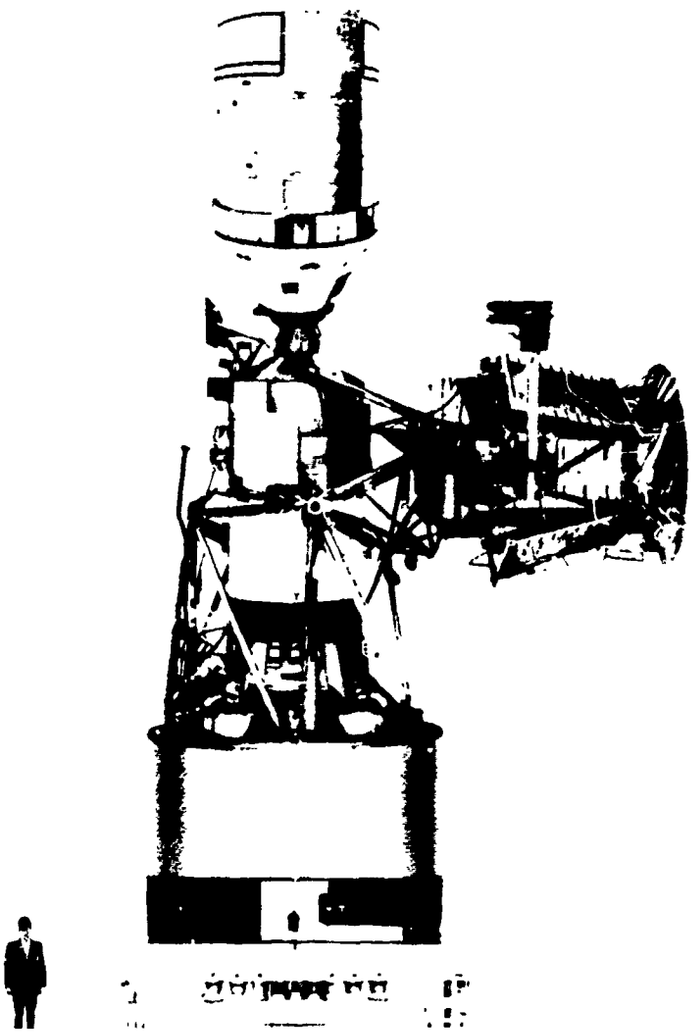

FIGURE 8. PAYLOAD ASSEMBLY ORBITAL CONFIGURATION STACK IN SPACECRAFT VIBRATION LABORATORY

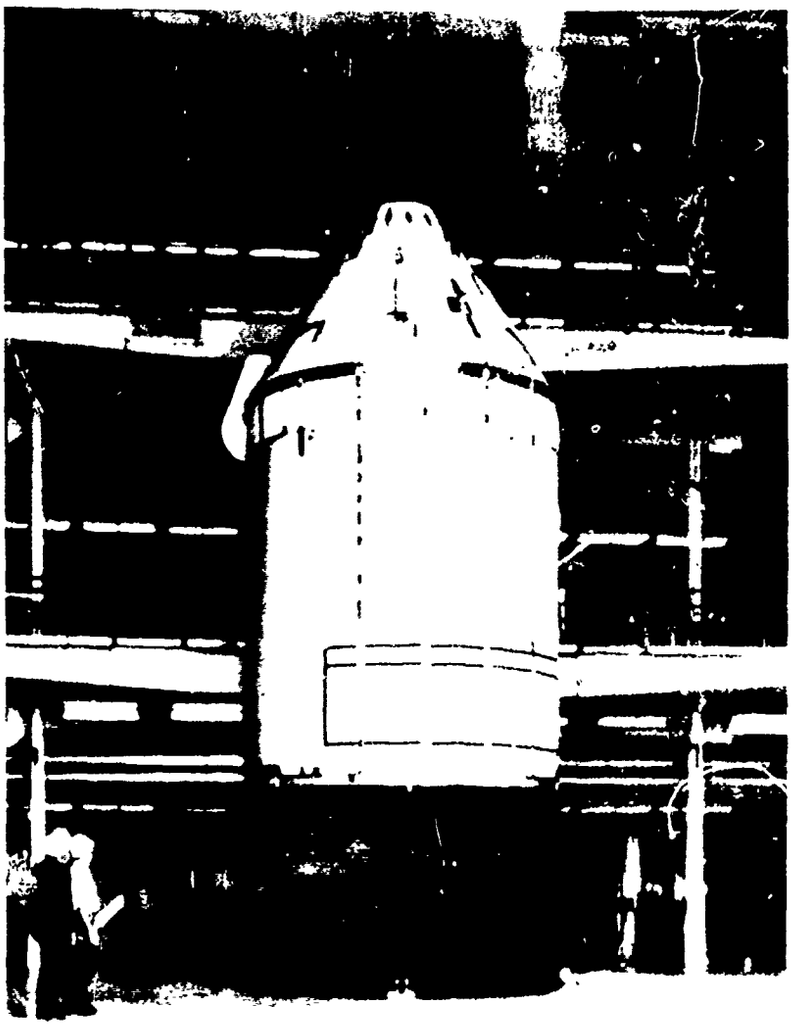

FIGURE 9. COMMAND/SERVICE MODULE ACOUSTIC TEST

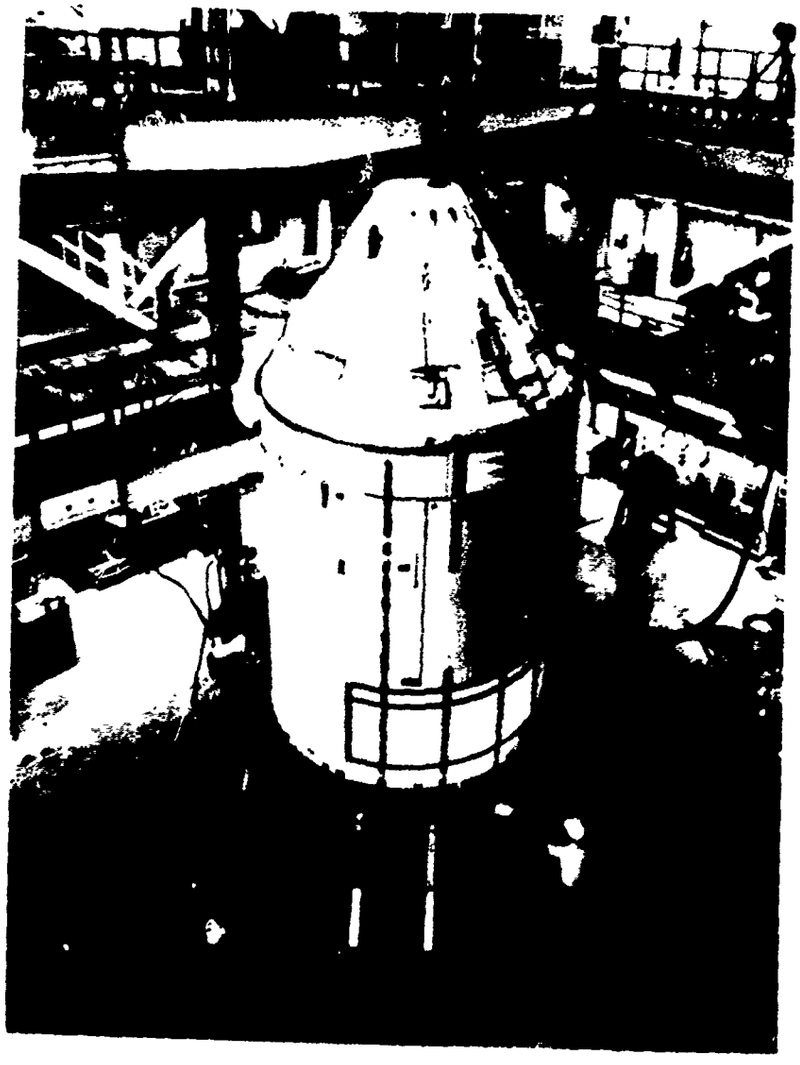

FIGURE 10. COMMAND/SERVICE MODULE VIBRATION TESTING

TABLE I. SKYLAB PAPERS PREPARED FOR THE 43rd SHOCK AND VIBRATION SYMPOSIUM

	Paper Title	Author(s)
1.	SKYLAB VIBROACOUSTIC TESTING - AN OVERVIEW	G. M. MOSELEY, Teledyne Brown Engineering Company, Huntsville, Alabama.
2.	SKYLAB VIBRATION AND ACOUSTIC STRUCTURAL TEST SYSTEMS	J. D. JOHNSTON, NASA-MSC, Houston, Texas. D. L. KNITTLE, Northrop Services Inc., Houston, Texas.
3.	ORBITAL WORKSHOP VIBROACOUSTIC TEST PROGRAM	W. H. KELLER, J. R. DONAHUE and E. YOSHIDA. McDonnell Douglas Astronautics Company, Huntington Beach, California.
4.	SKYLAB PAYLOAD ASSEMBLY - VIBROACOUSTIC TEST PROGRAM	P. RADER, Martin Marietta Corporation, Denver, Colorado.
5.	DEVELOPMENT OF AN AUTOMATIC MODAL TUNING AND ANALYSIS SYSTEM FOR PERFORMING SKYLAB MODAL SURVEYS	R. A. SALYER, TRW Systems, Redondo Beach, California. E. J. JUNG, NASA-MSC, Houston, Texas. S. L. HUGGINS and B. L. STEVENS, Northrop Services Inc., Houston, Texas.
6.	SKYLAB MODAL SURVEY TESTING	J. J. NICHOLS, NASA-MSFC, Huntsville, Alabama. R. E. HULL and B. BEJMUK, Martin Marietta Corporation, Denver, Colorado.
7.	USE OF GENERALIZED MASS CONTRIBUTIONS IN CORRELATION OF TEST AND ANALYTICAL VIBRATION MODES	R. E. HULL and B. BEJMUK, Martin Marietta Corporation, Denver, Colorado. J. J. NICHOLS, NASA-MSFC, Huntsville, Alabama.
8.	VIBRATION AND ACOUSTIC TESTS OF THE RECONFIGURED SERVICE MODULE ADAPTER FOR SKYLAB MISSIONS	R. A. COLONNA, NASA-MSC, Houston, Texas. D. E. NEWBROUGH, General Electric Company, Houston, Texas. J. E. WEST, JR. North American Rockwell Corp. Downey, California.

SKYLAB VIBRATION AND ACOUSTIC STRUCTURAL TEST SYSTEMS

James D. Johnston, Jr.
NASA Manned Spacecraft Center

and

Donald L. Knittle
Northrop Services, Incorporated

A detailed description is given of the vibration and acoustic test systems located at the Manned Spacecraft Center, Houston, Texas, which were used in dynamic structural evaluation of the Skylab Orbital Workshop and Payload Assembly. The test systems discussed include those required to impose a high level reverberant acoustic field on large test articles and those necessary for high force vibration testing of large, softly suspended test articles.

INTRODUCTION

The NASA Skylab is a manned orbital scientific laboratory scheduled for launch in early 1973. Since the launch of the laboratory leads directly into an operational mission without a preceding development flight, an extensive structural dynamic test program prior to flight was required to assure success of the Skylab mission. The test program (described in References 1, 2, and 3) entailed: (1) high-level acoustic testing to qualify the Skylab for resistance to lift-off noise and ensuing aerodynamic fluctuating pressure; (2) high-force vibration testing to assure the Skylab ability to withstand booster staging transients and other low frequency flight phenomena; and (3) low-force modal and impedance testing to acquire data for structural analyses. This extensive and complex testing was performed at the Vibration and Acoustic Test Facility (VATF) at the Manned Spacecraft Center, Houston, which provided and operated the test systems necessary to accomplish all of the Skylab test objectives. Acoustic, vibration, and instrumentation systems of the VATF were developed, modified, or adapted to meet the test requirements, and as a result of this effort, the VATF test capabilities are at the forefront of the state-of-the-art for structural dynamic testing.

This paper characterizes most of the dynamic test capabilities of the VATF (Figure 1) by describing its test laboratories and equipment and, in certain instances, how these laboratories and equipment were applied to Skylab testing. In particular, a unique reverberant acoustic chamber with closed-loop computer control along with the VATF data system used for acquisition, processing, and display of excitation and response measurements is described in "Test Systems of the Spacecraft Acoustic Laboratory"; a high-force vibration system with versatile excitation, control, and spacecraft suspension techniques is covered in "Test Systems of the Spacecraft Vibration Laboratory". Since the scope of this paper is broad, only the unique, new, or especially salient capabilities of the VATF systems for dynamic structural testing have been covered. Furthermore, substantial effort was devoted to upgrading VATF modal test hardware and capabilities, and, due to the wide scope of this effort, a separate paper (Reference 4) is devoted to this topic.

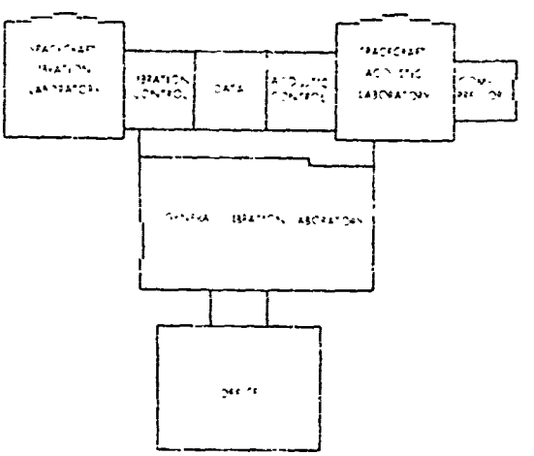

Figure 1. Plan View of Vibration and Acoustic Test Facility

TEST SYSTEMS OF THE SPACECRAFT ACOUSTIC LABORATORY

BACKGROUND

The Skylab acoustic test program objectives required that a reverberant sound field be imposed on each of the two major Skylab components, the Orbital Workshop (OWS) and the Payload Assembly (PA), to simulate the relatively uniform spatial conditions of both launch acoustic noise and aerodynamic fluctuating pressure environments. These simulations included overall sound pressure levels up to about 158 dB and 155 dB, respectively. Since the most severe launch noise and aerodynamic pressures occur at different flight times and differ in spectral content, two separate tests were required for each of the two Skylab components. However, the preceding Apollo program testing (Reference 5), which was the major VATF effort prior to Skylab, had employed progressive-wave acoustic fields to excite test article responses. For this reason, the facility had not been equipped with a large reverberant chamber to complement its extensive inventory of progressive-wave fixtures. In order that the Skylab testing could be achieved with maximum effectiveness, a suitable chamber was constructed and equipped.

Significant construction economy was realized by building the required reverberant chamber within the existing Spacecraft Acoustic Laboratory tower (Figure 2). The chamber walls were attached to existing tower structure, so that no new major structure was necessary. Also, construction of the reverberant chamber within the tower provided double wall (the tower outer wall and the reverberant chamber wall) isolation of the reverberant sound field from laboratory areas which were occupied by personnel during tests; thus, the chamber walls and ceiling were made much lighter than would have been required for noise isolation by only a single chamber wall. Furthermore, the reverberant chamber made full use of existing SAL tower services and equipment, such as air-conditioning, exterior doors, test article handling crane and hoist, electrical power, and noise generating equipment.

The major SAL test systems are defined here as the reverberant chamber together with its spacecraft handling equipment; the noise generation system which consists of air modulator noisemakers and an air compressor system for supplying pneumatic power to the noisemakers; and the acoustic environment control system which controls noise generation equipment to produce the necessary acoustic test spectra in the reverberant chamber. In the following acoustics discussion, the characteristics of these systems which pertain to the acoustic test capability of SAL will be discussed. The data acquisition and processing systems which complement the test capabilities of the VATF laboratories are briefly discussed in this part of the paper.

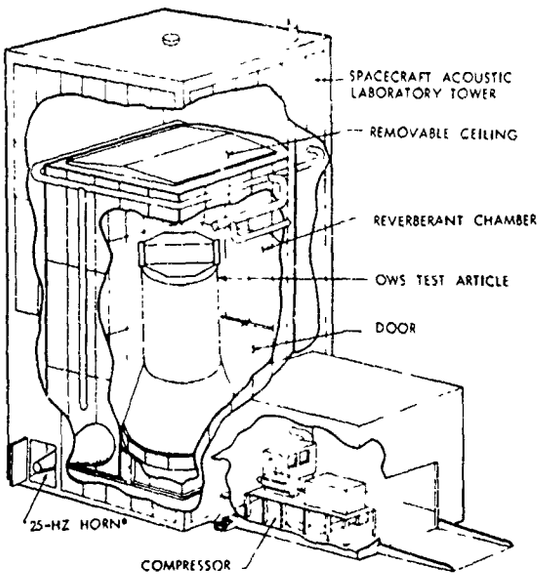

Figure 2. Configuration of Reverberant Chamber (* Other Horns Deleted from Illustration)

REVERBERANT CHAMBER

The reverberant chamber used for the Skylab acoustic tests (Figure 2) is a rectangular enclosure 44.4 x 47.3 x 75 feet high within the SAL tower. Three of the chamber walls are supported externally (internal to the tower) by the steel frame structure of the tower and are smooth and flat on the inside to minimize potential sound absorbing surface area; the fourth wall, which coincides with a part of the tower north wall, has a test article access door 32 feet wide and 40 feet high and an internal support structure both of which interrupt flatness of the wall. All four of the walls are fabricated from 6-inch thick precast reinforced concrete panels. Nineteen circular openings for horns are distributed among the room walls; these openings accommodate one 25 Hz horn, two 50 Hz horns, two 100 Hz horns, and 14 horns for use in the frequency range above 250 Hz. The chamber ceiling, which utilized work platforms once employed in the original tower, is made in nine removable pieces 5 feet wide by 49 feet long from steel beams faced on the chamber side with 1/4-inch steel plate to achieve a flat inner surface. Floor, ceiling, and wall surfaces of the chamber are all sealed with epoxy paint to minimize their sound absorption.

The reverberant chamber is well equipped to provide the test article handling necessary for access to the chamber; assembly within the chamber, if required; and positioning on the chamber floor. Test

articles which exceed the door size of 32 feet wide by 40 feet high (and can be disassembled) can be assembled from components within the chamber with the use of a 75-ton fixed point hoist and a 5-ton circular bridge crane. The hoist and crane are located in the tower above and external to the chamber and can service the chamber when the chamber ceiling is partially removed. Test article handling and assembly are expedited by supporting the test article with air pallets. An air pallet, about 2 feet square and 2-inches thick, inflated with shop air, can mobilize a load of several tons on a smooth floor. Twelve of these units were used to facilitate the assembly and positioning of the Skylab PA in the chamber. The use of the 2-inch thick air pallets rather than a more cumbersome supporting structure (and dolly) will permit a test article to be almost as tall as the chamber height. The PA was actually a few inches taller than the chamber so a 3.5 foot diameter hole was cut in the ceiling to allow the PA nose cone to protrude; in this case, the use of air pallets minimized the required ceiling modification.

NOISE GENERATION

Air modulated sound generators are used in the reverberant chamber for horn drivers. Five air modulators each rated at 20,000 acoustic watts output are used for low frequency (below 300Hz) chamber excitation; high frequency excitation (300 to 2,000 Hz) is provided by 14 air modulators, each rated at 10,000 acoustic watts output. The SAL air compressor can produce 27,000 SCFM at 30 PSIG. This flow supplies air for simultaneous operation of various combinations of air modulators; for instance, five low frequency and eight high frequency air modulators or two low frequency and 14 high frequency modulators consume the full compressor capacity. The SAL air compressor system can also operate with nitrogen rather than air to reduce high frequency acoustic absorption and thereby obtain more effective use of the sound energy in the chamber, as delineated in a later section. Also, the compressor provides virtually unlimited test durations.

ACOUSTIC SPECTRUM CONTROL

Acoustic test spectra generated in the reverberant chamber are automatically controlled by a closed-loop digital computer based system represented schematically in Figure 3. The control system samples noise data from up to 30 microphones, compares the average of these data to a preprogrammed 1/3 octave band spectrum, and then gives appropriate commands to a

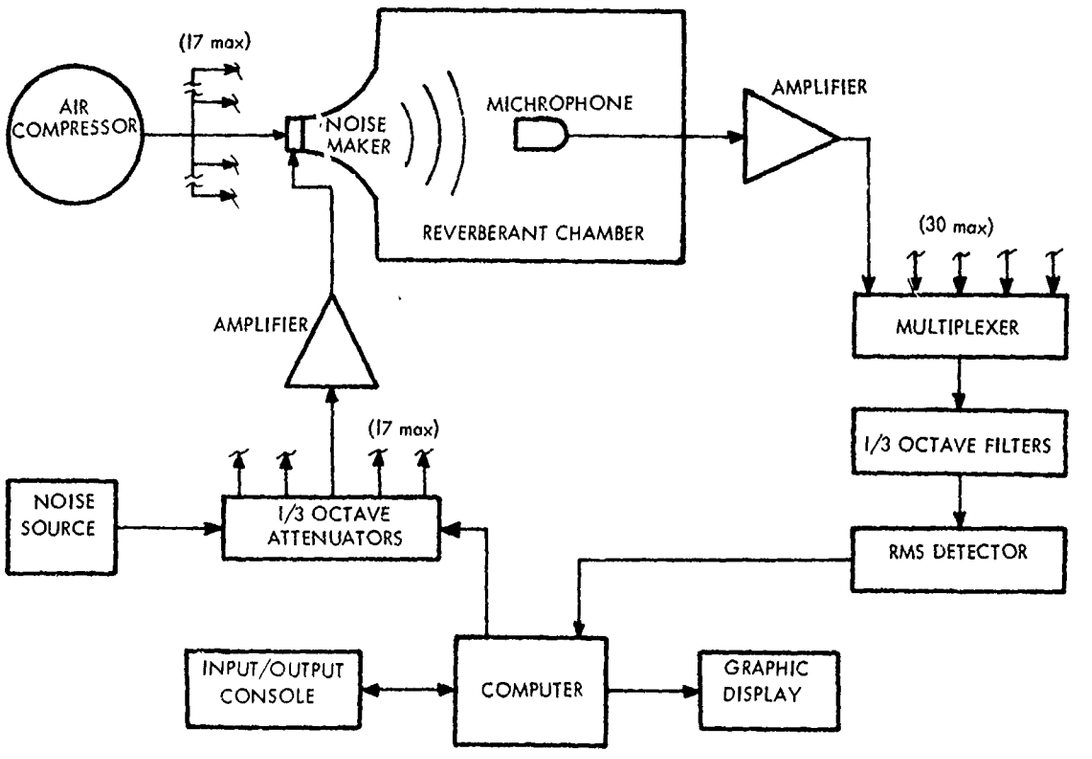

Figure 3. Diagram of Automatic Acoustic Control System

set of digital attenuators which regulate the air modulator power amplifiers. This system is capable of simultaneously shaping and raising the acoustic spectrum from 10 dB below nominal to the nominal sound pressure level in eight to 20 seconds.

The use of an automatic spectrum shaping system has proven to be advantageous both in test quality and in manpower utilization. Refinement of the test sound field has been obtained by basing the acceptability of a spectrum on the average response of up to 10 microphones (with a capability of 30); more microphones than could be conveniently used without the aid of a computer. A major improvement in test quality also results from the fast buildup to full test level of the computer controlled spectrum shaping, since, thereby, a test article is subjected to only a few seconds of noise prior to the actual test start. The previously used manual spectrum shaping procedure, on the other hand, required extensive undesirable exposure of the test article to high level nontest noise (albeit below the full test level) to accomplish the iterative procedure of exposing the test article to noise while recording microphone signals, data reduction and analysis, and subsequent manual adjustments to the individual air modulator power amplifiers. This entirely manual operation, which typically spanned several days, has been replaced by the minimal manual adjustments of the individual air modulator amplifiers for use with the digital control system and only seconds for spectrum buildup to test level.

REVERBERANT CHAMBER ACOUSTIC CHARACTERISTICS

Modal Properties

At low frequencies in a reverberant chamber (frequencies below some nominal frequency for which only a few wave lengths are equal to a typical room dimension), the acoustic energy available to excite test articles is largely concentrated at discrete acoustic modal frequencies of the chamber. The frequency locations of these acoustic modes with respect to structural modes of the test article are therefore important. Specifically, the proper excitation of the test structure by acoustic energy requires that one or more chamber modal frequencies fall within the modal bandwidth of each structural response mode. The bandwidth B for a structural mode is defined as that frequency band between the modal halfpower points: $B = f_o/Q$ where f_o is the mode frequency and Q is the mode amplification factor. A rectangular room, such as the SAL reverberant chamber, has modal frequencies (F_{lmn}) given by the formula:

$$F_{lmn} = \frac{c}{2}\left[\left(\frac{l}{L}\right)^2 + \left(\frac{m}{M}\right)^2 + \left(\frac{n}{N}\right)^2\right]^{1/2}$$

where l, m, and n have integer values; c is the speed of sound in feet per second; and L, M, and N are the room dimensions in feet. All of the calculated modes below 112Hz (788 modes) are shown in Figure 4.

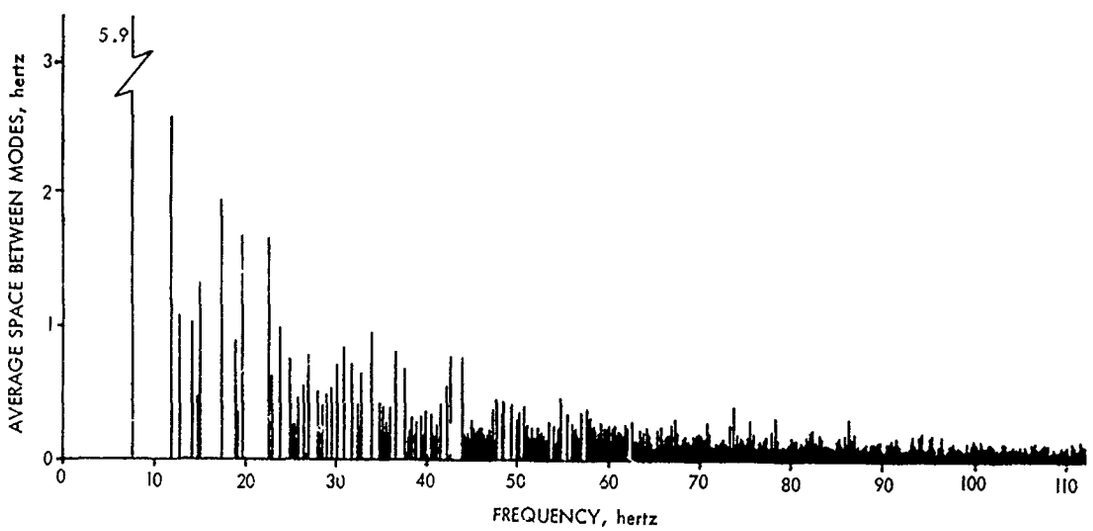

Figure 4. Reverberant Chamber Modal Characteristics

(These calculations assume an air medium at standard atmospheric conditions.) The modal frequencies are indicated on the abcissa of the modal plot by vertical lines. The height of each line is proportional to the sum of the two frequency spaces between the indicated mode and its nearest neighboring mode on each side; thus, the line heights give an indication of the uniformity of modal spacing. The figure shows that the average modal density of the reverberant chamber is good enough in all 1/3 octave frequency bands above the 20 Hz band to excite typical structural modes which have Q's of 50 or less.

Chamber Absorption

As previously mentioned, nitrogen or air can be used as the acoustic medium in the reverberant chamber. Nitrogen, which provides greater sound pressures in the high frequency range for a given acoustic power input to the reverberant room, is introduced into the compressed air loop by bleeding off air from the compressor return line and using dry nitrogen stored in gaseous form as the makeup supply until the desired nitrogen content is achieved. The effect of nitrogen content on the absorption of sound in the chamber is shown in Figure 5 which compares the chamber sound absorption in air to the sound absorption after most of the oxygen in air has been replaced by nitrogen (the gas is 95.5% nitrogen). As expected, these data show no significant difference in absorption below 400 Hz, but above 400 Hz, it can be seen that the benefits of replacing the oxygen in air with nitrogen increase with frequency. The effect of these absorption data on the generation of a sound spectrum is shown in Figure 6. The same input power to the room

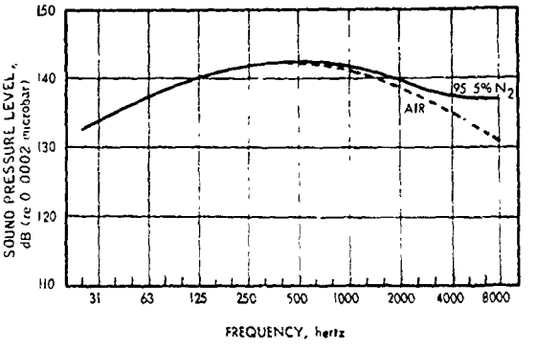

Figure 6. Sound Spectra in Air and in a Mixture of 95.5% N_2 and 4.5% O_2

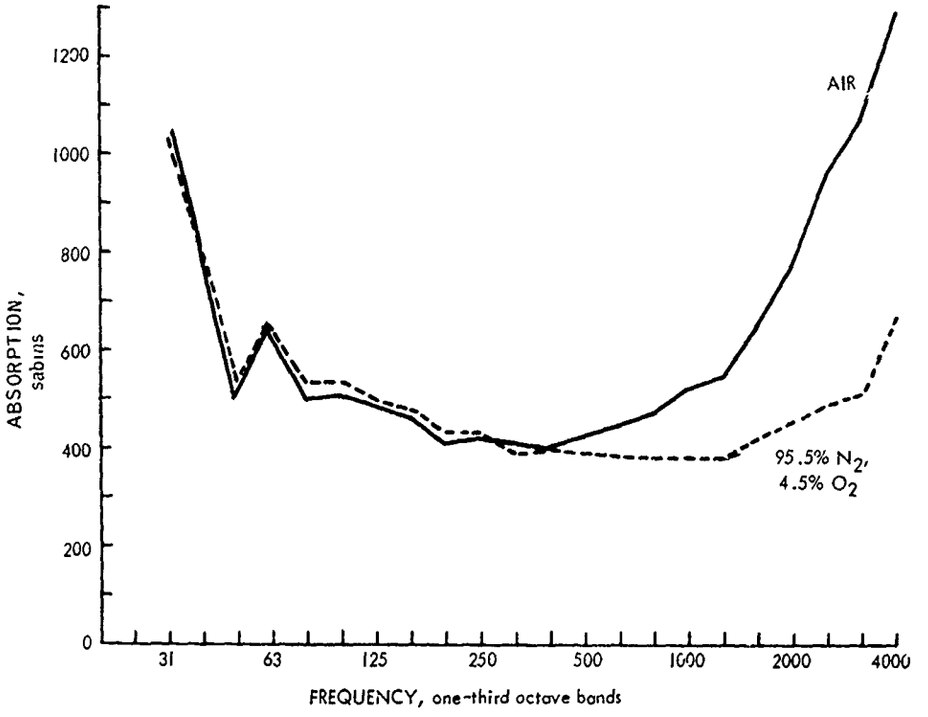

Figure 5. Reverberant Chamber Sound Absorption in Air and a 95.5% N_2, 4.5% O_2 Atmosphere

was used to generate both spectra, but the high frequencies are enhanced in the acoustic medium with oxygen replaced by nitrogen.

Spectral Flexibility

Two spectra generated in an air environment within the empty reverberant chamber in preparation for the Skylab tests are shown in Figure 7. One can see from these spectra that the SAL systems have a high sound generation capability for spectra which peak at high or low frequencies. Both of the spectra of Figure 7 were generated with the use of a mixture of high and low frequency air modulators and horns, were obtained with air, and are representative of Skylab test conditions.

DATA SYSTEMS

A Central Data Acquisition System (represented schematically in Figure 8), located between the Vibration and Acoustic Control Rooms, supports the VATF laboratories in Building 49 (Figure 1). The acquisition capacity consists of 312 channels of 0 to 2,500 Hz data recorded on four FM multiplexed tape recorder subsystems and 91 channels of 0 to 20,000 Hz data recorded on seven FM Simplex tape recorder subsystems. During a test, limited real-time information in raw form can be displayed on oscillographs, oscilloscopes, and meters paralleled with data recording systems.

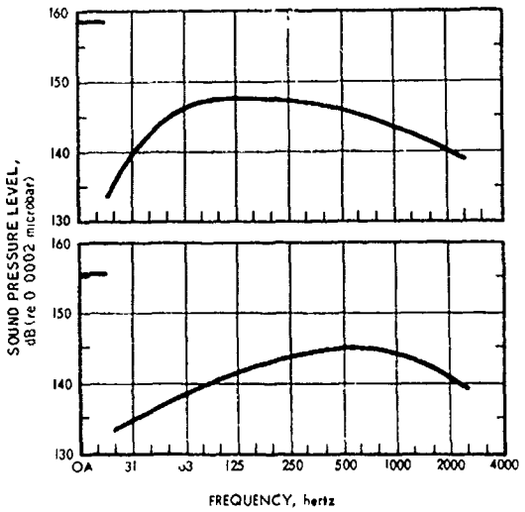

Figure 7. Acoustic Spectra Shaped Automatically in the SAL Reverberant Chamber

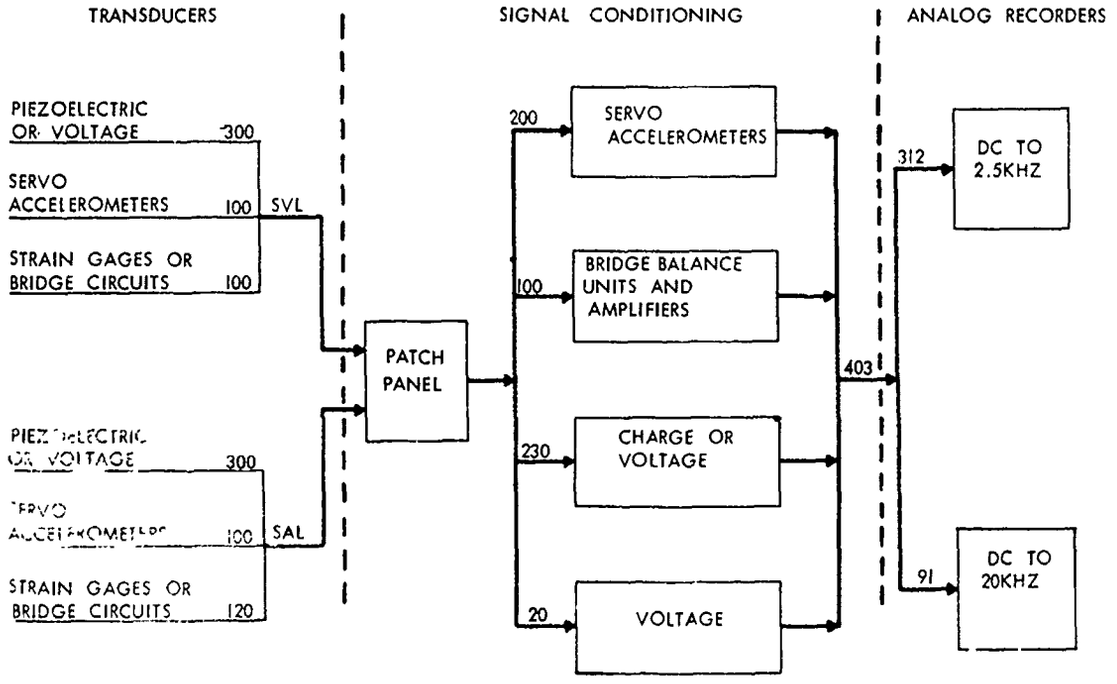

Figure 8. Central Data Acquisition System

Bulk data processing is performed using digital techniques at the MSC central computer complex. The processing for both random and sinusoidal waveform records is based on fast-Fourier-transform algorithms, and the data can be displayed in a wide variety of formats (e.g., power spectral density, 1/3 OB spectrogram, amplitude/phase vs frequency, force-normalized coincident and quadrature acceleration vs frequency, etc.). For quick-look test visibility, limited data are processed at VATF by analog methods; for instance, twelve 1/3 octave spectrograms or six power spectral density plots per hour can be produced.

This broad range of data acquisition and reduction capabilities permits full realization of the state-of-the-art testing potential inherent in VATF.

TEST SYSTEMS OF THE SPACECRAFT VIBRATION LABORATORY

BACKGROUND

The Skylab vibration test program required testing of the spacecraft in two sections, the Orbital Workshop and the Payload Assembly; the PA was required to be tested in two configurations, launch and orbital (shroud removed, Apollo Telescope Mount (AMT) deployed, and Command and Service Modules (CSM) docked.) Testing of the OWS consisted of low-level and high-level programmed-motion sine sweeps. Excitation of the PA in the launch configuration consisted of low-level constant force sine sweeps, high-level damped-sinusoidal transients, and a modal survey. Vibration testing in the orbital configuration consisted of a modal survey only. The spacecraft were oriented with the longitudinal (flight) axis vertical, except that the Apollo Telescope Mount was deployed 90 degrees to a horizontal attitude in the orbital configuration. The maximum vertical dimension for these spacecraft was 76 feet for the Payload Assembly (launch configuration), and the maximum horizontal dimension was 40 feet for the PA with the ATM deployed. Approximate weights of the test articles were 60,000 pounds for the OWS, 110,000 pounds for the PA, and 120,000 pounds for the combined PA and CSM in the orbital configuration. This section describes the test systems of the Spacecarft Vibration Laboratory which were utilized to perform the high-force testing and also describes the suspension of the PA in the orbital configuration. (Modal survey testing in that configuration is described in Reference 6.) The test systems of the SVL may be conveniently divided into four parts: the vibration tower, the spacecraft suspension systems, the spacecraft excitation system, and the vibration control system. Brief descriptions of these systems and explanations of how they were utilized for the Skylab testing are presented in the following paragraphs.

VIBRATION TOWER

The Spacecraft Vibration Laboratory, in which Skylab vibration testing was performed, consists of a vertical test tower, spacecraft suspension systems, high-force excitation systems, control and monitoring systems, and auxiliary equipment. The overall size of the tower is 60 feet square by 106 feet high, and it contains a test space 37 by 47 feet that has a vertical clearance of 93 feet. Spacecraft installation is accommodated by a main door clearance 32 feet wide by 40 feet high; a fixed 75-ton hoist, plus two bridge cranes of 10 and 20-ton capacity, respectively, provide for the handling of spacecraft and heavy equipment. Fixed platforms of 10 foot vertical intervals, starting at the 15 foot elevation, line the test space on three sides and provide for test hardware support and personnel access. Full and intermediate length movable platforms are provided for support and additional access within the test space. The tower is air-conditioned and connections for lighting, electrical power, air, water, instrumentation, intercom, and closed-circuit television are distributed throughout the laboratory. These support systems are operated in conjunction with the special test systems described in the following sections to perform spacecraft vibration testing.

SPACECRAFT SUSPENSION SYSTEMS

Suspension systems for the Skylab spacecraft were selected on the basis of spacecraft weight and geometry, vibration displacement and frequency range, and hardware availability. The Orbital Workshop test article weighed 77,000 pounds including force fixtures, was 22 feet in diameter by 40 feet high, and had a CG (center of gravity) at the geometric center. The Payload Assembly (launch configuration) weighed 123,000 pounds including fixtures, had a diameter of 22 feet and overall height of 76 feet, and had a CG 33 feet high. The Payload Assembly in the orbital configuration weighed a total of 130,000 pounds including the Command and Service Modules. High-force and modal vibration test specifications required that the test articles be freely supported with one inch displacement capability for high-force testing and three inch displacement clearance for modal testing. To minimize the influence of the supporting system, the suspension resonance frequencies were required to be below one and one-half hertz for the OWS and below one hertz for the PA, while damping was limited to five percent of critical with one percent desirable.

Two basic types of suspension were available in the SVL; hydrostatic bearings and pneumatic springs. Bearings are employed when test article motion must be constrained to uniaxial translation, and springs are used primarily for free-free support;

however, the two types may be used together for special requirements. Pneumatic springs were available in two configurations; first, bellows of reinforced rubber; second, steel piston assemblies with rolling rubber diaphragm seals. The bellows type is suitable primarily for underneath support, while the piston assemblies are designed for overhead suspension. Both of these spring types provide low spring rates in the vertical direction and the bellows type is soft horizontally, as well. However, the piston units are very stiff in the horizontal plane and must be used in conjunction with suitable pendulum attachments to the spacecraft if lateral freedom is desired. The requirements given above led to the use of air spring suspension and both available types of pneumatic springs in three separate configurations were utilized. Free-free suspension with sufficient stability to omit snubbers or cable restraints was achieved in all three setups.

The moderate weight and CG height of the Orbital Workshop permitted the selection of bellows air springs in a simple underneath support configuration. The OWS was mated to an existing ring fixture which was supported by four springs as shown in Figure 9. Each of the four springs consisted of one double-convolution commercially fabricated rubber element; this item was attached to an integral orifice/plenum assembly which was mounted on a support stand; the stands also provided hard support for the spacecraft when the springs were deflated. The vertical resonance frequency attained by this combination was 1.1 Hz and the stability ratio (which is defined as the ratio of restoring moment to overturning moment) was 4.6. Suspension characteristics of this and the other two configurations are summarized in Table 1.

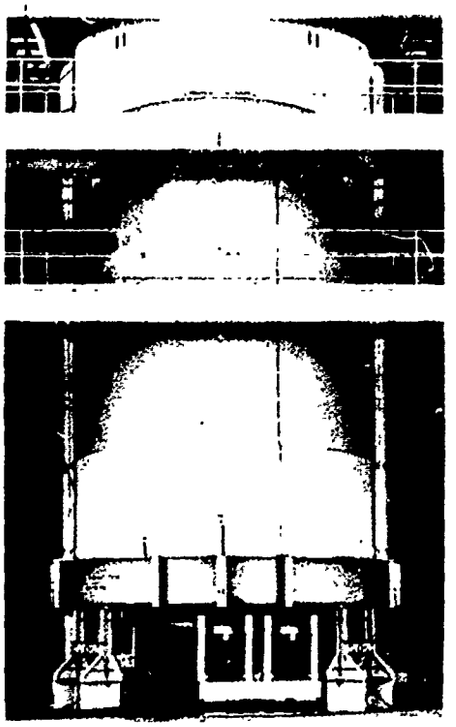

Figure 9. Orbital Workshop Suspension

Suspension of the Payload Assembly in the two configurations introduced some new considerations. The high vertical CG of the launch configuration required a support with either an extended base radius or an increased spring rate to provide sufficient static stability for underneath support. The extended radius was structurally undesirable and the increased spring rate would result in a resonance frequency higher than the specified limit. Furthermore, it was desirable to use as much common spring hardware as possible for the two PA configurations, and to have nearly identical spring characteristics for each of the three spacecraft assemblies in the orbital configuration. The spring rate of an air spring is proportional to the absolute air pressure and inversely proportional to the volume according to the relation

$$K = \frac{\gamma A^2 P}{V}$$

where K is the spring rate, A is the effective piston area, P is the absolute pressure, V is the volume, and γ is the ratio of specific heats (γ is 1.4 for air). The absolute pressure required to support a given load, W, is given by

$$P = \frac{W}{A} + P_{atm}$$

where P_{atm} is the atmospheric pressure. When the load, W, is fixed and the resonance frequency is limited (as was the case for the PA spacecraft), then it is extremely desirable to be able to change both the piston area and the volume of the air springs. The area is then selected to obtain a reasonable working pressure, and the volume is adjusted to obtain the desired resonance frequency. The existing VATF piston air springs were modified to allow incremental changes to the piston area and to provide continuously adjustable volumes. The variable area was achieved by installing 10 cylinders on the plenum tank such that any even number of pistons from two to 10 might be used according to the load. At a nominal working pressure of 100 PSIG, each assembly could be set up to support any load from 10,000 to 50,000 pounds. The volume change in the horizontal cylindrical plenum tank was accommodated by provisions for partially filling the tank

TABLE I. CHARACTERISTICS OF THE OWS AND PA SUSPENSION SYSTEM

PARAMETER	OWS	PA			
		Launch Config	Orbital Configuration		
			Base Assembly	Apollo Telescope Mount	CSM
Degrees of freedom	Six	Six	Six	Six	Six
Type of suspension	Underneath, bellows air springs	Overhead, piston air springs/pendulum	Overhead, piston air springs/pendulum	Overhead, piston air springs/pendulum	Overhead, piston air springs pendulum
Number of springs	Four	Three	Three	One	One
Total supported weight	77,000 lb	123,000 lb	78,000 lb	25,500 lb	29,000 lb
Operating air pressure	70 psig	82-94 psig	87-103 psig	87 psig	107 psig
Resonance frequency: vertical translation	1.1 Hz	0.75 Hz	0.5 Hz	0.5 Hz	0.5 Hz
horizontal translation	0.3 Hz	0.3 Hz	0.3 Hz	0.25 Hz	0.3 Hz
Damping ratio, vertical	Less than 1%	Approx 2%	Approx 2%	Approx 2%	Approx 2%
Stability ratio *	4.6	1.9	Not Applicable	Not Applicable	Not Applicable

* Ratio of restoring moment to unbalance moment.

with hydraulic oil. The total volume is 39,000 cubic inches and this may be reduced to 13,000 cubic inches by adding 113 gallons of oil. Therefore, a volume change and consequent spring rate change of about three to one may be effected. Accordingly, five of the piston air springs were so modified and utilized with the PA spacecraft. Three of these assemblies with 10 pistons each were setup to suspend the PA in the launch configuration shown in Figure 10. The PA was mated to the same ring fixture used with the OWS, and the fixture was suspended on 104-inch long pendulum rods attached to short outriggers on the ring. Note that a load cell was inserted in each pendulum assembly to obtain the load on each spring. The three spring plenums were filled with calculated quantities of oil to obtain the same resonance frequency.

Five air spring assemblies (piston type) were required for suspension of the PA and CSM in the orbital configuration as seen in Figure 11. The spacecraft were supported as three subassemblies: the lower subassembly was hung on three springs in the same manner as the launch configuration vehicle, but only six pistons per spring were required; the CSM and the ATM subassemblies were each suspended from single springs also fitted with six pistons, and the spring plenum volumes were adjusted to provide identical resonance frequencies for each subassembly. After mating of the three spacecraft components, the suspension of the combined assembly was essentially operated as a single system. Characteristics of the suspension systems for the PA in both launch and

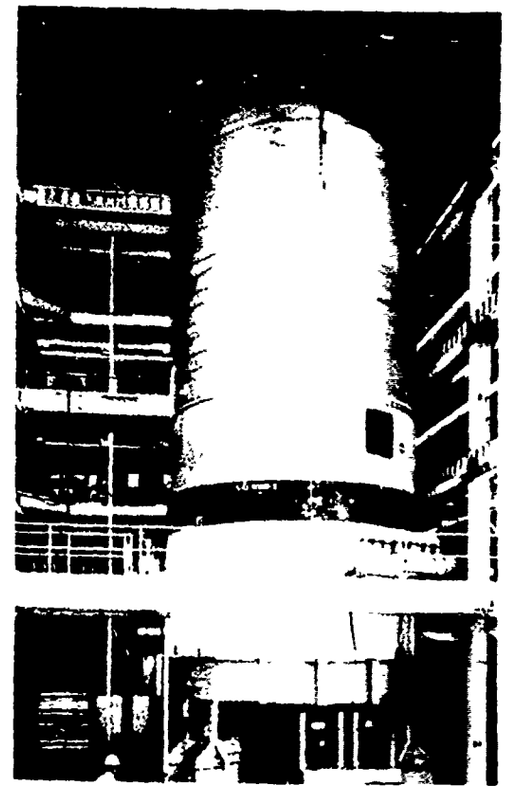

Figure 10. Payload Assembly Launch Configuration Suspension.

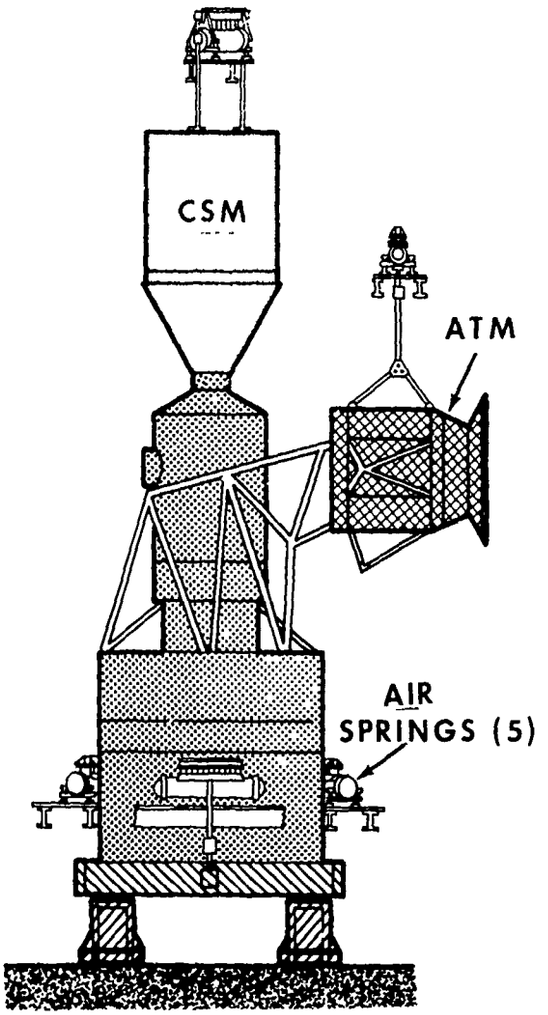

Figure 11. Suspension System for Skylab Payload Assembly, Orbital Configuration

orbital configurations are given in Table 1. In the three configurations, each air spring assembly could be operated manually at a local control panel and could be operated manually or automatically from the control room. Automatic operation utilized individual closed-loop control of the spacecraft elevation at each spring. Linear potentiometers were used as sensors and solenoid valves were used as control elements. The solenoid valves were driven in a random sequence to prevent rythmic interaction of the springs. Automatic operation of the suspensions maintained the mean spacecraft position within 0.05-inch.

SPACECRAFT EXCITATION SYSTEM

The vibration test specifications for the Skylab spacecraft required excitation within the frequency band from three to 60 Hz, displacements up to 0.5-inch double amplitude, acceleration up to 3.6 g peak, and maximum calculated forces of 100,000 pounds. The spacecraft excitation system of the SVL includes eight thrusters (electrodynamic shakers equipped for single point force attachment) each rated at 10,000 force pounds continuous output, three power amplifiers rated 175kva each, and a central switching console capable of establishing all useful combinations of series and parallel thruster/amplifier connections.

Eight thrusters were utilized for longitudinal excitation of the OWS and six in each of two lateral axes. Since neither inertial mass nor structural stiffness was available to react thruster forces within the test frequency range, the thruster masses were augmented with steel billets attached to the field structure, and those inertial assemblies were isolated from the facility floor and structure. For vertical operation, eight thrusters were mated in pairs with six-inch thick steel billets into assemblies weighing 30,000 pounds as shown in Figure 12. These assemblies were isolated from the floor by air spring units which had mechanical position control valves. For horizontal operation, shown in Figure 13, six thrusters were individually increased in weight from 4,000 to 8,000 pounds, and each assembly was mounted on a modified support base which utilized four linear ball bushings on twin horizontal shafts in a cast steel base. The thruster body with the augmenting steel billets was free to slide along the shafts in the direction of thrust, thus isolating vibration forces from the tower structure. Thrusters were driven in series to aid in obtaining uniform amplitude and phase of excitation forces; actual force amplitudes which were required for Skylab testing varied from 200 to 12,000 force pounds per thruster with one, two or three series-connected power amplifiers used as required.

VIBRATION CONTROL SYSTEMS

Skylab test specifications required the implementation of a number of control system configurations. For the sinusoidal, fixed and swept frequency tests, automatic control of input force for constant force tests, and automatic programmed control of input motion for the launch and boost simulation were required. Maximum allowable acceleration amplitudes at selected locations on the spacecraft were specified for all tests and the input force was required to be limited to preclude exceedance of these amplitudes. (For the damped sinusoidal transient tests, the spacecraft response limiting requirements were deleted.)

Figure 14 shows the SVL control room located on the second level immediately adjacent to the tower. Standard and special equipment are available for generation and control (automatic or manual) of sinusoidal, random, and transient excitation, and for monitoring test article response and test system status.

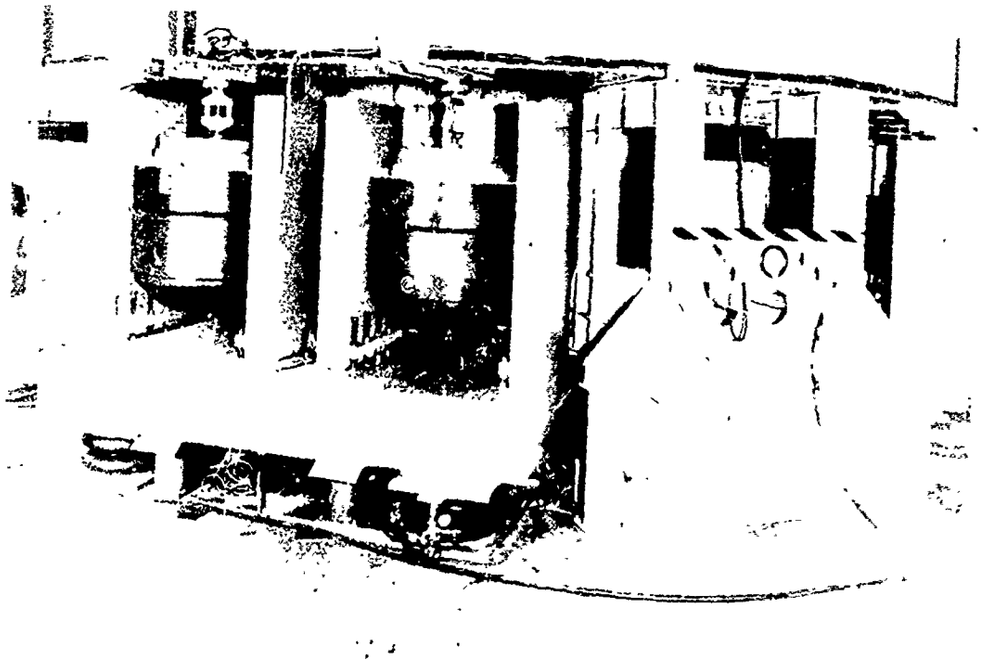

Figure 12. Vibration Isolated, Vertical, Dual Thruster Assembly

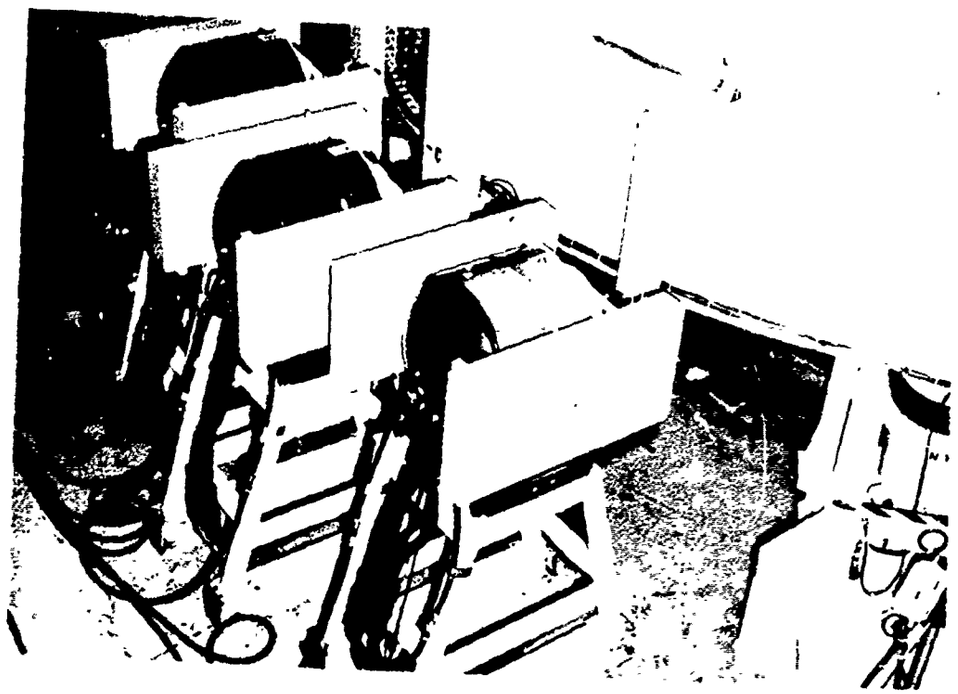

Figure 13. Vibration Isolated, Horizontal, Single-Thruster Assemblies

Figure 14. Spacecraft Vibration Laboratory Control Room

This equipment may be easily configured by patching and switching into systems capable of satisfying complex test requirements, such as those of the Skylab program. The equipment was configured as shown in Figure 15 for vibration testing of the Orbital Workshop. For constant force testing, excitation force signals (not shown in the figure) were fed to the maximum level selector and the maximum signal was used for automatic control. Exploratory tests resulted in switching of control to spacecraft response motion in certain frequency regions. Force levels and limiting response amplitudes were adjusted and a successful constant force sweep was attained. Analysis revealed that the eight thruster force amplitudes and phases were nearly identical. For the programmed input motion tests of the OWS, 23 input and response motion signals (acceleration) were filtered and weighted and fed to the maximum level selector. The selected signal was programmed and fed to the servo controller. Six additional motion signals, selected to represent cross-axis motion, were fed to a multichannel limit detector which was connected to effect an abort upon the detection of any limit exceedance. Figure 16 shows how the system performed during the OWS test. Note that servo control was excellent and that spacecraft response was actively controlling the input excitation at most frequencies above 12 Hz.

For the PA tests, constant force input sine sweeps were controlled by instantaneous summing of the eight force signals and filtering out the fundamental total force as the control signal. Spacecraft response motion at 23 locations was continuously compared with pre-established limit amplitudes, with an automatic abort for any limit exceedance as a mandatory action.

For simulating booster cutoff and separation excitation, the Payload Assembly was also subjected to damped sinusoidal transient excitation using the control system shown in Figure 17. The transient signal was generated by modulating the amplitude of a sinusoidal signal. Control was open-loop and proper amplitude was established by determining the response/excitation transfer function at low level. Two to four iterations were required at each of the nine specified frequencies to attain the required peak acceleration amplitude. Examples of typical transient excitation and spacecraft response are presented in Figure 18.

CONCLUDING REMARKS

A major test capability was developed at the Vibration and Acoustic Test Facility (VATF) to meet the needs of the Skylab program for dynamic

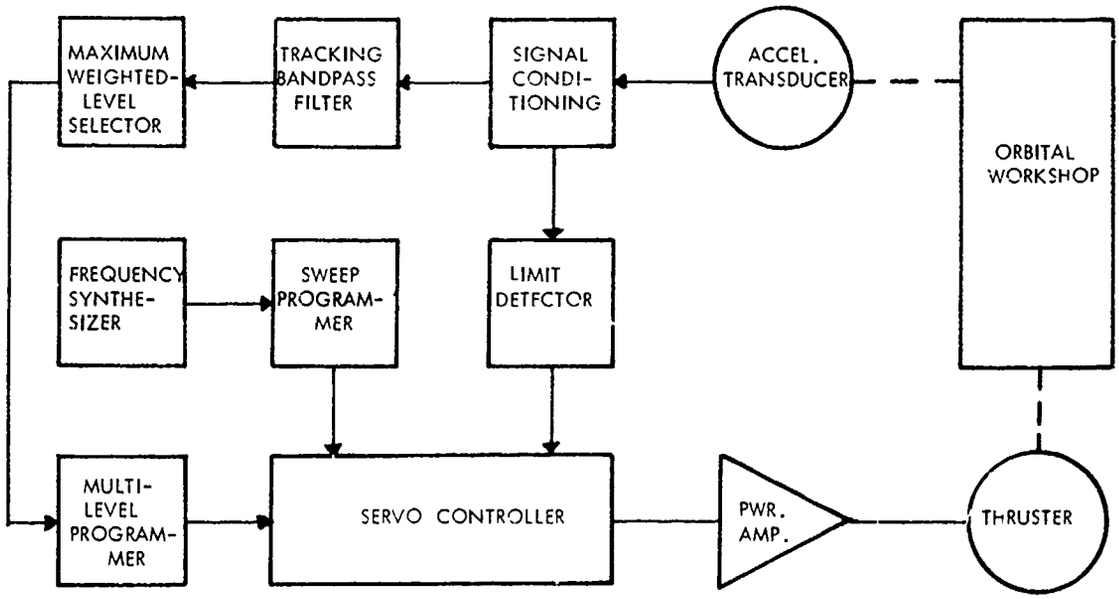

Figure 15. Vibration Control System for the Orbital Workshop

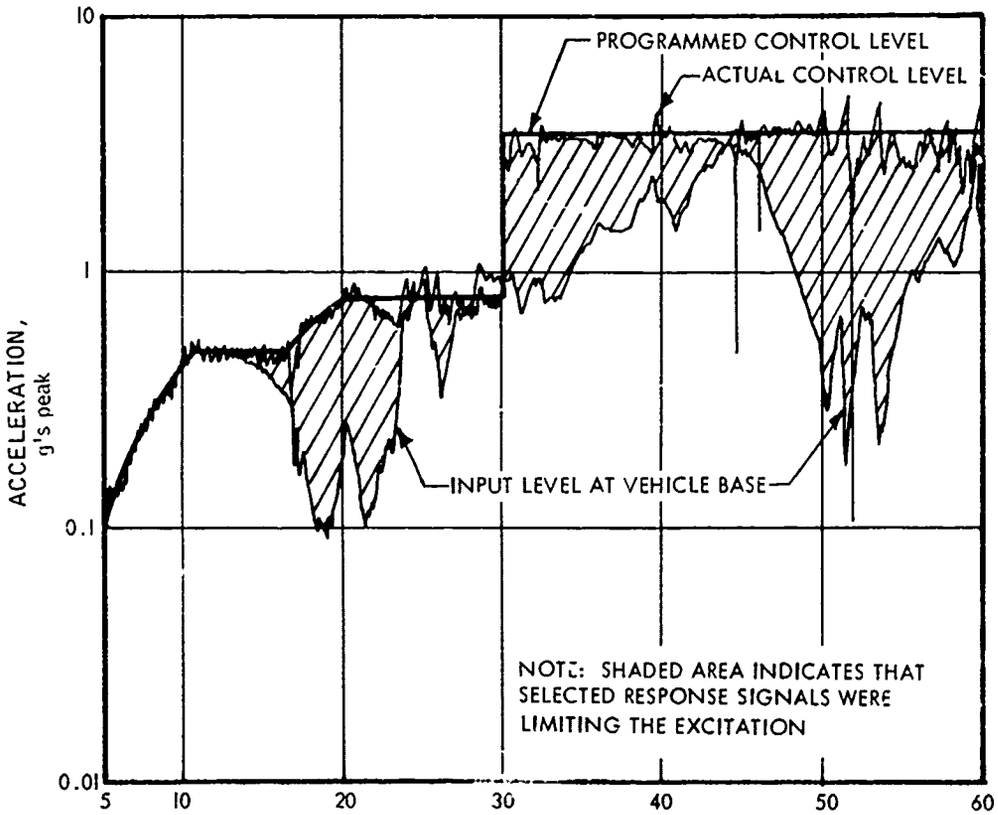

Figure 16. Control System Performance, Orbital Workshop Vibration

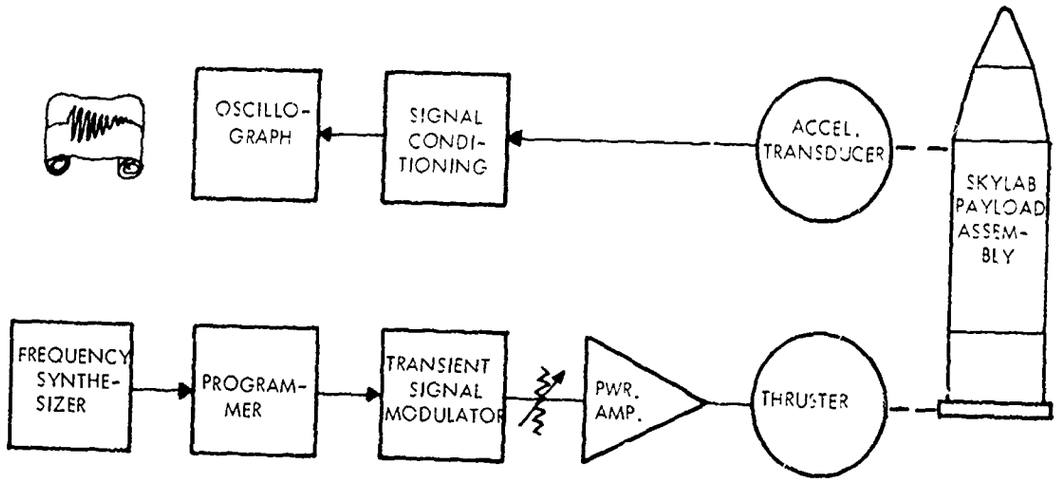

Figure 17. Transient Excitation System for Payload Assembly Vibration

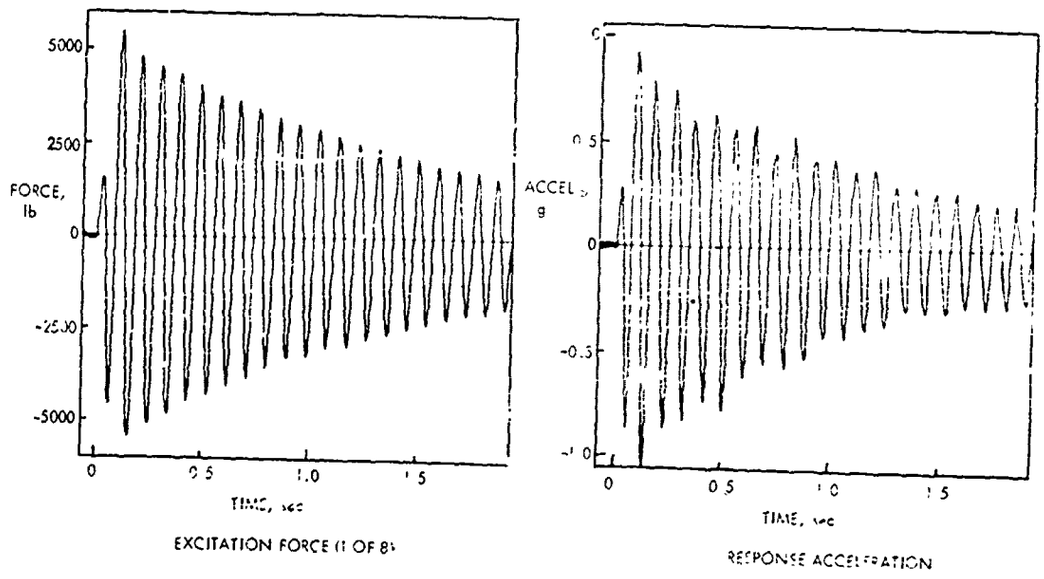

Figure 18. Typical Transient Excitation and Response, Payload Assembly Vibration

structural evaluation of the OWS and the PA. The structural effects of the severe high frequency (approximately 40 to 4,000Hz) portions of mission environments, such as lift-off acoustics and aerodynamic fluctuating pressures, on the Skylab spacecraft were determined by tests in the Spacecraft Acoustic Laboratory (SAL) reverberant chamber. The ability of the Skylab hardware to withstand the vibrations induced during launch and boost by staging transients, rough fuel burn, wind loads, and other low-frequency phenomena was determined by high force testing in the Spacecraft Vibration Laboratory (SVL). This paper has described the wide-ranging, state-of-the-art, capabilities of the SAL, the SVL, and their complementary data acquisition and reduction systems; all of these VATF capabilities contributed significantly to the success of the Skylab structural evaluation program.

REFERENCES

1. G.M. Moseley, "Skylab Vibroacoustic Testing - An Overview," Shock and Vibration Bull., 43 (Part 3) (1973).

2. W.H. Keller, J.R. Donahue, and E. Yoshida, "Orbital Workshop Vibroacoustic Test Program," Shock and Vibration Bull., 43 (Part 3)(1973).

3. P. Rader, "Skylab Payload Assembly - Vibroacoustic Test Program," Shock and Vibration Bull., 43 (Part 3) (1973).

4. R.A. Salyer, E.J. Jung, S.L. Huggins, and B.L. Stephens, "Development of an Automatic Modal Tuning and Analysis System for Performing Skylab Modal Surveys," Shock and Vibration Bull., 43 (Part 3),(1973).

5. R.A. Colonna, D.E. Newbrough, and J.R.West, Jr.,"Vibration and Acoustic Tests of the Reconfigured Apollo Service Module Adapted for Skylab Missions," Shock and Vibration Bull, 43 (Part 3) (1973).

6. J.J. Nichols, R.E. Hull, and B. Bejmuk, "Skylab Modal Survey Testing," Shock and Vibration Bull., 43 (Part 3)(1973).

DISCUSSION

Mr. Arthur (Aerojet Propulsion Co.): On your acoustic testing program, how do you determine the modal density of that acoustic chamber?

Mr. Dorland (NASA Manned Spacecraft Ctr.): The plot that you saw was of analytical results calculated for a rectangular room. We attempted to get an experimental verification of that but we never could because the modes in practice always tended to be smeared out and less distinct than shown here. This is a more rigorous measure of the success,or lack of it, of being able to meet the criteria.

Mr. Schell (Shock and Vibration Information Center): You showed by your control accelerometers that you didn't allow overtesting at certain points. It occurs to me that there might be other points on the structures which should be getting a much higher input during the test. Wouldn't this therefore result in an undertest at certain other points?

Mr. Dorland: This was a source of endless hours of debate on philosophy and rationale. The upshot of it was that we felt that we had to control on the weakest condition or on the item that was most resonant. We also had a criteria that the test level had to maintain a certain minimum value, which it always did. We never had to face the issue what as to would have happened if it hadn't.

ORBITAL WORKSHOP VIBROACOUSTIC TEST PROGRAM

W. H. Keller and E. Yoshida
McDonnell Douglas Astronautics Company
McDonnell Douglas Corporation
Huntington Beach, California

Acoustic and low frequency sinusoidal vibration tests were performed on the Orbital Workshop Dynamic Test Article, a full-scale, high fidelity flight article simulation, weighing approximately 80,000 pounds. The test control techniques, results, and use of data to verify component qualification test criteria and analytical models are described.

INTRODUCTION

Acoustic and low frequency sinusoidal vibration tests were performed on the Orbital Workshop Dynamic Test Article, a full-scale, high fidelity flight article simulation weighing approximately 80,000 lb. Testing of the Dynamic Test Article (DTA) was conducted in two phases. In the first phase, acoustic tests were conducted in which the maximum sound pressures and resulting random vibration responses were produced to simulate environment of the Orbital Workshop (OWS) during liftoff and boost. In the second phase, low frequency sinusoidal vibration tests were conducted to obtain modal response data and to produce the maximum transient response to simulate environment of the OWS during launch, engine cutoff, and stage separation. A two-volume report [1] covers each test phase.

TEST OBJECTIVES AND TEST SPECIMEN

The objectives of the DTA test program were to:

A. Verify acoustically induced vibration design and test criteria previously selected for components and subsystems

B. Demonstrate structural integrity of bracketry and secondary structure exposed to launch acoustic and vibration environments and transient loads during staging

C. Verify analytical models used for dynamic load analyses

The DTA was a full-scale, high fidelity simulation of the OWS flight stage structure, which is shown in Fig. 1. The DTA was assembled from previously built tankage and skirt sections. The tankage came from the Facilities Checkout Vehicle. The forward and aft skirts had been used on the Saturn S-IVB/V High Force Vibration Test Program.

Secondary structure and brackets were of a configuration to provide proper stiffness, strength, and geometry to the flight hardware. All components mounted on brackets, panels, basic structure, and isolators were mass simulated. Weights of the mass simulations were defined by the existing weight mathematical model for the OWS [2]. Fig. 2 and 3 show some typical component simulations. In Table 1 are presented baseline mass simulation requirements for components. These values provided initial guidelines and values and were subject to negotiation on an individual component basis if significant cost or schedule impacts became apparent. The mass of plumbing and wiring was integrated and added to the associated equipment mass substitutes except for lines greater than 2-in. in diameter or wire runs greater than 1-in. in diameter in which stiffness and/or mass might significantly affect dynamic response. In such cases, production line attachments and terminals were installed.

Some of the major components which were simulated are as follows:

Item	Weight (lb)	Remarks
Solar Array	2,160 (each)	Simulated mass, center of gravity, and stiffness
Radiator	436	Simulated mass and center of gravity
Film Vault	2,993	Simulated mass and center of gravity
Water Container	909	Filled with tap water
Power Distribution Display Console	741	Simulated mass and stiffness
Thruster Attitude Control System Sphere	150 (each)	Simulated mass and center of gravity

ACOUSTIC TEST

Acoustic testing was conducted at the Manned Spacecraft Center in Houston, Texas during February 1971. The volume of the 60- by 70- by 105-ft reverberant acoustic test chamber (the Spacecraft Acoustic Laboratory) had to be reduced to attain the sound pressure levels specified for the DTA. To accomplish this, a prestressed concrete chamber was fabricated inside the original facility. The new chamber size was 46- by 49- by 75-ft (Fig. 4). To permit achievement of the required DTA spectrums in the new acoustic test chamber, special acoustic horns were designed, built, and installed. WAS-300 and EPT-200 air modulators were coupled to the horns.

The test specimen included a mass simulated IBM Instrument Unit, the Dynamic Test Article, and a Saturn

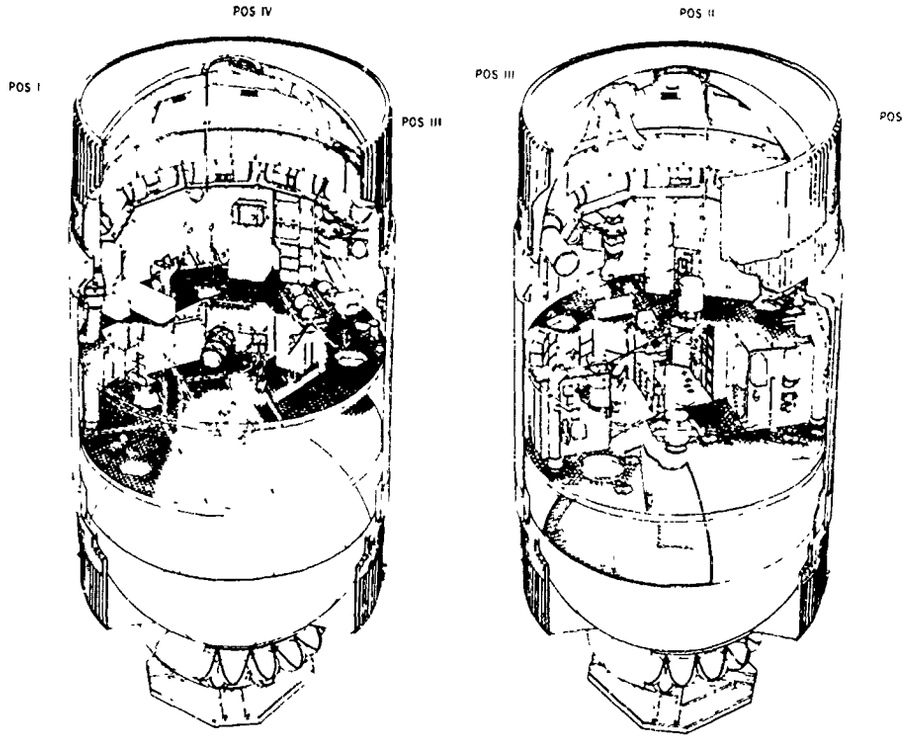

Figure 1 Cutaway View of the Orbital Workshop

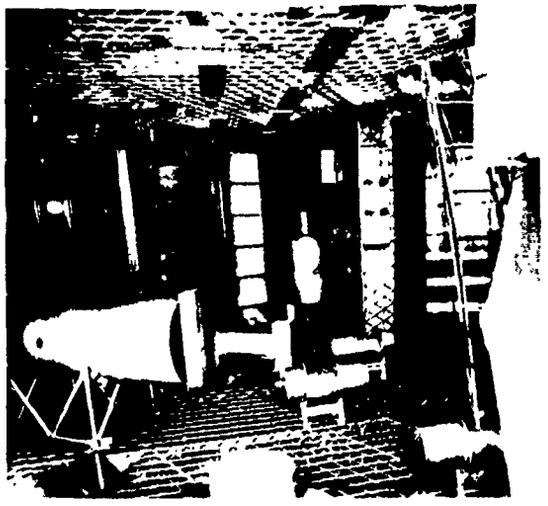

Figure 2 Dynamic Test Article Crew Quarters Simulation

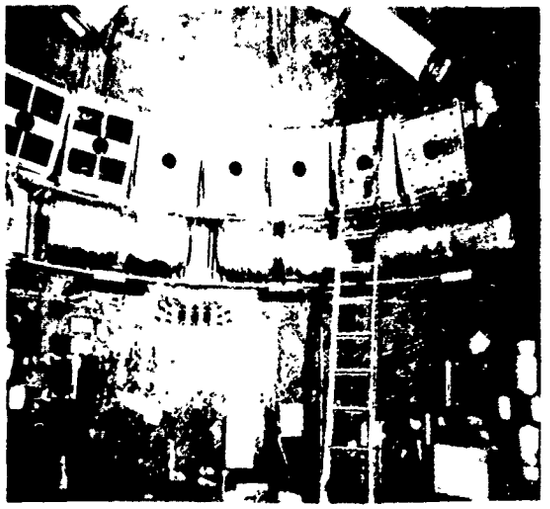

Figure 3 Dynamic Test Article Forward Compartment Simulation

Table I

DYNAMIC TEST ARTICLE MASS SIMULATION REQUIREMENTS AND TOLERANCES

Component Category	Simulation Parameter			
	Weight	CG (Reference Component)	Moment of Inertia (Reference Installation)	Moment of Inertia (Reference Component)
Individual items mounted on display or equipment panels				
For items weighing less than 1 lb*	(total) ±10%	N/A	N/A	N/A
For items weighing 1.0 to 10.0 lb	(individual) ±0.5-lb	N/A	N/A	N/A
For items weighing more than 10 lb	±10%	±5% of component dimension or ±0.25-in., whichever is greater	±10%	N/A
Assemblies and components on brackets, basic structure, or isolators				
For items weighing less than 20 lb	±10% or 0.5-lb, whichever is greater	N/A	N/A	N/A
For items weighing between 20 lb and 100 lb	±10%	±5% of component dimension or ±0.25-in., whichever is greater	N/A	N/A
For items weighing more than 100 lb	±5%	Same as above	±10%	±10%

**For equipment panels, tolerance on total weight on panel not to exceed ±0.5 lb or ±10%, whichever is greater*
Items weighing less than 1 lb should be integrated in the basic panel simulation with the total weight within the tolerance noted

S-IVB/V aft interstage structure (Fig. 5). The habitation and waste tanks were pressurized at 8 ± 0.5 psid throughout the acoustic tests. Acoustic closeouts which provided at least a 15 dB overall noise reduction were installed forward of the Instrument Unit and aft of the aft interstage. The forward closeout was made of 1/4-in. steel plates and the aft was made of wooden sheets spaced approximately 6 in. apart and filled with sand. Rubber tires were utilized to isolate the test specimen from the chamber floor. The acoustic test specimen was instrumented with 200 accelerometers, 19 dynamic strain gages, and 18 microphones. An additional 10 microphones were located in the reverberant chamber.

The intent of the acoustic tests was to simulate the maximum sound pressure levels expected during liftoff and boost. The maximum expected levels are represented by the OWS acoustic qualification test criteria, which are based on measured Saturn V data [3-6] with a factor of safety added (Fig. 6). However, structural vibration can be more efficiently induced in a reverberant acoustic chamber than in a free field or flight situation [7]. It was therefore necessary to determine the degree of this efficiency for the DTA chamber and to adjust test criteria accordingly. The following procedure was used.

Nine vibration and two acoustic measurements were made on the DTA which were identical in installation to past Saturn flight measurements, and which, in structural areas where the least amount of difference between flight and DTA dynamic response was expected. These measurements were on the forward and aft skirts. The ratio of vibration level to acoustic level in each 1/3 octave band was calculated from flight data. For the same measurement location on the DTA, the vibration/acoustic level ratio was determined from DTA test data taken during a low-level acoustic run. The degree of test chamber efficiency was determined by subtracting the DTA vibration/acoustic ratios from the flight data ratios. The acoustic qualification test level was then lowered by this difference.

The following equation was used to calculate the vibration/acoustic ratios or transfer functions (TF) in dB for one-third octave bandwidths.

$$TF = 20 \text{ Log } \frac{g/gref}{P/Pref}$$

$$= 20 \text{ Log } (g/gref) \quad 20 \text{ Log } (P/Pref)$$

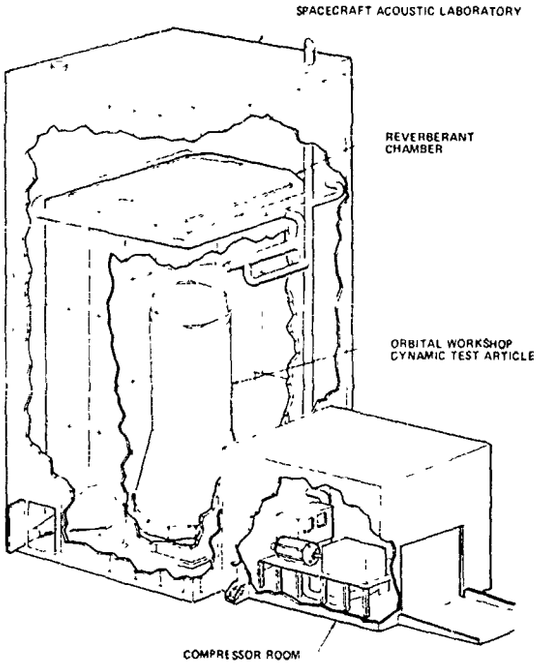

Figure 4 Spacecraft Acoustic Laboratory

where

g = vibration amplitude, rms

g ref = 1 0 g rms

20 Log (P/Pref) = Sound pressure level (SPL) in dB (re 2 x 10^{-5} N/m^2)

therefore

TF = 20 Log (g) - SPL

A comparison of typical flight and DTA transfer functions is shown in Fig 7. The test chamber efficiency factor was defined as the difference between the DTA and flight transfer functions Only three of the nine flight measurements were ultimately used in comparing transfer functions to determine the average efficiency factor Selection of the three measurements was based on directional sensitivity of instrumentation to the acoustic environment and a minimum amount of scatter in the data. The plotted points on Fig 8 are the average delta decibel (dB) difference between DTA and flight transfer functions, using the three noted measurements The smoothed curves on these plots define the final efficiency factors used to correct the qualification level acoustic specification for the tests

The efficiency factors were applied to the OWS acoustic criteria to obtain the adjusted DTA test levels shown in Fig 9 The outputs of nine microphones located on the surface of the test specimen were averaged and used to control the adjusted test

Figure 5. Dynamic Test Article Acoustic Test Specimen

levels The acoustic control system utilized a digital computer operated in an automatic closed loop mode to fully control the test levels to within plus or minus 2 dB In the automatic closed loop mode, the computer would first sample the 1/3 octave band levels from two microphones, which were determined to be stable and generally representative of all the microphones If necessary, the outputs of the appropriate noise generators were automatically varied until the average of the two microphones reached the preset dB level (for example, −9 dB below the final levels) At this point the computer would sample all nine microphones and modify the outputs of the appropriate noise generators until the average of all nine microphones were within ±2 dB of the specified level The final acoustic test spectra are also shown in Fig. 9.

Durations of the full power liftoff level and boost level tests were 1-min. and 2-min , respectively The DTA was inspected after the completion of each full level test run There were no

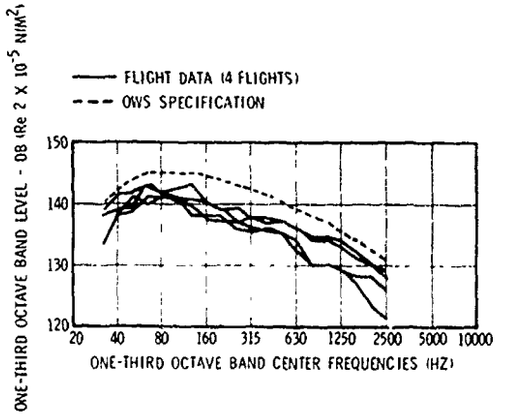

Figure 6. Typical OWS Acoustic Test Specification Versus Flight Data

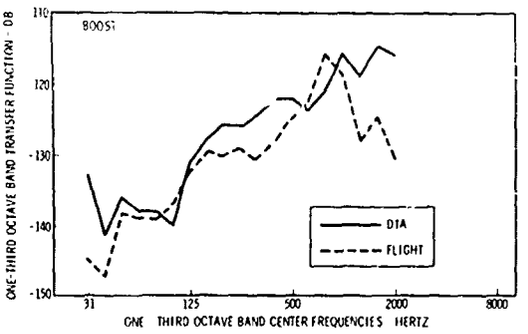

Figure 7. Typical Comparison of DTA and Flight Transfer Functions

structural failures during the acoustic tests Several minor anomalies were encountered which were primarily attributed to differences between the actual flight hardware and the simulated hardware used in the DTA. Examples of anomalies were

Description	Disposition
Seven mass simulators became loose	Production drawings specify use of self-locking bolts
Mounting bolts of four units backed off from torque alignment markers	Production drawings specify use of proper torquing techniques and proper self-locking fasteners

The DTA vibration data were reduced to acceleration spectral density plots and were evaluated by a joint McDonnell Douglas and Marshall Space Flight Center review team to determine adequacy of the existing OWS vibration specifications Where significant differences were found between the data and the original criteria [8], the criteria were revised [9] The criteria were raised in 6 (11 percent) of the environmental subzones and unchanged in 14 (27 percent) of the subzones In 33 (62 percent)

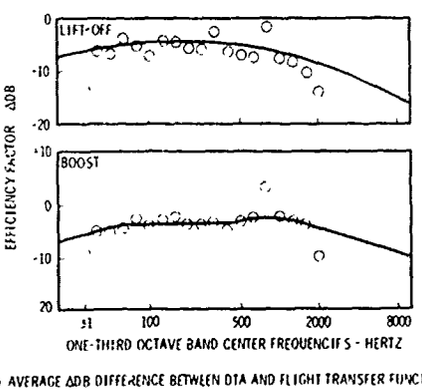

Figure 8 Dynamic Test Article Acoustic Test Chamber Efficiency Factor

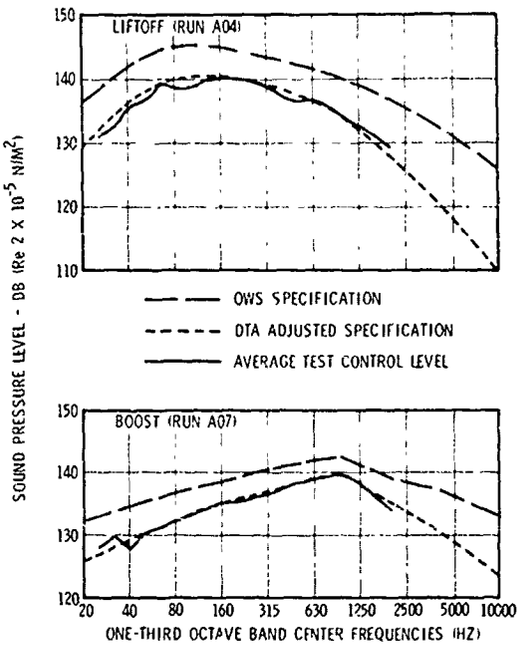

Figure 9 Comparison of OWS Specification, DTA Adjusted Specification and Computer Average Test Control Level

of the subzones, the criteria were lowered, resulting primarily from lowering the "in-plane" criteria for all shell structure subzones These criteria had previously been conservatively defined to be 3 dB below the test levels in a direction normal to the shell surface; DTA data allowed a greater reduction. Twenty new subzones resulted directly from DTA data Many of these were generated to define vibration test levels for specific components, rather than use the more general subzone specification. The DTA mass simulations of these components were specifically instrumented for this purpose. The habitation tank internal acoustic criteria were lowered by applying calculated DTA noise reductions to the external acoustic specification These changes in test criteria were made before qualification tests were performed with the exception of the habitation tank sealing device; however, no requalification of this sealing device was required because a functional sealing device was tested in position on the DTA and this device passed special post-DTA leakage tests Fig 10 shows a typical comparison of the DTA data with the OWS criteria.

LOW FREQUENCY VIBRATION TEST

Vibration testing was conducted at the Manned Spacecraft Center in the Spacecraft Vibration Laboratory The excitation system consisted of Ling Model 310 vibration thrusters, each with a force rating of 10,000 lb. Eight thrusters were used in the longitudinal axis as shown in Fig. 11. In the lateral axis tests, six thrusters (3 aft and 3 forward) were utilized as shown in Fig 12 and 13. The thruster armatures were connected in series and provided essentially in-phase excitation at each drive point The thrusters were used in conjunction with ring fixtures and an

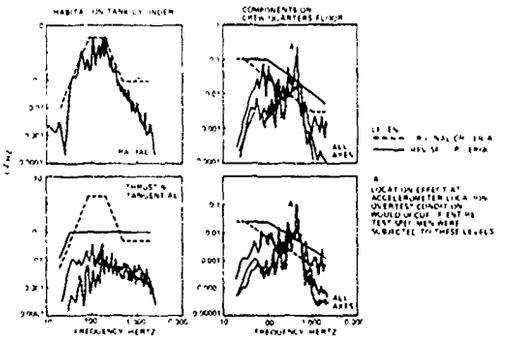

Figure 10. Dynamic Test Article Typical Data Versus Component Criteria

air-bag suspension system Major changes in test configuration of the low frequency vibration from the acoustic test were

A. The aft interstage and simulated Instrument Unit were not installed

B The DTA was not pressurized

C. 150 low frequency servo accelerometers were added

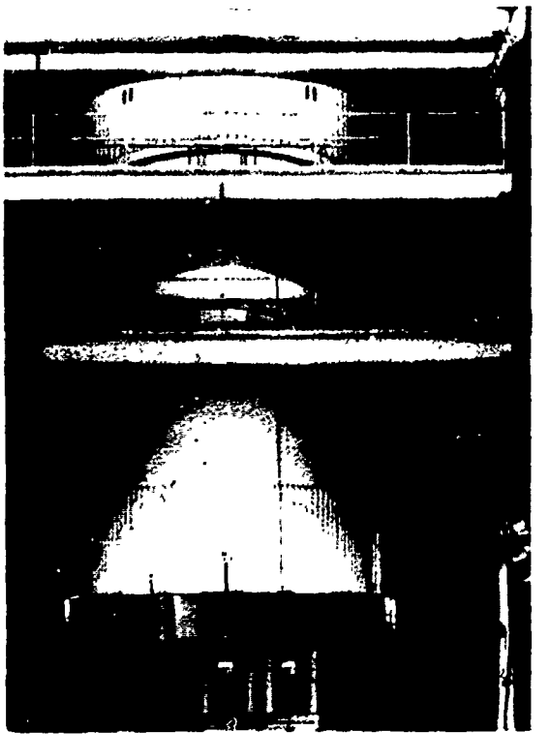

Figure 11. Dynamic Test Article Longitudinal Axis Vibration Test

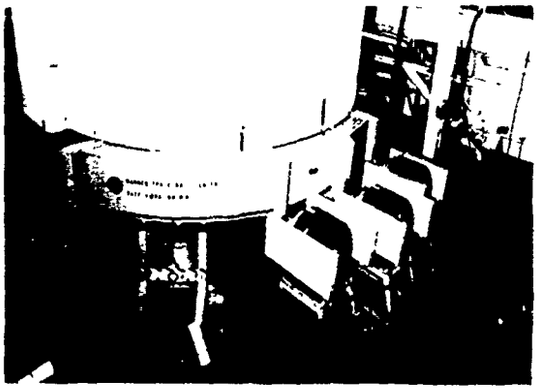

Figure 12. Dynamic Test Article Lateral Axis Vibration Test (Aft Section)

D 75 high frequency piezoelectric accelerometers were deleted

The OWS low frequency vibration specifications are based on the maximum expected vibration levels predicted for the OWS prime structure during flight transients such as launch, engine cutoff, and stage separation Response of the entire flight vehicle to these transients is at discrete frequencies, as is shown by the "line spectra" presented in Fig 14 [10] It was recognized that the sinusoidal sweep test could produce much higher dynamic response levels in the major subassemblies than those levels that would be induced by actual flight transient phenomena Therefore, a constraint put on the test was that when the response of a major subassembly reached calculated design dynamic load, the vibration test level was to be limited This response limiting was accomplished automatically with the computerized control system

Measurements on the DTA were made with 269 vibration and 19 strain transducers. Up to 8 accelerometers mounted on the OWS prime structure were used for test level control A maximum of 18 vibration measurements were used in the

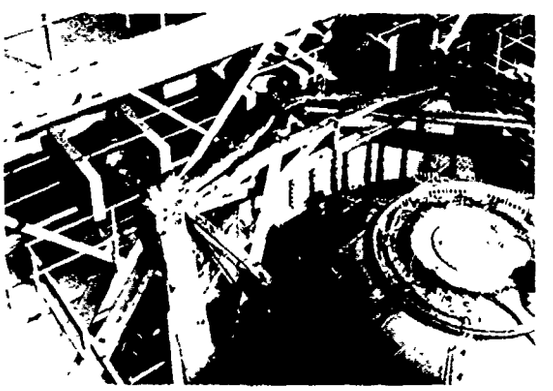

Figure 13 Dynamic Test Article Lateral Axis Vibration Test (Forward Section)

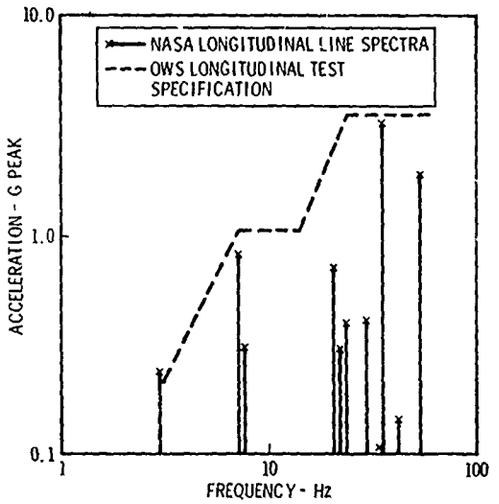

Figure 14. Predicted Longitudinal Axis Line Spectra Versus OWS Test Specification

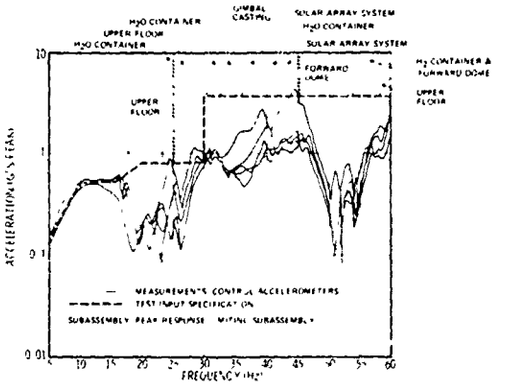

Figure 15. Dynamic Test Article Longitudinal Vibration Test Control Parameters

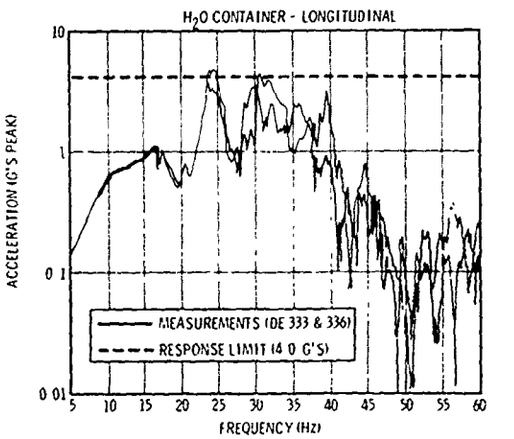

Figure 16 Dynamic Test Article Vibration Response of Peak Limiting Subassembly

acceleration peak limiting control system and six were used in the out-of-plane acceleration automatic abort system. Test control measurements were also monitored in real time on oscillographs with red line requirements to be used as a manual test abort.

The vibration tests were conducted in several steps prior to the qualification test runs These steps included low level runs to verify phase and instrumentation, to identify resonant frequencies and amplification factors, to obtain mode shape information for major subsystems, and to check out the automatic control and abort systems Several deviations were made to the original requirements primarily due to limitation in the testing equipment. The sweep rate was reduced from 3 to 0 9 octaves/min the sweep was conducted in small incremental "step dwells," the lowest frequency was changed from 3 to 5 Hz in the longitudinal axis and from 2 to 4 Hz in the lateral axis, and the levels below 30 Hz were reduced for the longitudinal axis

The major test axis was the longitudinal direction (the only major component that responded to the lateral axis specification [4 to 20 Hz] was the solar array wing assembly) The longitudinal test control plot is shown in Fig 15 The notches in the data represent the frequency at which the limiting response of the subassembly has been reached A typical response limited plot is shown in Fig 16 Inspections revealed no structural failure or degradation, one test anomaly occurred which was attributed to the configuration of one of the flight hardware simulations that was used. Specifically, 6 out of 23 TACS sphere straps loosened because the spheres, which were simulated with hard plastic, were slightly out of round and had no bosses to prevent rotation.

The data were used to verify major OWS structural subsystem dynamic models There was generally good agreement with modes and frequencies of analytical models used for dynamic load analyses A minor correction to the stiffness model for the crew quarters floor assembly was made as a result of the DTA data In Table 2, response of major subassemblies with design criteria is compared and in Tables 3 and 4 predicted and measured resonant frequencies of selected major subassemblies are compared

CONCLUSIONS

Overall conclusions

A Sufficient data were obtained to either verify the dynamic design and test criteria for OWS components and subassemblies or to revise them as necessary

B The structural integrity of primary and secondary structure was verified with regard to structural capacity for withstanding simulated maximum expected acoustic and acoustically induced random vibration environments and the integrity of the major subsystems was verified with regard to capacity for withstanding launch and staging transients

C The low frequency dynamic responses of the DTA verified the adequacy of the analytical dynamic models

Table 2

COMPARISON OF OWS DESIGN CRITERIA AND DTA RESPONSE DATA IN LONGITUDINAL AXIS

Major Subassembly	Load Factor	
	Design Criteria Compensated for 1g Effect	DTA Response at Fundamental Frequency
Upper Floor Assembly	±3.1g	±3.3g
Lower Floor Assembly	±3.1g	±1.9g
Water Container Assembly	±4.0g	±4.0g
Thruster Attitude Control System Sphere Assembly	±9.0g	±5.0g
Solar Array Fairing	±3.0g	±3.0g
Water Ring Stowage Container Assembly	±4.0g	±4.0g

Table 3

COMPARISON OF PREDICTED AND MEASURED RESONANT FREQUENCIES OF THE CREW QUARTERS FLOORS

Mode No.	Predicted Frequency Hz	Measured Frequency Hz	Percent Difference
1	10.07	11 31	12
2	13.65	18.83	38
3	16.52	20.71	25
4	17.49	31.45	23
5	20.28	26.23	29
6	20 40	*	– –
7	21.06	28.27	34

**Not identified from DTA/OWS test data.*

used to calculate dynamic loads for the OWS during launch, boost, and staging events.

Conclusions regarding test techniques:

A. The schedule for this test was optimum because the test was late enough in the OWS program to permit the structural configuration to be established and early enough to precede component qualification

B. Reverberation chamber efficiency factor was significant and must be considered.

Table 4

COMPARISON OF PREDICTED AND MEASURED RESONANT FREQUENCIES OF WATER CONTAINERS AND STOWAGE CABINETS

Mode No	Predicted Frequency Hz	Measured Frequency Hz	Percent Difference
1	12 6	12 5	–0 80
2	13 1	13 0	–0 77
7	17 7	17.0	–4 1
8	18 4	19 5	+5 65
19	24 4	24.5	+0 49
22	28 6	28 0	–2 15
26	33 1	30 5	–8 25
29	34.3	38 0	+9 72
31	38 1	38 0	–0 26
33	40 9	40 0	–2 25
39	47.2	46 0	-2.61
– –	– –	54 0	– –

C Peak limiting accelerometers maintained satisfactory control of the vibration test specimen

REFERENCES

1. "Orbital Workshop Dynamic Test Article Vibro-Acoustic Test Report", Volume I (Acoustic Test), and Volume II (Low Frequency Vibration Test), McDonnell Douglas Astronautics Company Report MDC G2445, October 1971.

2. "Skylab A Dynamic Test Article Mass Properties Report, Model No DSV7-DTA", McDonnell Douglas Astronautics Company Report MDC G0869, December 1970

3 "Saturn S-IVB-501 Stage Flight Evaluation Report," Volume II, Douglas Report SM-47004, April 1968.

4. "Saturn S-IVB-502 Stage Flight Evaluation Report," Douglas Report SM-47005, July 1968.

5. "Saturn S-IVB-503N Stage Flight Evaluation Report," Douglas Report SM-47006, March 1969

6 "Saturn S-IVB-505N Stage Flight Evaluation Report," McDonnell Douglas Astronautics Company Report MDC G0008, August 1969.

7. V Mason, "Investigation of the Possible Structural Over-Test Due to the Qualification of Spacecraft Structures in a Reverberant Room," Wyle Laboratories Report WR 71-1, January 1971

8. "Orbital Workshop Acoustic, Shock, and Vibration Test Criteria," McDonnell Douglas Astronautics Company Report DAC 56620B, April 1970

9 "Orbital Workshop Acoustic, Shock, and Vibration Test Criteria," McDonnell Douglas Astronautics Company Report DAC 56620C, May 1971

10 "Saturn V Dry Workshop Vehicle Composite and Modal Accelerations," NASA Memorandum S&E-ASTN-ADL-70-14, February 1970

DISCUSSION

Mr. Kertesz (Lockheed Missiles & Space Co.): How did you establish the flight transfer functions?

Mr. Keller: The flight transfer functions were determined by using flight vibration data measured on the structure and ratioing that to acoustic levels measured at the same structure. This was done by ratioing data in third octive bandwidths.

Mr. Kertesz: You hadn't flown this structure when you ran the test?

Mr. Keller: We flew a Saturn V vehicle with a Saturn S IV B stage on it. If you look at the configuration of the workshop, it looks essentially the same. We know that inside the workshop we are filled with equipment rather than fuel, but in the structural areas of the skirts the similarities are expected to be good.

Mr. Kertesz: You measure the dynamic load at 17 or 18 locations and clip the input. Originally, the input was described as some kind of excitation coming from the Saturn which was given, but then you modified that excitation presumably not to exceed certain precomputed peaks at a given number of locations. If you modified it in that way, why do you run the test in the first place?

Mr. Keller: The objective was to make sure that the large structure which heretofore had just been shown adequate by analysis was, in fact, adequate for the analysis load factors. Each of those large structures with the exception of the lower floor and the gas spheres at the base of the workshop did in fact reach their limit load factors. Therefore the structural analysis confirmed that they were adequate. It's interesting to note that the upper floor did reach its limit load factor and it weighs more than the lower floor. You might feel that since the analysis approach was confirmed on the upper floor, the lower floor should be adequate by comparison. The gas sphere which was not adequately tested, was tested later as a component rather than as a cluster of spheres.

Mr. Koen (Bell Laboratories): Were vibration tests run on electronic equipment? If so, what kind of vibration tests were run?

Mr. Keller: There was no electronic equipment on this dynamic test article, however we did perform component tests of hardmounted electronic equipment to specifications which were confirmed by this dynamic test article.

SKYLAB PAYLOAD ASSEMBLY VIBROACOUSTIC TEST PROGRAM

Paul Rader
Martin Marietta Corporation
Denver, Colorado

and

Jack Macpherson
Marshall Space Flight Center
Huntsville, Alabama

The acoustic and vibration tests of the Skylab payload assembly are described. Test conditions for liftoff and boundary layer acoustical environments were determined by comparing the vibroacoustic transfer functions calculated from measurements of the test article and Saturn V flight vehicles. The test results, including special additional tests necessitated by the analyses of data from initial testing, are discussed.

INTRODUCTION

The Skylab payload assembly vibroacoustic test program conducted at the Manned Spacecraft Center from September 1971 thru July 1972 was one of the most ambitious of its type ever conducted on a spacecraft. This paper describes two phases of the total program--the acoustic and vehicle dynamics tests. The objectives of the tests were to:

1) Verify the dynamic design and test criteria for components and subassemblies;

2) Verify the structural integrity of bracketry and secondary structure;

3) Qualify selected flight hardware components.

These tests formed a part of the total test program designed to insure the flightworthiness of the Skylab.

The following tests are discussed in this paper:

1) Acoustics,

   a) Liftoff environment,

   b) Boundary layer environment,

   c) Instrument unit (IU) acoustic test,*

   d) IU modal survey,*

   e) Additional IU acoustic tests,*

   f) Apollo telescope mount/control moment gyro (ATM/CMG) qualification test;

2) Vehicle dynamics.

TEST CONFIGURATION

The test article was assembled from the major structural articles shown in Figure 1. The configuration included a number of flight-type components and subassemblies for qualification or verification of response characteristics. All other components weighing more than 5 pounds were simulated by mass mock-ups installed on flight-type brackets. The payload assembly in the launch configuration was approximately 28 feet in diameter at the base, 76 feet long, and weighed approximately 129,000 pounds.

*These tests were added to the original program as a result of analysis of data from tests 1a) and b).

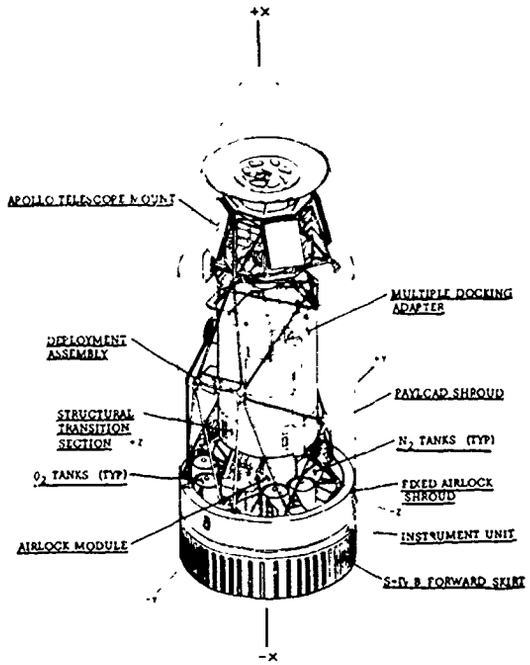

Fig. 1 - Payload assembly test article launch configuration

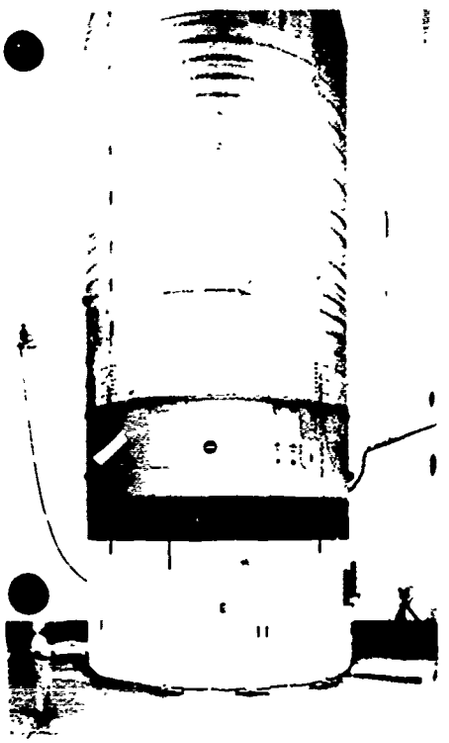

Fig. 2 - Skylab payload assembly installed in reverberation chamber

ACOUSTIC TESTS

Payload Shroud Liftoff and Boundary Layer Tests

The payload assembly was installed in the reverberation chamber at the Manned Spacecraft Center's Vibration Acoustic Test Facility as shown in the photograph in Figure 2. The article was instrumented with 43 microphones, 303 piezoelectric accelerometers, and 32 strain gages.

Liftoff and boundary layer acoustic spectra (Fig. 3) derived from Saturn V flight data were modified to account for the reverberation chamber efficiency factor to achieve the required vibration levels. The initial test environments were based on chamber efficiency factor corrections obtained during the Orbital workshop dynamic test article (DTA) tests. Since the acoustic field, and, consequently, the chamber efficiency factor depend on the test article geometry, absorption characteristics, and relative volumes of the article and test chamber, low-level (-6 dB) runs were conducted to determine vibroacoustic transfer functions with which to establish the correct acoustic environment for the payload assembly. The transfer functions were calculated for measurements corresponding to flight locations in the S-IVB forward skirt and instrument unit modules.

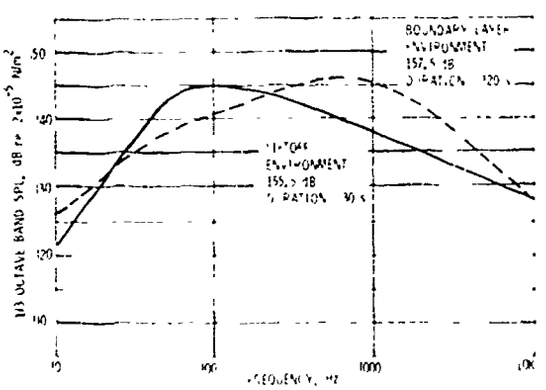

Fig. 3 - Liftoff and boundary layer spectra from Saturn V flight data

These data indicated that an additional correction should be made to the liftoff spectrum in the frequency region below 100 Hz. Comparisons of the spectra derived from flight data, initial test environments, and final test environments are presented in Figures 4 and 5 for liftoff and boundary layer conditions.

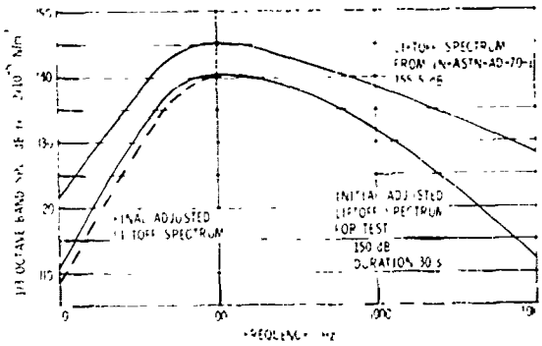

Fig. 4 - Comparison of liftoff spectra from flight data, OWS/DTA test and payload assembly test

The test environment was controlled within the specified tolerances by averaging the signals from 10 microphones distributed over the exterior surface of the test article. Spectrum equalization of the acoustic generators and the broadband sound pressure level (SPL) were controlled by a digital computer. The spatial distribution of the sound field over the surface of the vehicle was quite good, as shown by the typical example plotted in Figure 6.

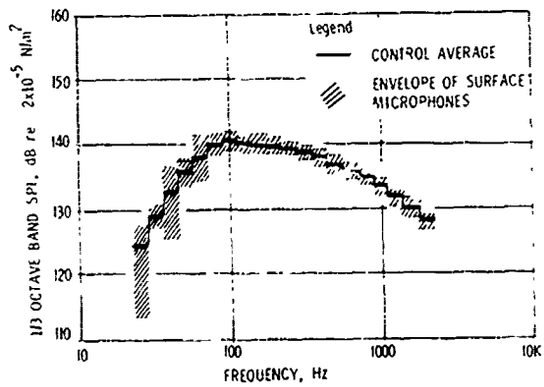

Fig. 6 - Envelope and average of control microphones

Analyses of the vibration data indicated that vibration levels exceeded the qualification test levels for components in the instrument unit and Apollo telescope mount modules. As a result, additional acoustic and vibration tests were conducted on the IU and ATM to evaluate the response characteristics related to major components in the IU and to qualify the control moment gyro in the ATM.

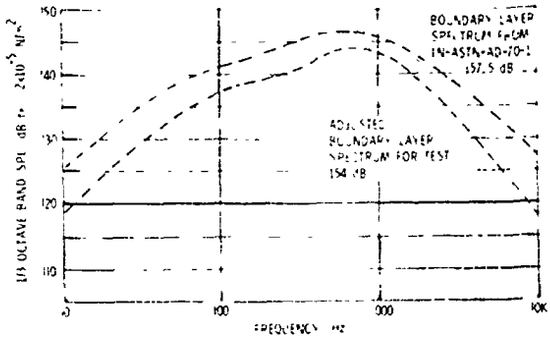

Fig. 5 - Comparison of boundary layer noise spectra from flight data and payload assembly test

Instrument Unit Tests

For the IU acoustic tests, liftoff and boundary layer spectra were derived for the IU area from Saturn V flight data, and the chamber control microphones were located on the IU circumference. Comparisons of the IU test spectra with those used for the entire payload assembly are shown in Figure 7. These tests were conducted to ensure that the exceedances observed were not a result of an overtest in the IU area because of the use of the payload shroud spectra for the payload assembly. It should be recognized that the liftoff environment for the IU resulted from a tight envelope of flight data, whereas the payload shroud (P/S) spectrum represents the 97.5% confidence level of the flight data population.

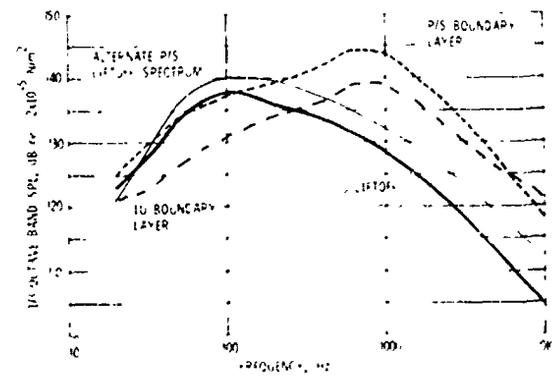

Fig. 7 - Comparison of payload shroud and IU spectra

Further diagnostic tests were conducted to investigate the IU dynamic response anomaly. These included special measurements to determine the effects of the 25-Hz horn and of chamber standing waves. In addition, modal surveys were conducted with both a flight control computer (FCC) dynamic simulator and an FCC prototype unit installed in the IU. There were significant differences in response between the FCC mockup and FCC prototype units. None of the diagnostic tests provided an explanation of the increase in vibration levels over the previous levels observed from Saturn flights. These increases were attributed to the difference in IU boundary conditions between the Skylab launch configuration and the Apollo launch configuration.

ATM/CMC Qualification Test

A special test program was conducted to qualify the ATM control moment gyro. The test environments were controlled from eight microphones internal to the payload shroud. Other instrumentation included eight external microphones and 70 piezoelectric accelerometers. The test installation is shown in Figure 8. As in the previous payload assembly tests, the maximum environment runs were preceded by low-level tests to properly range the instrumentation and provide data to derive the vibroacoustic transfer functions. These functions are necessary to adjust the acoustic environment to establish the required test article vibration responses. The basic objectives of the test were achieved in that a high-fidelity test bed for the CMG was provided, and the acoustic test conditions necessary to produce the required structural vibration response were achieved. The CMG was qualified by the test.

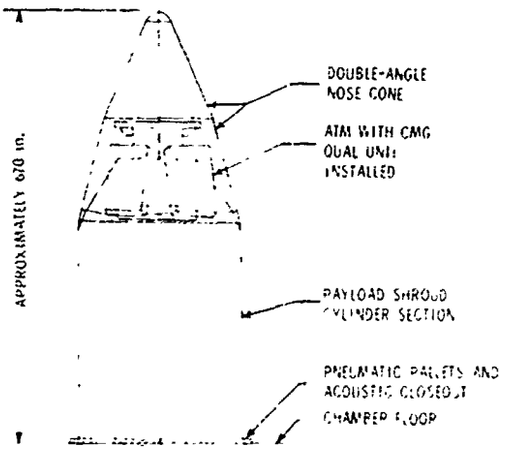

Fig. 8 - ATM CMG acoustic test configuration

VEHICLE DYNAMICS TEST

Vibration tests of the entire payload assembly were conducted to simulate the low-frequency environment resulting from the launch vehicle engine cutoff and separation transients. The test article was installed on a 12,000-pound base ring and the entire assembly was suspended on three air springs, providing a longitudinal suspension system frequency of approximately 0.7 Hz. A photograph of the test installation is shown in Figure 9. Excitation was provided by eight 10,000-pound-force electrodynamic thrusters located in pairs at the vehicle axes as shown in Figure 10. The assembly was instrumented with 232 accelerometers and eight force gages and was protected by an automatic abort system that monitored and controlled response levels at selected, critical load points.

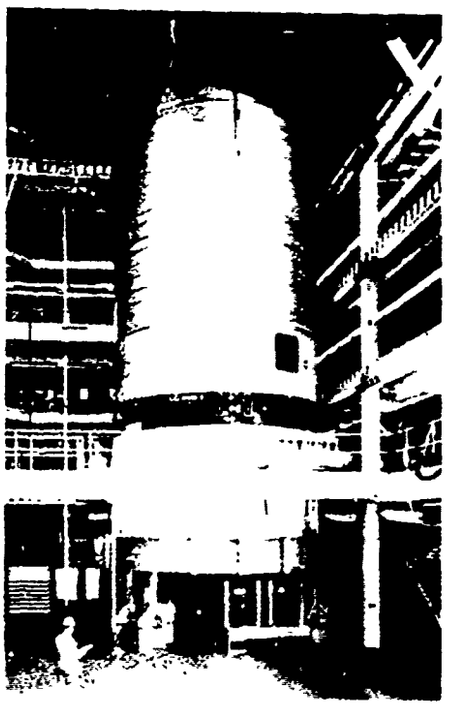

Fig. 9 - Payload assembly installed in vibration test facility

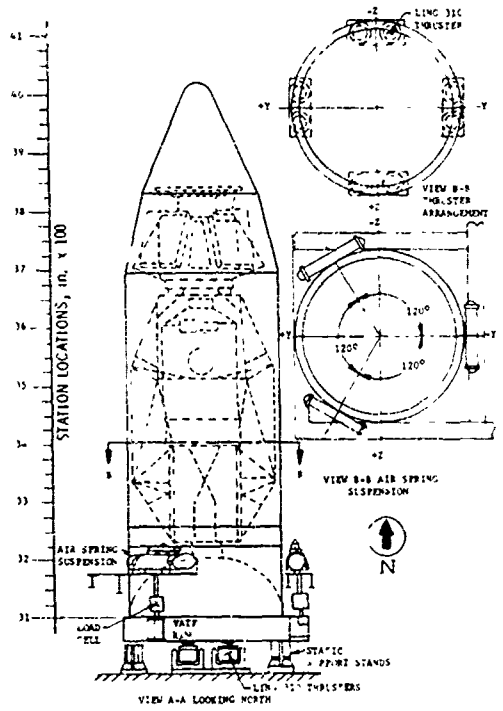

Fig. 10 - Vehicle dynamics test setup

The test sequence consisted of a 4-Hz dwell to verify instrumentation, force-controlled sinusoidal sweeps (2400 and 5600 lb at 1 octave/minute) to identify resonances and transmissibility characteristics, and vibration transients at selected frequencies to evaluate the payload assembly structure for simulated engine cutoff, separation, and ignition transients. The selection of the nine transients listed in Table 1 was based on a review of the sine sweep data and the prior mathematical analysis of the launch vehicle.

TABLE 1
Payload Assembly Vehicle Dynamics Test Transients

Frequency, Hz	Input Acceleration, g, peak	Input Force, lb
34.78	0.37	8,000
28.24	0.20	5,328
18.70	0.09	4,000
17.80	0.19	8,640
14.50	0.11	9,320
10.60	0.26	50,400
7.69	0.38	66,800
7.45	0.28	68,800
6.92	0.29	66,720
G_p	Decay equivalent to that provided by 1% of critical damping	
Note: Transients between 6.0 and 35 Hz were selected based on review of sine sweep data.		

SUMMARY OF TEST RESULTS

The acoustic and vehicle dynamics tests of the payload assembly were completed with no failures of flight-type structure, either primary or secondary. Sufficient data were acquired to evaluate component qualification test criteria. These evaluations, termed exceedance studies, were performed by the applicable hardware contractors with the following results:

1) Instrument unit - Twenty-three components were recommended for retest to increased qualification levels. As an example, a revised specification for the flight control computer is compared to the original qualification test level and the test data envelope in Figure 11;

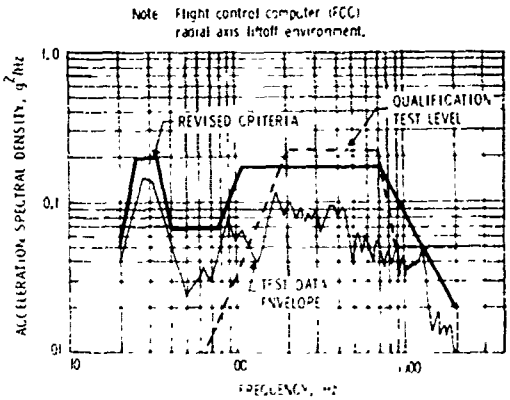

Fig. 11 - Comparison of test data and criteria for the flight control computer

2) Multiple docking adapter,

   a) Weight classifications in two environmental subzones were changed,

   b) Nine new environmental subzones were added,

   c) No component requalification was required;

3) Airlock module, payload shroud, deployment assembly, and fixed airlock shroud,

   a) Test criteria were increased in 11 environmental subzones,

   b) Three new environmental subzones were added,

   c) Special environmental criteria were established for seven components,

d) Four components were recommended for requalification tests;

4) Apollo telescope mount,

a) Test criteria were increased in two environmental subzones,

b) The control moment gyro was recommended for requalification test. Requalification was accomplished during the ATM/CMG acoustic test previously described in this paper.

CONCLUSIONS

The testing program described in this paper demonstrated the structural integrity of bracketry and secondary structure of the payload assembly for the expected flight dynamic environments. In addition, data were acquired to either verify or establish realistic test criteria for components, resulting in the requirement to requalify a number of components.

The total Skylab vibroacoustic test program, which included the tests described in this paper, the orbital workshop program, and the modal survey tests described in other papers during this session, has served to develop a high degree of confidence in the flightworthiness of the Skylab vehicle.

DEVELOPMENT OF AN AUTOMATIC MODAL TUNING AND ANALYSIS SYSTEM FOR PERFORMING SKYLAB MODAL SURVEYS

Robert A. Salyer
TRW Systems
Redondo Beach, California

Ed J. Jung, Jr.
NASA-Manned Spacecraft Center
Houston, Texas

and

Stacy L. Huggins and Barry L. Stephens
Northrop Services, Inc.
Houston, Texas

A digitally based automatic modal tuning and analysis system was developed to provide an operational capability beginning at 0.1 Hz. The system provides unique control features, maximum operator visibility, and complete data reduction and documentation within minutes after data acquisition is complete. The automatic modal tuning and analysis techniques were proven during the successful application of the system to a modal survey of the Skylab payload.

The elements of the system are briefly described and the operational flow is discussed to illustrate the full range of capabilities and the flexibility of application.

INTRODUCTION

The automatic modal tuning and analysis system (AMTAS) was developed to perform a modal survey of the Skylab payload which weighs approximately 120,000 pounds and is approximately 76 feet high. The complexity of the task required an automatic control and data analysis system to provide positive excitation control and broad real-time data bandpass beginning at virtually zero Hertz.

The purpose of this paper is to present a general overview of the hardware and software components of the system and a functional description of the system capabilities.

SYSTEM DESCRIPTION

General Features

Digital techniques are utilized to provide a low frequency operating bound of virtually zero Hertz without compromise of capability. Positive excitation control is achieved through force feedback digital control of the forcing function. The narrowband filtering and co-quad analysis capabilities are extended to essentially zero Hertz through software for digital filtering and data reduction.

Six elements constitute the automatic modal tuning and analysis system: 1) computer; 2) excitation control subsystem; 3) data acquisition subsystem; 4) excitation subsystem; 5) monitoring subsystem; and 6) software support package. The conceptual layout of the system is shown in Figure 1.

System Director

A general purpose computer with 32K of core memory is used to direct the system. The computer supports the following peripherals: card reader, card punch, line printer, disk drive, tape deck, console typewriter, input signal selectors, A/D converter and multiplexer, alphanumeric CRT with keyboard, alphanumeric-graphic CRT with keyboard, force and acceleration detector, and digital plotters.

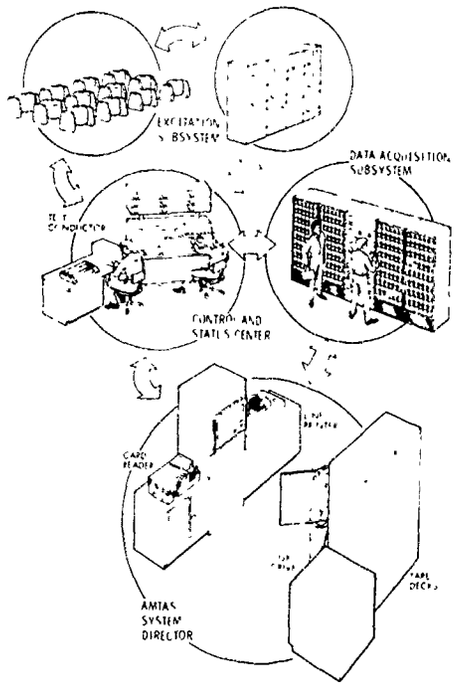

Figure 1.

Conceptual Layout

The computer operates under a group of programs (supplied by the manufacturer) for generating, organizing, testing, and executing programs for real-time data acquisition and control. The major components of this software include a machine language assembler, FORTRAN compiler, loader, disk utility program, supervisor, and real-time system director.

The system director controls the real-time data acquisition and control programs. It consists of time-sharing control, program sequence control, master interrupt control, interval timer control, and error alert control. A subroutine library consists of input-output conversion, arithmetic, functional, and selective dump, debug, and miscellaneous programs. In addition, three other categories of software are required for the system: I/O handlers for nonstandard peripherals; application programs (real-time and off-line); and test and validation routines. These three groups of software, referred to as the software support package, were written specifically for the AMTAS application.

Software Support Package

The software support package provides process control, data acquisition, data reduction, and modal documentation.

The control, data acquisition, and excitation subsystems are interconnected with the computer through the peripherals (see Figure 9). Man-computer interactive control of system functions is provided by the keyboard display units at the control console. Real time data reduction, modal purity, and data validity assessment results are displayed on the alphanumeric CRT display. Quick-look graphic documentation is presented on the graphic CRT hardcopy unit and digital plotter.

Five process control functions are provided by the software support package: sweep direction and linear rate, response channel selection, phase-lock control, force distribution control, and limiting of critical accelerations. Data acquisition is inhibited when any servo correction (force level or frequency) is in progress.

Bookkeeping data, force data, and engineering unit response data are acquired and stored in the computer for subsequent listing and reduction.

Data reduction under control of the software package includes binary to decimal conversion, voltage to engineering unit conversion, co and quad component resolution, geometric transformation, generalized mass computation, normalization of generalized coordinate data, and auto- and cross-orthogonality checks.

The modal documentation operations by the software support package are real-time CRT displays of process control parameters and engineering unit data; real-time line printer listings of raw voltages, engineering unit data, and generalized coordinate data; off-line listings of auto-and cross-orthogonality results; punched cards for raw data and normal mode data; and near-real-time quick-look and permanent records consisting of a set of 15 stick plots.

The process control sequence during modal sweeps is shown in Figure 2. The sweep parameters and reference accelerometer are selected by keyboard entry. Frequency incrementing is initiated by command. The individual force distribution and limit accelerations are checked and corrected if required. Data samples are acquired and total response data from three reference accelerometers are resolved into co-quad components. The co-quad data are plotted and the frequency is incremented. This sequence is repeated until the sweep is completed.

The process control sequence during a modal dwell is shown in Figure 3. After the modal decay indicates that the desired mode has been separated from adjacent modes, the run number and mode number are entered on the CRT keyboard. All other bookkeeping and test data are acquired by the computer to completely eliminate manual recording errors. Phase lock and data acquisition are initiated by keyboard

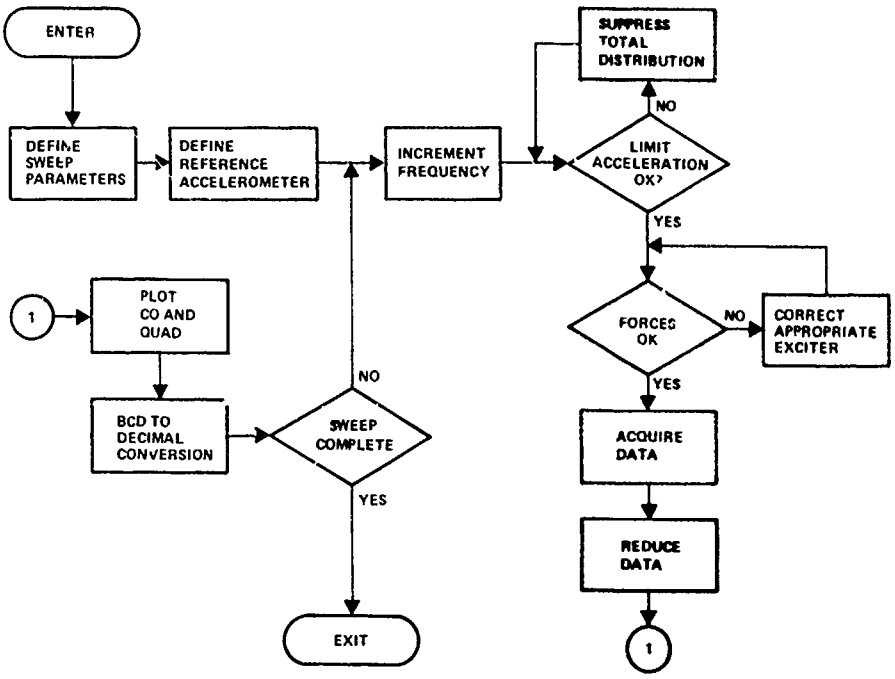

Figure 2.
Sweep Operational Flow Chart

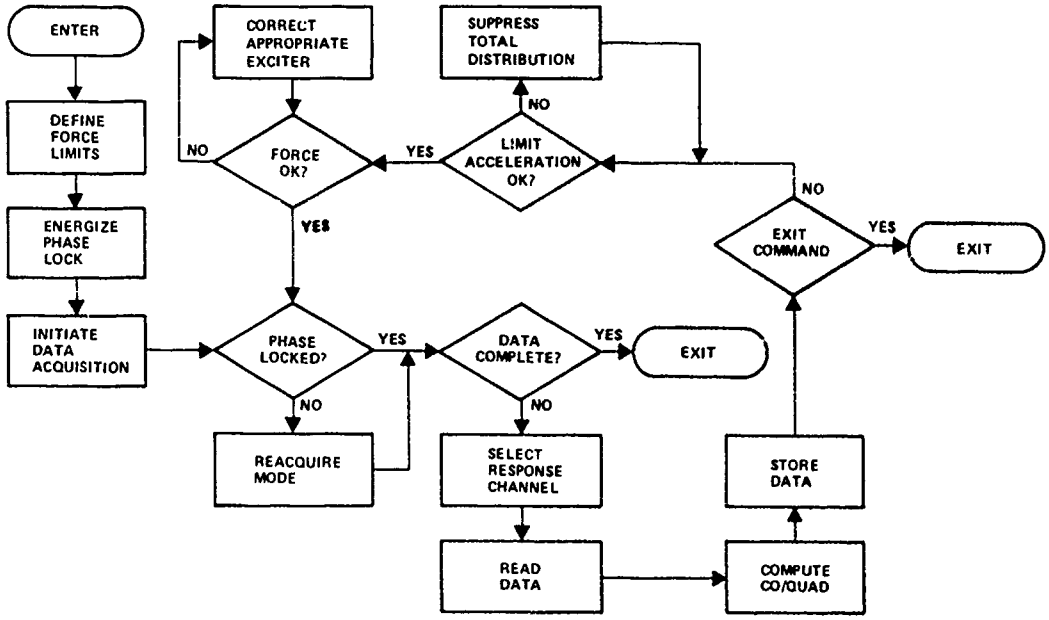

Figure 3.
Modal Dwell Operational Flow Chart

entry. The first set of three response channels are selected for co-quad analysis. When data sampling is complete, the next set of response accelerometers is selected for priority level sampling, while data reduction, documentation, and storage continue on the mainline level of software operation. If an exit command has not been entered on the keyboard, the force distribution and limit acceleration are corrected, if required. The sequence is repeated until all response data are acquired or until an exit command is received. Fourteen digital servos are active during the modal dwell: twelve individual force servos, the total energy servo, and frequency servo (phase lock).

Data Acquisition

Several data acquisition functions are common to both sweep and dwell modes of operation. Bookkeeping data (run number and mode number) are entered by manual CRT keyboard, shown at the left of Figure 9. The format is printed out on the display such that the letter X appears where data must be entered by the operator. After data entry, the send key is depressed to initiate a read by the computer. The format is updated and the input stored on disk. The run and mode numbers are used to subscript the incoming data for proper organization and storage in disk and tape files.

A view of the control console is given in Figure 4. The keyboard display units are shown on the right side of the control console. Overall views of the AMTAS are shown in Figures 5 and 6.

The force level of each active exciter is displayed on the alphanumeric CRT. Limit acceleration status is displayed at the bottom of the CRT at each force level update time.

Response data are acquired by a keyboard selected load cell and a set of three accelerometers. These transducers are fixed throughout a sweep. However, in the tuning mode, the load cell and response accelerometers may be selected or changed at any time, providing the flexibility required to examine response characteristics of the structure as the forcing distribution and frequency are varied to optimize a desired mode. In the dwell mode the reference load cell is selected by keyboard entry. The data acquisition sequence, initiated on the keyboard, consists of acquiring response data from all accelerometers (maximum of 200) in groups of three.

The software support package provides

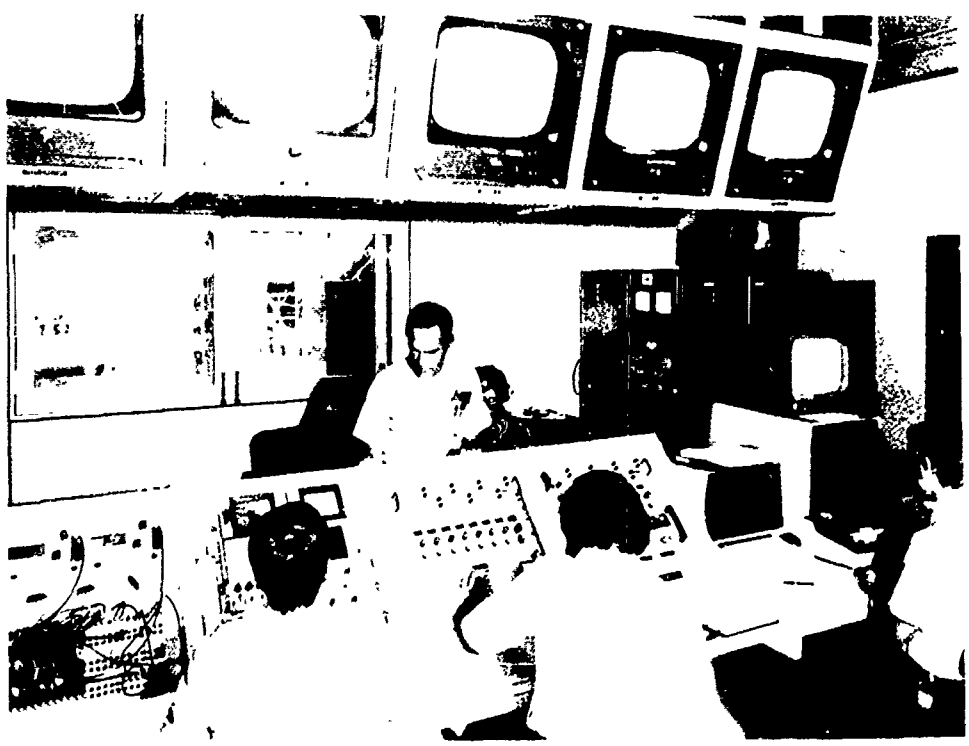

Figure 4.
AMTAS Control Console

Figure 5.
Overall View Of AMTAS

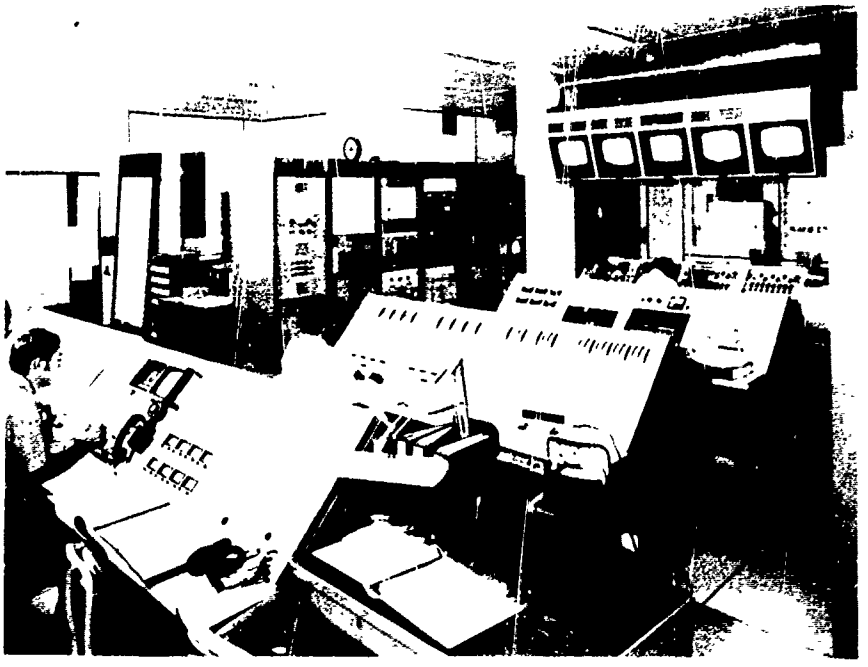

Figure 6.
Overall View Of AMTAS

maximum real time visibility and immediate post test documentation. The raw data is converted to engineering unit data, co-quad components are computed and translated from accelerometer to mass model (generalized) coordinates, and all data is stored in disk and tape files for off-line reduction (plots and orthogonality checks).

Documentation (Figure 7) consists of co-quad plots, decay curves, listing of raw voltage, engineering unit and generalized coordinate data, orthogonality matrix printout, modal plots, and a punched card deck of modal response data. This documentation is available immediately after modal acquisition is completed.

The CRT display unit presents a dynamic real-time status display. Parameters included are force levels, frequency, error and status messages. Subroutine execution is initiated by a command entered on the keyboard.

Data listing by the line printer is initiated by keyboard entry. This listing is available for single modes or total set of modes. The listing includes status and bookkeeping, raw voltage, engineering unit and generalized coordinate (normal mode) data. An additional keyboard entry will result in an orthogonality printout.

Modal deflections for a given mode can be output in the form of cards with a non-process program in an off-line time-share computer mode.

A set of stick plots (15 maximum) documents a mode in the form of node deflections versus vehicle station.

All structure dependent data exists in files that are easily maintained during model updates and revisions. The operational program, file creation program, and file input program with data modules are stored and maintained separately. For a future modal test, only the file input modules need be revised to include the structure-peculiar data; other modules are independent of structure.

The data file creation module creates the files required by the program for the program for execution, including the structure-dependent data. The structure-dependent files can be revised at any time without disturbing the other programs by replacing the data deck and reloading and executing the file input program.

Data Acquisition Subsystem

A diagram of the data acquisition subsystem is shown in Figure 8. The analog front end of the subsystem includes the following:

A strain gage signal conditioning system with patching capabilities to the test laboratory junction boxes. This system supplies power, signal amplification, calibration capability, and bridge balancing for one, two, three, and four active element strain gage bridge circuits and strain gage bridge transducers, such as load cells.

A servo accelerometer signal conditioning system with patching capabilities to the test laboratory junction boxes. This system supplies power, output signal balancing, and calibration for

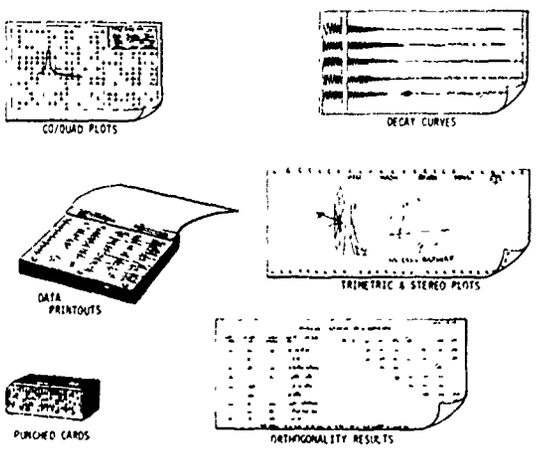

Figure 7.
AMTAS Documentation Package

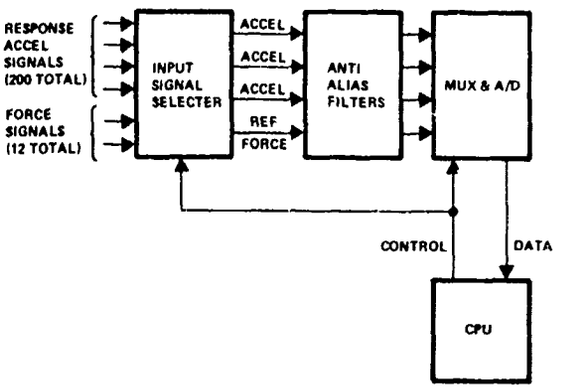

Figure 8.
Data Acquisition Subsystem

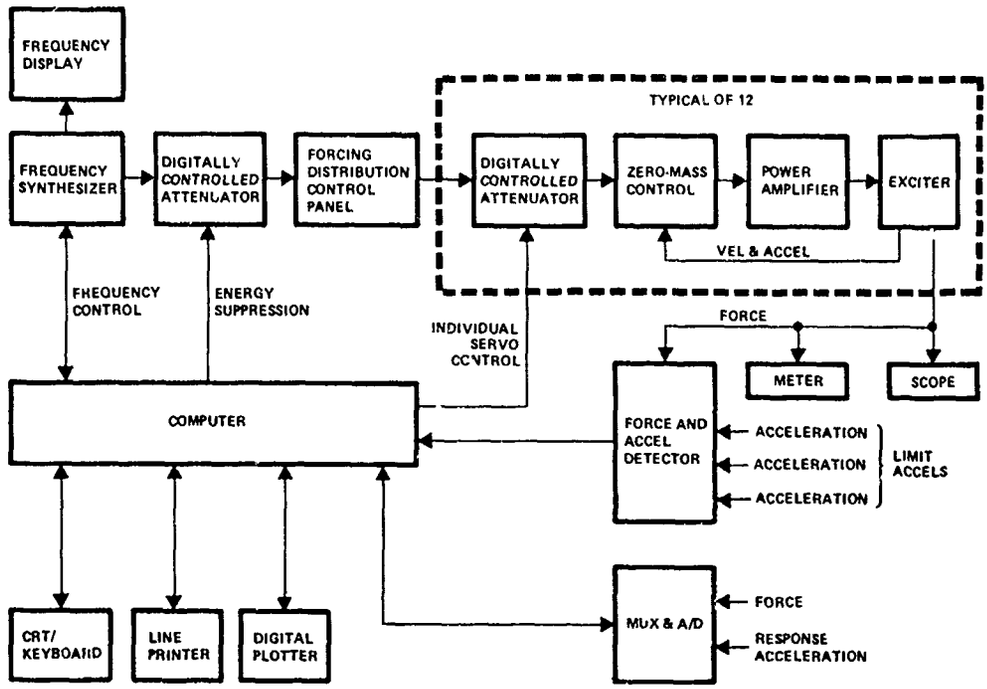

Figure 9.

Excitation Control Subsytem

sensitive servo type acceleration transducers.

The analog front end conditions the acceleration and force signals. Groups of transducers are selected automatically by the computer as inputs to the low-pass anti-aliasing filters. Digitized samples of the inputs are acquired by an A/D converter and multiplexer. Fourier analysis of these digitized data provides complex Fourier transform coefficients for the computation of co and quad values.

Excitation Control Subsystem

Digital feedback force control techniques avoid the need for constant bandwidth tracking analyzers and an analog servo unit, either of which imposes a low frequency limit on the system.

The frequency synthesizer, controlled by the computer (Figure 9) provides the desired frequency. Finest resolution is 0.01 Hz.

The system master gain, which controls the total forcing distribution is manually initialized but is adjusted under direct program control to suppress the total energy supplied to the structure if critical acceleration levels are exceeded. The signal from the ensemble of critical locations, which is sensing the highest signal level, is selected with a force and acceleration detector. The output of this unit is fed to the computer to control the total energy level.

The forcing distribution is manually initialized by level set and phase selection for each individual exciter. Phase adjustment is by sense only (0 to 180 degrees). Other phase manipulation is undesirable because normal mode motions and damping forces act, respectively, in a 0 or 180 degree sense. The driving forces are continuously variable to cancel the internal damping shears and moments to preserve the steady-state natural mode. To assure preservation of the forcing distribution and natural mode, a detected signal from each amplifier representing force is monitored by the computer to allow computer adjustment of the current supplied to each individual exciter. If the system amplitude is corrected by the computer (energy suppression), the individual forcing distribution digital control output is factored to prevent recompensation.

A separate component of the excitation control subsystem is the zero mass control unit needed to eliminate the effects of the armature and stinger mass during modal decays and when no drive signal is applied to the exciter. In addition, since the armature circuit remains active, the unit must compensate for back electromotive force generated by the moving coil. A secondary effect of the control unit

is to transform a voltage amplifier into an approximation of a current amplifier. A velocity transducer measures the differential velocity between the exciter body and armature (back EMF is directly proportional to the differential velocity). Mass cancellation is directly proportional to the acceleration of the armature-stinger assembly alone. Therefore, use of the acceleration signal measured on the vehicle at the stinger interface is appropriate. The signals generated by the two transducers are correctly phased, summed instantaneously, and then summed with the excitation drive signal, if present, resulting in a positive feedback system. The feedback signal is summed with the drive signal in lieu of switching the feedback signal into the amplifier input circuit upon initiating a decay.

Excitation Subsystem

A single channel of the excitation subsystem consists of a solid state, direct-coupled power amplifier; field supply and control unit; low-frequency-long-stroke exciter assembly; and mechanical-force-input coupler (stinger). A maximum of 12 channels can be excited simultaneously utilizing a combination of 16 power amplifiers/field supplies and 24 exciters. A patching network provides access from a given exciter to any power amplifier.

The primary consideration in application of the excitation system is to assure that there is no phase shift between any of the inputs to the structure. Phase shifts may occur electrically in the input circuitry to the power amplifiers or in the power amplifiers themselves. A phase shift can also occur mechanically in the shaker support structure or the stinger. Direct coupling is advantageous in minimizing or deleting phase shifts in the input and drive circuits and is a necessity for very low frequency operation. Direct coupling is used in the system principally because of the low frequency design criterion.

The stinger assemblies were designed to be stiff enough to transmit the force input with no appreciable phase shift (less than 5 degrees) up to the upper frequency limit. Nominal guidelines are to have the first mode of the stinger, axial or bending, at a minimum frequency of three times the upper frequency limit of the test band.

Monitoring Subsystem

The peripheral monitoring subsystem consists of a group of analog meters, analyzers and display units to aid in tuning operations and for continuous verification of nominal system operation. The function of the monitoring subsystem is to display 12 lissajous patterns simultaneously to aid the operator in tuning.

Twelve dual-channel dynamic analyzers act as narrowband filters (5 Hz) to provide high quality output signals of force and acceleration to the display units. In addition, a 90-degree phase shift is introduced between the two channels of the analyzer so the lissajous figure at resonance is a straight line rather than an ellipse. The paired outputs of the analyzers are hard wired to signal multiplexing units and then to bistable storage display units, which display four patterns on a single unit (storage display units are highly advantageous over standard oscilloscopes when operating below 5 Hz). Two options are available to the operators for tuning at frequencies below 3 Hz, where the analyzers cannot function. Since response signals are of much higher quality at lower frequencies, the main function of the analyzers is to provide the 90-degree phase shift between the force and acceleration signals. Therefore, the raw acceleration can be used to tune on elliptical patterns. An alternative is to use the raw velocity signal available from the shaker mounted velocity transducers. By using these transducers only at the very low frequencies, the phase problems associated with shaker body motion are avoided.

Other features of the monitoring subsystem include miniature oscilloscopes for continuous display of the raw force wave shape and analog voltmeters connected through a signal selector from the analyzer outputs. The analog meters are used to monitor force and acceleration when the central processor is not on line and to cross-check the digital data acquisition system during dwell operations by comparing analog and digital readings.

Ancillary Support Systems

The soft-spring suspension system provides a simulated free-free environment in which to excite and measure the natural elastic vibration modes of a structure. A maximum of 16 units can be used to suspend the test article. Each unit can support up to 50,000 pounds while maintaining a very low resonance frequency.

The closed circuit television capability consists of eight video channels, including cameras and controls. The video control console permits adjusting the position of each camera image. Patch panel and push button selection capability are available for matching cameras and monitors. Scan conversion, split screen special effects, waveform monitoring, and video signal conditioning are also available.

Analog data recording systems including the following:

Analog magnetic tape recorders with multiplex input capability (used to record data for off-line co-quad reduction).

Oscillograph chart recorders utilizing dry development, light sensitive papers on which galvonometer deflections are recorded.

An off-line co-quad analysis capability was developed to process data acquired from a large number of transducers during an incremental sinusoidal sweep over a large frequency band. The wideband sweep is performed to define the structural modes. The processed data is used in conjunction with the analytical data to define target modes and predicted forcing distributions.

SYSTEM APPLICATION

Two keyboard CRT terminals are used for entering test parameters, initiating commands to the software system, and displaying data and computations.

The system controller provides a logic procedure (Figure 10) for selecting the basic options for tuning and acquiring data for a mode or manipulating and displaying modal response data for assessing purity and validity of a previously acquired mode. The options are discussed below in the nominal operational sequence.

Supervisor Option

The excitation control and data acquisition supervisor is composed of the software modules for tuning and data acquisition. All excitation, real-time monitoring and control, and data acquisition are conducted with this supervisor. The remaining options of the controller are associated with data analysis, display, and assessment.

Eight operational possibilities are available within the supervisor:

1) SUPSS - Single shaker, wideband, sinusoidal sweep with digital data acquisition. Three accelerometers can be selected for generating co and quad plots on the digital plotter during one sweep. The raw co-quad data is stored on magnetic tape and listed on the line printer.

2) ASUPS - Single shaker, wideband, sinusoidal sweep with analog data acquisition for off-line co-quad reduction (not shown in Figure 10).

3) SUPTS - Tuning operations with a single shaker for approximate frequency settings.

4) SUPTM - Tuning operations with multiple shakers (maximum of 12). Fine tuning is accomplished with this software module.

5) SUPSM - Multiple shaker, narrowband, sinusoidal sweep to define the resonance condition. Three accelerometers can be selected for generating co and quad plots on the digital plotter during one sweep. The raw co-quad data is stored on magnetic tape and listed on the line printer.

6) SUPMD - Modal decay with signals from a maximum of 24 selected accelerometers recorded on an oscillograph.

7) SUPDW - Modal dwell operation for digital data acquisition in co and quad format. The system director checks the phase lock, if in use, the force distribution status while selecting input signals and resolves the data into co and quad components. The data is stored on magnetic tape, displayed on the CRT, listed on the line printer, and transferred to cards as a backup data file.

8) Return to Controller - Provides the initial display on the CRT and awaits a selection by the operator (not shown in Figure 10).

Print Option

This entry from the controller provides for additional printing of the generalized coordinate data from the disk unit to the line printer. Any mode previously stored on disk can be printed.

Plot Option

This option provides access to the plot routines. The two options are listed below.

1) Stick plots on the digital plotter or graphic CRT generated by this routine are composed of node displacements or rotations as a function of elevation or station number about three mutually perpendicular axes. The shape of the perturbed structure is derived from the deflection data of the mass points.

2) The routine for orthographic and stereographic plots on the digital plotter generates three orthographic and two stereographic views of the structure. Plotting parameters are manually entered on the keyboard to allow the structure to be viewed at any angle and at any focal point. The stereo plots, viewed with a stereoscope, provide a three dimensional view of the structure.

ORTHO Option

The orthogonality routine provides for selecting the type of check, auto or cross, to be made between analytical or experimental modes. In addition, the particular set of desired modes for orthogonality is entered through the CRT keyboard.

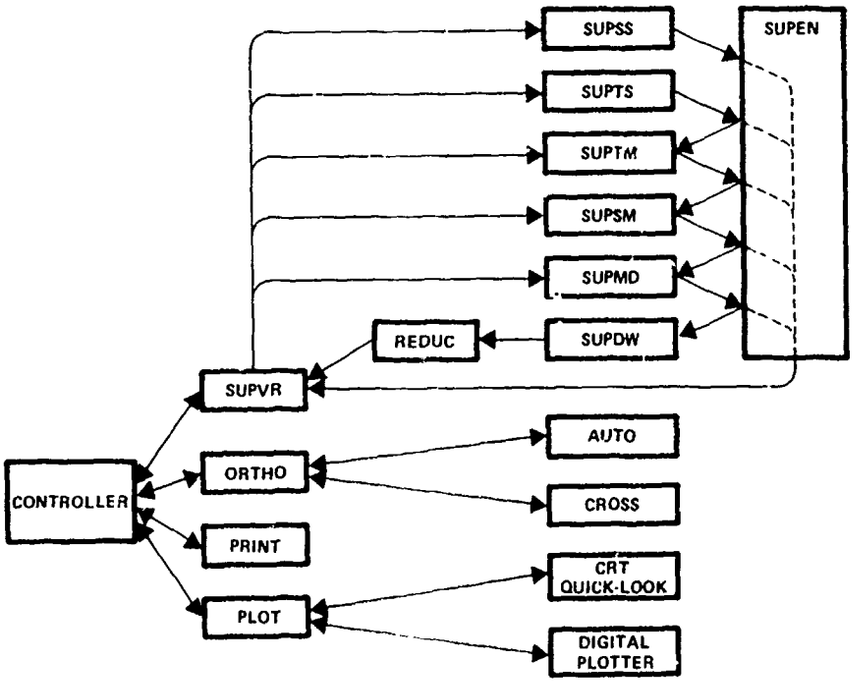

Figure 10.
AMTAS Operational Logic

TEST TECHNIQUES

Modal Tuning and Data Acquisition

The supervisor provides the algorithms for excitation control, real-time monitoring, and data acquisition for all modal operations. Upon selection of the supervisor through the controller, the initialization procedure is performed, followed by keyboard entry of the limit accelerometer parameters and respective response limits. The first operational entry is utilized to perform a wideband sinusoidal sweep with a selected exciter to obtain preliminary data of vehicle response to uniaxial single point force input. This data provides modal definition for use during tuning. Generally, the majority of these sweeps are conducted before advancing to the other sequences. (In either the SUPSS or the ASUPS mode two shakers can be driven simultaneously, although only one is actively servo controlled. The second shaker improves the quality of the excitation for better definition of bending or torsional modes when driving tangentially attached shakers.) In the SUPSS mode, three accelerometers can be selected for digital recording and concurrent co-quad plotting. Any number of accelerometers can be selected for analog tape recording in the ASUPS mode for subsequent off-line data reduction. This mode of operation is advantageous when a large number of accelerometers is desired for preliminary data analysis.

The information resulting from wideband sweeps is gross mode shapes or pairing with predicted analytical modes, approximate frequency of a mode, preferred shakers for a mode, and initial phase settings for shakers.

After the initial wideband sweeps and subsequent data analysis, modal tuning follows. The next four options of the selection menu, SUPTS, SUPTM, SUPSM and SUPMD, are associated with the tuning operation. Modal tuning with multiple exciters, SUPTM, is the main process of modal excitation and mode identification and separation. Tuning with a single exciter, SUPTS, is a short form of tune multiple.

The modal tuning and acquisition sequence is initiated by selecting a target mode and determining the appropriate forcing distribution. A nominal force level is manually initialized on the master (primary) exciter. This exciter is selected by analysis of the analytical model data (plots and listings) and the experimental co-quad data derived from the single exciter (ASUPS and SUPSS) sinusoidal sweeps.

The operator directs the operation by keyboard entry. After manual initialization of the forcing distribution, the LO command returns the display update rate to the slow mode (the HI update mode is automatically activated upon entry to a software module requiring forcing distribution initialization). Returning to the slow update mode allows most of the computer time to be devoted to acquiring and reducing data. The data acquired from the accelerometers and reference load cell is entered into the CRT format before the operation begins. These transducers can be changed by the appropriate entry at any time during a given operation.

The modal response of the structure is optimized by varying the frequency of excitation and the forcing distribution (phase and level of the active exciters). While increasing quadrature values are noted on the co-quad displays, the frequency is incremented to optimize the quad value and to close the lissajous pattern. The lissajous pattern complements the co-quad displays and is useful in approaching an effective distribution. However, fine tuning is best achieved by observing small changes in the quadrature values since these effects cannot be detected in the lissajous patterns. Lissajous patterns are normally formed by pairing exciter forces and respective driving point accelerations. However, accelerations from other points of the structure may also be used, particularly when fine tuning the mode. As more exciters are activated, the resonance frequency will tend to shift downward. As this occurs, the frequency is incremented to below resonance, then increased in fine steps to peak the quadrature values (see the comments below on hysteresis).

In some instances it may be advantageous to suppress the participation of a neighboring mode rather than to attempt to excite the target mode. A decrease in the co values indicates suppression of the undesired mode. The quad values must not decrease appreciably during the process.

After the forcing distribution is optimized, the frequency of resonance is established from a lower frequency to eliminate effects of hysteresis; hysteresis often distorts response level versus frequency curves and may result in erroneous indications of resonance conditions.

Accelerometers at key points of the structure are surveyed to assess the adequacy of tuning. Co-quad values from several primary locations are tabulated for reference during subsequent operations.

The four options of the tuning process automatically sequence in a logical order: tune single proceeds to tune multiple, then to sweep multiple, and then to modal decay. However, any desired operation can be entered directly through the operation selection menu, as shown in Figure 10.

A sweep multiple operation can be conducted at any time in the tuning process as an aid in defining the resonance condition, particularly if difficulties arise in the tune multiple operation. A narrowband sweep can identify any neighboring problem mode and provide insight on suppression techniques. After completion of the final tune multiple sequence, a sweep multiple operation is normally performed for data purposes. The co-quad plots from these narrowband sinusoidal sweeps are utilized in post-test analysis for an index of modal separation and for the calculation of damping values. One or more sweeps can be performed depending on the number of different accelerometers to be plotted.

When the co-quad data of the tune multiple and sweep multiple operations indicates that a mode has been properly separated and tuned, a modal decay is performed. Shaker excitation is removed and the unfiltered signals from selected accelerometers are recorded on an oscillograph. The quality of the decay curves provides another index of modal purity. If the structure decays smoothly with the absence of beating for the tuned mode, modal purity is good. If the modal purity is satisfactory, the sequence will be cycled automatically to the modal dwell operation for data acquisition. If modal purity is poor, the tuning iterations can be repeated. In tuning problem modes it is sometimes helpful to acquire dwell data despite the impurities and to generate plots of the existing mode. These plots provide the visibility to define problem areas and to assess the adequacy of the existing exciter locations to properly excite the target mode.

The modal dwell operation begins with the operator entering bookkeeping data, mode identifier, and run number for documentation and data retrieval purposes. Excitation is reinstated and the force servo maintains the predetermined forcing distribution. The automatic phase lock feature can be activated if desired. After stabilization of the forcing distribution and response, data is acquired on the operator's CRT. Upon completion of data acquisition, the data is automatically reduced and stored on disk (note the position of the REDUC module in Figure 10).

Data Reduction

Co and quad components are normalized to force. Force normalized co-quad provides a common basis of comparison for dwell data acquired when an individual exciter level varies within the tolerance band of the servo, causing minor variations in response levels. The normalized co and quad values are output to the line printer, CRT and plotter.

Co-Quad Plots

The data obtained from a typical sine sweep

is in the form of three sets of force normalized coincident (CO) and quadrature (QUAD) component values displayed on a digital X-Y plotter. The wideband force normalized co-quad plots provide a means of identifying the resonant frequencies of the structure.

At a resonance frequency the quad component of the data rises to a peak value and then declines while the co component decreases to a minimum, rises sharply crossing the zero axis when the quad is at a peak value, increases to a maximum, and gradually returns to the zero axis, assuming a positive quadrature peak; polarities of the co value will reverse for a negative quad peak.

Line Printer Listings

The sequence log is generated automatically as a given operation progresses. Bookkeeping data, type of operation, and data are displayed in the listing on the line printer.

The forcing distribution is logged on the sequence log when the operation is initiated by keyboard entry. At this time the force servo is activated by the computer to maintain the logged forcing distribution.

A printout of bookkeeping data and engineering unit data in global and generalized coordinates is obtained in the off-line mode by the appropriate keyboard entry. A listing of this complete summary of modal data may be obtained at any time.

Modal Plots

The stick plots are useful as a diagnostic in addition to their normal function of providing a graphic description of a mode. The trimetric (three planar views) set and stereo pair provide a graphic capability for assessing the adequacy of a particular forcing distribution in exciting a given mode.

Up to 15 stick plots can be produced by the appropriate keyboard entry in the off-line mode. Actually only six plots (three translation and three rotation) are required to describe a structure, but the capability of plotting separate parts of the structure on different plots was developed to increase the clarity of presentation. The maximum of 15 plots is divided into three sets of translation (nine plots) and two sets of rotation (six plots).

An automatic scaling feature provides maximum resolution (the operator may override this feature and specify a particular scale, if desired). For comparison purposes, however, scaling for the total set of translation plots is calculated on the basis of all data to be plotted. Similarly, the scale for rotation is calculated for all plots.

A set of stick plots may be made on the alphanumeric graphic CRT (quick-look) or the digital plotter (report quality hardcopy). These plot degree-of-freedom versus station number and are formatted to provide perturbance definition along each axis.

Decay Curves

This display is used to assess the purity of a mode by noting the amount of beating present. Curves generated during a modal decay with only the target mode excited will reflect no beating.

Off-Line Co-Quad Analysis

This processing (by a central reduction laboratory) is accomplished by digitizing and reducing the taped analog data to the desired engineering unit output.

This reduced data permits an assessment of the operation of the force servo subsystem and detection of the approximate frequencies at which the response of the structure is significant.

CONCLUDING REMARKS

The automatic modal tuning and analysis system described herein is capable of meeting the requirements of a modal survey of any structure comparable in size and complexity to the Skylab payload. The techniques and methods employed in the AMTAS will allow the system to be expanded to meet the requirements of larger structures During the application of AMTAS to the Skylab modal survey, several improvements to the system were defined. Those improvements, representing significant increases to overall capability, are discussed below.

Suspension System

The ancillary suspension system should become an integral part of the system to permit computer control of the suspension system. Single parameter (position) or dual parameter (load or pressure and position) feedback can be utilized for positive control of the test article suspension.

Technical Writer's Log Input

An additional CRT/KBD display unit should be incorporated for use by the technical writer. Test comments could be composed in the local mode utilizing the edit features of the unit. After the text is completed, the comments could be entered by a send command. The entire sequence log, including comments, should be displayed on the line printer and stored on digital magnetic tape.

Modal Survey Simulator

Training could be facilitated if a simulator software package were developed and included as an on-line option. Data stored

during the Skylab modal survey could be utilized for a realistic simulation of a modal survey, including wideband and narrowband sweeps, tuning operations, modal decays and dwells. This approach would eliminate the need for a structure for training purposes.

Test Procedure Display

A separate CRT (monitor only) unit should be incorporated to display the test procedure with slaved monitor units at each test station. This would eliminate the complexity of following the test operation as the mainline program will automatically display the correct page of the procedure and scroll it forward as the test progresses.

BIBLIOGRAPHY

1. R. A. Salyer, "Hybrid Techniques for Modal Survey Control and Data Appraisal", Shock and Vibration Bulletin, December 1970.

2. R. A. Salyer, "Purity Criteria for Modal Survey Data", Proceedings, 17th Annual Technical Conference, Institute of Environmental Science.

DISCUSSION

Mr. Hodge (Lockheed Missiles & Space Co.): In your post processing, what was your orthogonality criteria? What determined whether the mode was acceptable?

Mr. Salyer: That is really covered in the next paper("Skylab Modal Survey Testing"). We shot for ten percent.

SKYLAB MODAL SURVEY TESTING

J. J. Nichols
NASA-Marshall Space Flight Center
Huntsville, Alabama

and

R. E. Hull and B. I. Bejmuk
Martin Marietta Corporation
Denver, Colorado

Recently completed modal surveys of two Skylab orbital laboratory configurations are described. Included are discussions of test philosophy, pre-test analyses, testing methods, the test results, and correlation of the test modes with analytically derived vibration modes. The phase-separation techniques used and the multi-shaker excitation proved to be a highly successful method for testing coupled, complex structural systems.

INTRODUCTION

The Skylab orbital laboratory was designed to provide a long-term living and working environment for three men in orbit around the earth. A Saturn V upper stage was converted into living quarters and a primary working area for the laboratory. Compatible hardware was designed to provide docking ports, airlocks, and supports for heavy, sensitive experiments. This paper describes recently completed full scale modal survey tests of two configurations of the Skylab, excluding the living quarters and primary working area.

Since normal vibration modes provide the basis of all dynamic loads and stability calculations, it is necessary that these data be accurately determined to assure the total dynamic adequacy of a system. On new and complex structural systems, modal survey tests are usually mandatory to obtain the accuracy required. This is particularly true on complex structures that must support highly sensitive equipment or be man rated. The Skylab vehicle had to satisfy both of these requirements. The philosophy governing the subject modal tests was to acquire all structurally significant vibration modes in the frequency range affecting structural loads and flight controls computations. Comparison of the normal modes acquired during the tests with analytically predicted modes facilitated the verification of the mathematical model and exposed specific areas where modeling was inadequate.

Modal surveys were conducted on two physically distinct configurations. These consisted of the Skylab launch and orbital configurations shown in Figs. 1 and 2. The launch configuration consisted of all hardware above the Saturn S-IVB stage workshop, including the S-IVB forward skirt. The total system tested weighed approximately 130,000 lb and was 80 ft long. The orbital configuration consisted of the same structure, but with the payload shroud jettisoned and the Apollo Telescope Mount deployed. The Apollo command and service module was docked to the axial port. An air bag support system simulated a free boundary condition for both tests. The modal survey of the launch configuration structure was performed first and provided valuable experience which was used to alter several areas in the approach to the orbital configuration modal survey. These differences in the conduct of the two tests and their effects on the results obtained are emphasized in the discussion of the testing techniques.

Prior to the Skylab program, large rockets and space vehicles were excited during dynamic tests by placing shakers in one plane only and recording the resulting motion. This type of testing is adequate on simple structures that have very little mass and stiffness coupling between planes and when modes are fairly well separated. Skylab is a highly coupled system with a dense concentration of modes below 20 Hz. This made a multiple plane excitation system mandatory if individual modes were to be isolated and mapped. A unique multi-shaker control and online data acquisition system known as AMTAS (Automatic Modal Tuning and Acquisition System) was utilized on these tests.

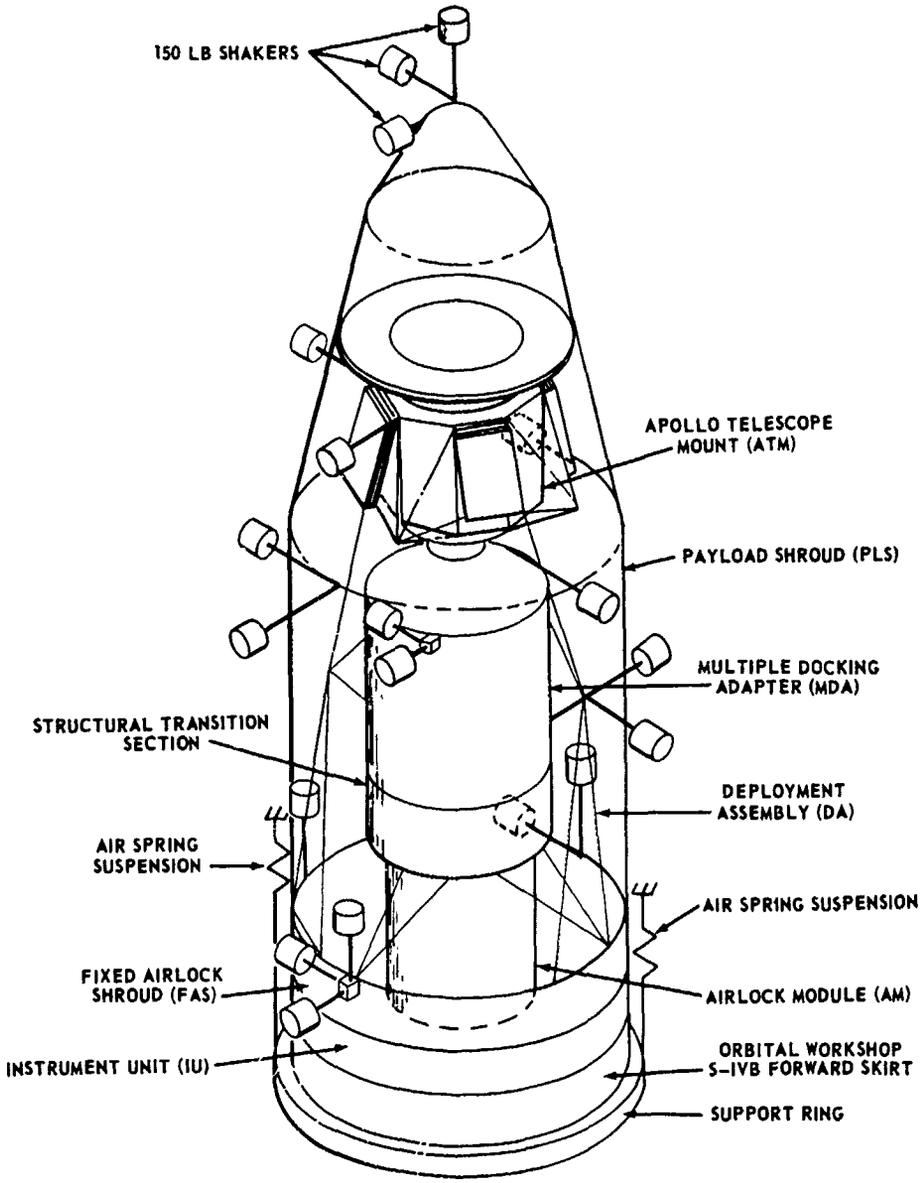

Fig. 1. Schematic of the launch configuration dynamic test article

The AMTAS measures the total acceleration response and resolves it into vector components in phase with a selected force and one 90 degrees out-of-phase with the force. These components are defined as the coincident (CO) and quadrature (QUAD) response vectors, respectively. At resonance the quadrature component represents the total response, since the in-phase component is zero. The phase-separation technique had been used with previous success in the aerospace industry, but this was the first time on a system as large as Skylab. The phase-separation technique coupled with multi-shaker excitation proved to be an efficient and accurate method for defining system modal characteristics.

Because of the physical size and complexity of the Skylab structure, several problems were encountered in formating and evaluating the vast amount of experimental data obtained. Also, a schematic

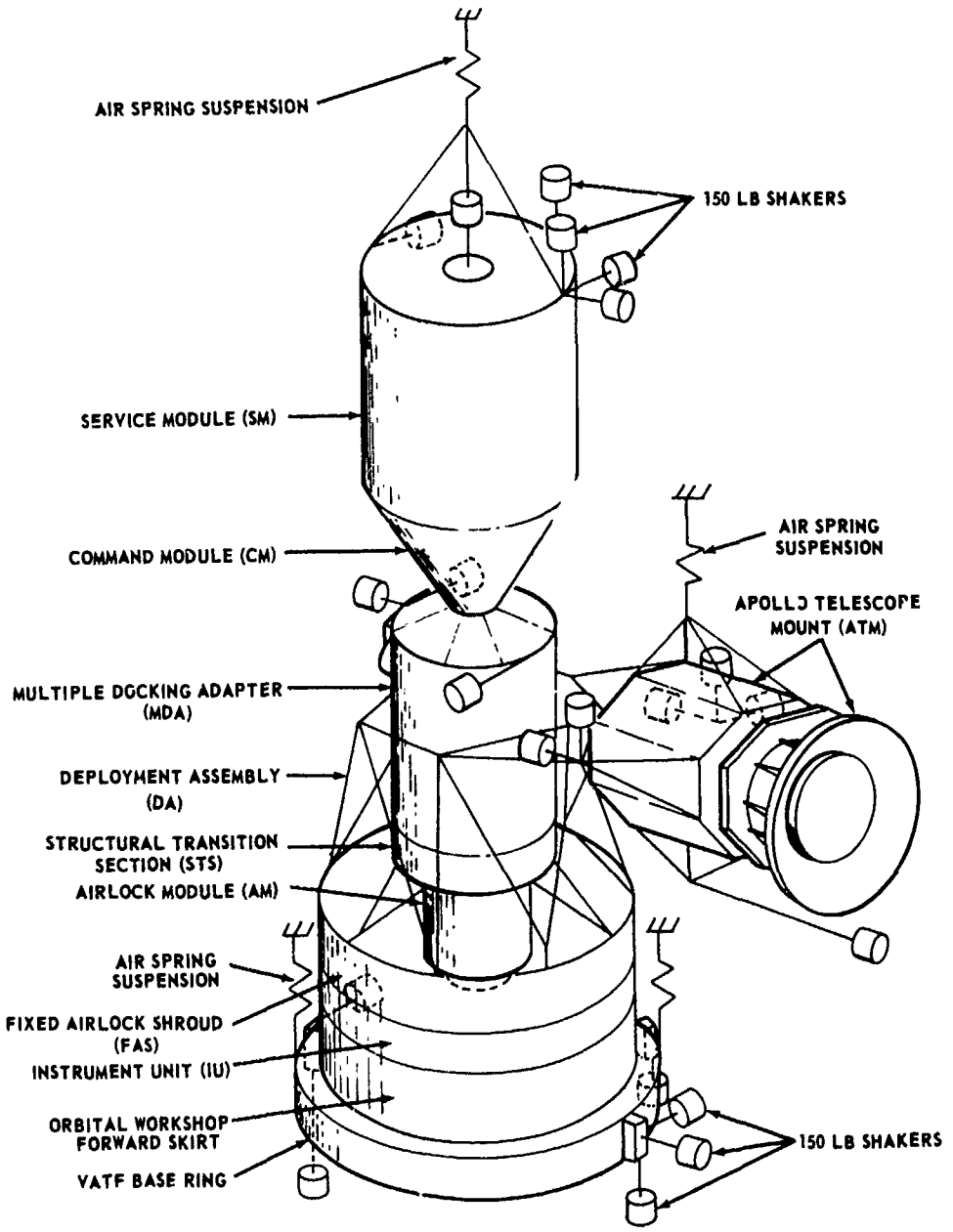

Fig. 2. Schematic of the orbital configuration dynamic test article

approach to correlating the test data with analytical results had to be formulated before assessments could be made. These topics, along with refinements made in other areas and helpful aids in acquiring data, are discussed in the following sections of this paper.

PRETEST ANALYSES

Prior to starting actual modal testing, mode shapes and frequencies for both test configurations were calculated. The results of these analyses were used for further analytical pretest studies and

subsequent post-test correlations with the test data. The mode shapes and frequencies were derived using the same technique as was used in calculating modal data for design loads purposes. The technique is known as the Modal Synthesis Method and is described in detail in Reference 1. Briefly, in applying this technique, the structure to be analyzed is considered to consist of an assemblage of structural components. One of the components is designated as the "main beam", while the remaining components are considered to be "branches" which are to be inertially coupled to the "main beam." The process involves calculating mode shapes and frequencies for each "branch" when constrained at the various "main beam" interfaces. The "branch" mode shapes along with the "main beam" mode shapes are mathematically combined to form the coupled system for which coupled mode shapes and frequencies are calculated for the entire structure.

Figs. 3 and 4 indicate the various "branches" and "main beams" used in calculating the coupled mode shapes and frequencies for the launch and orbital configurations, respectively. The results of the coupled analyses indicated 205 modes in the launch configuration test frequency range of 0 to 50 Hz. The orbital configuration analysis resulted in 78 modes within the 0-to 20-Hz test frequency range. The final coupled models contained 425 and 630 net discrete degrees of freedom for the launch and orbital configurations, respectively.

Further pretest analyses were performed for the purposes of determining accelerometer measurement and modal shaker locations, measurement transformation equations for data reduction, and mass matrices for on-site orthogonality checks.

Due to limitations in data acquisition and reduction capabilities, along with availability of accelerometers, each test was limited to 200 accelerometer measurements per test mode. As a result, kinetic energy studies of the analytical modes were performed in order to determine optimum measurement locations for each of the test articles. In determining the 200 locations, emphasis was placed on instrumenting those areas which could be expected to have significant kinetic energy contributions in the greatest number of highly-coupled modes within the test frequency range. After determining the locations, transformation equations were generated (based on accurate laboratory accelerometer location measurements) for the purpose of transforming the measurements to the mathematical collocation points. These transformations were used along with analytically derived mass matrices to transform and normalize the test data and obtain on-site orthogonality checks and plots of the test modes. The mass matrices were derived from analytical component matrices using static reduction techniques.

A further pretest analytical effort involved determining physical locations for the 150-pound modal shakers used to excite and isolate the test modes. These studies were necessary due to limitations on quantities and implementation of the shakers. The studies were further complicated by physical clearance limitations in the laboratory.

For each test, a limit of twelve shakers could be simultaneously activated during modal tuning. In addition, the shakers could not be arbitarily moved about the structure during tuning operations. As a result, nineteen permanently located shakers were designated for the launch configuration and twenty-one for the orbital configuration. As previously indicated, any combination of twelve of these shakers could be used for modal tuning. The shaker location studies were concerned with determining which of the physically possible shaker locations could be used to excite the modes of interest. The selection process was analytically conducted and the final locations were based on maximizing the accelerations of the modes of interest while simultaneously suppressing accelerations in neighboring modes in order to maximize modal purity.

MODAL TUNING METHOD

The "co-quad" method of modal tuning was used for both Skylab modal survey tests. The following paragraphs briefly describe the essential features of the method. Detailed discussions of co-quad tuning are found in References 2 and 3.

The co-quad method involves resolving the total acceleration at each measured point on the structure into coincident (co) and quadrature (quad) components which are in- and out-of-phase, respectively, with a reference force signal ("master" shaker). These components are expressed mathematically as

$$\text{Quad} = |F|\ |A|\ \sin\theta \qquad (1)$$

$$\text{Co} = |F|\ |A|\ \cos\theta \qquad (2)$$

In the above equation, F is the value of the reference force, A is the total acceleration at a point on the structure, and θ is the phase angle between the reference force and acceleration vectors. Clearly, as the phase angle approaches 90°, the quad component will approach a maximum while the co will approach zero. Fig. 5 depicts the classical relationship between these components and the total acceleration as frequency is increased through a resonance. In addition, it can be seen that, if the total acceleration is expressed as a complex quantity, the imaginary portion is analogous to the

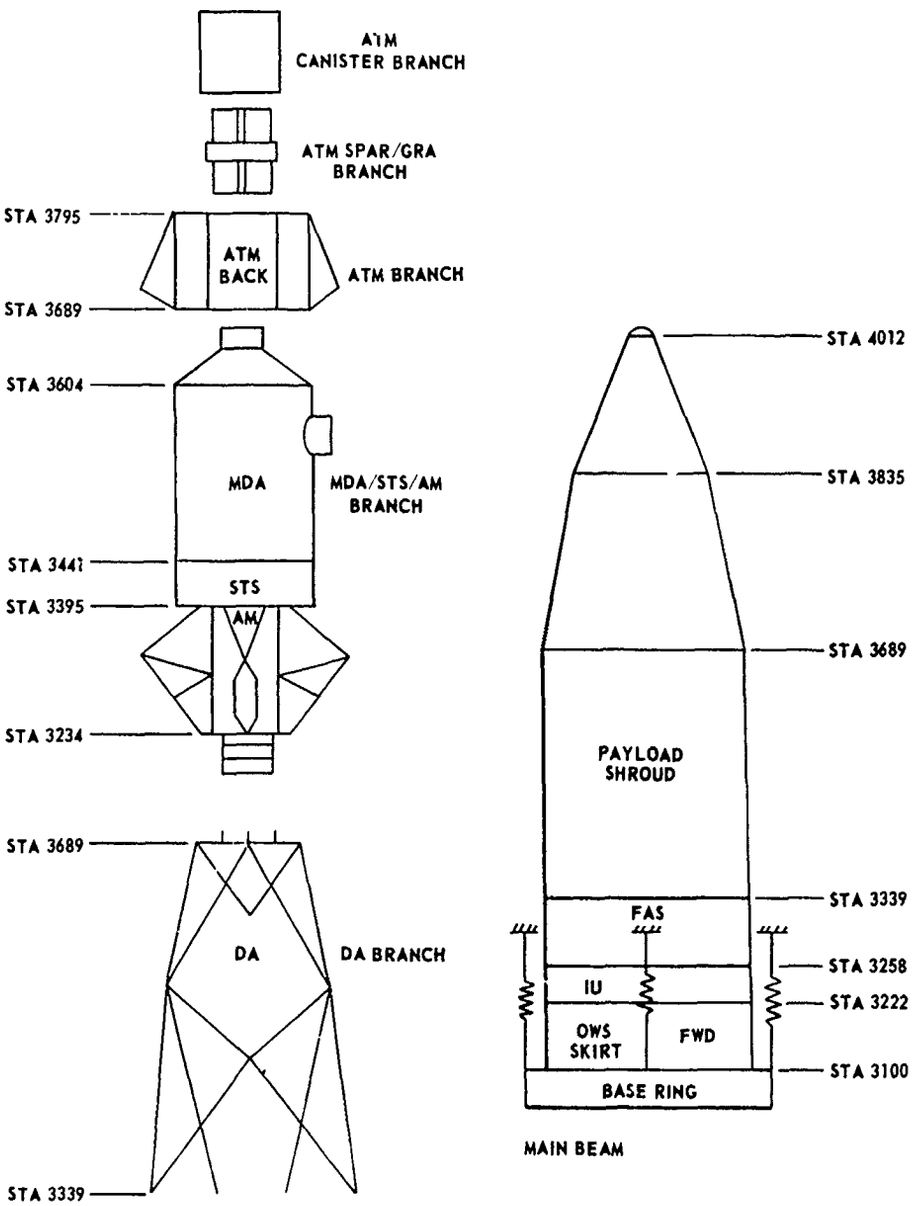

Fig. 3. Breakdown of launch configuration dynamic test article into components for vibration analysis

quadrature while the real part is analogous to the coincident component.

In actual laboratory practice, structural resonances are identified by first performing single-shaker "wide band" sweeps through the frequency range of interest. A portion of a typical single-shaker sweep is shown in Fig. 6. This figure shows the variation of co and quad components with frequency. After completion of the sweeps, the identified resonances are dwelled upon with the intention of exciting and isolating the attendant mode. This "tuning" process essentially consists of attempting to maximize the quadrature response for the mode of interest by varying shaker force amplitudes and phases. In practice, the quadrature responses will be comprised of components from neighboring modes as well as the mode of interest

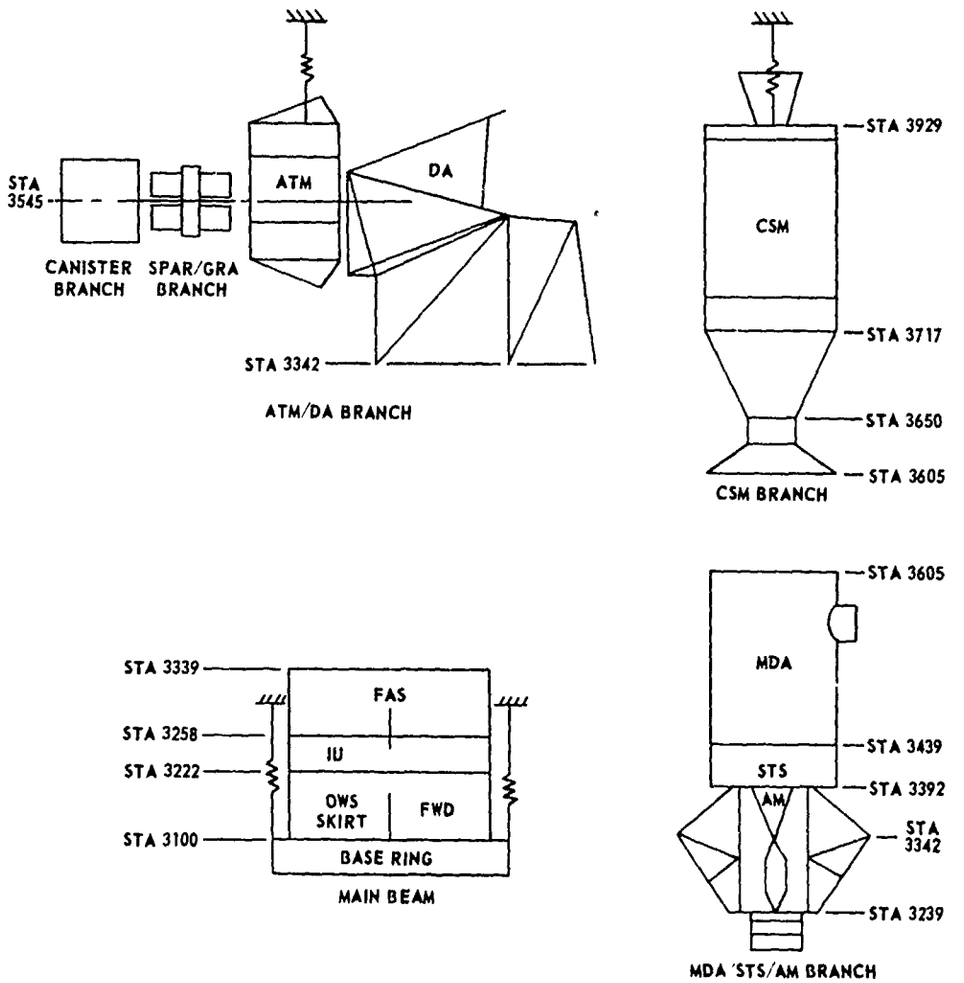

Fig. 4. Breakdown of orbital configuration dynamic test article into components for vibration analysis

As a result, the "ideal" relationship shown in Fig. 5 seldom exists. "Narrow band" shaker sweeps are utilized during the tuning process as an aid in identifying the neighboring modes and the severity of coupling with the mode of interest. These sweeps may cover a range, for example, of one cycle on either side of the desired modal frequency and yield high resolution online plots of co and quad variations in this range. The effects of each change in shaker amplitude and phase is determined using the narrow band sweeps. Once the quadrature responses have been satisfactorily optimized throughout the structure, the degree of success in isolating the mode of interest is determined by recording decay histories of acceleration after all shakers are simultaneously deactivated. The presence of "beating" during decay will indicate lack of purity. A further check on modal purity can be obtained through orthogonality checks.

The co-quad method of modal tuning was used quite successfully during both Skylab modal surveys. The greatest advantage of this method over other methods lies in the high degree of visibility provided by automatic online decomposition of the total acceleration into co and quad components.

TEST PROCEDURES AND DATA EVALUATION

Since the objective of the Skylab modal survey tests was to acquire only significant vibration modes of the launch and orbital configurations, emphasis was placed on modes characterized by the motion of major components of the system.

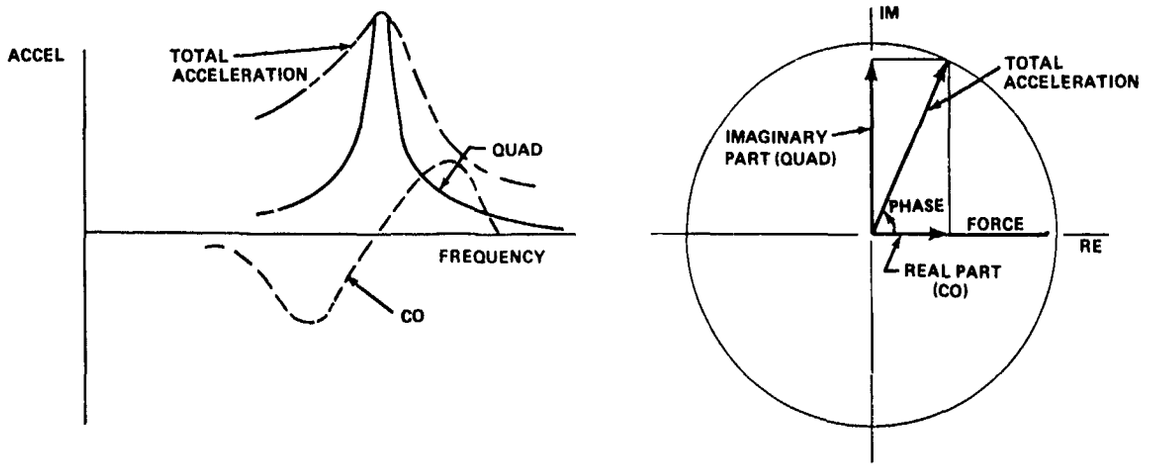

Fig. 5. Relation of co and quad to real and imaginary part of steady state response vector

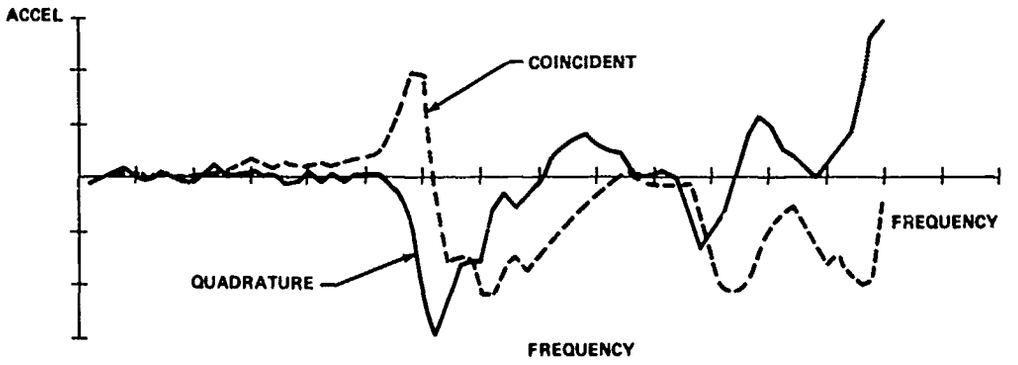

Fig. 6. Typical section of a wide band single shaker sweep

A large number of modes involving small, isolated components was not mapped since they were not considered significant to the scope of these tests. The following dicussion gives an overview of the tests conducted and the problems encountered during the course of testing.

a. Pretest System Checkout

Occasionally, at the start of testing, the significance of a thorough system checkout is overlooked in favor of obtaining test data on or ahead of a planned schedule. It should be recognized that the pretest system checkout does yield valuable data which can save many days of man effort and schedule time. This is accomplished by eliminating instrumentation and data acquisition problems at the start through the use of efficient and systematic planned procedures. Because of the large number of accelerometers used on the Skylab tests and complexity of the online data acquisition system, considerable effort was allocated to the pretest checkout.

The polarities of accelerometers were verified by exciting the test articles in suspension system modes and observing the resulting rigid body motion. A unity quadrature check was also performed to verify the operational capability of the data acquisition system downstream from the co-quad analyzer. Input of a quadrature value of unity was used to simulate the reading of accelerometers in all coordinate axes. In each case, these simulated readings were processed through all of the data reduction channels, including transformations of motion to the analytical modal mass points and then producing the corresponding online plots. Several errors in the transformation equations were exposed and corrected, as well as some hardware problems that would have been difficult, if not impossible, to spot without an attentive systematic check. Additional routine data checks were made

throughout the test program as part of the test procedures to verify the quality of data obtained. Failures in data acquisition equipment and configuration change errors were uncovered by these routine checks that would otherwise have gone undetected for days as piles of data were accumulated. Obviously, this would have resulted in an unforgivable waste of time and resources.

b. Wide-Band Frequency Sweeps

At the outset of each test, wide-band frequency sweeps were made to experimentally identify significant modes of the Skylab system. During the launch configuration test, single-shaker sweeps were made from 5 to 50 Hz at each of the 19 shaker locations. Likewise, on the orbital configuration test, frequency sweeps were conducted from 1 to 20 Hz. Only selected shaker locations were excited on the orbital test. In some cases, two shakers with either 0 or 180° phase were excited simultaneously to obtain the desired response spectrum. Accelerometer data were acquired at selected measurement points, decomposed into the coincident and quadrature components, and plotted as a function of frequency. The frequency sweep rate of 0.5 Hz/min yielded near-steady-state response during these sweeps. Examination of the co-quad plots facilitated approximate definition of the mode shapes and their frequencies. During the single-shaker sweeps performed on the launch configuration test article, only three accelerometer measurements were acquired for each sweep. Estimation of mode shapes from these limited measurements was difficult and in some cases, impossible. As a result of experience gained from these tests, the number of accelerometers was increased to 56 for the orbital configuration sweep test. This allowed a more accurate estimation of the mode shapes and greatly enhanced the tuning of the orbital configuration modes.

A typical section of a wide band, single-shaker sweep plot is shown in Fig. 6. The measured amplitude at resonant peaks was tabulated as a function of frequency and location for each accelerometer. Data from all the accelerometers were listed in matrix form so that the existence of a mode would be more readily apparent. This type of formating worked exceptionally well when there was good separation between modes. At the higher frequencies, identification became more difficult because of the higher modal density. This might be eliminated on future tests by taking smaller frequency increments when conducting the frequency sweeps. It should be mentioned that separation can be difficult even at the lower frequencies, since some modes appear in pairs and very close in frequency. This occurred at some of the lower bending modes due to slight stiffness and mass differences between the pitch and yaw planes. A pretest analysis was used as an aid in identifying these conditions. Once their existence was recognized, it was no problem separating them during the modal tuning operation.

c. Tuning and Acquisition of Modes

The approximate shapes of frequencies of major modes were acquired from the tabulated wide-band frequency-sweep data. Three-dimensional vector plots made for each deflection pattern aided in selecting shaker locations, phasing shakers, and choosing instrumentation to be monitored during the tuning process. Considerable effort was expended in analyzing the data and making the above selections. However, it was time well spent. Modes that could be approximately defined in this manner were tuned in only a fraction of the time required for ill-defined modes.

A total of 12 shakers could be controlled simultaneously during the modal dwells. A photograph of the control panel is shown in Fig. 7. Approximate tuning of the modes was accomplished by varying force amplitudes while monitoring Lissojous patterns of selected accelerometers and the master shaker. Final tuning required further manipulation of the shaker forces and phases while observing quadrature and coincident component vector amplitudes. A mode was considered to be well-tuned when the quadrature was maximized at points of largest displacement and the co vector was less than 10 percent of the quad amplitude.

Prior to the acquisition of data, the purity of a mode was verified first by performing a narrow band frequency sweep through the established resonance. Several selected acceleration measurements were acquired and plotted as shown for the wide-band sweep data. If the plots showed that neighboring modes had been depressed, the next step was to acquire decay traces of several selected accelerometers and examine them for beating. If any one of the purity checks was negative, additional tuning was required. When this occurred, new shaker locations were usually selected with the aid of the co-quad data from the unsuccessful dwell. The entire tuning process was then repeated.

Acquisition of a mode using AMTAS involved recording the 200 acceleration measurements followed by analog-to-digital data conversion. Digital decomposition of the total acceleration into coincident and quadrature components and transformation of the quadrature data from the accelerometer locations to the mathematical model mass collocation points was then accomplished. Online printouts of total acceleration, coincident and quadrature components, and the co-quad ratio were generated. Quadrature data, normalized with respect

Fig. 7. Vibration test control room

to the mass matrix to yield a generalized mass of unity, were used to produce two-dimensional plots of the mode shape immediately following acquisition of the mode.

During the launch configuration modal survey, 24 unique modes were acquired in the frequency range below 50 Hz. Orthogonality of these modes with respect to the mass matrix is shown in Table 1. Table 2 shows the orthogonality between the 25 modes acquired during the orbital configuration test. The off-diagonal terms shown in the orthogonality matrices are not squared. Therefore, they represent true-coupling between the modes involved. In most cases, the orthogonality results are excellent. Some modes do show strong coupling, but a few high off-diagonal terms should be expected due to the limited number of accelerometers and shaker locations used.

The first elastic mode of the launch configuration test article is shown in Figs. 8, 9, and 10. Two-dimensional plots similar to those produced on-line during the test are shown in Figs. 8 and 9. Fig. 10 provides a pictorial display of the same mode. Only motion of large components pertinent to the description of the character of this mode is shown. Figs. 11 and 12 depict the first elastic mode of the orbital configuration test article in the same fashion.

CORRELATION OF TEST AND ANALYSIS

The correlation process leads to either confirming the mathematical model or exposing its deficiencies. The Generalized Mass Contribution (GMC) method, described in Reference 4, greatly aided in this correlation. The fractional distribution of the normalized kinetic energy throughout the structure was computed for both the test and analytical modes. A least-squares fit method was then used to find the best match between the GMC distribution of a test and an analytical mode. Frequency and mode shape plots were used to further confirm

TABLE 1
Orthogonality of Launch Configuration Test Modes with Respect to the Mass Matrix

MODE	FREQUENCY	MODE NUMBER																							
		1	2	3	4	5	6	7	8	9	10	11	12	13	14	15	16	17	18	19	20	21	22	23	24
1	0.73	100	2.8	2.1	2.4	0.8	0.8	0.8	2.1	2.1	1.5	2.5	13.1	3.4	3.2	0.4	3.1	2.4	1.4	2.3	4.7	0.7	0.3	1.1	3.5
2	1.371		100	5.9	3.6	2.3	2.9	0.0	1.2	2.0	1.8	2.2	5.2	0.4	0.6	2.7	4.0	2.3	0.6	2.2	3.3	11.5	4.8	2.0	1.0
3	5.837			100	3.8	0.1	1.7	3.7	12.3	1.7	0.0	5.6	3.8	8.9	4.7	8.3	2.0	1.3	2.8	4.1	2.2	8.4	0.6	8.0	2.4
4	7.541				100	3.2	3.8	12.1	6.6	17.4	16.7	0.9	7.5	17.9	5.3	7.5	4.0	5.8	3.6	11.7	1.2	4.1	14.4	1.0	10.8
5	8.791					100	7.2	10.2	5.4	6.3	9.6	11.9	3.9	10.1	1.9	1.5	1.7	1.9	6.6	16.7	5.8	6.2	1.8	3.6	1.5
6	9.208						100	1.5	4.1	0.0	8.2	5.2	4.3	4.1	5.0	0.4	5.2	1.5	2.0	4.7	16.0	2.1	5.2	12.7	1.0
7	10.39							100	16.1	7.6	4.9	2.8	2.0	4.4	4.6	0.3	7.6	0.9	2.2	7.7	5.6	0.7	2.2	4.0	2.5
8	11.30								100	2.3	11.1	0.3	1.0	10.2	3.4	0.2	2.5	3.5	5.8	2.6	0.4	4.2	4.9	5.7	2.1
9	13.48									100	21.3	5.9	17.8	11.8	10.0	3.0	13.0	5.0	19.1	19.8	11.1	2.4	1.0	6.9	13.8
10	16.16										100	8.1	6.9	36.0	14.5	4.2	29.5	1.2	4.9	29.9	3.3	21.9	12.1	2.1	3.8
11	16.87											100	12.1	11.5	11.1	1.1	19.7	6.1	8.5	5.8	4.3	17.2	5.0	4.5	8.1
12	16.26												100	5.1	3.7	13.5	9.0	22.4	18.4	16.6	0.9	2.3	5.5	9.5	7.6
13	16.56													100	0.8	3.5	30.6	14.3	5.9	31.5	5.3	12.0	14.7	0.3	2.3
14	17.82														100	9.3	9.3	2.9	9.5	5.4	1.8	19.1	1.8	3.1	1.9
15	18.78															100	4.7	18.9	15.6	4.4	10.2	7.6	0.9	7.5	3.4
16	20.28																100	2.8	2.0	7.1	7.1	0.6	11.8	2.5	2.3
17	21.96																	100	18.5	1.9	4.7	29.0	5.1	1.0	3.0
18	22.22																		100	38.2	41.1	12.5	11.4	5.7	19.2
19	23.00																			100	23.1	3.3	0.7	1.8	8.2
20	23.86																				100	30.8	2.5	2.0	2.4
21	26.93																					100	9.6	5.0	0.4
22	40.89																						100	2.9	0.8
23	43.63																							100	18.0
24	43.99																								100

TABLE 2
Orthogonality of Orbital Configuration Test Modes with Respect to the Mass Matrix

MODE	FREQUENCY	MODE NUMBER																							
		1	2	3	4	5	6	7	8	9	10	11	12	13	14	15	16	17	18	19	20	21	22	23	24	25
1	0.31	100	1.0	2.4	1.8	0.2	0.6	1.8	1.2	1.2	3.2	3.4	11.9	8.4	6.7	2.4	0.6	2.9	1.4	0.9	6.6	2.4	0.3	10.3	1.9	7.6
2	0.3		100	0.3	3.0	9.2	19.6	1.8	5.1	1.2	0.5	4.6	8.1	17.5	2.1	0.3	15.9	1.5	0.6	1.4	2.5	1.6	2.7	6.0	8.5	11.3
3	1.31			100	3.7	0.9	2.5	1.4	1.8	0.6	1.1	1.8	0.1	1.5	0.2	2.8	1.2	0.4	0.9	2.4	0.2	0.3	0.7	8.6	3.0	0.3
4	1.43				100	7.4	1.0	2.0	0.4	1.1	7.5	1.3	0.5	0.2	0.7	24.2	0.5	0.1	1.4	2.5	1.1	0.7	2.3	2.2	0.3	2.2
5	1.66					100	10.8	1.4	0.5	0.2	0.2	1.5	3.4	1.2	3.4	16.5	1.1	1.5	2.8	2.8	1.8	0.3	3.7	3.1	1.8	4.8
6	1.74						100	0.6	1.8	4.7	0.7	5.4	2.7	1.5	7.3	1.1	2.5	0.0	2.1	1.3	1.3	1.2	0.3	0.0	2.4	7.7
7	2.51							100	1.7	2.9	1.2	0.7	0.4	3.5	4.0	10.8	1.0	0.1	2.0	9.4	3.0	1.8	0.7	5.2	8.2	0.8
8	3.06								100	3.1	3.9	0.8	1.5	9.4	3.4	5.2	0.1	1.3	0.8	2.4	3.9	4.1	1.8	2.2	4.0	2.6
9	4.10									100	13.0	0.3	3.2	4.8	2.0	9.2	2.9	2.7	1.5	0.8	3.8	3.1	1.8	3.9	3.0	3.4
10	4.86										100	4.9	2.9	2.9	4.6	46.2	1.5	4.6	1.2	0.5	3.1	1.7	2.5	0.2	9.1	0.6
11	5.03											100	2.3	1.3	1.4	1.9	0.3	1.2	0.1	1.6	0.4	0.7	0.8	0.9	3.0	0.8
12	5.86												100	0.0	0.5	24.2	2.0	1.4	2.9	0.6	3.3	2.3	6.1	0.0	1.3	6.4
13	6.36													100	2.8	0.0	3.7	2.9	1.1	2.5	0.7	0.9	0.3	2.4	1.5	0.7
14	6.73														100	63.8	0.9	3.0	1.4	7.2	5.5	1.8	0.8	11.2	0.1	4.5
15	7.59															100	4.3	1.6	7.1	0.9	1.2	0.8	0.6	8.9	5.4	0.8
16	8.96																100	0.6	1.1	1.4	2.5	1.1	1.2	1.6	0.4	8.7
17	11.89																	100	8.9	9.1	4.1	2.6	9.2	4.6	2.5	2.8
18	12.66																		100	7.7	5.2	11.3	27.5	7.7	1.4	1.2
19	13.30																			100	32.4	9.5	13.8	1.3	9.4	5.7
20	13.88																				100	20.3	11.5	6.4	7.4	1.1
21	14.86																					100	23.5	2.9	11.8	0.5
22	15.40																						100	32.0	7.8	1.2
23	16.20																							100	6.5	2.5
24	16.63																								100	16.8
25	17.01																									100

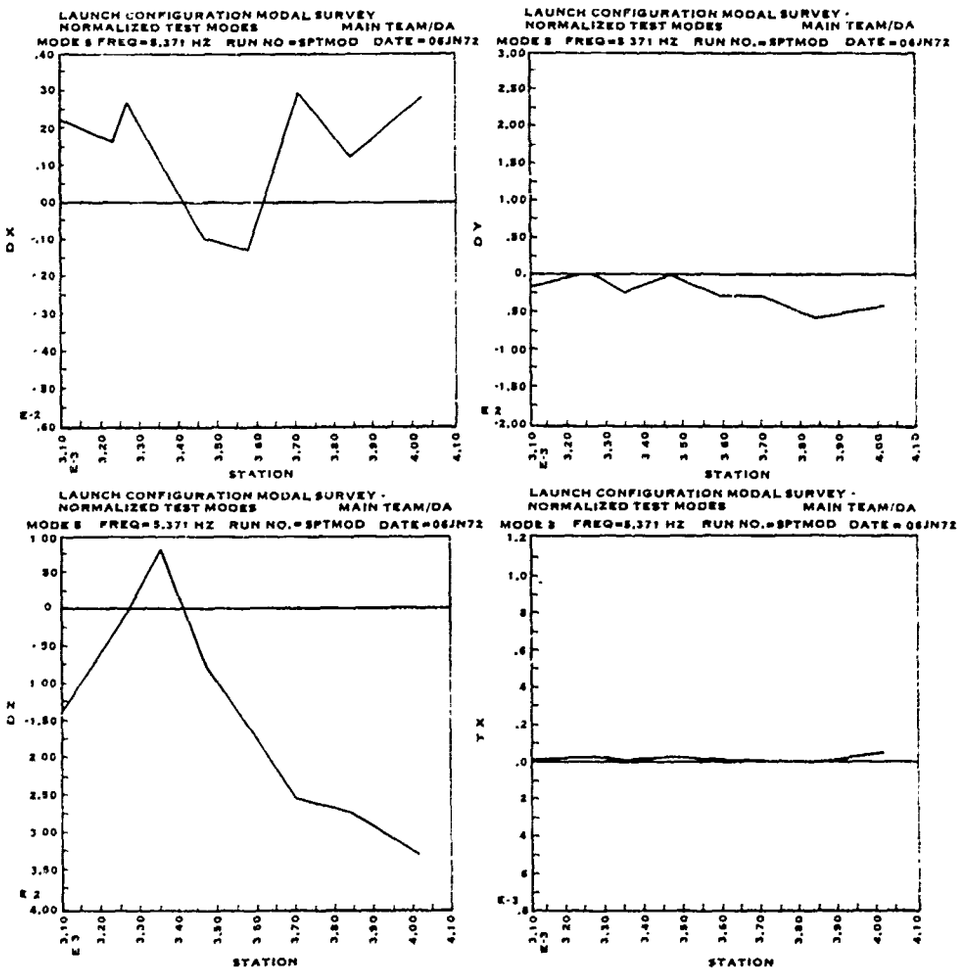

Fig. 8. Launch configuration first elastic mode, main beam deflections

the GMC correlation. A summary of the frequency correlation results is shown in Tables 3 and 4 for the launch and orbital configurations, respectively.

The launch configuration correlation analysis exposed a serious modeling error in the airlock module tunnel and at the MDA/STS interface representation. The frequency of modes involving large elastic deformation of these areas was up to 25 percent lower than analytically predicted. The first elastic experimental mode was found at 5.35 Hz compared to 7.25 Hz, as analytically predicted. Change in a local area stiffness of the math model was required to make analyses agree with the test results. The airlock module nitrogen storage tank supports were also found to be in error and were remodeled. Differences between the test and analytical frequencies of the FAS oxygen storage tanks were attributed to structural differences between the test and flight hardware. A correct representation of the test hardware eliminated these discrepancies.

The orbital configuration confirmed the modeling problem in the AM/STS area that was exposed by the launch configuration test. A stiffness error in the ATM deployment assembly and the command/service module interface representations was also found and corrected. Post test frequencies in Table 4 reflect these changes in the math model. Some of the higher frequencies of the launch configuration shifted to give worse correlation frequency-wise than before model rework. However, modal amplitudes and phasing between different parts of the structure were greatly improved to give a better overall correlation.

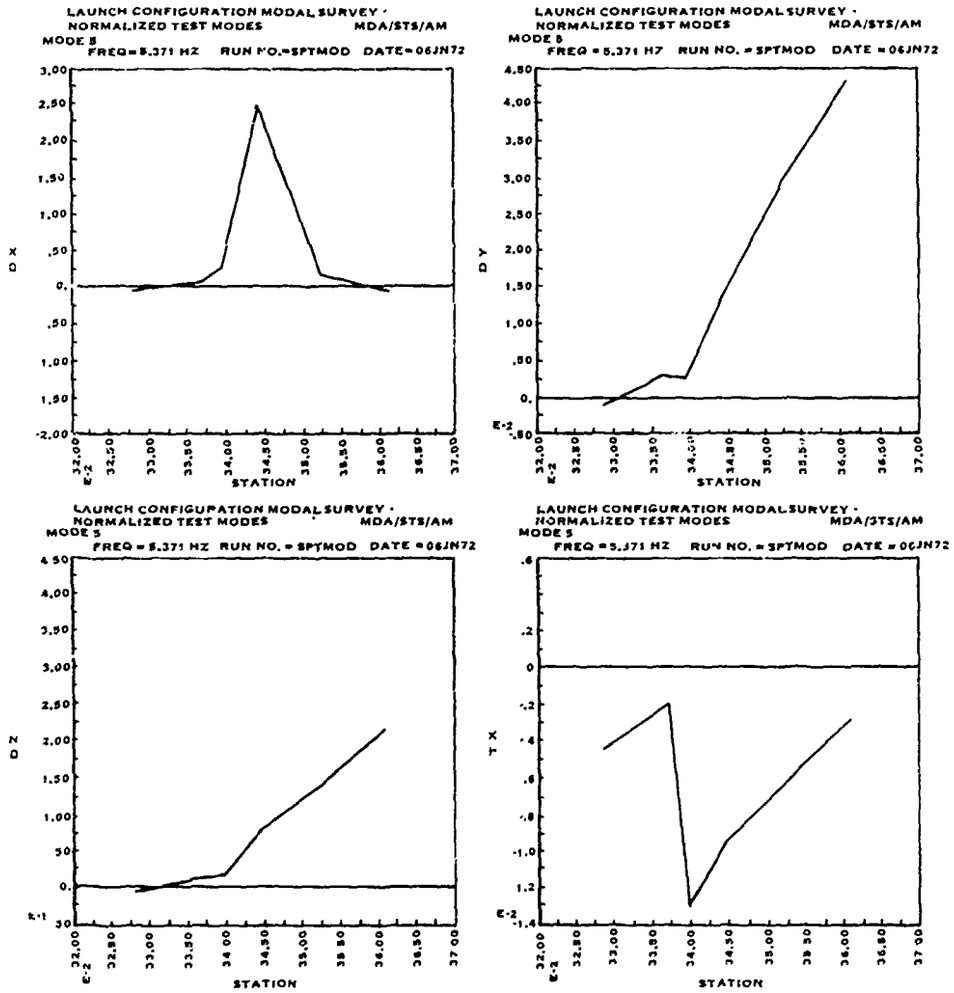

Fig. 9. Launch configuration first elastic mode, MDA/AM deflections

SUMMARY

The co-quad technique, coupled with multi-shaker excitation, proved to be an efficient and accurate method for defining the Skylab system's modal characteristics. Refinements in test techniques and procedures were made as the testing progressed. Only three accelerometers were monitored for each wide-band frequency sweep on the launch configuration. This proved to be an inadequate amount of instrumentation to allow gross definition of the required modes. This problem was corrected on the orbital configuration since assessment of mode shapes prior to the tuning process was extremely helpful in tuning a mode.

Several purity checks were made during the course of acquiring modal data. The online orthogonality checks and the narrow band frequency sweeps proved to be the most useful evaluations. Orthogonality calculations were particularly helpful in the evaluation of modes with close frequencies.

During the post-test data evaluation and subsequent correlation with analysis, modal plots failed to provide the information required for accurate detailed comparisons. The generalized mass-contribution method, as previously described, provided the necessary tool for defining and sorting the characteristics of both the analytical and test modes. From the distribution of the generalized mass, the dominant subsystem or active structural areas in each mode was easily defined.

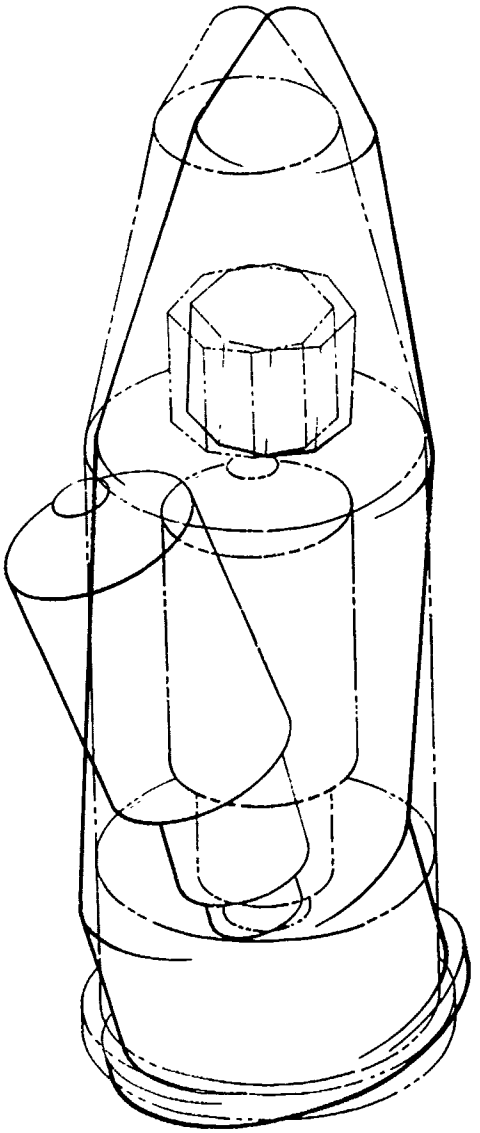

Fig. 10. Launch configuration first elastic mode, pictorial representation

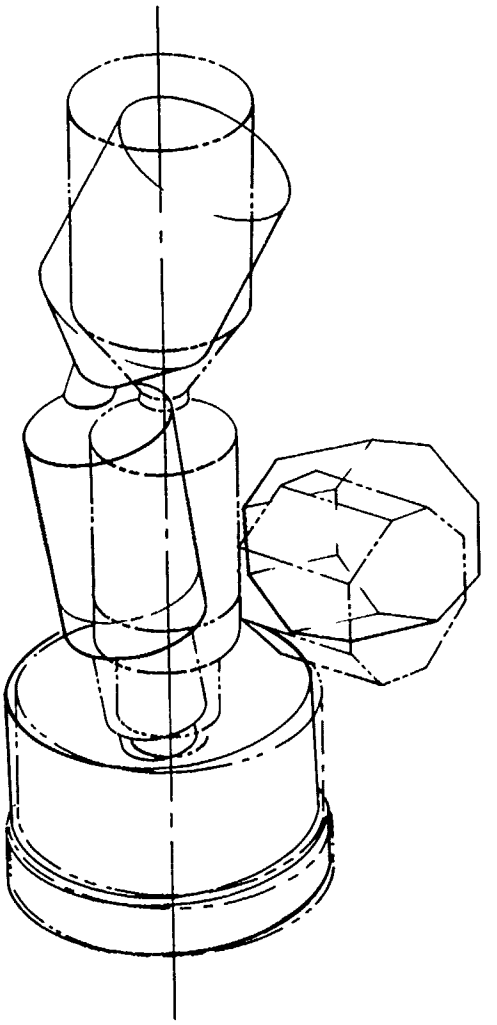

Fig. 11. Orbital configuration first elastic mode, pictorial representation

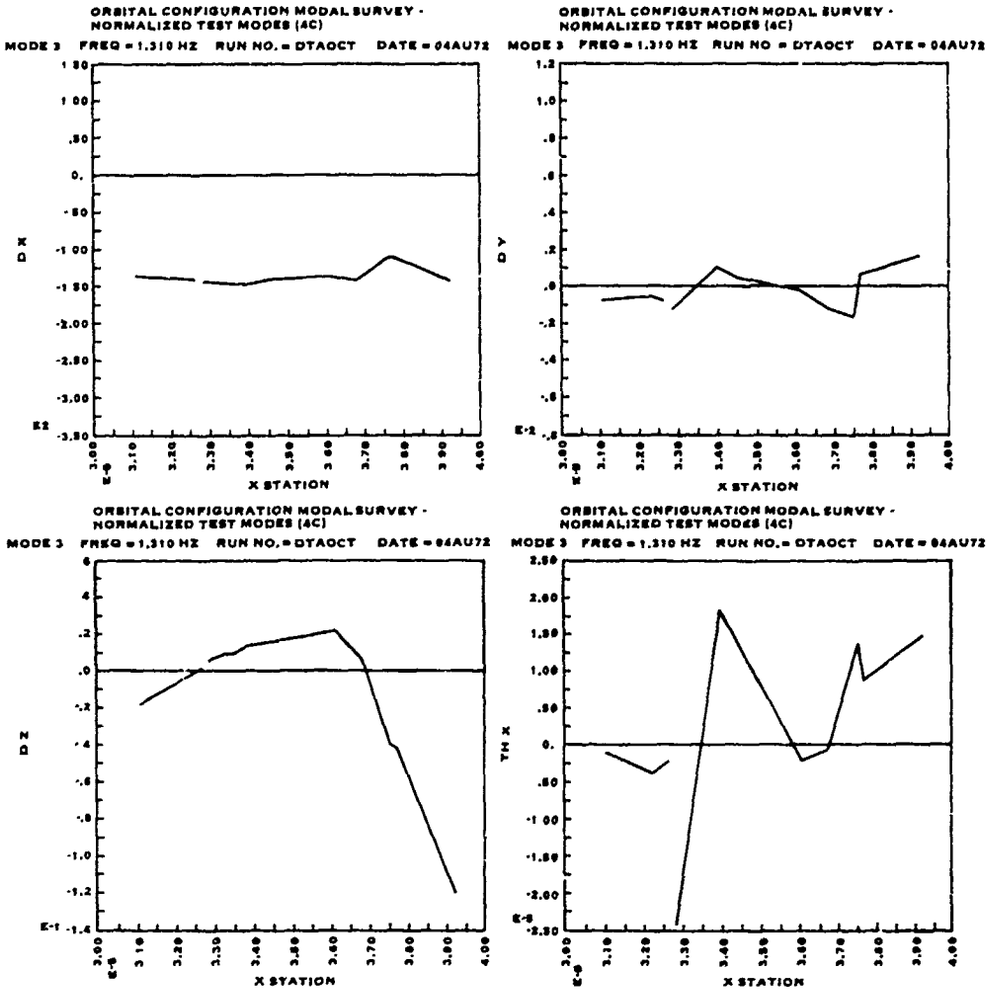

Fig. 12. Orbital configuration first elastic mode, main beam deflections

The test data and correlation technique described provided valuable information for verifying dynamic math models of the Skylab. Several errors were uncovered and have been corrected. The impact of these math model changes on loads and stability analysis results is still being assessed at the time of writing of this paper.

TABLE 3
Summary of Test and Analytical Modes Correlation, Launch Configuration

Test Mode		Correlating Pre test Analytical Mode Frequency, Hz	Correlating Pre-test Analytical Mode Frequency, Hz
No	Frequency, Hz		
1	0.73	0 721	0,720
2	5.371	7.256	5,235
3	5.537	7.856	5,460
4	7.541	7.766	7,766
5	8.791	10 257	9,018
6	9.208	10 325	9 083
7	10.39	11.073	9,891
8	11.30	12 608	10,862
9	13.45	13 985	13,220
10	15.15	16.325	15,373
11	15.87	18.119	15,072
12	16.28	16.667	16,780
13	16.56	20.150	16,201
14	17.92	20.378	19,165
15	18.78	19.083	18 815
16	20.28	21.783	19,956
17	21.96	23.992	30,249
18	22.2?	23 360	28,904
19	23.1	24.926	22,640
20	23.2	*	*
21	26.93	*	*
22	40.89	*	*
23	43.63	42.052	42,050
24	43.99	43.088	34,380

*No Analytical Mode Could Be Correlated

TABLE 4
Summary of Test and Analytical Modes Correlation, Orbital Configuration

Test Mode		Correlating Pre-test Analytical Mode Frequency, Hz	Correlating Post-test Analytical Mode Frequency, Hz
No.	Frequency, Hz		
1	0.31	0.28	0,28
2	0.3?	0 28	0,28
3	1.31	1.37	1,279
4	1.43	1.57	1,377
5	1.66	1.96	1,670
6	1 74	1.99	1,643
7	2.51	2.66	2,338
8	3.06	3.52	3,151
9	4.10	3.28	3,531
10	4.50	5 32	4,323
11	5.03	6 07	4,888
12	5.76	5.78	5,706
13	6.30	7.04	6,552
14	6.73	9.10	9,192
15	8.85	9.38	9,405
16	11.59	12.64	*
17	12.65	13.75	12,072
18	13.30	13.01	12,566
19	13.68	13.28	13,323
20	14.55	14.97	14,855
21	15.40	13.97	14,855
22	16.20	17.14	17,553
23	16.53	18.32	18,361
24	17.01	19.51	19,644

*No Analytical Mode Could Be Correlated

REFERENCES

1. W. A. Benfield and R. F. Hruda, "Vibration Analysis of Structures by Component Mode Substitution," AIAA Journal, Vol 9., No. 7, July 1971.

2. Salyer, Robert A., "Hybrid Techniques for Modal Survey Control and Data Appraisal," Shock and Vibration Bulletin 41, Washington, D. C., 1970,

3. Stahle, C. V., "Phase Separation Technique for Ground Vibration Testing," Aerospace Engineering, July 1962.

4. Hull, R. E., Nichols, J., Bejmuk, B., "Use of Generalized Mass Contributions in Correlation of Test and Analytical Vibration Modes," (to be published in Shock and Vibration Bulletin 43).

5. Vibro-Acoustic Modal Test Evaluation Report (Launch Configuration), ED-2002-1494, and Vibro-Acoustic Modal Survey Test Evaluation Report (Orbital Configuration), ED-2002-1522, Martin-Marietta Corporation, Denver Division.

6. White, C. W., Dynamics Modal Verification Report, Launch Configuration (ED-2002-1546) and White, C. W., Dynamics Modal Verification Report, Orbital Configuration (ED-2002-1551), Martin-Marietta Corporation, Denver Division.

DISCUSSION

Mr. Arthur (Aerojet Solid Propulsion Co.): You said that the main reason that you did the modal survey was to check your mathematical modal. I'm wondering why you didn't just check a simple frequency response test against your mathematical results.

Mr. Bejmuk: There are several philosophies as to whether one should perform a full scale modal survey or whether monitoring the frequency response will suffice. We felt that performing a modal survey of the type we did, short of actually monitoring the flight data, was the only effective method of learning the correctness of the mathematical modal. If you recall, this was a man-rated, single-flight mission with a lot of new hardware involved. We felt we needed a modal survey. In fact, I wish I had a little more time. I would have gotten into some of the results that we obtained and the impact or the analysis which was done on a pretest basis, as well as improvement which were made as results of the test. I think it would have become obvious that the money on the test was well spent.

Mr. Hodge (Lockheed Missiles and Space Company): What was your orthogonality criteria? What determined whether you accepted a mode or rejected it?

Mr. Bejmuk: Criteria for acceptance or rejection of a mode was not exclusively based orthogonality? We were looking at narrow band sweeps that we performed just prior to mode acquisition. We have looked at the print-out of answers. We have looked at the appearance of coincidence and quadrature at the coordinates recorded. That served in part for assessment as to whether the mode was good or required additional retuning. We felt, due to the complexity of the structure and the limitation of only 12 shakers that we could control at a time, that if we had thirty percent non-squared terms in our diagonal it would have been a successful test. Of course, our results looked much better than that.

Mr. Hodge: How did your results compare to your analytical modal?

Mr. Bejmuk: On launch configuration we found a little greater disagreement between test and analysis. For example, the first elastic mode was predicted at 7.2 Hz and found at 5.3 Hz. Now, that looks like a considerable frequency span but, if we consider that the mode actually involved elastic motion on one of the interfaces, we found it was extremely easy to correct. In fact the involved contractor did correct the model. We have rerun the analysis and we have excellent agreement now. We could not have assessed that disagreement without the test.

Mr. Hodge: How about the first mode in the orbital configuration?

Mr. Bejmuk: The mode in the orbital configuration was right on the bottom. The simple reason is that, prior to going into the orbital configuration test, we already had some knowledge with respect to the problem of our model derived from the launch configuration tests. So our analysis was not exactly the pretest analysis. We already had some knowledge of the modeling problems which were incorporated into our analytical model. The results were excellent. The first mode was something like 1.3 versus a predicted of 1.41. It was a few hundredths of a Hz.

USE OF GENERALIZED MASS CONTRIBUTIONS IN CORRELATION OF TEST AND ANALYTICAL VIBRATION MODES

Robert E. Hull and Bohdan I. Bejmuk,
Martin Marietta Corporation
Denver, Colorado

and

J. Nichols
National Aeronautics and Space Administration,
Marshall Space Flight Center
Huntsville, Alabama

A technique for the use of generalized mass contributions of discrete structural degrees of freedom as an aid in correlating analytically derived vibration modes with modes acquired from modal survey testing is described. Examples of the application of this method in the correlation of Skylab vibration modes are presented.

INTRODUCTION

After completing a spacecraft modal survey test program, the structural dynamicist is confronted with the task of comparing or "correlating" measured spacecraft vibration characteristics with corresponding analytically derived characteristics. The data to be compared consist of mode shapes and corresponding modal frequencies. The usual procedure is to compare directly plots of the test and analytical mode shapes. If the plot of an analytical mode appears similar in shape and amplitude with a given test mode plot, the two modes are said to correlate. The frequencies corresponding to the correlating mode shapes may or may not differ significantly.

Although this procedure may be adequate for use in relatively simple structures, the structure may be quite complex, consisting of an assemblage of many large truss and shell components, with the components containing some type of "local" appendages. During forced excitation, the responses of the appendages couple with the responses of the overall structure and these responses may be very closely spaced in frequency. The modal shape of the overall structure in one of the coupled appendage modes may closely resemble that of a truly overall structural mode. Because in a highly coupled system these modes are very easily mistaken for each other, before attempting to correlate test modes with the analytical modes for a complex structure, one must be able to "sort out" the local modes from the overall structural modes.

The generalized mass contribution (GMC) technique presented here provides a tool for determining the characteristics of each mode shape by determining the distribution of kinetic energy throughout a mode. With this information, the analyst can then differentiate between overall structural and local modes. In addition, GMC distributions for both test and analytical modes can be directly compared in attempting to correlate the modes.

The technique for determining GMC distributions is commonly employed in vibration analyses. The essential purpose here is to illustrate the use of these distributions as a tool for correlating test and analytical vibration modes.

The following discussion reviews the method for determining GMC distributions The results of a simple beam analysis are presented to illustrate the method. Finally, the application of the method of the correlation of Skylab vibration modes is presented.

DETERMINATION OF GMC DISTRIBUTIONS

A GMC distribution indicates the contribution of each discrete structural degree of freedom to the total generalized mass for each of the normal modes of a vibrating structure. The determination of this distribution is based on the kinetic energy expression for the vibrating structure given as

$$KE = 1/2 \left\{\dot{q}\right\}^T [M] \left\{\dot{q}\right\} \quad (1)$$

where $\dot{q}$ is a column matrix of discrete velocities at a finite number of points located throughout the structure, and M is a mass matrix representing the vibrating mass at each of these points. For a linear structure, the velocity at any point in the structure, $\dot{q}_i$, can be expressed as the sum of the velocities in each of the normal vibration modes for the structure, that is

$$\dot{q}_i = \sum_{j=1}^{N} \dot{q}_i^j \quad (2)$$

where the superscript refers to a normal mode number. Transforming equation (2) to modal coordinates and using matrix notation gives

$$\left\{\dot{q}\right\} = [\phi] \left\{\dot{\xi}\right\} . \quad (3)$$

In equation (3), $[\phi]$ is a matrix of orthogonal mode shapes for the structure, and $\{\dot{\xi}\}$ is a column matrix of modal velocities with each element corresponding to the generalized velocity of the modes. Each column in $[\phi]$ is a mode shape containing the modal amplitudes for each discrete degree of freedom in the mathematical model. These modal amplitudes can be normalized in an arbitrary manner, and it is convenient to normalize them so a generalized mass of unity is obtained for each mode. Substituting equation (3) into the kinetic energy expression (eq 1) gives

$$KE = 1/2 \left\{\dot{\xi}\right\}^T [\phi]^T [M] [\phi] \left\{\dot{\xi}\right\} . \quad (4)$$

The inner triple matrix product in equation (4) is defined as the generalized mass matrix. If the mode shapes have been previously normalized to give unity generalized masses, this triple product will yield an identity matrix. If the modes have not been previously normalized in this manner, it is accomplished by letting

$$[GM] = [\phi]^T [M] [\phi] \quad (5)$$

where [GM] is a diagonal matrix of generalized masses for each mode. The normalization process consists of dividing each modal amplitude in a given mode by the square root of the generalized mass corresponding to that mode. A typical normalized modal amplitude for the ith degree of freedom in the jth mode is

$$\phi_{ij}^{\text{Norm}} = \phi_{ij}^{\text{Non norm}} \Big/ \left(GM_{jj}\right)^{1/2} . \quad (6)$$

The GMC matrix is calculated by first letting

$$\underset{[D]}{nxm} = \underset{[M]}{nxn} \; \underset{[\phi]}{nxm} \quad (7)$$

where n is the total number of discrete degrees of freedom and m is the total number of modes. It can be seen that equation (7) represents a portion of the generalized mass triple matrix product contained in equation (4). That is, if equation (7) is premultiplied by the transpose of the modes matrix, the unity generalized mass matrix will result. If, however, we only multiply corresponding elements of the modes matrix (nontransposed) and the matrix result of equation (7), the GMC matrix is obtained. That is

$$GMC_{ij} = \phi_{ij} D_{ij} . \quad (8)$$

Each column in the GMC matrix corresponds to a given mode shape. Each element in that column corresponds to a discrete degree of freedom, and the value of that element is that degree of freedom's "generalized mass contribution" toward the total generalized mass value of 1.0. The column, taken in total, represents the generalized kinetic energy distribution of the degrees of freedom for that mode.

It can now be seen that, if both analytical and test mode shapes are normalized (per equation 6) using the same kernel mass matrix, the generalized mass contributions for analysis and test may be directly compared.

To provide a simple example, a uniform beam with an attached concentrated mass Fig. 1(a) was analyzed. The purpose of this example is to demonstrate the value of the GMC matrix in evaluating the dominant characteristics of mode shapes. Plots of the first two elastic modes for this system are shown in Figures 1(b) and (c). It can be seen that both shapes exhibit "first bending" characteristics in the beam portion of the system, with the concentrated mass first in phase and then out of phase with the beam. Examination of the mode shape plots does not readily reveal where the dominant motions lie. To determine this, GMCs were calculated for each mode. The individual degree of freedom GMCs for the beam were summed to determine the total beam contribution in each mode. The results, as shown in Figures 1(b) and (c), indicate that the first elastic mode is dominated largely by the response of the concentrated mass (GMC of 0.73), while the second mode is dominated by the beam with a total GMC of 0.78. For a complex structural system containing many "local" systems such as the concentrated mass in this example, a GMC calculation based on the analytical model is of great value in determining whether a given "local" system should be instrumented for a modal survey of the structure in the laboratory. In the above example, if the concentrated mass were not instrumented during modal testing, only the beam portion of the mode shapes would be

measured and correlation with analytical shapes could be quite difficult since the first and second modes exhibit similar shapes along the beam.

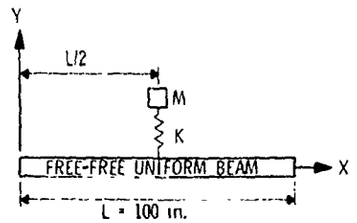

BEAM EI = 8.333×10^9 lb-in.^{2}

TOTAL BEAM MASS = $20.0 \frac{\text{lb-s}^2}{\text{in.}}$

$M = 1.0 \frac{\text{lb-s}}{\text{in.}}$

$K = 0.146 \times 10^6$ lb/in.

(a) UNIFORM BEAM EXAMPLE

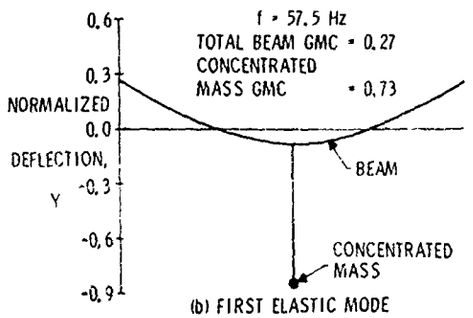

(b) FIRST ELASTIC MODE

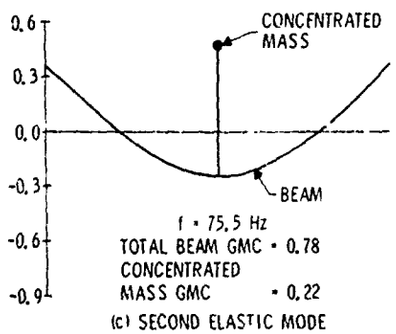

(c) SECOND ELASTIC MODE

Fig. 1 - Uniform Beam with Concentrated mass

USE OF GMC MATRICES IN MODAL SURVEY TESTING

Prior to starting a modal survey test, mode shapes derived from a mathematical model of the structure to be tested are usually available. If a GMC matrix is calculated using the analytical modes and mass matrix, the results can be used to determine the number of accelerometers required and their locations in the structure. That is, the GMC matrix provides information as to which portions of the structure have significant contributions to the total kinetic energy in each of the analytical modes included in the test frequency range. Since practical limitations in test instrumentation usually require compromises in the total number of degrees of freedom to be measured, a study of the analytical GMC matrix will help ensure that the most significant degrees of freedom are retained for measurement.

After completing testing, a GMC matrix can be calculated for the test modes and compared with a corresponding matrix for the analytical modes as an aid to the correlation effort.

The correlation phase of modal testing requires a large amount of engineering judgment. The GMC matrix comparison aids the engineer in making the best judgments by providing a tool that goes beyond direct mode shape plot comparisons. However, it is emphasized that since the GMC matrix provides no information in regard to relative phasing of the various structural components in a given mode, the plot comparisons must be employed in conjunction with the GMC matrices.

If the mathematical model of the test structure is not suspected to be grossly inadequate, a "least-squares" method of comparing test and analytical GMC matrices can be satisfactorily employed. This method consists of determining the sum of the squares of the differences in the GMCs for each test mode, taken one at a time, with every analytical mode. The analytical mode for which the sum of the squares is a minimum would constitute the "best fit" of the GMCs for the test mode. To perform this calculation, a column matrix of GMCs for a given test mode is selected and subtracted from every column of the analytical modes GMC matrix. This results in a matrix of GMC differences having the same size as the analytical GMC matrix. Each element in the differences matrix is then squared and the sum of all the elements in each column of the result is calculated. The column that yields the least sum will correspond to the analytical mode having the "best fit" of GMCs for the particular test mode. The resulting information provides the analyst a starting point in the correlation task.

The GMC matrix can be further used by summing, for example, all the GMCs corresponding to the torsional degrees of freedom in each mode to determine if the mode is largely a torsional mode. Or, if the structure is composed of several subassemblies, the GMCs for the degrees of freedom contained in each subassembly can be summed in each mode to determine the relative participations.

APPLICATION TO SKYLAB MODAL SURVEY RESULTS

Extensive modal survey tests of two full-scale Skylab configurations were performed at the Manned Spacecraft Center in Houston, Texas during the first half of 1972. The configurations tested were the launch and orbit configurations shown in Figures 2 and 3. It can be seen that in the orbital configuration, the payload shroud is not present, the Apollo telescope mount has been rotated 90 degrees to the deployed position, and an Apollo command and service module has been axially docked to the multiple docking adapter. During test, each configuration was supported by a low-frequency air spring system, rendering the end conditions to be essentially free-free.

The modal survey of the launch configuration was first in the test sequence and 24 unique test modes in the 0- to 50-Hz frequency range were obtained. Two-hundred degrees of freedom in each mode were measured using a corresponding number of accelerometers. During the posttest correlation study for the launch configuration test modes the need for GMC calculations developed. Due to the complexity of the launch configuration test modes and the large number of degrees of freedom in each mode, it became difficult to discern the essential dominant characteristics of each mode shape by simply inspecting two-dimensional mode shape plots. Because of shaker placement during testing, it was expected that the test modes would not be "local" in nature but would be overall structural modes exhibiting motions in all areas of the structure. However, as the correlation study progressed, it became increasingly clear that some of the test modes were possibly local in nature. To resolve this question, GMC calculations were performed on the test modes. The results showed that many of the modes did display significant local characteristics. For example, four of the test modes had total GMCs for the six fixed airlock shroud oxygen tanks ranging from 0.59 to 0.71. Many other modes contained significant contributions from these tanks, ranging from 0.20 to 0.36 of the generalized masses of unity.

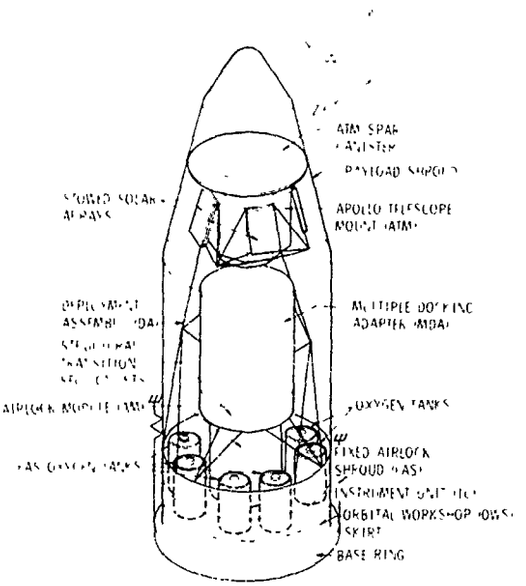

Fig. 2 - Skylab launch configuration for modal survey testing

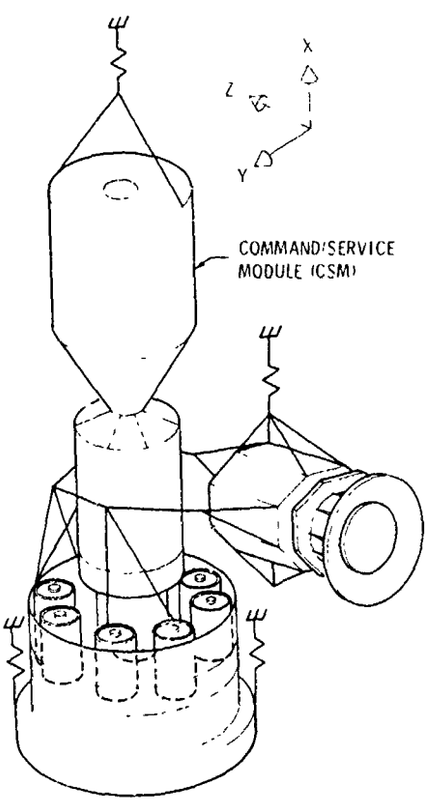

Fig. 3 - Skylab orbital configuration for modal survey testing

As the test mode GMC results were being studied, it was found inconvenient and time-consuming to examine the GMC matrix in the usual form of a computer printout. As a result, a small computer program that arranged the GMC matrix into convenient tables for each mode was written. One of these tables showed a summary of GMCs for various major areas, or components, of the structure by indicating the GMC sums for each degree of freedom contained in each component. A second table generated indicated the GMC for each individual degree of freedom at each collocation point with a description of the collocation point. Hence, if it was desired to determine which component degrees of freedom contributed to a particular component sum given in the first table, the second table provided this information. Examples of the two types of tables are shown in Table 1(a) and (b). Table 1(a) shows GMC summaries for seven major components of the Skylab launch configuration. The first portion of this table indicates the GMC sums by degrees of freedom for each component. For example, the numbers in the column labeled (DX) represent the sums of the GMCs for all the X degrees of freedom. The second portion of the summary table indicates the total GMC for each component and is the sum for all the degrees of freedom of each component. Table 1(b) gives the GMCs for degrees of freedom corresponding to Table 1(a) summary. The test mode represented in these tables was selected as an example of a mode that could easily be misinterpreted by examining only the mode shape plots. Referring to the GMC summary Table 1(a) , it can be seen that the six FAS oxygen tanks contribute a GMC of almost 0.71, largely in the Y and Z degrees of freedom. However, this is not apparent in the two-dimensional plots shown in Figure 4(a) and (b). Figure 4(a) is a plot of the normalized Y deflections versus station for the payload shroud/FAS/IU/OWS portion of the structure, while Figure (b) is a corresponding plot of the normalized Z deflections. These plots indicate apparent bending in the Y and Z directions of the plotted components. It can be seen that the FAS tank deflections appear to be significant but that the relative significance of the bending deflections is not apparent. The question is immediately answered by the GMC summary table indicating that the bending deflections represent a total GMC of about 0.14. The mode is therefore classified as local in nature due to the large GMC of the FAS tanks. GMC tables were also generated for the analytical mode shapes and used along with the mode shape plots for determining correlating modes.

As a result of the knowledge gained in using GMCs to correlate the launch configuration test modes, the correlation effort following the subsequent orbital configuration test could be performed in a rapid and systematic manner. In addition to generating GMC tables for the orbital configuration test and analytical modes the least-squares GMC fit technique previously described was employed with excellent results. The least-squares results were used as a starting point in the correlation effort followed by mode shape plot and GMC distribution comparisons. Many of the least-squares GMC fit results were further verified by performing an orthogonality calculation of the test modes with the analytical modes ("cross-orthogonality") after normalizing each set to the same mass matrix. This calculation indicated significant coupling between correlating modes. It should be noted that neither of these techniques would have yielded satisfactory results if the analytical modes or the mass matrix were grossly in error.

An example of the orbital configuration correlation results is shown in Figure 5. The plots shown in Figures 5(a) and (b) are the test and analytical centerline bending deflections in the X-Z plane of the main portion of the structure from the OWS skirt forward through the CSM. Figure 5(a) is the test mode plot while Figure 5(b) is a corresponding plot for the correlating analytical mode. These plots represent only a portion of the entire mode shape but serve to illustrate the excellent shape correlation, which is verified by the agreement in the corresponding GMC summary tables shown in Table 2(a) and (b) directly below the plots.

CONCLUSION

The GMC matrix is an invaluable tool in correlating test and analytical vibration modes and provides real insight in determining the dominant characteristics of the individual modes. The use of GMC matrices in correlating Skylab modal survey test modes provided a systematic approach and increased confidence in the results. Further modal survey tests could utilize on-line GMC calculations as the test modes are acquired. The correlation effort could then be commenced during actual testing.

ACKNOWLEDGEMENT

The authors wish to express their appreciation to Messrs. R. F. Hruda, H. D. Wilkening, and C. W. White of the Martin Marietta Corporation for their contributions and guidance in developing the systematic utilization of generalized mass contributions for correlating test and analytical vibration modes.

TABLE 1
Generalized Mass Contributions

(a) Launch Configuration Modal Survey

Test Modes Generalized Mass Contribution Summary

Test Mode No. 10 Test Frequency = 9.208 Hz

Component Name	GMC (DX)	GMC (DY)	GMC (DZ)	GMC (TX)	GMC (TY)	GMC (TZ)
Shroud/FAS/IU/OWS/SS	.0002	.0609	.0623	.0056	.0041	.0064
6-FAS 02 Tanks	.0248	.2783	.2942	.0565	.0268	.0262
Deployment Assembly	.0015	.0204	.0069	.0000	.0000	.0000
MDA/STS/AM	.0008	.0252	.0309	.0025	.0074	.0049
6-AM N2 Tanks	.0009	.0107	.0302			
ATM-Rack, CMGS, SAS	.0000	.0034	.0024	.0001	.0002	.0000
ATM-Spar/Can/GRA	.0000	.0013	.0032	.0000	.0005	.0003
SUM	.0282	.4002	.4301	.0647	.0390	.0378

Total GM Contribution for each Component	
Shroud/FAS/IU/OWS/SS	.1395
6-FAS 02 Tanks	.7068
Deployment Assembly	.0288
MDA/STS/AM	.0717
6-AM N2 Tanks	.0418
ATM-Rack, CMGS, SAS	.0061
ATM-Spar/Can/GRA	.0053

(b) Generalized Mass Contributions by Degree-of-Freedom

Launch Configuration (DTA)

Test Mode No. 10 Test Run No. 200

Test Frequency = 9.208 Hz

Node No.	GMC (DX)	GMC (DY)	GMC (DZ)	GMC (TX)	GMC (TY)	GMC (TZ)	Node Description
1	.0001	.0520	.0454	.0003	.0023	.0010	OWS Skirt/Base Ring
2	.0000	.0016	.0033	.0001	.0008	.0005	OWS/IU I/F
3	.0000	.0006	.0012	.0000	.0002	.0002	IU/FAS I/F
4	.0001	.0061	.0101	.0047	.0007	.0043	FAS/PLS/DA/AM I/F
5	.0000	.0000	.0019	.0000	.0000	.0001	Payload Shroud
6	.0000	.0000	.0001	.0000	.0000	.0000	Payload Shroud
7	.0000	.0005	.0002	.0004	.0001	.0001	PLS/ATM I/F
8	.0000	.0001	.0000	.0001	.0000	.0000	Payload Shroud
9	.0000	.0000	.0001	.0000	.0000	.0001	Payload Shroud Nose
10	.0032	.0649	.0016	.0019	.0017	.0010	FAS 02 Bottle
11	.0040	.1017	.0323	.0313	.0031	.0148	FAS 02 Bottle
12	.0011	.0189	.0000	.0045	.0047	.0014	FAS 02 Bottle
13	.0011	.0026	.0387	.0064	.0038	.0028	FAS 02 Bottle
14	.0079	.0535	.1346	.0123	.0135	.0038	FAS 02 Bottle
15	.0075	.0367	.0870	.0001	.0000	.0024	FAS 02 Bottle
16	.0006	.0000	.0000	.0000	.0000	.0000	DA EREP Package
17	.0000	.0112	.0008				DA Trunnion
18	.0009	.0023	.0045				DA Trunnion
19		.0069	.0016				DA/ATM Support Frame
20	.0000	.0064	.0083	.0001	.0002	.0001	AM Tunnel
21	.0000	.0046	.0068	.0007	.0005	.0007	AM Tunnel
22	.0000	.0038	.0063	.0007	.0010	.0008	AM/STS I/F
23	.0008	.0010	.0016	.0005	.0001	.0000	STS/MDA I/F
24	.0000	.0021	.0014	.0005	.0038	.0026	MDA
25	.0000	.0073	.0065	.0000	.0018	.0007	MDA
26	.0000	.0053	.0000				AM N2 Tank T3A
27	.0003	.0030	.0001				AM N2 Tank T3F
28	.0001	.0010	.0124				AM N2 Tank T2A
29	.0003	.0011	.0058				AM N2 Tank T2F
30	.0001	.0003	.0070				AM N2 Tank T4F
31	.0001	.0000	.0049				AM N2 Tank T4F
32	.0000	.0034	.0024	.0001	.0002	.0000	CG ATM Rack + SAS
33	.0000	.0013	.0032	.0000	.0005	.0003	CG Spar/Canister
SUM	.0282	.4002	.4301	.0647	.0390	.0378	

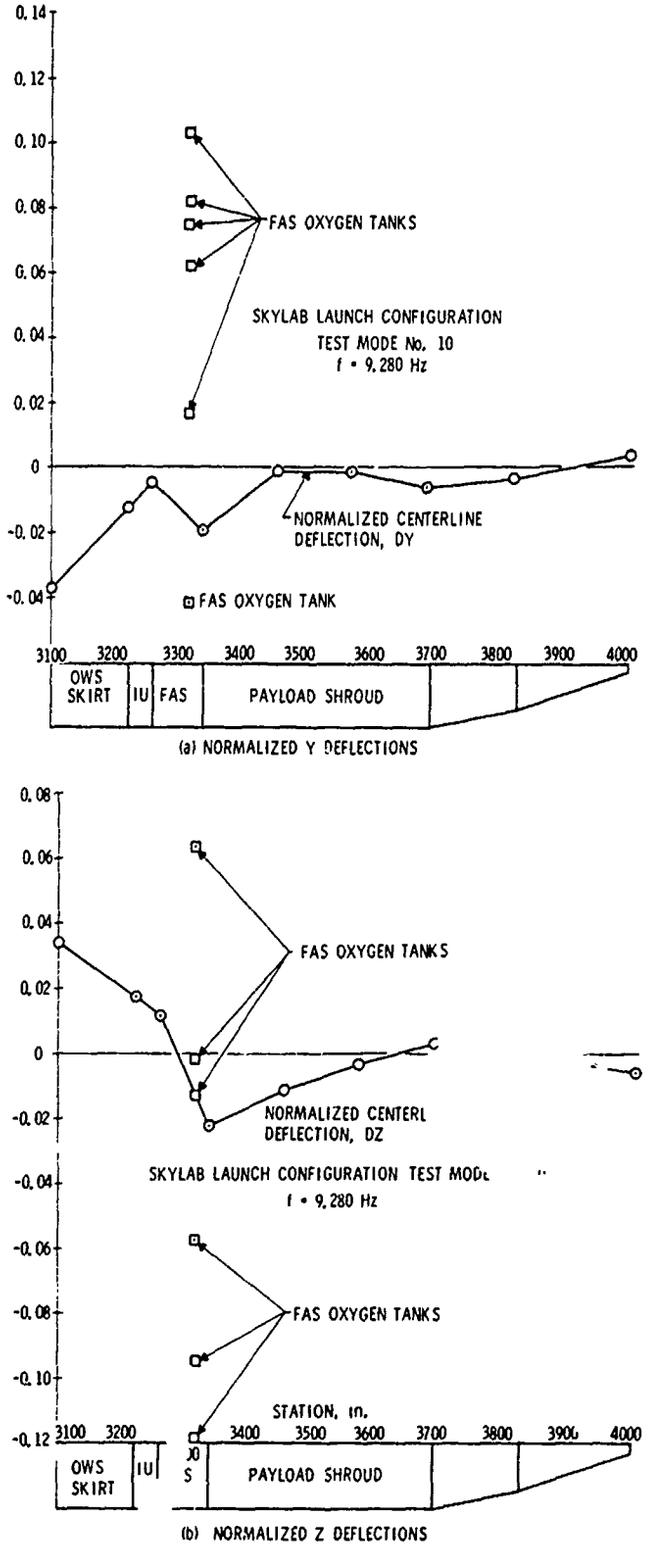

Fig. 4 - Partial plot of Skylab launch configuration test mode 10

TABLE 2
GMC Summaries

(a) Orbital Configuration Modal Survey

Test Mode Generalized Mass Contribution Summary

Test Mode No. 3 — Test Frequency - 1.31 Hz

Component Name	GMC (DX)	GMC (DY)	GMC (DZ)	GMC (TX)	GMC (TY)	GMC (TZ)
BR OWS Skirt IU FAS	.0180	.0001	.0152	.0000	.0102	.0000
6-FAS 02 Tanks	.0209	.0000	.0025			
MDA STS/AM	.0112	.0000	.0130	.0000	.0007	.0000
6-AM N2 Tanks	.0034	.0000	.0007			
Command Service Mod	.0135	.0001	.4132	.0004	.0078	.0013
Deployment Assembly	.0022	.0000	.0097			
ATM-Rack, CMGS, 4-SAS	.1823	.0026	.1187	.0000	.0091	.0000
ATM-Spar Center	.0536	.0001	.0246	.0000	.0026	
ATM-GRA Can Center	.0506	.0000	.0163	.0000	.0033	.0000
SUM	.3568	.0028	.6140	.0004	.0247	.0013

Total GM Contribution for each Component	
BR OWS Skirt/IU FAS	.0435
6-FAS 02 Tanks	.0234
MDA STS AM	.0249
6-AM N2 Tanks	.0042
Command Service Mod	.4362
Deployment Assembly	.0129
ATM-Rack, CMGS, 4-SAS	.3037
ATM-Spar Center	.0610
ATM-GRA Can Center	.0702

(b) Orbital Configuration Modal Survey

Analytical Modes Generalized Mass Contribution Summary

Analytical Mode No. 7 — Analytical Frequency - 1.372 Hz

Component Name	GMC (DX)	GMC (DY)	GMC (DZ)	GMC (TX)	GMC (TY)	GMC (TZ)
BR OWS Skirt/IU FAS	.0152	.0000	.0315	.0000	.0188	.0000
6-FAS 02 Tanks	.0192	.0000	.0020			
MDA/STS/AM	.0091	.0000	.0184	.0000	.0011	.0000
6-AM N2 Tanks	.0024	.0000	.0007			
Command Service Mod	.0132	.0001	.4367	.0019	.0090	.0000
Deployment Assembly	.0023	.0000	.0118			
ATM-Rack, CMGS, 4-SAS	1591	.0019	.1125	.0000	.0000	.0000
ATM-Spar Center	.0460	.0000	0216	.0000	.0016	
ATM-GRA Can Center	.0412	.0000	.0190	.0000	.0028	.0000
SUM	.3078	.0022	.6546	.0019	.0335	.0000

Total GM Contribution for each Component	
BR OWS Skirt IU FAS	.0060
6-FAS 02 Tanks	.3212
MDA STS AM	.0286
6-AM N2 Tanks	.0031
Command Service Mod	.4609
Deployment Assembly	.0141
ATM-Rack, CMGS, 4-SAS	.2736
ATM-Spar Center	.0624
ATM-GRA Can Center	.0631

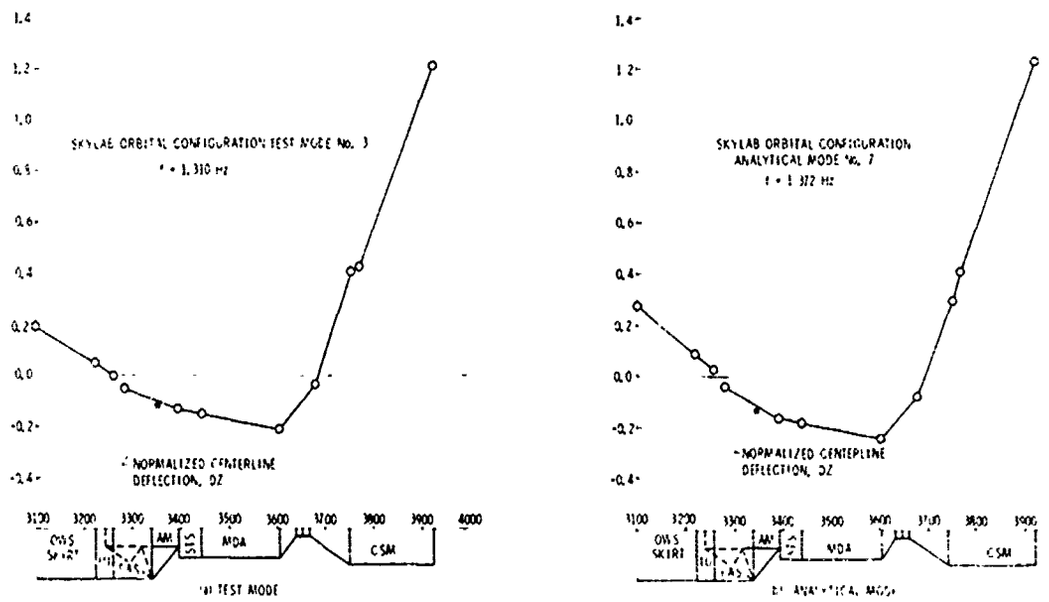

Fig. 5 - Partial plot of Skylab orbital configuration test mode 3

VIBRATION AND ACOUSTIC TESTS OF THE RECONFIGURED APOLLO SERVICE MODULE ADAPTED FOR SKYLAB MISSIONS

Richard A. Colonna
NASA Manned Spacecraft Center
Houston, Texas

Dan F. Newbrough
General Electric Company
Houston, Texas

and

James R. West, Jr.
North American Rockwell Corporation
Downey, California

Substantial modifications were made to the Apollo service module (SM) to adapt it for use on Skylab missions. These modifications required that structural integrity be demonstrated by a series of vibration and acoustic tests and that analytically developed random and sinusoidal test requirements be verified.

Extensive vibration and acoustic tests were conducted on the Apollo SM and the techniques used for the Skylab SM were similar. The Skylab SM acoustic tests were not conducted in the same reverberant test facility used for the other Skylab payload modules, but were conducted using the NASA's Manned Spacecraft Center Vibration and Acoustic Test Facility progressive wave mode of excitation. Sinusoidal vibration tests were accomplished using combinations of electrodynamic shakers. Data acquired from the Skylab SM acoustic and vibration tests were use to refine and determine test requirements for new Skylab SM components and experiments.

This paper discusses the vibration and acoustic tests conducted, the effectiveness of these tests, and the data evaluation used to develop component and subassembly vibration test requirements.

INTRODUCTION

The Skylab command and service modules are subjected to severe vibration and acoustic environments during launch and boost. Although these dynamic environments have been measured and test requirements verified on Apollo flights, the changes to the service module to adapt Apollo hardware for Skylab missions made prediction of vibration requirements and demonstation of structural adequacy difficult without vehicle-level dynamic tests. The vibration and acoustic tests briefly described herein were used to demonstrate Skylab service module structural integrity for the vibration environment, and to verify analytically developed random vibration criteria for equipment testing.

SPACECRAFT DESCRIPTION

The Skylab spacecraft, as shown in Fig. 1, is similar in exterior appearance to the Apollo spacecraft, consisting of two modules stacked end-to-end. The command module contains the flight crew with associated life support, spacecraft control, stowage, docking, and landing systems. The service module contains the propulsion, electrical power and environmental control systems as well as some scientific experiments. For the Skylab mission, the command and service modules were modified to support extended earth orbital missions. Changes to the command module were primarily associated with components, while primary and secondary structures remained the same. None of these component changes required retesting of the command module at the structural assembly level. On the other hand, modifications were quite significant for the service module. The Apollo "J" mission scientific experiments and cryogenic storage tanks, located in Bay 1 of the service module, were replaced with additional propellant storage for the reaction control system (RCS), as well as a scientific equipment shelf and a battery shelf as shown in Fig. 2. The service propulsion

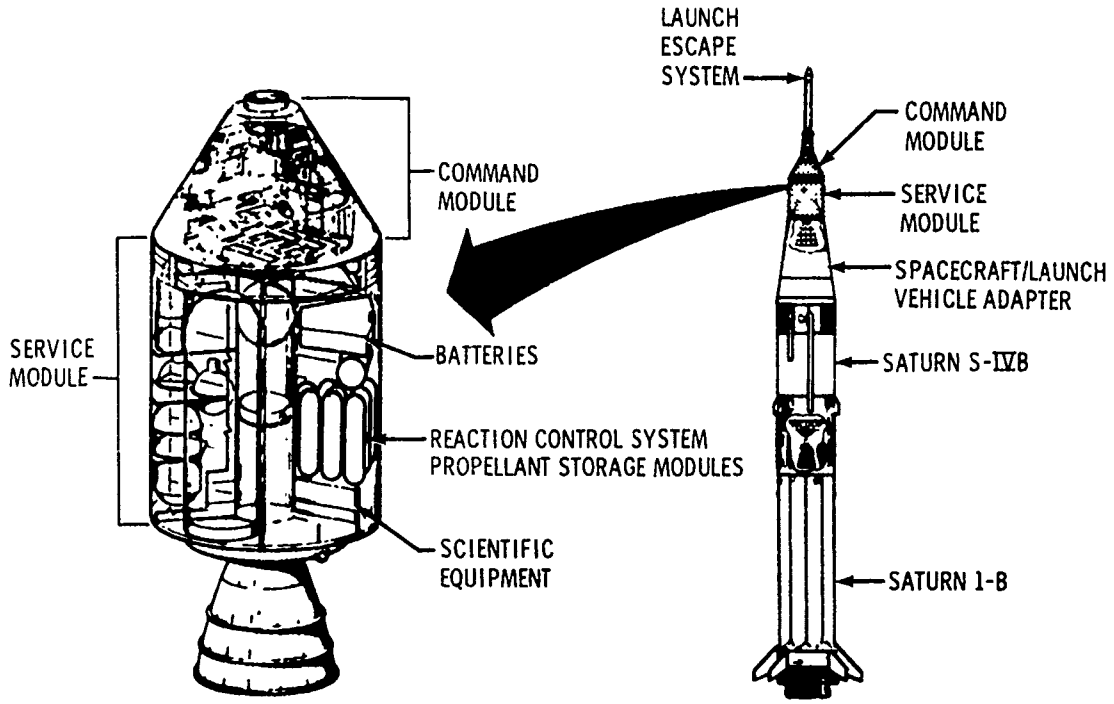

FIGURE 1.- SKYLAB SPACECRAFT AND LAUNCH VEHICLE.

system (SPS) propellant required for an earth orbital mission is significantly less than that needed for lunar orbital operation, and allows two of the four SPS propellant tanks and one of the two helium pressurization tanks for the SPS to be removed from the Skylab service module. One of the three fuel cells located in Bay IV and the "J" mission batteries on the Bay IV aft bulkhead were also removed These changes completely reconfigured service module Bay I and required significant changes to plumbing lines and electrical cables throughout the service module. The service module configuration changes were sufficient to warrant vibration and acoustic testing of a fully assembled Skylab service module.

DYNAMIC ENVIRONMENTS

It should be noted that the Skylab spacecraft will be launched on the Saturn IB booster, whereas the Apollo spacecraft were launched on the Saturn V launch vehicle. However, the vibration and acoustic environments induced by both launch vehicles are generally similar and Apollo design and test requirements account for both Saturn launch vehicles. The vibration induced in the command and service modules during atmospheric flight is intense and the content is both random and sinusoidal. Detailed descriptions of the command and service module vibration environments are presented in Refs. 1, 2, 3, and 4. Initial vibration test requirements for Skylab hardware were based on extrapolations of Apollo requirements which utilized scaling factors derived from the differences in mass and stiffness for the Apollo and Skylab primary structure.

SKYLAB VIBRATION AND ACOUSTIC TESTS

Because of the extensive modifications to the Apollo service module to adapt it for the Skylab mission, an Apollo service module, modified to the Skylab configuration, was subjected to a series of vibration and acoustic tests in the Manned Spacecraft Center (MSC) Vibration and Acoustic Test Facility. These tests were conducted to verify the design of Skylab structural elements and to refine predicted vibration criteria for new Skylab functional components. In addition, these tests provided margin to verify that Apollo components will function for the new Skylab application. The service module used for this test, designated SM 3D-2, was originally Apollo SM 105, described in Ref. 3. Bay I of the service module was modified to include:

a. A propellant storage module (PSM) and mounting provisons. (The tanks were filled with referee fluids to simulate the launch loading.)

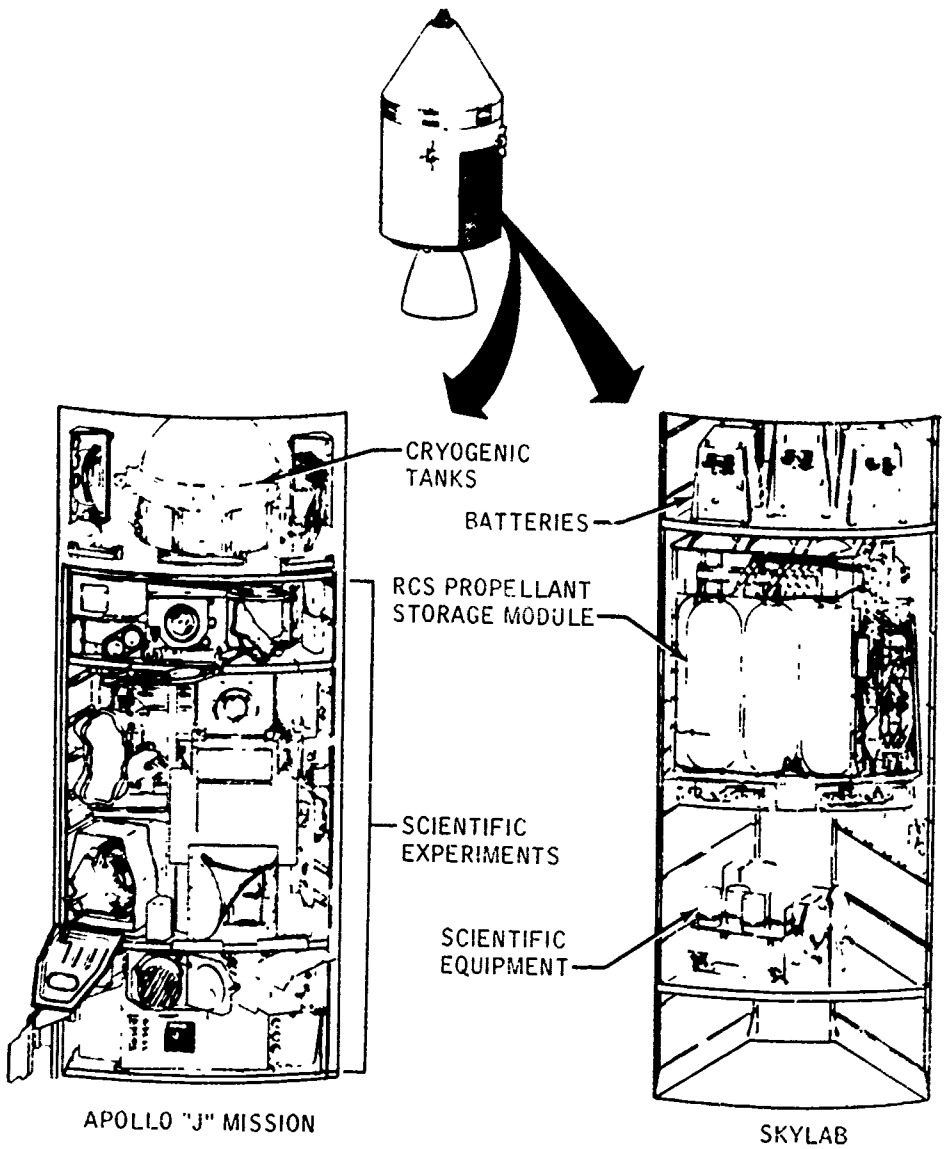

FIGURE 2.- SERVICE MODULE BAY I - APOLLO "J" MISSIONS AND SKYLAB

b. A scientific experiment shelf with mass simulated experiments.

c. A battery shelf with the necessary battery cases containing ballast for mass simulation.

d. A new outer shell structural panel, reworked to include the battery and experiment access provision. Plumbing for the RCS propellant storage and portions of wire harnesses were also included on this panel.

Mass simulations of the RCS tanks and engines, mounted on the outer shell, were used at all four engine locations. At one of these locations, the new Skylab components and associated plumbing were included to provide an interface with the new propellant storage provisions. The additional plumbing and valves required

to distribute this propellant to the four engine locations was also installed.

Only one of the SPS helium tanks was installed, and the SPS engine used for this test did not have a nozzle extension. The SPS tanks in Bays II and V were filled with referee fluids to simulate the Skylab launch loading conditions.

INSTRUMENTATION

The instrumentation employed during testing consisted of piezoelectric accelerometers and microphones. All output signals for the acoustic and vibration measuring systems were recorded on magnetic tape. The data on each recorded channel consisted of calibration signals, instrumentation ambient noise floor signals, and the test data. More detailed descriptions of the characteristics of the data acquisition systems are presented in [illegible] 3.

A total of 180 accelerometers were used to measure vibration responses of primary and secondary structure and responses at the interfaces of new Skylab equipment support structures. A total of 32 microphones was used to measure and control the acoustic tests.

VIBRATION TESTS

Figure 3 shows the overall vibration test configuration. The test fixture was a ring constructed to be rigid in the frequency range of interest, 5 to 35 hertz. An air spring type suspension system was attached to the bottom of this ring. The service module was secured to the top of the ring, and the vibration thrusters were attached as shown in Figure 3. The suspension system consisted of four air springs located at 90-degree intervals around the ring. The thruster system for longitudinal excitation consisted of four Ling model 310 thrusters attached to the ring. For lateral excitation, two thrusters were attached to the aft end of the service module on primary structure.

Selection of the sinusoidal vibration spectrum for control was difficult because of uncertainties in the response of the test structure. From evaluation of Apollo flight data, it was determined that bending or longitudinal modes of the launch vehicle would produce sinusoidal amplitudes of the spacecraft no greater than 0.2g peak. The flight data also indicated that sinusoids could occur up to 35 hertz and analysis indicated that no component resonances existed below 5 hertz. Therefore, the control procedure that evolved was to subject the service module to a 0.25g peak swept sinusoidal vibration environment over the frequency range of 5 to 35 hertz at a rate of 0.5 octave per minute in the three major axes; longitudinal (X-axis), radial (R-axis: parallel to the horizontal Bay I centerline), and tangential (T-axis: orthogonal to the X and R axes and tangential to the horizontal Bay I centerline). The acceleration amplitude was controlled at either the service module aft bulkhead or forward bulkhead (whichever was greater). Table 1 summarizes the vibration tests performed in each of the three axes.

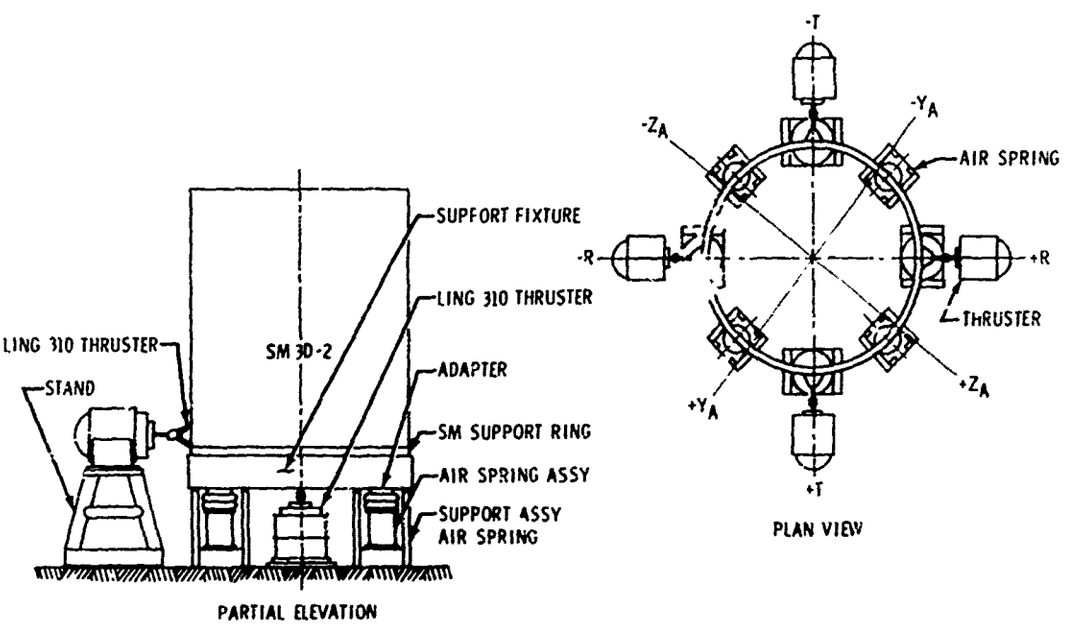

FIGURE 3. - SM 3D-2 VIBRATION TEST CONFIGURATION

TABLE 1.- SINUSOIDAL SWEEP VIBRATION TESTS[a]

Run number	Axis	Planned frequency band, Hz	Test run time, sec	Sweep rate, octaves/min	Comments
1	X	5-35	292.229	0.568	Successful test.
2	R	5-35	292.230	0.568	Successful test.
3	T	5-35	253.623	0.568	Aborted at a frequency of 27.06 hertz.
4	T	10-35	285.846	0.2845	Aborted at a frequency of 25.90 hertz.
5	T	10-35	230.012	0.2845	Aborted at a frequency of 25.72 hertz. Test article damaged.

[a]Input level for tests was 0.25g peak.

Testing in the X and R axes was successfully completed with no anomalies. Three attempts were made to conduct the T-axis test, but anomalous conditions resulted in premature termination of each attempt. During the first two T-axis sweep tests, a resonant condition in the test setup caused test termination due to insufficient thruster control system capability. In the first attempt, the resonant buildup rate was greater than the response speed of the control system. Accordingly, the sweep rate was reduced. In the second attempt, the desired vibration level could not be maintained because of the inability of the amplifier to provide sufficient power to achieve the required thruster force levels. For the third attempt, one control accelerometer was relocated and an amplifier was connected in series with the original amplifier to provide a greater dynamic range. The last T-axis attempt was manually terminated at 25.72 hertz because the test article sustained damage at both thruster attach points.

ACOUSTIC TESTS

The Skylab service module acoustic tests were conducted in the MSC progressive wave acoustic test facility, Ref. 5, which allows variation in spectrum and levels in each of 16 separate ducts located around the service module. Figure 4 shows the test setup. The sound pressure levels used successfully to test the Apollo service module were also used for SM 3D-2. Comparison of flight-measured vibration environments with those generated during Apollo ground tests proved the validity of simulating flight noise levels with acoustic tests. The derivation of the test spectrum is treated in greater detail in Refs. 1, 2, and 3. The acoustic tests were controlled to the levels shown in Fig. 5 by monitoring microphones located in each duct, midway along the service module.

The service module outer shell damage sustained during the vibration testing was repaired to the extent necessary to proceed with the acoustic tests. Damaged parts were not replaced with new parts and the repair did not restore the structure to its full static strength. The service module was then subjected to a progressive wave acoustic environment, which produced random vibration levels in the service module outer shell equal to those experienced during the transonic and maximum dynamic pressure portions of flight. Table 2 summarizes the acoustic tests performed.

TEST RESULTS AND DATA EVALUATION

The service module outer shell structural failure was a result of improper application of the sinusoidal forcing function. The thruster force required to maintain the desired vibration level and the configuration of the thruster attachment (single point) to the test article resulted in local overloading of the structure. Evaluation of the data obtained during the attempts to conduct the T-axis test resulted in the conclusion that the test setup exhibited a unique resonance at approximately 26 hertz with an antinode condition at the thruster attachment plane. The single point attachment of the thrusters is unrealistic when compared to the actual load path across a spacecraft module-to-module interface. Vibration loads are transmitted over the entire interface, rather than at two discrete points. Therefore, the local loading conditions producing the outer shell failure were not considered representative of flight conditions, and the failure does not represent a structural design deficiency. Further attempts to complete the T-axis testing were terminated because of program schedule considerations. The risk involved with not having tested in the range of 25 to 35 hertz for the T-axis was considered to be very small since Apollo flight data indicated only minor

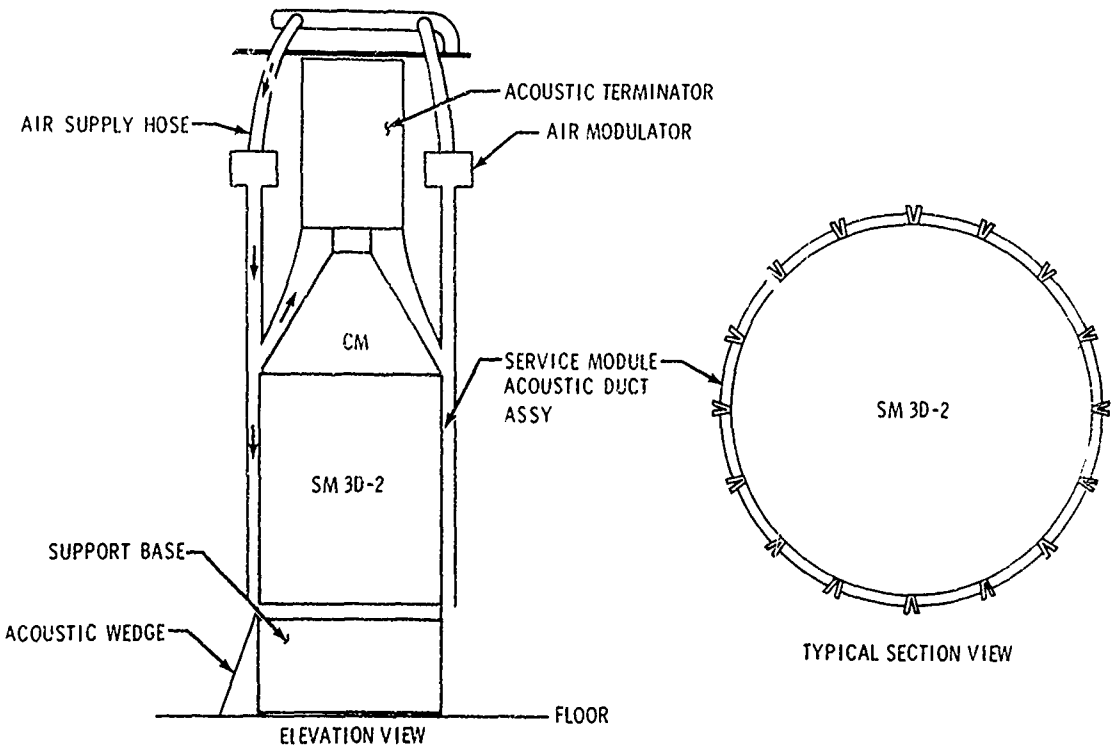

FIGURE 4.- ACOUSTIC TEST ASSEMBLY, MODIFIED SERVICE MODULE 3D-2.

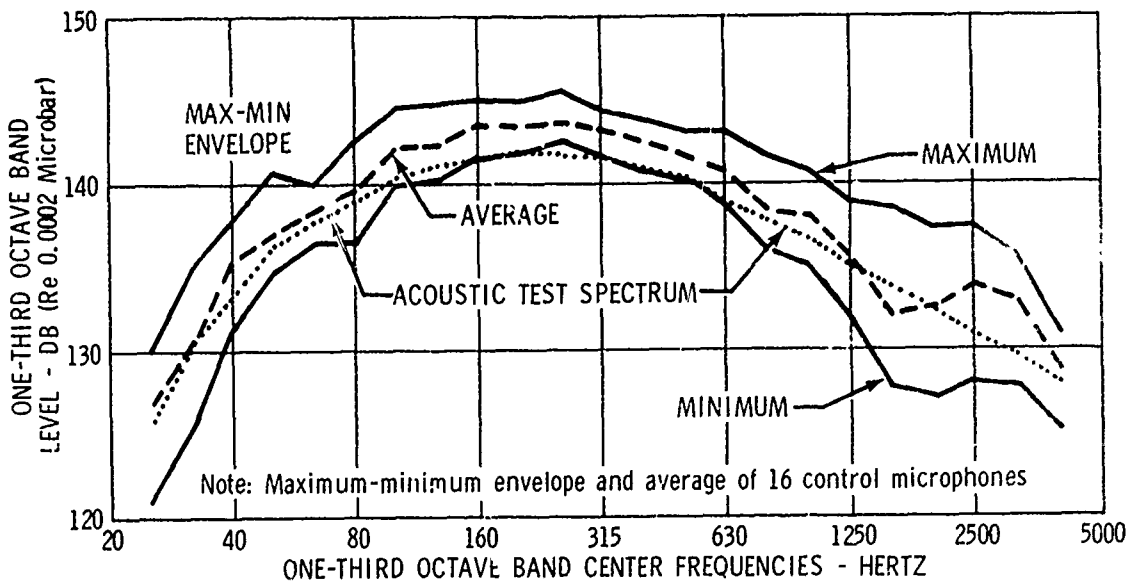

FIGURE 5.- ACOUSTIC SPECTRA - CONTROL DATA FROM SM 3D-2

TABLE 2.- ACOUSTIC TEST SUMMARY

Run number	Average overall sound pressure level, dB	Test run time, sec	Comments
1	146	60	Successful test.
2	152	15	Successful test; response measurement ranging confirmed.
3	152	15	The second short high-level run was made to optimize spectrum levels.
4	152	112	Successful long duration run; all required excitation time accumulated.
	156	10	
ACCUMULATED EXCITATION TIMES:			
	146	60	
	152	142	
	156	10	
	Total	212	

sinusoidal forcing functions in this frequency range. Moreover, the absence of equipment resonances over 25 hertz during the R-axis test and the similarity of the equipment in the . and R directions tended to indicate that T-axis resonances were unlikely.

Table 3 summarizes the sinusoidal vibration test criteria derived from the SM 3D-2 tests for the Bay 1 batteries, the scientific experiment shelf, and the PSM. These vibration criteria were established by adjusting the X, R, and T axis response vibration data for SM 3D-2 by the correction factors defined in Fig. 6. The correction factors represent a 2-sigma peak amplitude envelope of a composite of several measurements recorded on two Apollo flights. These factors were used to account for differences between SM 3D-2 vibration inputs and the in-flight service module sinusoidal forcing function.

The data recorded during the acoustic tests from all accelerometers were reduced to acceleration spectral density plots which were then grouped into composites to represent the maximum environments for each Skylab item of equipment on SM 3D-2. Figure 7 presents a typical composite of several measurements and the resulting envelope which was then used as the component random vibration test criteria.

The SM 3D-2 tests allowed derivation or refinement of vibration test requirements for approximately ten Skylab equipment items and assemblies.

CONCLUSION

The Skylab SM 3D-2 vibration and acoustic tests were successfully completed and the required vibration response data obtained. Structural integrity of the Skylab service module was demonstrated for the vibration environment and evaluations of measured data provided the necessary refinement to predicted Skylab equipment test requirements.

TABLE 3.- SKYLAB SINUSOIDAL TEST CRITERIA DERIVED FROM SM 3D-2 ACCELERATION DATA

Location	Amplitude		Frequency, Hz
	g peak	in. D.A.	
Inputs to batteries on bay I battery shelf			
X-axis		0.13	5 - 15
	0.15		15 - 20
	0.8		20 - 35
R-axis	0.25		5 - 15
	0.4		15 - 20
	0.25		20 - 35
T-axis		0.125	5 - 16
	1.5		16 - 20
	0.35		20 - 35
Inputs to equipment on scientific experiment shelf			
X-axis	0.25		5 - 14
		0.025	14 - 27.5
	1.0		27.5 - 32.5
	0.25		32.5 - 35
R and T axes	0.25		5 - 35
Inputs to PSM at structural attach points			
X, R, and T axes	0.25		5 - 35

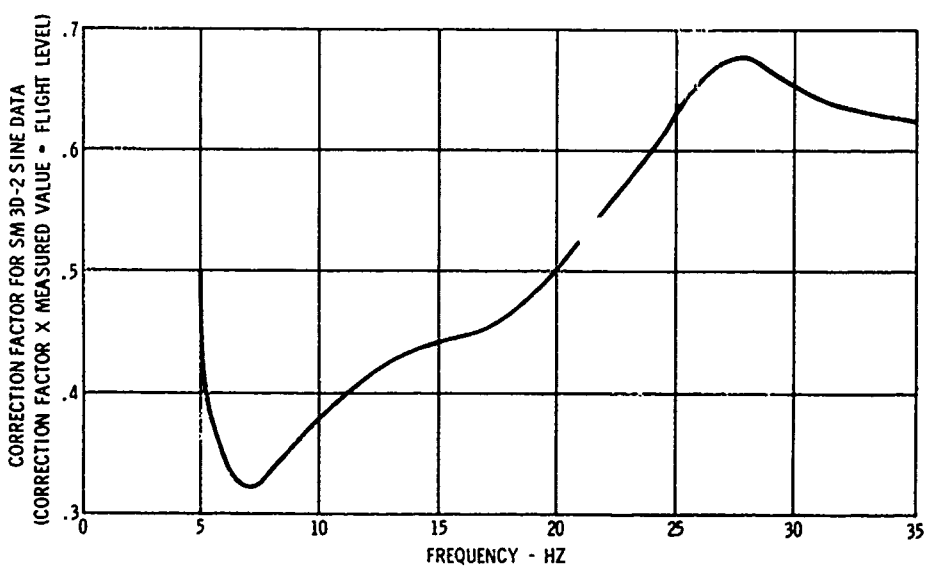

FIGURE 6.- CORRECTION FACTOR FOR SM 3D-2 SINUSOIDAL DATA

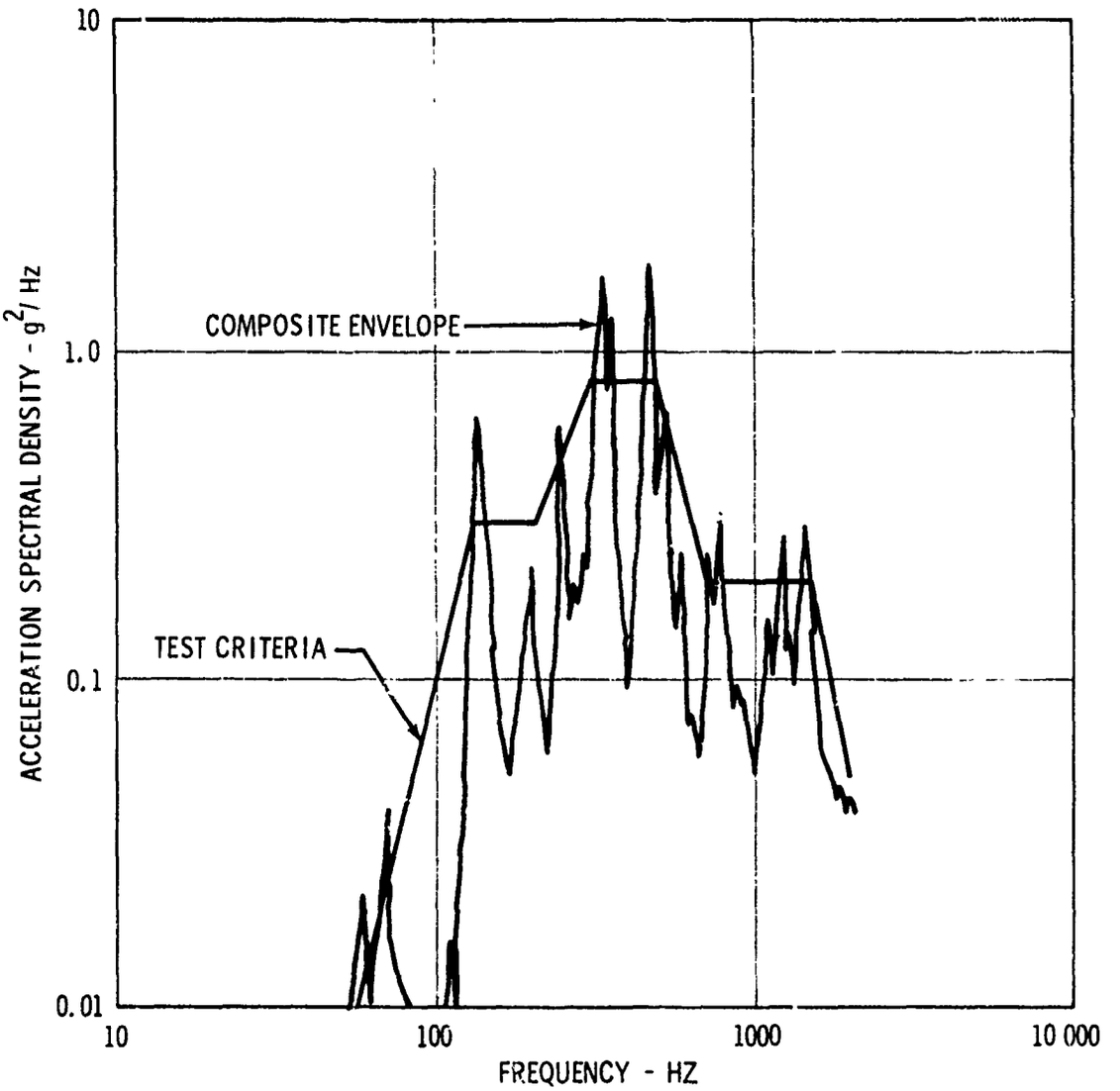

FIGURE 7. - RANDOM VIBRATION - TYPICAL COMPOSITE AND CORRESPONDING TEST REQUIREMENT ENVELOPE

REFERENCES

1. D.E. Newbrough, R.A. Colonna, J.R. West,Jr., "Development and Verification of the Apollo Command and Service Module Vibration Test Requirements," Shock and Vibration Bull. No. 37, Part 5, 1968.

2. D.E. Newbrough, Murray Bernstein, and Eugene F. Baird, "Development and Verification of the Apollo Lunar Module Vibration Test Requirements," Shock and Vibration Bull. No. 37, Part 5, 1968.

3. A.E. Chirby, R.A. Stevens, W.R. Wood, Jr., "Apollo CSM Dynamic Test Program,"Shock and Vibration Bull. No. 39, Part 2, 1969.

4. C.L. Stevens, "Vibration Response of Apollo Shell Structures to Acoustic and Aerodynamic Noise," Proceedings of the 13th Meeting of the Institute of Environmental Sciences, Vol. II, 1967.

5. R.J. Wren et al., "Concept, Design, and Performance of the Spacecraft Acoustic Laboratory," Shock and Vibration Bull. No.37, Part 5,1968.

VIBRATION TESTING AND ANALYSIS

THE EFFECTIVENESS OF ENVIRONMENT ACCEPTANCE TESTING ON THE APOLLO SPACECRAFT PROGRAM

Richard W. Peverley +
The Boeing Company
Houston, Texas

The Apollo environmental acceptance test program was unique in the the vibration and thermal test levels were generally uniform for all components regardless of the flight environment. Some components, in fact, were requalified because the acceptance levels exceeded the qualification levels. During a three year period, 14,994 individual components were subjected to thermal and vibration acceptance testing with a failure rate of 9.4%. Thermal testing appeared to be more effective with a failure rate of 17.5% as compared to 6.7% for vibration. Of the total 1,406 failures, 23.5% were caused by design inadequacies while 57% were caused by workmanship defects The remaining failures were caused by test errors. A survey was made of failures on components that had not been subjected to environmental acceptance testing. Less than 4% of those units not subjected to this type of test had a failure during ground checkout of a flight spacecraft that might have been detected during an environmental acceptance test. No flight failures were considered to have been an escape from the environmental acceptance test screen. A detailed description of the test program and the data analysis is presented in this paper.

INTRODUCTION

Environmental acceptance* tests are conducted to screen latent or incipient defects which might otherwise be undetectable in a quiescent environment. The environments utilized for this purpose on the Apollo Spacecraft Program were high and low temperature and vibration. The unique aspect of the Apollo tests was the selection of common environmental test levels which were the same for all components and were generally independent of the flight environment.

The environmental acceptance test levels were selected to be sufficiently severe to detect workmanship faults but passive enough to preclude the overstressing and weakening of a component.[1] It had become an accepted practice in the aerospace industry to conduct acceptance vibration tests at a nominal mission level. This practice assured that the design stresses were not exceeded since qualification levels were generally set at the design level plus some margin. Testing at the mission environment, however, did not always assure that parts were adequately stressed so that workmanship faults would be detected. This problem was particularly acute on the Apollo spacecraft where some qualification vibration levels were as low as 0.005 g^2/Hz. The philosophy adopted on the Apollo program was that the environmental acceptance tests were to be conducted to verify the quality of manufacturing; and, since quality must be uniform, the environmental acceptance tests levels must be the same for all components.

The Apollo environmental acceptance test program was initiated in mid-1967. At the time, several spacecraft were in various stages of assembly, and a number of components had completed their qualification tests. A decision had been made to test only selected components. The selection process was conducted through a series of joint reviews between NASA/MSC* and each of the major Apollo contractors (the criteria for this selection process are described in the following section of this paper). A total of 174 electronic, electrical, and electromechanical components were selected for acceptance vibration and 119 for thermal acceptance testing. All production units of these component types were then tested with the exception of those components that had been previously installed on spacecraft. Additional consideration was given to these components and some units were removed from the spacecrafts for environmental acceptance tests. From mid-1967 through mid-1970, a total of 14,994 components had been subjected to acceptance vibration tests and/or to acceptance thermal tests. In addition eight manned Apollo flights with three lunar landings had been completed. Thus, a sufficient quantity of failure data is available to properly assess the Apollo environmental acceptance test program. Prior to discussing the failure rate, however, a brief summary of the test requirements will be presented to insure that the significance of those failures is understood.

The background of this paper was described in papers by Mr. C. Low[1] and Mr. S. Simpkinson[2]. The purpose of this paper is to present any analysis of the additional data that have become available since their papers were written and to present some data in more detail.

* The Apollo environmental acceptance test program was the result of the joint effort of several organizations within NASA/MSC; primarily, the Apollo Spacecraft Program Office, the Engineering and Development directorate, the Reliability and Quality Assurance Office, and the Safety Office.

+ Formerly with the General Electric Company, Houston, Texas

TERMINOLOGY

CERTIFICATION

The combined testing and analysis required to determine that the design of the hardware meets the requirements.

QUALIFICATION

A test structured to demonstrate that design performance can be realized under design limit mission environments. Tests are conducted on a representative sample of production hardware and are part of the certification program.

ENVIRONMENTAL ACCEPTANCE

Test structured to demonstrate the manufacture is adequate to meet the requirements. This is a screening test conducted under specified environments on every production component.

QUALIFICATION/CERTIFICATION ENVIRONMENTS

Environmental test levels that simulate the maximum environmental conditions encountered in the specified design limit mission.

ACCEPTANCE ENVIRONMENTS

Environmental test levels arbitrarily assigned for the environmental acceptance test. These levels were derived on the basis of inducing stresses that would identify latent defects and were not derived on the basis of flight environments. Certification was required to be some factor above the acceptance environment, as a minimum.

FAILURE

The inability of an item to perform its prescribed function within established limits and within operating environments.

TEST REQUIREMENTS

Environmental acceptance tests were conducted to screen manufacturing and workmanship flaws in flight and test hardware that are not readily detectable by normal inspection techniques. The requirements established for these tests were primarily for electrical, electronic and electromechanical components. Additional failure data were also to be provided to assist in the detection and elimination of the causes of the failures produced. The test environment was to be defined by hardware sensivity and could include vibration, thermal cycling, or both. These tests were normally conducted by the vendor as a part of the customer acceptance test.

Environmental acceptance tests were conducted at the same component level of assembly as the certification* tests. All components were not necessarily subjected to environmental acceptance testing. Components were selected by the application of the following criteria:

1. Components that cannot be effectively inspected during manufacture, or components whose assembly processes and techniques are not readily quality controlled.
2. Components that have marginal or questionable environmental sensitivity. The following defects were expected to be uncovered:

   Vibration

   - Loose electrical connections
   - Loose parts
   - Relay contact chatter
   - Switch contact chatter
   - Contamination
   - Cold solder joints
   - Incomplete weld joints
   - Close tolerances
   - Incomplete crimp connections

   Thermal

   - Voids in potting
   - Short run wires
   - Welded solder connections
   - Bimetallic effect of leak springs
   - Insulation penetrations
   - Close tolerance mechanisms
3. Items for which additional confidence is desired through the elimination of infant mortality failures.

Once a component was designated for environmental acceptance testing, all manufactured items of that part number were tested.

The acceptance vibration test levels are shown in Figure 1. These vibration levels were based on Gemini experience where the failure rate following exposure to such test levels was reduced. As shown in Figure 1, the qualification level must exceed the acceptance level, as a minimum, by a factor of 1.66. When this program was initiated, most of the Apollo hardware had completed qualification testing. Those components that had not been qualified to 1.66 times the acceptance level were requalified. Some exceptions were made when the qualification vibration levels were near 1.66 times the acceptance level, but each case required an individual deviation from NASA. All new programs required the minimum qualification level to be at 1 times the acceptance level. The acceptance vibration test duration was a minimum of 30 seconds, but one minute was considered optimum. The thermal test levels are shown in Figure 2. These levels were more nearly related to qualification levels than were the vibration acceptance levels. On the testing of Apollo hardware, some deviations were granted while some items were requalified. For hardware that was qualified after the environmental acceptance program was initiated, it was required that qualification tests include, as a minimum, the 100°F acceptance range, plus the 40°F spread between acceptance and qualification.

Functional and/or continuity checks were performed on all components before, during, and after the test. If a functional verification

* The term "certification" is used in place of the term "qualification" in Apollo terminology. Specifically, the term certification defines those environmental tests which combined with other tests and analyses, constitute the certification of a component for flight.

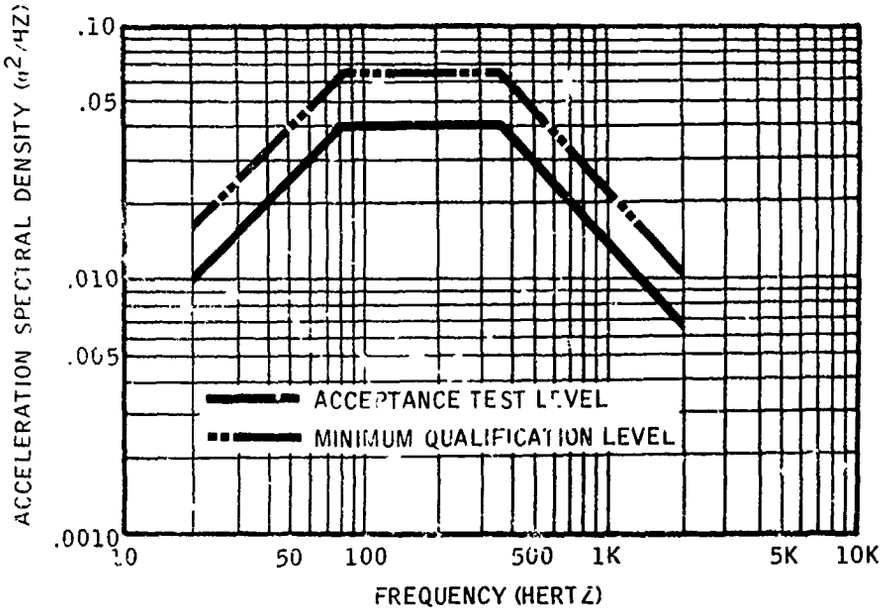

Figure 1. Environmental acceptance vibration test requirements.

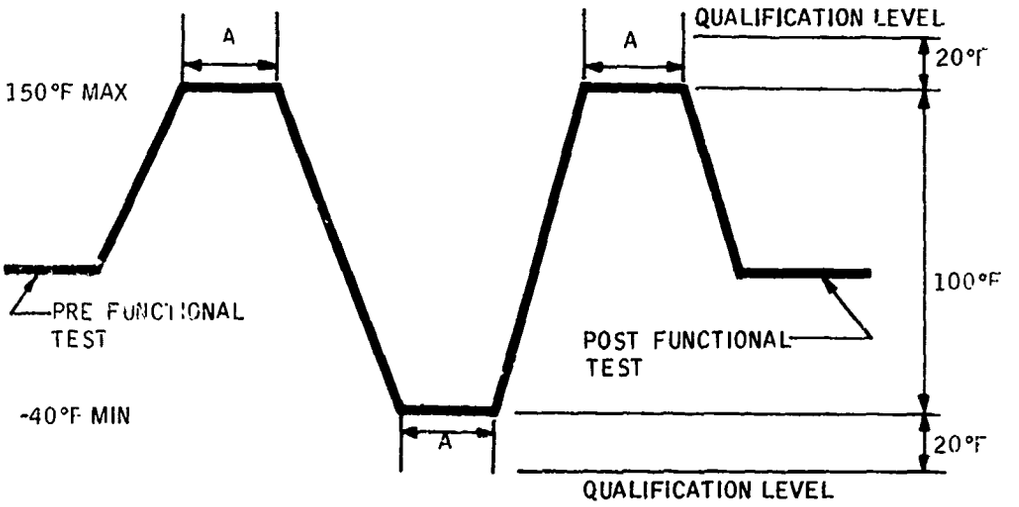

- A IS THE TIME REQUIRED TO STABILIZE TEMPERATURE PLUS ONE HOUR MINIMUM
- EQUIPMENT TO BE OPERATED AND MONITORED DURING THE TEST
- FUNCTIONAL TESTS TO BE PERFORMED BEFORE AND FOLLOWING THE TEST
- CONTROL TEMPERATURE RANGE BETWEEN MAXIMUM AND MINIMUM TEST CONDITIONS SHALL BE AT LEAST 100° F

Figure 2. Environmental acceptance thermal test requirements.

could not be performed during the test because of time limitations, then only those functions that were critical to crew safety and mission success were continuously monitored.

All contractors were required to report all acceptance test failures through the NASA/MSC (Manned Spacecraft Center) failure reporting system. They were, in addition, required to summarize these failures in periodic reports. These reports constitute the basis for the assessment described below.

FAILURE SUMMARY

Table I shows a tabulation of the number of component types, number of individual component tests, number of failures, and the failure rate for the Apollo Command and Service Module (CSM) and the Lunar Module (LM). The tabulation is for both thermal and vibration testing. The data analyzed were acquired over a three year period of time, beginning in mid-1967 and ending in mid-1970. Although additional data have been taken since mid-1970, the bulk of the testing was completed prior to that time. Hence, the newer data would have a negligible effect on the analysis. A component type in Table I is defined as those with the same basic part number. There were approximately the same number of LM and CSM component types tested. Of the 293 component types tested, 76 were subjected to both vibration and thermal testing. The total number of units tested only approximates the total number of tests that were conducted, since some components were tested more than one time. The number of failures represents the number of failure reports that were written, some of which were subsequently found to be caused by testing errors (this subject will be discussed in more detail later in the paper). The failure rate is simply the number of failures divided by the number of units tested.

TABLE I

SUMMARY OF ACCEPTANCE VIBRATION AND THERMAL TESTING FOR CSM AND LM COMPONENTS

VIBRATION	
Number of component types	174
Total number of units tested	11,467
Number of hardware failures	741
Failure rate in percent	6.7
THERMAL	
Number of component types	129
Total number of units tested	3,809
Number of hardware failures	665
Failure rate in percent	17.4

The failure rate for thermal testing was substantially higher than for vibration testing. There was no conclusive explanation for this phenomenon, but its existence was not only substantiated by the higher overall failure rate but was also obvious during the detailed analysis of individual failures.

A further breakdown for the failure rate by individual subsystem is shown in Table II, below, where failure rate is based on the number of units tested versus the number of failures that occurred.

As might be expected, the failure rate is higher for those subsystems with a higher percentage of electronic equipment. The failure rate for the display panels is not significant. These tests were conducted on removable panels which contained various numbers of individual components. Thus, the failure rate per number of components would be much less than shown in Table II. The failure rate obtained on one subsystem, the abort guidance subsystem, was over 100%. A total of 100 failures occurred during the thermal testing of 88 units of 5

TABLE II

SUMMARY OF ACCEPTANCE VIBRATION AND THERMAL TESTING FOR THE LM AND CSM BY INDIVIDUAL SUBSYSTEM

SUBSYSTEM	CONSTRUCTION TYPE		VIBRATION TESTS				THERMAL TESTS			
	ELECTRONIC	ELECTRO-MECHANICAL	COMPONENT TYPES	UNITS TESTED	FAILURES	PERCENT	COMPONENT TYPES	UNITS TESTED	FAILURES	PERCENT
SEQUENCERS	90%	10%	10	169	11	6.5%	8	[illegible]	13	8.2%
ENVIRONMENTAL	10%	90%	14	339	32	9.4%	13	197	22	11.2%
ELECTRICAL	80%	20%	53	847	103	12.2%	30	449	28	6.2%
STABILIZATION	80%	20%	11	184	28	15.2%	11	386	71	18.3%
COMMUNICATION	90%	10%	23	441	105	23.8%	21	273	73	26.6%
INSTRUMENTATION	90%	10%	7	118	30	25.4%	5	469	26	5.6%
REACTION CONTROL	20%	80%	1	543	7	1.3%	3	757	71	9.3%
PROPULSION	15%	85%	9	234	16	6.8%	3	22	1	4.5%
ABORT GUIDANCE	80%	20%	9	257	17	30 0%	5	88	100	114.0%
MECHANICAL	0	100%	1	74	7	10.6%	1	51	6	11.7%
RADAR	80%	20%	4	52	32	6.2%	0	0	0	0%
DISPLAY COMPONENTS	90%	10%	32	8208	353	4.9%	18	848	177	21.0%
DISPLAY PANELS	90%	10%	0	0	0	0%	11	106	77	7.3%
TOTAL			174	11467	741	6.7%	129	3807	665	17.4%

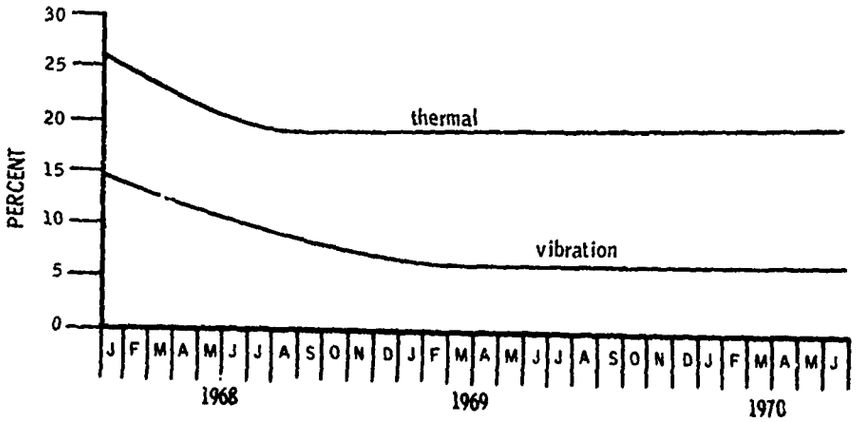

Figure 3. Percent failures for those units tested versus time showing that the failure rate has remained relatively constant.

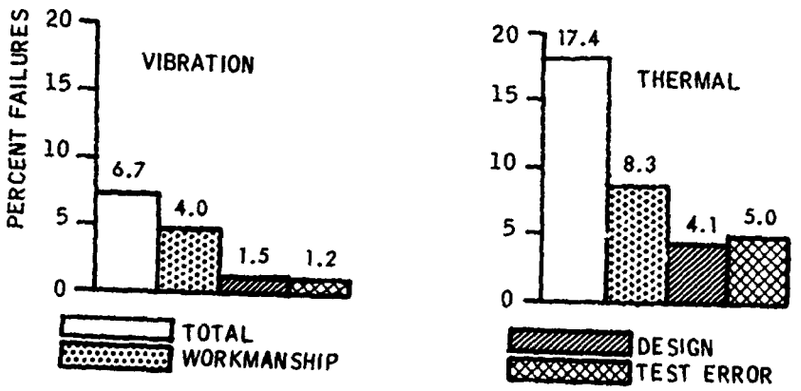

Figure 4. Failure classification by percentage based on workmanship, defects, design defects, and test errors for both CSM and LM failures.

different component types in this subsystem. There were 29 failures on one component type and 47 failures on another type. There were a number of circumstances which caused the failure rate in this subsystem to be so high. As an example, several components incurred multiple failures. One individual component, in fact, incurred six different failures before it passed. Also, all units from one component type were reworked, and an additional environmental test was required for all units. This subsystem is by no means typical, but shows the value of an environmental acceptance test in screening out failures in a subsystem that was particularly failure prone.

The failure rate versus time is shown in Figure 3. The significance of this figure is to show that having overcome the high failure rate at the beginning of the program, the failure rate remained constant.

Each failure was analyzed to determine if its origin was a workmanship, design, or testing deficiency. A breakdown of this failure classification by percentage is shown in Figure 4.

The following are definitions of the failure classifications:

1. Test Error - Failure occurring during the acceptance test caused by the test operator, test equipment, and/or improper procedures.

2. Workmanship - Failure caused by the improper application of approved manufacturing processes and techniques. Also includes failures caused by the inherent piece part failure rate.

3. Design - Failure caused by design deficiency requiring a drawing and/or process specification change.

In many cases, a single design fix was used as corrective action for several failures. Discounting the test errors, Table I can be revised to show definite hardware failures as shown in Table III below:

TABLE III

SUMMARY OF ACCEPTANCE VIBRATION AND THERMAL TESTING FOR CSM AND LM COMPONENTS DISCOUNTING TEST ERROR FAILURES

VIBRATION

Number of component types	174
Total number of units tested	11,467
Number of hardware failures	559
Failure rate in percent	4.7

THERMAL

Number of component types	119
Total number of units tested	3,809
Number of hardware failures	470
Failure rate in percent	12.4

As might be expected, the number of workmanship failures was the highest. The number of design faults that escaped the certification program and were detected during the acceptance program is significant.

A breakdown of environmental acceptance test failures by failure mode that has been previously presented[1] is shown in Figure 5 below:

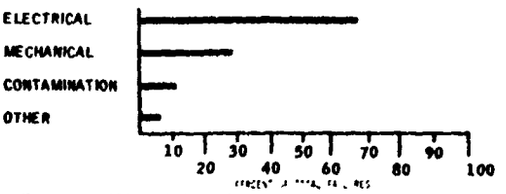

Figure 5. CSM and LM environmental acceptance test failures by failure mode.

These results are to be expected, since the large majority of the monitored functions are electrical.

At this point in the assessment, we have shown that 9.4% of the 14,994 units subjected to environmental acceptance testing incurred some type of failure (test errors not included). Thus, the effectiveness of the program has been demonstrated. One might now question how many escapes from this screen occurred. The following analysis was made to provide an answer to this question.

POST TEST FAILURES

An analysis was made of post-acceptance test failures to determine how many defects were found that could have been (or should have been) detected during an environmental acceptance test. This analysis was conducted by reviewing the post-acceptance test closeout of CSM failures to determine if the failure could have been (or should have been) detected by the environmental acceptance test screen. Such an analysis called for a large amount of judgement by the reviewer.

As previously mentioned, 144 CSM component types were considered to be candidates but were eliminated. Of those component types that were not subjected to environmental acceptance testing, there were 1101 post-acceptance test failures that occurred during later ground test operations; mostly during integrated vehicle testing. Only 44 or 4% of these could have possibly been detected during an environmental acceptance test. Twenty of these failures occurred on one component type. Thus, only 2.2% of the remaining 1100 failures could possibly

have been screened by this method. None of these failures occurred on 90 of the 116 component types, and 11 incurred only one failure of the type that might have been screenable.

CONCLUSIONS

The current Manned Spacecraft Center programs have included environmental acceptance testing at the lowest practical component level of assembly. The conduct of a rigorous program of this type on components, plus repeated integrated checkout tests on the spacecraft, have been used to provide the necessary screens for defective hardware.

The results have been encouraging. Since the adoption of the environmental acceptance testing techniques, there have been no flight failures on equipment that have been subjected to this type of test. The environmental acceptance tests have uncovered defects which could have produced flight problems. As a bonus, some design defects were also uncovered which had not been detected during qualification testing. In terms of cost and effectiveness, these tests have more than justified their existence.

REFERENCES

1. G. M. Low: "Introduction to a Series of Nine Articles Covering Major Facets of Design Development and Operations in the Apollo Program," Astronautics and Aeronautics, March 1970, pp 27-45.
2. S. H. Simpkinson: "Testing to Insure Mission Success," Astronautics and Aeronautics, March 1970, pp 50-55.
3. R. W. Peverley and D. E. Newbrough: "An Assessment of the Apollo Spacecraft Vibration Test Program," The Journal of Environmental Sciences, March/April 1971, pp 12-19.

ACKNOWLEDGEMENTS

The author wishes to express his appreciation to Mr. C. Laubach of the NASA/MSC Test Division for supplying some of the data used in this analysis. Credit must also be given to North American Rockwell and Grumman Aerospace Corporation personnel who generated the data. Credit must also be given to the NASA/MSC personnel who participated in this program, but who are too numerous to list.

ON THE DEVELOPMENT OF PASSENGER VIBRATION RIDE ACCEPTANCE CRITERIA

Sherman A. Clevenson and Jack D. Leatherwood

NASA Langley Research Center
Hampton, Virginia

This paper contains a description of the Passenger Ride Quality Apparatus (PRQA) and discusses the full range of its capabilities. In addition, a brief discussion is included of a pilot test program to obtain subjective reactions of bus passengers in a rapid transit system and correlations of the reactions with the ride motions.

INTRODUCTION

Environmental factors such as vibration, noise, and temperature are important considerations in the design of transportation systems since such factors may adversely affect passenger acceptability of the system. Future transportation systems such as STOL aircraft and high-speed ground vehicles are expected to experience larger vibration amplitudes than those encountered in currently operating systems. The question arises as to whether the passenger will accept these levels and, if not, how much reduction in vibration level will be needed to achieve acceptability. To answer these questions the relations between vibration and passenger comfort must be understood. To provide such relations, or comfort criteria, a vibration ride comfort program is now underway at the Langley Research Center of the NASA. In this paper, two studies that are part of this program are described. First, the development of a laboratory simulator for systematically studying the effect of vibration on people will be discussed, and then the development of a method for determining passenger subjective response, or comfort rating, of the vibratory environment will be described.

Unlike environmental factors such as noise and temperature, vibration effects on comfort perception are difficult to characterize due to the inherent complexity of the vibration (random and multidirectional) and also the unique effect of vibration on various portions of the human body. In comparison with studies conducted in the field under real world conditions, laboratory simulation and study offers several important advantages. These advantages include generally lower cost, the ability to sort out and study vibration parameters separately, broad spectra-shaping capability, control of subject population, separation of axis effects, and elimination of other environmental parameters such as noise and temperature.

Practically no studies have been reported with the traveling public in simulators that resemble and reproduce a multidegree-of-freedom transportation environment. Although many moving base simulators exist, they are usually of the single-degree-of-freedom type. In general, the larger moving base simulators are configured as a crew compartment. In most instances, test personnel are experienced pilots or crew who are not representative of the traveling public. The large motion simulators are excellent for the study of kinetosis (motion sickness). The Passenger Ride Quality Apparatus (PRQA) described herein has been developed to study subjective response to vibration in the frequency range above the kinetosis (0 to 0.4 Hz) range and below the acoustic (30 Hz) range, and in an environment closely resembling the passenger environment in aircraft or surface vehicles.

The development of an acceptable ride comfort criteria requires the assessment of the passenger comfort associated with specific vibration environments. Since comfort is highly subjective, its measurement has many of the problems inherent in psychological research such as choice of subject population, elimination of psychological bias, and so forth. Thus, a psychologically valid comfort rating scale is required. Many different comfort rating scales have been used as evidenced from the papers presented at a recent ride quality symposium held at Langley Research Center [1]. These scales are generally interger-valued ranging from 4-point to 10-point scales with varying descriptive adjectives. It is therefore difficult to evaluate and compare the results available in the literature [2]. The research presently underway is directed toward the development of a "standard" subjective response rating scale and demonstration of its validity for measuring human response.

The role of the simulator and the subjective response rating scale in the development of a ride vibration criterion can be explained using Figure 1. Specified inputs are applied to the PRQA resulting in a desired ride environment which the subjects are asked to rate for vibration comfort. The inputs and resulting ride environment can be ideal (such as sinusoidal, white noise, or shaped-spectra) or actual tape recordings from field vehicles can be used. It should be noted that extensive field measurements have been made on various vehicles using a portable measuring/recording system developed by Langley as reported in Reference [3]. Data representing the ride environments of more than 30 vehicles are presently stored in a data library and discussion of some of the vehicles and data can be found in References [4] and [5]. A correspondingly large library of subjective data measurements, however, does not exist at this time. The experimental program

described in this paper is intended to produce a comprehensive set of such subjective measurements.

The physical data, as shown in Figure 1, are analyzed for vibration characteristics such as power spectra, rms levels, exceedances, and so forth. The comfort ratings are obtained by asking the subjects to rate selected portions of the ride using comfort rating scales developed in the program described later in this paper. The results are then analyzed statistically to produce an indicator of comfort level. Finally, the comfort levels and associated vibration characteristics are correlated and regression models for ride comfort formulated. It is expected that results from these studies with the PRQA will provide (1) a "first cut" ride vibration acceptance criterion for use in design of future vehicles, and (2) a guide to procedures and data to be used in field tests to verify the ride criteria in a more realistic environment.

DESCRIPTION OF THE PASSENGER RIDE QUALITY APPARATUS

Overall System

The Passenger Ride Quality Apparatus (PRQA) is shown in Figures 2 to 6. To illustrate the assembly of the PRQA, a model is shown beside the passenger research compartment in Figure 2. The passenger cabin, referred to as a research model, is bolted to the table of the motion-base system in one of two positions 90° apart. The hydraulic actuators and restraints are indicated. The supports, one below each corner of the motion-base table, are used to support the table and cabin when not in use. The reaction mass is made of steel-reinforced concrete and weighs approximately 100,000 pounds. This PRQA is the only simulator capable of multidegree-of-freedom motion using a close simulation of a transportation system at vibration frequencies up to 30 Hz. Great emphasis is placed on human safety aspects.

Research Compartment

The initial research compartment was made to simulate the upper quarter of a passenger cabin of a modern jet aircraft. An exterior view of the cabin is shown in Figure 3. The base of the cabin is 7 feet by 7 feet. Interior head room is just over 7 feet. The interior as shown in Figure 2 is closely configured like the real aircraft as to seating, overhead rack, and so forth. However, the interior wall has a mirrored finish to supply an impression of width and the forward and rear bulkheads have two-way mirrored panels. That is, they appear as mirrors on the inside, but can be seen through from the outside.

Motion Base System

The motion base system is more clearly defined in the closeup photograph of the model in Figure 4 and with drawings (Figs. 5 and 6) showing locations of the actuators and restraints.

Actuators. Three hydraulic servocontrolled actuators are used to control the vertical motion. The actuators are located such that one is on the roll axis (see Fig. 5). By forcing the other two actuators with a phase difference of 180°, the motion base table is forced to rotate.

A fourth actuator used for obtaining lateral motion is connected from the underside of the center of the table to a vertical extension of the reaction mass. The electronic servocontrols are compensated such that correction signals are directed to any actuators that are not directly controlling the motion. For example, for side-to-side motion of the table, the vertical actuators must extend to keep the table moving in only one plane. All four actuators are mounted on ball joints to allow side, vertical, and rolling motions of the table. Other motions are restrained.

Restraint System. The motion base restraint system is shown in Figure 6. This system of linkages is designed to allow the desired three degrees of freedom, roll, vertical and lateral, and restrain motions in the fore and aft, pitch, and yaw degrees of freedom. The restraint of the yaw and fore-and-aft motions is accomplished by the geometry of the restraint linkages and by the use of pin end connections at the reaction mass and table and ball joints at the centers of the linkages. Pitch motion is prevented by appropriate control of the signals to the vertical actuators.

Performance

The distinctive operating feature of the PRQA is its ability to reproduce three degrees of freedom of the ride recorded from an actual vehicle. Furthermore, it can do it in single or multiple degrees of freedom under control of the operator. The three motions are heave (vertical), lateral (sideways), and roll. The amplitude and phase relationships are infinitely variable between axes.

Motion. The performance of the PRQA is limited by its actuators and controls. Curves showing its capabilities are given in Figure 7. The capability in the vertical and lateral directions is identical; namely, the displacement is limited to 6 inches double amplitude from 0 to 1.28 Hz, the maximum velocity is 24 inches per second, and the acceleration is limited to ±0.5g up to 30 Hz. In the roll degree of freedom, the displacement is limited to 0.2 radian double amplitude from 0 to 1.28 Hz, the maximum angular velocity is 7 radians per second, and the acceleration is limited to 6 radians per second squared in the frequency range from 1.28 to 5 Hz.

Control. The control console (Fig. 8) for the PRQA is located in an adjoining room where the operator can observe the PRQA and its occupants while controlling its motion. Considerable versatility is built into the control console. Some examples are: (1) a program selector allows selection of up to six programs including random noise, tape recorders, and signal generators for each actuator; (2) a program conditioner to allow an adjustable rate of turn-on and turn-off of the signal selected and allows master programing of each or all degrees of freedom; (3) limit detectors to limit displacement, velocity, and acceleration; and (4) controllers that allow complete preprograming. When the test program has been preset, a push of the start/stop button initiates testing. For any repetitive testing, after the preset

number of cycles have occurred, the system comes to rest at the preselected rate.

Operation. The PRQA is operated by two certified operators. Prior to the initiation of a series of tests, both operators use a checklist and set the controls for the prescribed test. In addition to adjusting the potentiometers for the desired motions, displacements, accelerations, frequencies, and time for the particular test, limiters are also adjusted. These limiters are for displacements, accelerations, or pressures. They are adjusted such that a visual indicator, a light on the controller panel, shows when the signals are off by a preselected value, say 5 percent. When the signal has a greater discrepancy, say 10 percent, the system automatically shuts down. For conducting a test, one operator pushes the start/stop button and monitors a four-beam oscilloscope to be assured that the expected test is being conducted. The particular signals monitored are selected by wire connections on the scope matrix board. Typical signals of interest include actuator control signals, table displacement, passenger cabin accelerations. The test either finishes automatically, or the operator pushes the start/stop button a second time. The second operator observes the test and the subjects from a position outside the passenger cabin and notifies the control console operator of any conditions requiring test termination. The test subjects can also abort the test by pushing any of the "chicken" switches.

Reproducibility. An indication of the reproducibility of the PRQA is shown in Figure 9. Signals proportional to the accelerations measured on the floor of a bus were used as input to the PRQA. These signals were integrated twice to obtain control signals for the actuators. The resulting motions on the floor of the PRQA were measured using the same portable vibration measuring/recording system [3] used to obtain the bus measurements. From the figure, it is seen that accelerations measured on the floor of the PRQA passenger compartment closely resemble those measured on the floor of the bus. When a sinusoidal input representing either displacement or acceleration was used, the reproducibility was excellent.

Another indication of the PRQA reproducibility is shown in Figure 10, again using the acceleration measurements obtained during the above-mentioned bus ride. The upper curve in Figure 10 shows the power spectral density (PSD) of the accelerations measured on the floor of the bus. The data used for this PSD encompass the 1-second interval of data shown at the top of Figure 9. The lower curve in Figure 10 shows the PSD of the response measured on the floor of the PRQA compartment for the same time period as the upper curve. With the exception of the responses below 2 Hz, excellent agreement exists between input and output. For frequencies below 2 Hz, the control console has rolloff filters to reduce the response of the PRQA to quasi- or steady-state accelerations. This reduction is necessary due to the limited excursion available to the PRQA.

Man Rating and Safety Considerations

All equipment in NASA that is used in man-machine research is required to be man-rated. In general, this means that the operation of the PRQA equipment is foolproof and safe in all respects. The intent of the PRQA is to expose passengers to the dynamic environments typical of existing ground transportation systems or commercial jet aircraft. Passengers will not be exposed to vibrations resulting in pain or injury. The following discussion of safety aspects has to do with potential emergency conditions only. The safety considerations for the PRQA as shown in Table I fall in two categories: the apparatus and its location.

TABLE I. SAFETY CONSIDERATIONS

- Apparatus
  - Electrical and Hydraulic
  - Mechanical
- Facility

Among the electrical safety devices are those that will shut down the system automatically such as activating a limit switch by exceeding a preset voltage representing displacement, velocity, or acceleration. Hydraulic safety devices consist of temperature and pressure controllers, oil level in reservoir, and preset valves called load limiters to prevent any nonprogramed loads to the research compartment.

Examples of mechanical devices are microswitches at the limits of the travel of the motion base table. If the table does not stop due to electronic control, four mechanical supports (see Fig. 4) are provided to insure that the table cannot proceed more than 1/2 inch farther. Shock-absorbing material is attached to the motion-base table to reduce impact forces during emergency conditions. Metal-to-metal impact is prevented. Other mechanical switches that will stop the system are activated upon opening either access door or by pressing the "chicken" switches located above each seat. The research compartment is designed to withstand a more severe vibratory environment than conventional aircraft. The structural analysis of the compartment showed the first structural frequency to be 38 Hz.

Some of the safety considerations of the facility include hinged cover plates that cover the space between the table and the platform. These plates are kept closed except during tests. They prevent anyone from accidentally stepping where there is no platform. Warning flashing lights stating "tests in progress" are activated during tests to prevent unauthorized entrance.

PRQA Programs

Although not finalized, it is planned that initial programs utilizing the PRQA will be directed toward identifying and verifying the principal vibration parameters influencing human comfort

response. Physical parameters of interest include frequency, amplitude, narrow-band power, exceedance count, peaks, rms levels, and axes of vibration. Psychological parameters include such variables as crowding, attitudes, surroundings, and subject population.

One series of tests will determine the frequency and directional sensitivity of human subjects by exposing them to narrow-band white noise with center frequencies ranging from 1 Hz to 30 Hz along one axis at a time. The results should help to refine the human frequency dependent transfer function for each axis, and also to determine the relative weighting factors to be applied to each axis of vibration. Once frequency and directional sensitivity factors have been determined, another series of tests will be oriented toward identifying the vibration parameter(s) best correlating with measured comfort responses. This will involve application of correlation or regression techniques to the PRQA data. The outcome is expected to be a regression model for comfort.

DEVELOPMENT OF SUBJECTIVE RESPONSE SCALES

The Department of Psychology of Old Dominion University (ODU), under contract to LRC, is conducting an experimental study to develop and validate means for measuring and assessing the response of people to motion and vibration. Several condidate subjective response rating scales have been tested by exposing large groups of passenger subjects to ride motions under actual field conditions. The field vehicles used were City Rapid Transit buses that were operated over a preselected route which included segments of ride varying from relatively smooth (interstate highway) to relatively rough (isolated rural roads). A total of four candidate rating scales were investigated. Scales 1 and 2 are illustrated in Figure 11. Both are integer scales with point values ranging from one to five for scale 1 and one to six for scale 2. Note also in Figure 11 the differences in descriptive adjectives between the two scales. A third scale (scale 3) shown in Figure 11 was used in which the subjects were merely asked to rate the ride comfort as being satisfactory or unsatisfactory. The fourth scale (not shown) is a magnitude estimation scale in which the passenger subject assigns his own numbers to his perception of comfort. A discussion of the psychological factors influencing the selection of these scales for study is beyond the scope of this paper but will be reported in detail in a report to be prepared by ODU at a later date.

The basic ingredients of the experimental bus program are illustrated in Figure 12. The tests involved the leasing of City Rapid Transit buses to transport groups of passenger subjects over a preselected route approximately 54 miles in length and 2 hours in duration. A total of eight bus trips have been made to date with groups of 20 to 30 passenger subjects per trip. The subjects were asked to rate the comfort of 17 preselected portions of the total ride using one of the candidate rating scales. The comfort evaluations were taken at about 5- to 10-minute intervals with the subjects allowed about 15 seconds to indicate their ratings. Physical ride motion measurements were obtained during each 15-second rating period using the LRC ride measurement package [3]. These measurements consisted of the three-axis linear accelerations at forward and center locations in the bus floor. The acceleration time histories were then processed through the LRC time series analysis program to obtain power spectra (g^2/Hz) of the ride. The power spectra were then integrated over 2 Hz bandwidths and the square root of the results taken to obtain a measure of the average rms level of acceleration contained within each bandwidth. Typical examples for two rides, one of which was rated satisfactory and the other unsatisfactory, are shown in Figure 13. The upper graph shows the average rms acceleration levels associated with each of 12 frequency bands ranging from 1 to 25 Hz. These data correspond to vertical motions at the front of the bus and were obtained when scale 3 was in use. For this condition, 82.1 percent of the subjects rated the ride as satisfactory denoting a relatively smooth ride. In contrast, however, examine the lower graph of figure. This shows considerably large rms levels with only 17.6 percent of the subjects rating the ride as being satisfactory. Note also that the overall rms acceleration level associated with the rough ride is approximately three times the level for the smooth ride. The subjective data for each scale were analyzed by ODU to obtain interscale correlations, identify inconsistencies, and to identify a best scale. Data analysis and comparative evaluation of rating scales are still underway by ODU. Preliminary results, however, indicate that scale 2 appears to be the best at this point in time. Final selection of a scale awaits further analysis and will be published by ODU.

CONCLUDING REMARKS

A discussion of the Langley Research Center ride comfort program has been presented with emphasis on the development of a Passenger Ride Quality Apparatus and development of validated subjective response rating scales. The performance and safety features of the Passenger Ride Quality Apparatus have been described and some of the initial ride quality test programs outlined. A description of the experimental procedure employed by Old Dominion University to develop improved comfort rating scales has been given. Although data analysis is not yet complete, a tentative rating scale has been identified.

REFERENCES

[1] Symposium of Vehicle Ride Quality held at Langley Research Center, Hampton, Virginia, July 6-7, 1972. Papers No. 4, 6, and 11, NASA TM X-2620, October 1972.

[2] R. M. Hanes, "Human Sensitivity to Whole-Body Vibration in Urban Transportation Systems – A Literature Review," Johns Hopkins University, APL/JHU TPR 004, May 1970.

[3] John J. Catherines, Sherman A. Clevenson, and Harland F. Scholl, "A Method for the Measurement and Analysis of Ride Vibrations of Transportation Systems," NASA TN D-6785, May 1972.

[4] Sherman A. Clevenson, and Kenneth B. Ullman, "A Technique for Evaluating Track Condition Using Railcar Vibrations," Presented at the

AIAA/ASME 12th Structures, Structural Dynamics, and Materials Conference, Anaheim, California, April 19-21, 1971, AIAA Paper No. 71-384.

[5] John J. Catherines, and Sherman A. Clevenson, "Measurements and Analysis of Vibration Ride Environments," Presented at the Joint Symposium on Environmental Effects on V/STOL Designs, Arlington, Texas, November 1970, Preprint No. SW-70-21, American Helicopter Society, November 1970.

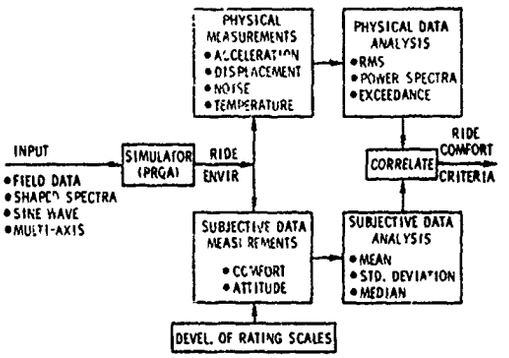

Figure 1. Langley Research Center ride comfort program plan.

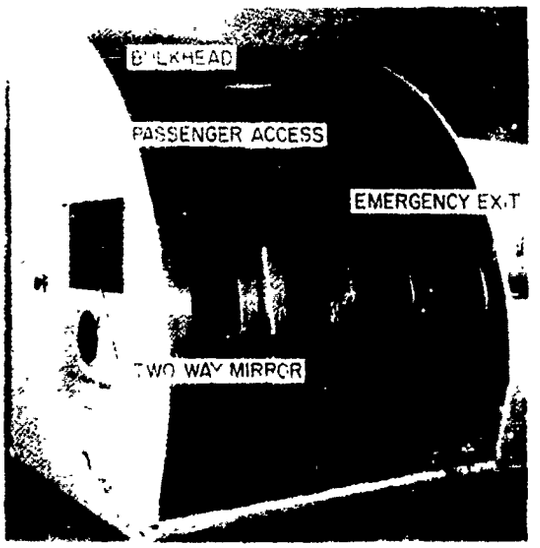

Figure 3. Exterior view of the PRQA.

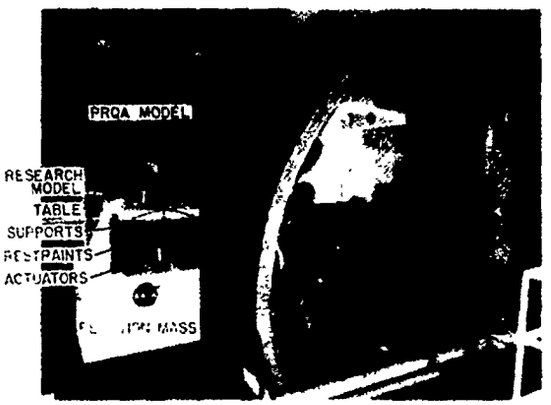

Figure 2. Interior view of the PRQA and a model of the PRQA.

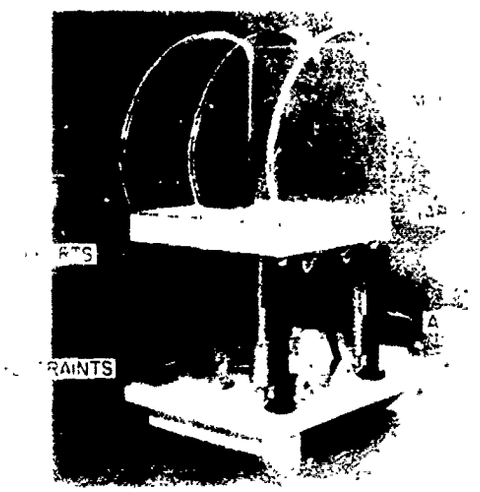

Figure 4. Model of the PRQA indicating the supports, actuators, and restraints.

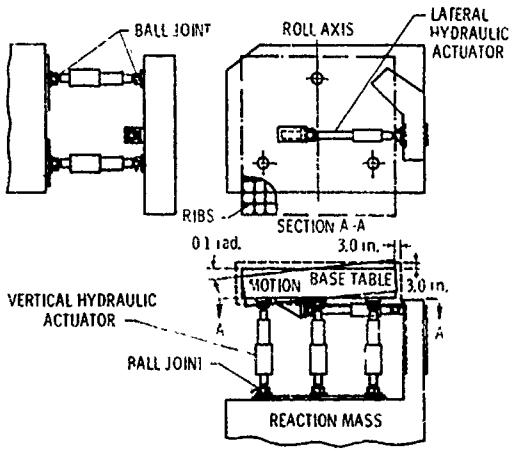

Figure 5. Motion-base actuator system.

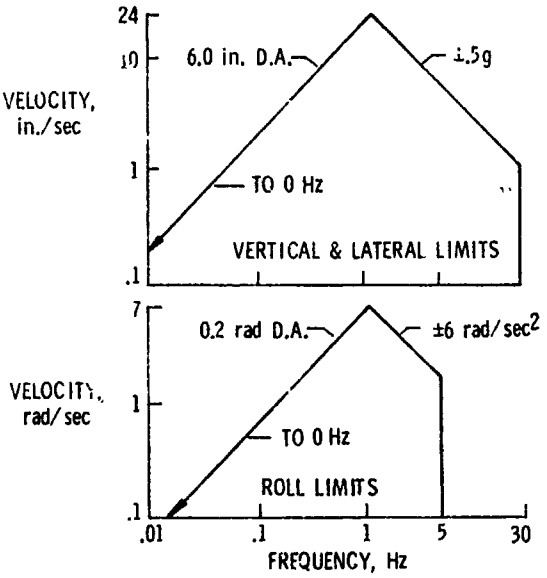

Figure 7. Displacement, velocity, and acceleration capabilities of the PROA.

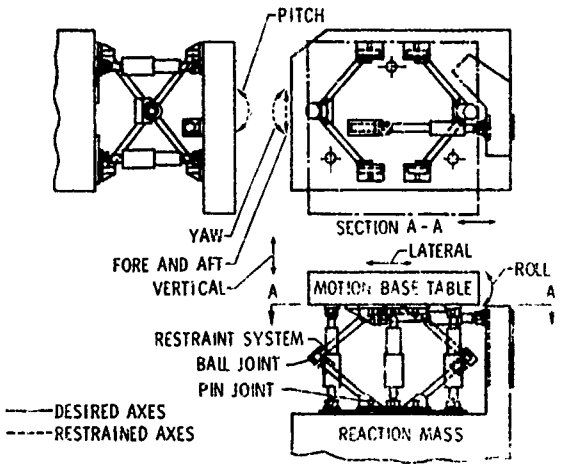

Figure 6. Motion-base restraint system.

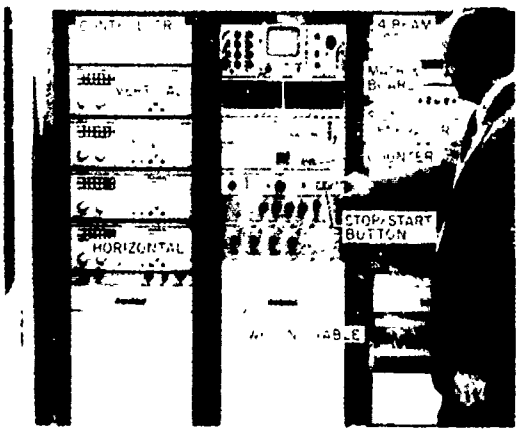

Figure 8. Control console for the PROA.

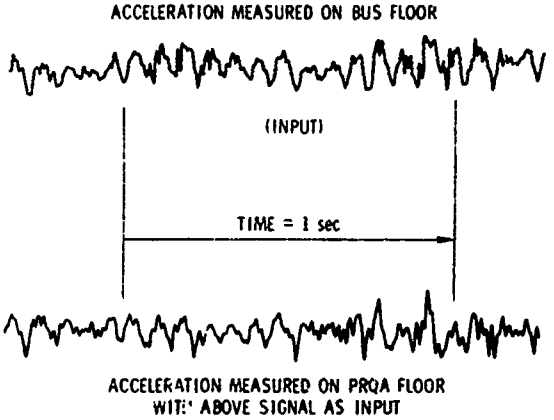

Figure 9. Comparison of PROA response to input.

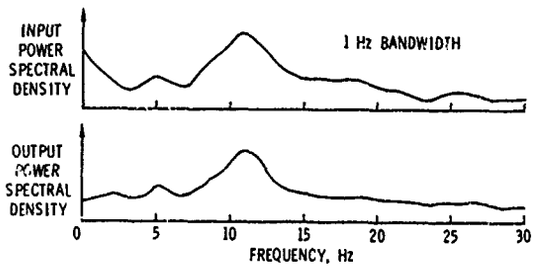

Figure 10. Comparison of PSD's of input and output of the PROA.

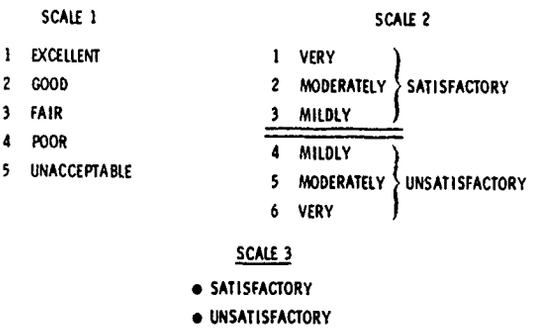

Figure 11. Candidate subjective response rating scales.

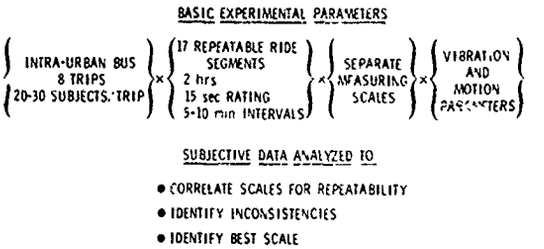

Figure 12. Basic ingredients of the experimental bus program.

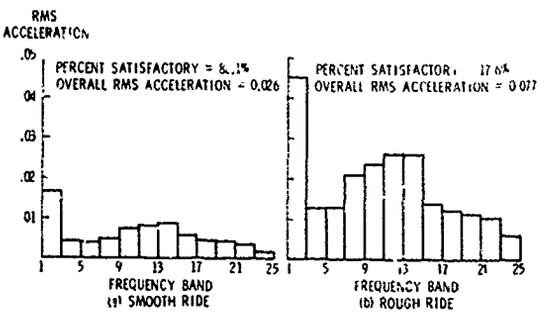

Figure 13. Typical acceleration levels for 2 Hz frequency bands illustrating smooth and rough ride for front-vertical measurements during a bus ride.

CAPTIVE FLIGHT ACOUSTIC TEST CRITERIA FOR AIRCRAFT STORES

Alan Burkhard
Air Force Flight Dynamics Laboratory
Wright-Patterson AFB, Ohio

This paper describes the development of an acoustic test criteria for assembled externally carried aircraft stores for their captive flight environment. This test method induces random vibration within the store which closely simulates the actual service environment at vibratory frequencies above 200 Hz. Because it requires application of the oscillatory force external to the store, there is no need to account for structural transmissability characteristics in the test development. The criteria were developed using the results of extensive captive flight and acoustic chamber measurements on aircraft stores and wind tunnel studies of typical store shapes. The test criteria are not rigidly established but are adaptable to a particular aircraft/store interface, aircraft's dynamic pressure and the store's geometric properties. The paper contains numerical examples that demonstrate the use of the developed acoustic test criteria.

INTRODUCTION

Externally carried aircraft stores are exposed to a very severe operational vibration environment. This environment has been known to cause malfunctions such as improper activation of fuzes, inadvertent jettison of stores, or other failures which compromise the mission of the weapon system.

AFFDL has conducted an extensive study of existing literature on the vibracoustic environment of externally carried aircraft stores and their qualification testing criteria (1). This study showed that new test methods are needed because the present qualification criteria do not provide adequate screening of stores before flight evaluation and operational deployment.

The study further showed that the vibration environment in captive carried aircraft stores stems from three principal sources: aircraft motion such as occurs during takeoff, landing, and air gusts; aerodynamics (oscillating air pressure at the store's surface) such as boundary layer turbulence, buffetting, jet engine noise, and propeller blade passage noise; and self induced motion such as internal pumps and motors or ram air turbines.

Generally the most significant of all these sources is the random aerodynamic pressure fluctuations which beat upon the skin of the store which in turn, produces random vibration throughout the store. A good store qualification test should, thus, cause the same random vibration patterns. It was pointed out in reference 1 and demonstrated in reference 2 that testing in an acoustic chamber would fulfill this requirement.

This paper describes the effects of turbulent airflow acting on the store's surfaces. The results of wind tunnel and flight studies are first discussed to define the characteristics of this flow field as it relates to stores of various geometric shapes. This is followed by a discussion of AFFDL acoustic chamber tests wherein studies were made to duplicate the measured in-flight vibrations of six distinct stores. The results of these independent studies are then correlated and generalized to develop acoustic qualification test criteria for captive carry of a wide range of assembled aircraft stores. The paper concludes with examples of the use of the test criteria.

Related random vibration tests for store components and assembled stores can be found in Method 514 of MIL-STD-810, "Environmental Test Methods." The acoustic criteria which are detailed in the appendix to this paper are contained in Method 515 of MIL-STD-810. All of these external store test criteria complement each other so that testing is done over the entire frequency range which vibration has been known to cause failures or malfunctions.

TRANSONIC WIND TUNNEL STUDIES

The turbulent airflow about a store's surface contains randomly oscillating air pressures which cause random vibration in the surface structure. This vibration is transferred throughout the stores structure and to internal equipment such as fuzes, electronic guidance and propulsion subsystems. The magnitude of these turbulent forces is sufficient to produce failure and malfunctions of internal equipment and sonic fatigue of light weight surface structure (4,5). Thus it is important to understand what influences various surface contours have on the pressure fluctuations in the airflow about a store.

Surface pressure fluctuations on various shaped rotationally symmetric bodies in transonic conditions have been measured by several investigators (6, 7, 8, 9). Their results show that the character of this fluctuating pressure field is highly dependent on the surface geometry of a store.

Close examination of this transonic wind tunnel data shows the following general characteristics of aerodynamic induced surface pressure fluctuations.

a. At transitions from conical to cylindrical sections, local flow separation occurs causing local increase in pressure fluctuations. The magnitude of these increases in pressure fluctuations is dependent on local cone angle.

b. The effect of local disturbances dies out within one store diameter down stream of surface irregularities.

c. The pressure fluctuations on a long cylindrical section at locations more than one store diameter down stream of surface irregularities do not increase in magnitude with aft station.

d. For regions where the vehicle profile is continuously changing with aft station, the magnitude of pressure fluctuations also increases with aft station.

e. The magnitude of pressure fluctuations is a linear function of dynamic pressure (q).

CAPTIVE FLIGHT ENVIRONMENT

The captive flight vibration and acoustic environments of externally carried stores in general have been extensively analyzed by Dreher, Lakin, and Tolle (1) and Piersol (3). The following general conclusions can be drawn from their analyses:

a. The vibration and acoustic spectrum of a store in captive flight does not significantly change in relative shape with Mach numbers from 0.45 to 0.90. The whole spectrum just shifts in amplitude with increasing q.

b. Linear relationships exist between store vibration and q ($G_{rms} \backsim q$) and between pressure fluctuations and q ($P_{rms} \backsim q$). These relationships provide conservative estimates of these environments if measured values at 0.85 to 0.90 Mach number are used to evaluate the proportionality constants.

c. Cluster carriage of a store increases its vibration levels above that which single carriage would produce. The largest increase in a TER (triple ejection rack) is 3 dB for those stores in the shoulder positions and a 6 dB increase for those stores in the aft shoulder positions of a MER (multiple ejection rack).

d. Tailfins which are exposed to the airstream in captive carriage can introduce significant vibratory energy into the whole store at the tailfin's natural frequencies.

ACOUSTIC CHAMBER STUDIES

Six different stores were selected for this program. These were selected because they possessed the different aerodynamic properties that are commonly used in aircraft stores. These store shapes are shown, not to scale, in Fig. 1. Each of these stores had been instrumented at various structural locations to measure vibration and several stores had two or three flush mounted microphones to measure the in-flight pressure fluctuations on the surface of the store. The instrumentation and flight measurement program for these stores was described by Dreher (10).

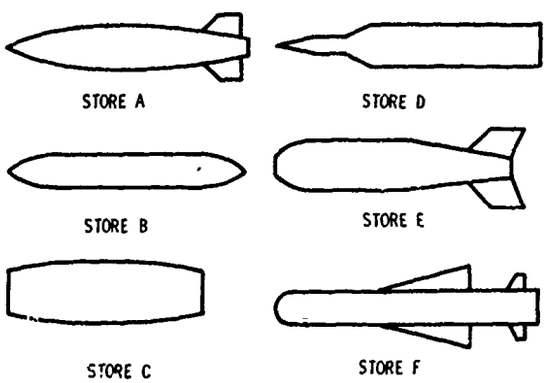

Fig. 1 - General profiles of stores used in this study

Because of a limited number of data recording channels available during the flight test program, the flush surface microphones were not in sufficient number to realistically define the total fluctuating pressure field about each store. Even in the cases where sufficient microphones were available, there is some concern that differences in the

turbulent flow field characteristics and acoustic chamber characteristics do not permit a one to one correlation between these environments (1). Thus, it was decided to place the flight instrumented stores into an acoustic chamber and adjust the chamber environment such that the captive flight vibration environment was duplicated.

The six flight instrumented stores were acoustically tested in the AFFDL Wide Band Acoustic Chamber which has a single noise source. This facility was described by Kolb and Magrath (11). The stores were suspended by their lugs by means of soft springs and installed horizontally with the long central axis of the store coinciding with the horizontal center axis of the horn. Most stores were positioned with their aft end toward the horn, as shown in Fig. 2.

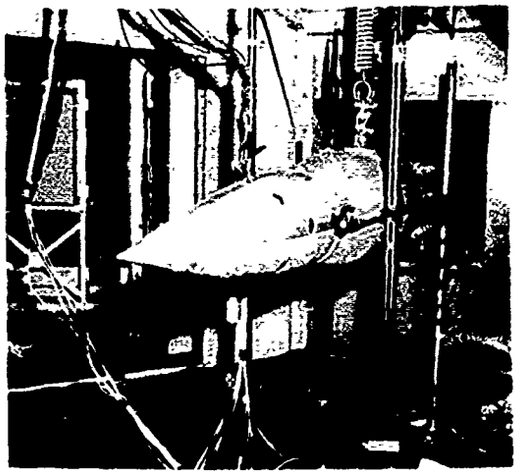

Fig. 2 - Store installed in acoustic chamber

The microphones and accelerometers used in the captive flight measurement program were supplemented by five to nine portable B&K condenser microphones, Type 41[illegible]. These additional microphones were located so that they were not close to any major discontinuity in the profile of the store. Microphones were located in each of the three regions of the store (nose, middle, and aft) as shown in Fig. 3. These microphones were used to define the average superimposed acoustic spectrum that acts on each of these three regions of the store. The outputs of all the transducers were recorded on tape by a Honeywell Model LAR 7400 tape recorder and analyzed by a B&K Model P-297 one-third octave band analyzer and a Time Data 100 Digital Spectrum Analyzer.

Each store was exposed to several

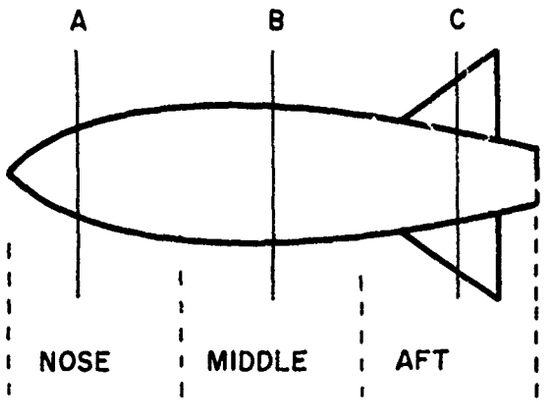

A, B, C PLANES WHERE ACOUSTIC SPECTRUM WAS MEASURED

Fig. 3 - Subdividing a typical store into three regions

different unshaped acoustic chamber environments that encompassed its measured captive flight acoustic levels. The responses of the store mounted accelerometers to the applied acoustic chamber spectra were then compared to their respective captive flight vibrations. The flight data used in this comparison was for Mach numbers 0.85 to 0.90 or maximum q condition if this Mach number range was not attainable. Fig. 4 shows how the applied acoustic chamber environments excited vibrations in the stores that had the same resonance peaks and valleys as the captive flight data. However, the relative amplitudes of the individual peaks and valleys were not necessarily reproduced since the chamber acoustic spectrum was not specially shaped.

It should be noted from the figure that an acoustic test does not subject a store's components to an artificial vibration environment, with high levels at frequencies where low levels occur in captive flight or vice versa. Therefore, an acoustic test with a properly shaped spectrum will realistically evaluate a store for its captive flight environment over its range of applicability as described later.

The response of all the accelerometers in each of the regions were averaged. The average one-third octave acceleration spectrum in each region was compared to the average external noise outside of its respective region. Fig. 5 shows a typical example of the linear relationship that exists between acoustic noise and store vibration. A strong relationship was found for one-third octave band levels having center frequencies above 160 Hz. This linear relationship permitted interpolation between

the various acoustic spectra to determine a shaped acoustic test spectrum that will exactly duplicate the measured captive flight vibration above 160 Hz.

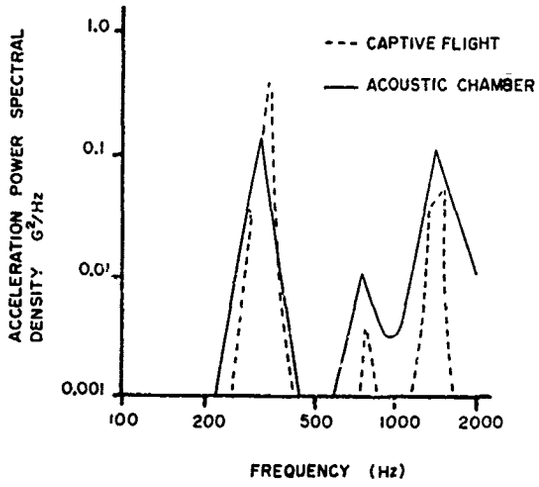

Fig. 4 - Comparison of captive flight and acoustic chamber vibration response for the same store station (Bandwidth of analysis = 20 Hz)

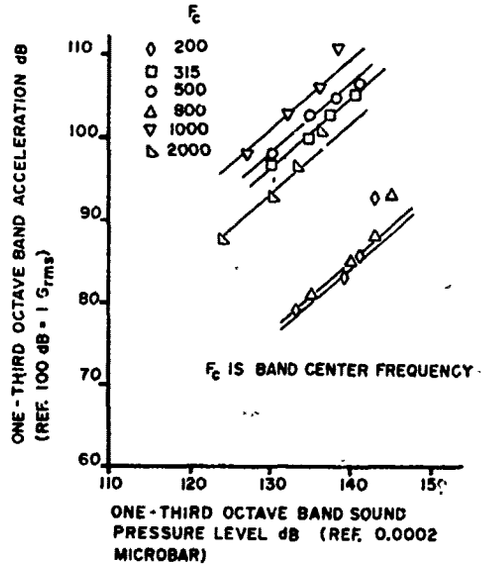

Fig. 5 - Linear relationship between average acoustic noise outside the store and average vibration for the same store region

Below 200 Hz, the acoustic chamber results exhibited an unusual phenomenon. The vibrations induced in this frequency range by the chamber noise were much lower relative to the flight measured vibrations even though the unshaped chamber acoustic environments encompassed the flight acoustic environments. In fact, using the interpolation/extrapolation techniques described in the last paragraph, the projected test levels were significantly different than the flight measured acoustic levels in this lower frequency range.

If we couple this fact with the assumption that acoustic fields only excite vibrations at the natural frequencies of the store surface (shell modes) and that these are generally above 200 cps (1), it can be rationalized that the vibrations induced in the store below 200 Hz stem from other sources such as aircraft motion, air gust, and buffeting. Thus, pending further investigation of this phenomenon, it was decided to cut off the acoustic test spectrum at 200 Hz. As a consequence, it is necessary to simulate this lower frequency vibration environment by direct application of vibration to the store using a shaker. Such a vibration test for assembled stores can be found in Method 514 of MIL-STD-810C.

Fig. 6 shows a typical comparison between the resultant shaped acoustic test spectrum and the measured captive flight acoustic spectrum for two store stations that were within one store diameter of each other (a store diameter is the maximum diameter in the store). Both spectra demonstrate similar profiles for the higher frequencies. However, the shaped acoustic spectrum is always less than the captive flight spectrum. This difference in levels could very well be attributed to the placement of the flush mounted microphones which measured the captive flight acoustic levels. These microphones were located next to major surface discontinuities which cause localized higher acoustic levels than that which was found on the surrounding store surface (8).

The shaped acoustic test spectrum represents the average aerodynamic pressure fluctuations profile along the store. Therefore, strongly localized effects are not included in these levels. To simulate these phenomena in conjunction with the distributed acoustic profile would require a multi-source acoustic facility. Such a facility is more expensive to operate and would not significantly improve on the excellent agreement between the captive flight and the acoustic test store vibrations that has been found using a single source acoustic facility. Moreover, a single source facility could be as simple as a jet engine with appropriate reflective walls and baffles.

The shaped acoustic test spectra for the individual stores differ considerably in both spectrum shape and level. To further analyze the results of this acoustic study the shaped acoustic test spectrum for each store was

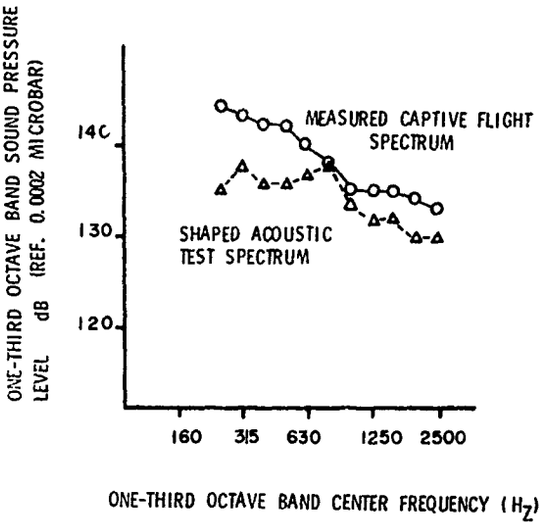

Fig. 6 - Comparison of measured captive flight acoustic spectrum with the shaped acoustic spectrum for store stations that were within one store diameter of each other

normalized to a dynamic pressure (q) of 1000 psf and to single carriage levels. Normalization to single carriage levels was done using the criteria discussed earlier (3) and normalization to a dynamic pressure of 1000 psf was accomplished using a linear relationship between vibration and dynamic pressure (1).

The normalized shaped acoustic test spectrum for each store was enveloped by a series of straight line segments as shown in Fig. 7. These envelopes were drawn for each store station where the B&K microphones were positioned in the acoustic test. The shaped acoustic test spectrum in each region of the store was quantized in terms of three variables, L_o, F_o, and A, where L_o is the maximun one-third octave band level in the envelope, F_o is the one-third octave band center frequency at which the acoustic envelope starts to roll off, and A is the high frequency roll off rate.

These three variables that defined the shaped acoustic test spectrum were analyzed for any general trends that could be identified for each store or group of stores. These trends were found to parallel the results of the transonic wind tunnel studies mentioned earlier. This correlation permitted the extrapolation and interpolation to flight regimes and vehicle shapes not investigated in this study.

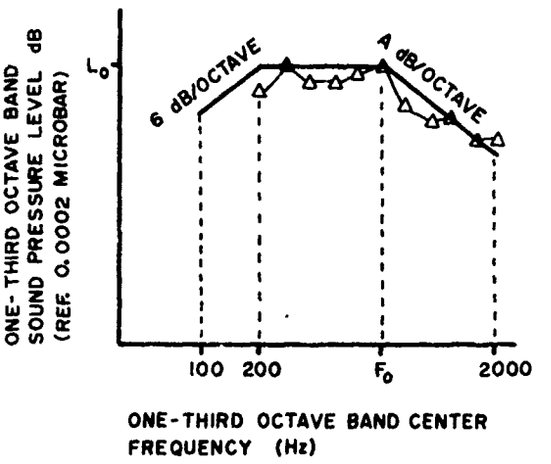

Fig. 7 - Envelope for typical shaped acoustic test spectrum

The detailed development of the prediction relationships for each parameter that defines the envelope for the shaped acoustic test spectrum can be found in an Air Force Flight Dynamics Laboratory Technical Report which is scheduled for publication in 1973. Pertinent results of the study which lead to the development of the acoustic test criteria are discussed in the following sections.

SPECTRUM SHAPE

Fig. 8 shows how F_o values tend to cluster into separate groups when plotted against nondimensional characteristic length ratio, X/R, where X is distance from the nose of the store measured along the longitudinal axis of the store and R is the local radius of the store at any store station. One group of data is for store stations that were either aft of reentrant angles or that were within one store diameter of the aft end of the store. The rest of the store stations cluster into the other group. This data can be approximated by Equation 1 below, when the calculated values of F_o are rounded off upwards to the next highest one-third octave band center frequency.

$$F_o = 600 \text{ Log}(X/R) + C \qquad (1)$$

where C = -200 for store stations that are within one store diameter of either the aft end of the store or aft of re-entrant angles

C = 400 for other store stations

The lower values of F_o at the aft end of the store and at stations that are aft of reentrant angles are characteristic of pressure fluctuations accompanying flow separation (12).

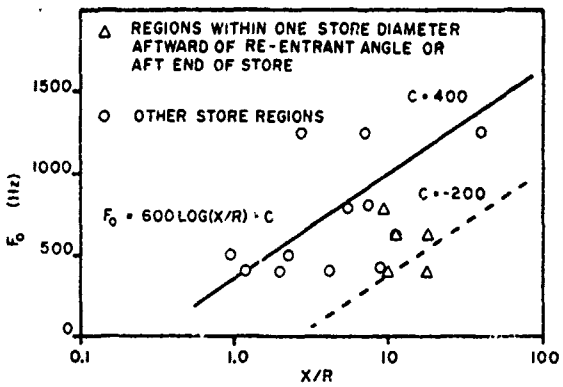

Fig. 8 - Shaped acoustic test envelope cut off frequency variation with characteristic nondimensional store length

ACOUSTIC LEVEL, L_o

The extensive analysis of captive flight vibracoustic data done by Dreher (1) and Piersol (3) shows that dynamic pressure has a strong influence on the acoustic and vibration levels in externally carried stores. A conservative approximation of this relationship is the assumption that acoustic levels and vibration levels are linearly dependent on dynamic pressure (q) provided data measured in the transonic flight regime is used to evaluate the proportionality constants. Therefore, a basic equation of the form $L_o = 20 \text{ Log}(q) + Z$ can be used, where Z represents the influence of the individual geometry of each store as discussed below.

Fig. 9 shows how the one-third octave band level, L_o, changes with store station. Three distinct trends are evident. Most of the stores tested had L_o increasing with aft store station. However, store C had L_o decreasing with aft store station, while stores B and D had L_o remaining relatively constant across certain store stations. All these trends can be related to their individual store profiles using the earlier mentioned wind tunnel results.

Stores with Changing Cross-sectional Diameter

For those stores which had gradually changing store profile (i.e., stores A and B), the one-third octave band level variation with store station can be enveloped by the following equation:

$$L_o = 20 \text{ Log}(q) + 11 \text{ Log}(X) + K \qquad (2)$$

K is evaluated by considering the nose of each store. A convenient measure of the amount of pressure fluctuations that the nose introduces into the environment about the store in captive flight is the local cone angle at station X = 1 inch as shown in Fig. 10. Using this measure of nose bluntness, a general equation for these types of stores is Equation 3 except when local nose cone angle approaches 90 degrees (ref. Eq. 5):

$$L_o = 20 \text{ Log}(q) + 11 \text{ Log}(X) + 7 \text{ Log}(1-\cos(\beta_1)) + 72 \qquad (3)$$

Stores with Long Cylindrical Sections

The overall pressure fluctuations on a long cylindrical section does not increase with aft station and is approximately $P_{rms} \approx 0.02q$ (12). The one-third octave band levels measured in captive flight for stores with long cylindrical sections are approximately flat from 200 to 2000 Hz. Therefore,

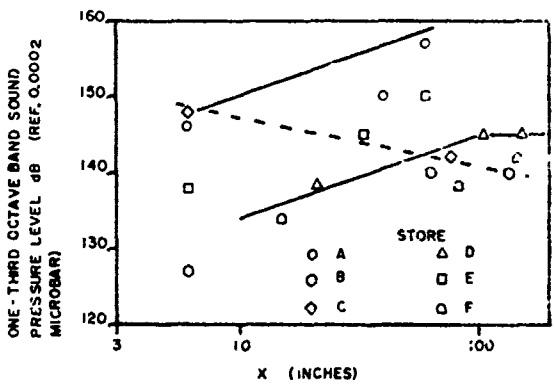

Fig. 9 - Aftward variation of maximum one-third octave band sound pressure level, scaled to q = 1000 psf.

the one-third octave pressure fluctuation level is approximately $P_{rms} \approx 0.006q$ or:

$$L_o = 20 \text{ Log}(q) + 84 \qquad (4)$$

Equation 3 is used for store stations up until one store diameter into a long cylindrical section and then Equation 4 is used for store stations in the long cylindrical section.

For a changing diameter region which is aft of a long cylindrical region use Equation 2. Redefine X and K so that X equals one at the aft end of the cylindrical section and K equals 84.

Stores with Blunt Noses

A very blunt nose (β_1 equal to 80-90 degrees) produces a very strong increase in pressure fluctuations at the nose of the store. The effect of this strong nose pressure rise over-shadows the influence of

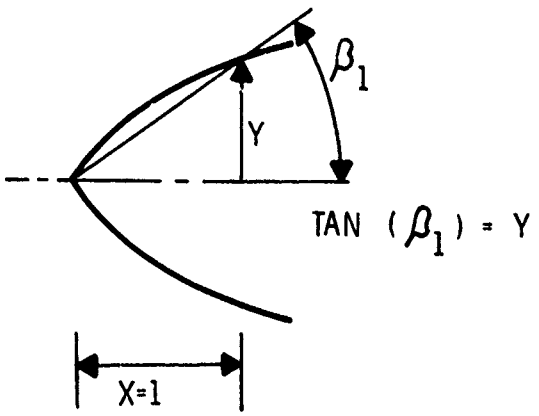

Fig. 10 - Local cone angle at station X equals 1 inch

gradual surface profile changes in the store (9). This is evident in store C where L_o decreases with aft store station (see Fig. 9). In this case Equation 3 is replaced with Equation 5, below.

$$L_o = 20 \text{ Log}(q) - 6 \text{ Log}(X) + 96 \qquad (5)$$

Equation 5 is used for store stations up until X equals 100. Aft of this station use Equation 3 or 4 depending which one is appropriate for the type of store profile in this region.

HIGH FREQUENCY ROLL OFF RATE, A

To best envelope the individual shaped acoustic test spectrum for each store and store station without being too conservative resulted in two different roll-off rates. 6 dB/octave for F_o greater than 400 Hz and 2 dB/octave for F_o equal to or less than 400 Hz.

ACCURACY OF PREDICTION RELATIONSHIP

To demonstrate the accuracy of the derived acoustic test prediction criteria, test parameters were calculated for the stores used to develop these criteria. A comparison of predicted values from equations 3, 4, and 5 and acoustic chamber values is shown in Table 1. All stores except store A were predicted within acceptable tolerances.

The L_o values for the three sections of store A were severely under predicted by 7 to 12 dB. This can be explained by considering the structural makeup of this store and the spectral characteristics of its flight data. As discussed by Dreher (10) the significant peaks in this flight data can be correlated to the natural frequencies of the tailfins on the store. He estimated that the vibrating tailfins could contribute as much as 13 to 20 dB to the measured vibrations levels throughout the store, which suggests that this under prediction is, in fact, largely due to the highly turbulent conditions around the aft fin section. Therefore, by removing the tailfin vibration from the flight data so that only the vibration due to surface pressure fluctuations on the main body of the store is considered, the acoustic chamber and predicted levels tend to fall in line.

The analysis of the flight measurements for the other finned stores (E and F) shows that tailfin vibration does not predominate to such a significant extent as occurred for store A. In the case of store E, flight acoustic measurements near the fins are, in fact, higher than flight measured levels from store A. However, store E's tail cone assembly is loosely attached (definite play observable) to the main body of the store such that its highly vibrating tail cone can be easily isolated. The tail cone on store A, on the other hand, is rigidly attached to the main store body resulting in no attenuation.

In the case of store F, its fins are more like wings (i.e., large with respect to the main body). As discussed in references 1 and 13, it is difficult or impossible to excite the the more fundamental natural frequencies of relatively large surfaces in flight because of the relatively poor space/phase correlation of the turbulent air flow. Thus, it follows that the wings on store F should not contribute significantly to its dynamic environments whereas the relatively small fins on store A should, and do, contribute significantly.

It thus appears that more work is necessary to establish a cutoff fin area (or size) below which the fin vibration effect is significant. In this case, then, the acoustic chamber predicted test level would be raised by a certain factor (say 12 to 15 dB) near the fins. This would provide both a sonic fatigue test for the fins (many fins have fatigued and fallen off in flight) as well as a vibration test for the rest of the store.

As an interim approach to qualifying stores with rigidly attached small tail fins, the use of the assembled store vibration test outlined in Method 514 of MIL-STD-810C is recommended. This test is designed so that most stores in this category receive a thorough vibration shake-down over a frequency range which extends to 2000 Hz.

TEST CRITERIA

A general acoustic test criteria for captive and free flight of assembled externally carried aircraft stores is contained in the Appendix and was constructed using the results of this investigation and the characteristics of normal mission profiles for aircraft that carry stores. Note how the criteria can be adjusted for frequency range, amplitude, and

TABLE 1

Comparison of Predicted and Acoustic Chamber Values for Shaped Acoustic Test Spectrum Envelopes

Store	Store Region	Chamber L_o	Predicted L_o	Chamber F_o	Predicted F_o	Chamber A	Predicted A
A	Nose	146	134	500	500	-6	-6
A	Middle	150	143	800	800	-6	-6
A	Aft	157	145	630	630	-6	-6
B	Nose	127	127	1250	630	-6	-6
B	Middle	140	138	1250	1000	-6	-6
B	Aft	140	142	1250	1600	-6	-6
C	Nose	148	150	500	400	-6	-2
C	--	--	--	--	--	--	--
C	Aft	142	143	400	400	-2	-2
D	Nose	138	136	800	1000	-6	-6
D	Middle	143	143	630	1250	-6	-6
D	Aft	143	144	630	500	-2	-6
E	Nose	139	139	400	500	-6	-6
E	Middle	145	144	400	800	-6	-6
E	Aft	150	150	800	400	-6	-2
F	Nose	134	144	400	630	-2	-6
F	Middle	138	140	400	1000	-2	-6
F	Aft	142	142	400	500	-2	-6

flight conditions. Thus overtesting and undertesting are minimized.

The free flight criteria were derived directly from the captive flight criteria because of the lack of any significant amount of free flight store data. In this regard, the acoustic test criteria for single carriage of a store during captive flight is used for the free flight criteria provided that the maximum free flight dynamic pressure is used to calculate the test levels. It is judged that this approach is slightly conservative to the extent of any addition to the test level caused by pylon/rack generated turbulence which is not present during free flight.

The captive flight criteria contain functional and fatigue (endurance) tests. A separate functional test was provided to allow performance evaluation of operating store equipment at realistic environmental levels. The fatigue test levels are generally higher and are adaptable to the testing time and the number of operational missions. The development of these fatigue criteria parallels those used in other store and aircraft equipment vibration tests (3, 14).

EXAMPLE CALCULATION USING ACOUSTIC TEST CRITERIA

Example I

A new store is being developed for captive carriage on a high performance aircraft. This store is designed for a life of 50 missions with an expected maximum dynamic pressure of 1400 psf. The shape of the store is shown in Fig. 11 and pertinent geometric properties of the store are listed in Table 2.

Plane A

f_o = 600Log(20/4.5) + 400 = 790

f_o ≈ 800 Hz

L_o = 20Log(1400) + 11Log20 + 7Log(1-cos 69) + 72 = 147.9 Functional Level

L_o = 20Log(1200/1400) + 2.5Log(50/9) + 147.9 = 148.3 Endurance Level

Plane B

f_o = 600Log(80/5) + 400 ≤ 1250 H_z

L_o = 20Log(1400) + 84 = 147 Functional Level

L_o = 20Log(1200) + 2.5Log(50/9) + 84

= 147.4 Endurance Level

Plane C

f_o = 600Log(140/5) + 400 ≤ 1600 H_z

L_o = 20Log(1400) + 84 = 147 Functional Level

L_o = 20Log(1200) + 2.5Log(50/9) + 84

= 147.4 Endurance Level

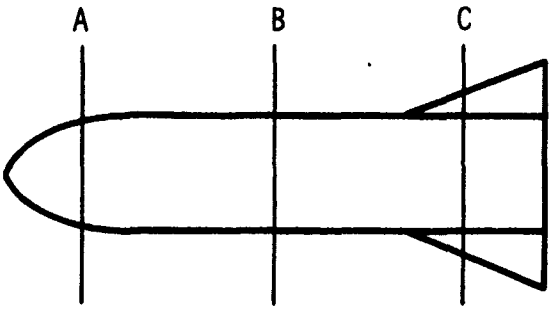

Fig. 11 - Store profile of Example I

TABLE 2

Properties of the Store in Example I

Reference Plane	Store Station (Inches)	Local Store Radius (Inches)
A	20	4.5
B	80	5
C	140	5

N = 50 q_{max} = 1400 psf
Length of Store = 160 inches
β_1 = 69° T = 3 hours

TABLE 3

Acoustic Test Criteria for the Store in Example I

Reference Plane	f_o (H_z)	*L_o Functional	L_o Endurance (T = 3 hours)	A
A	800	148	148	-6
B	1250	147	147	-6
C	1600	147	147	-6

* Since functional levels are the same as endurance levels, functional checks could be made during the endurance test. In this case, only 3 hours of testing is necessary.

Example II

Suppose a new store is being developed for use on a high performance aircraft. This store is designed for cluster carriage in either a TER or MER rack, total of 3 missions, and a maximum dynamic pressure of 1000 psf. The deployment of this store permits a maximum free flight dynamic pressure of 1500 psf. The shape of this store is shown in Fig. 12 and pertinent geometric data for this store is listed in Table 4.

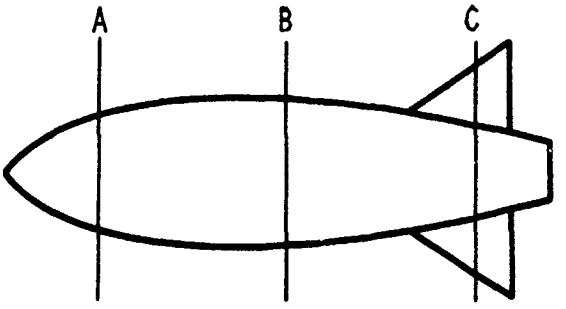

Fig. 12 - Store profile of Example II

Plane A

f_o = 600Log(16/6) + 400 ≤ 800 H_z

L_o = 20Log(1000) + 11Log(16) + 7Log(1-cos 24°) + 72 = 137.7 Functional Level

L_o = 20Log(1000/1000) + 2.5Log(3/3) + 137.7 = 137.7 Endurance Level

Plane B

$f_o = 600\text{Log}(50/10) + 400 \backsimeq 1000\ H_z$

$L_o = 20\text{Log}(1000) + 11\text{Log}(50) + 7\text{Log}(1\text{-cos } 24°) + 72 = 143.2$ Functional,

Endurance Levels

Plane C

$f_o = 600\text{Log}(84/7) - 200 \backsimeq 500\ H_z$

$L_o = 20\text{Log}(1000) + 11\text{Log}(84) + 7\text{Log}(1\text{-cos } 24°) + 72 = 145.8$ Functional,

Endurance Levels

Note: Since the store can be carried on a TER or MER rack these levels were raised 6 dB for the test criteria. Since functional and endurance test levels are the same for a test time, T = 1 hour, no endurance test is needed.

Free Flight Calculations

Plane A

$f_o = 800\ H_z$

$L_o = 20\text{Log}(1500) + 11\text{Log}(16) + 7\text{Log}(1\text{-cos } 24°) + 72$

$L_o = 141.2$

Plane B

$f_o = 1000\ H_z$

$L_o = 20\text{Log}(1500) + 11\text{Log}(50) + 7\text{Log}(1\text{-cos } 24°) + 72$

$L_o = 146.7$

Plane C

$f_o = 500\ H_z$

$L_o = 20\text{Log}(1500) + 11\text{Log}(84) + 7\text{Log}(1\text{-cos } 24°) + 72$

$L_o = 149.3$

Since the captive flight test levels are higher than the free flight levels no separate free flight test is required as long as the free flight functional checks are done during the captive flight test.

TABLE 4

Properties of the Store in Example II

Reference Plane	Store Station (Inches)	Local Store Radius (Inches)
A	16	6
B	50	10
C	84	7
Total Length of Store 100 inches		
$\theta_1 = 24°$ N = 3 T = 1 hour		

TABLE 5

Acoustic Test Criteria for the Store in Example II

Reference Plane	f_o H_z	L_o Functional MER Rack (T = 1 Hour)	A
A	800	144	-6
B	1000	149	-6
C	500	152	-6

REFERENCES

1. Dreher, J. F., Lakin, E. D., and Tolle, E. A., "Vibracoustic Environment and Test Criteria for Aircraft Stores During Captive Flight," Shock and Vibration Bulletin, No. 39, Supplement, April 1969.
2. Peverley, R. W., "Vibracoustic Test Methods for Vibration Qualification of Apollo Flight Hardware," Shock and Vibration Bulletin, No. 37, January 1968.
3. Piersol, A. G., "Vibration and Acoustic Test Criteria for Captive Flight of Externally Carried Aircraft Stores," AFFDL-TR-71-158, December 1971.
4. McGowan, P. R., Frasca, R. L., "Structural Design for Acoustical Fatigue," ASD-TDR-63-820, October 1963.
5. Ballentine, J. R., Plumblee, H. E., et. al, "Refinement of Sonic Fatigue Structural Design Criteria," AFFDL-TR-67-156, 1967.
6. Coe, C. F., and Nute, J. B., "Steady and Fluctuating Pressures at Transonic Speeds on Hammerhead Launch Vehicles," NASA TMX-778, December 1962.
7. Coe, C. F., "Steady and Fluctuating Pressures at Transonic Speeds on Two Space-Vehicle Payload Shapes," NASA TMX-503,

March 1961.

8. Wiley, D. R., and Seidl, M. G., "Aerodynamic Noise Tests on X-20 Scale Models," AFFDL-TR-65-192, November 1965.

9. Coe, C. F., "The Effects of Some Variations in Launch-Vehicle Nose Shape on Steady and Fluctuating Pressures at Transonic Speeds," NASA TMX-646, March 1962.

10. Dreher, J. F., "The Effect of Tailfins on the Vibracoustic Environment of Externally Carried Aircraft Stores," Shock and Vibration Bulletin, No. 41, Supplement, December 1970.

11. Kolb, A. W., and Magrath, H. A., "RTD Sonic Fatigue Facility, Design and Performance Characteristics," Shock and Vibration Bulletin, No. 37, Supplement, January 1968.

12. Lyon, R. H., Random Noise and Vibration in Space Vehicles, Shock & Vibration Monograph SVM-1, U. S. Government Printing Office, Washington D. C., 1967.

13. Eldred, K., Roberts, W., and White, R., "Structural Vibrations in Space Vehicles," WADD-TR-61-62, December 1961.

14. Dreher, J. F., "Aircraft Equipment Random Vibration Test Criteria Based on Vibrations Induced by Turbulent Airflow Across Aircraft External Surfaces," Shock and Vibration Bulletin, No. 43, 1973.

APPENDIX

METHOD 515, MIL-STD-810

3.5 Procedure II - Acoustic testing for assembled externally carried aircraft stores.

3.5.1 This acoustic test is performed to determine that the assembled store is constructed to withstand and perform in the expected dynamic environment. Procedure IIB of Method 514, assembled externally carried store vibration test, shall also be conducted to insure thorough testing from 20 to 2000 H_z. Acoustic testing of assembled externally carried stores is not required if the minimum value of f_o of para. 4.7.2.3 of Procedure IIB of Method 514 is greater than 1200 H_z.

3.5.2 Test Setup

The store shall be mounted in a suitable test facility as described in 3.4.1. A suitable acoustic noise source can be a jet engine on an open-air stand, a jet engine in test cell, or an acoustic test chamber. Provision for baffles shall be made so that the frequency spectrum can be shaped to the required profiles.

3.5.2.1 Microphone Placement

Three reference planes perpendicular to the longitudinal axis of the store shall be defined. The location of these reference planes is such that they are at positions which are one-sixth, one-half, and five-sixths of the length along the store. In each reference plane 3 microphones, 120 degrees apart, shall be positioned about the store. Each microphone shall be located within 18 inches from the surface of the store but no greater than one-half the distance from the nearest baffle, whichever is less.

3.5.3 Test Procedure

The response of the microphones which are in each reference plane shall be averaged giving one output for each reference plane. The one-third octave band sound pressure level about the entire store shall be shaped so that at the location of each of these three reference planes the frequency spectral profile shall envelope the frequency spectral profile of Figure 515.1-3 and the values of Table 515.1-II. A controlled acoustic environment below 100 H_z and above 2000 H_z is not required but these frequencies may be present because of the nature of the test facility.

For low power acoustic facilities which cannot excite the entire frequency range at one time, it is permissible to break the test into smaller frequency segments. The testing time for each of these segments shall be the same as that required if the entire spectrum is excited simultaneously.

3.5.3.1 Captive Flight Test

Two tests, functional and endurance, shall be conducted using their respective test levels given in Table 515.1-II. No endurance test is required if, for a one hour endurance test, the test level L_o is equal to or less than the corresponding functional test level. During the functional test, the store shall perform according to prime development specification operating requirements (ref. General Requirements para. 3.2.4). This test shall be for one hour. Proper performance of the store is only required after conclusion of the endurance test (ref. General Requirements para. 3.2.4).

3.5.3.2 Free Flight Functional Test

For stores that are deployed by separation from the aircraft (free flight) such as bombs and missiles, a free flight functional test shall be conducted in addition to the captive flight tests of para. 3.5.3.1. The equipment shall perform according to the equipment specification operating requirements (ref. General Requirements, para. 3.2) during the functional testing. Para. 3.5.2, para. 3.5.2.1, para. 3.5.3, Table 515-II, and Figure 515.1-3 shall be used to determine the test

procedures, levels and frequency spectra for the free flight test except as noted below. In this case, factor (N/3T) shall be set equal to one and no MER or TER cluster carriage factor shall be used. The value of q shall be the maximum value attainable during free flight. The duration of this functional test shall equal the maximum free flight time expected at maximum q, but not less than 30 seconds. In the event that all free flight functional checks are made during the captive functional test and the captive functional test levels are larger than or equal to those derived here (3.5.3.2), no free flight functional test is required.

3.5.4 References

Dreher, J. F., Lakin, E. D., Tolle, E. A., "Vibracoustic Environment and Test Criteria for Aircraft Stores During Captive Flight," Shock and Vibration Bulletin No. 39, Supplement, NRL, Wash, D.C., April 1969.

Dreher, J. F., "Effects of Vibration and Acoustical Noise on Aircraft/Stores Compatibility," Proc. Aircraft Compatibility Symp., Vol. 6, pp 245-272, Eglin AFB, Florida, November 1969.

Preliminary AFFDL Test Results of Laboratory Acoustic Chamber Simulation of Flight Vibration of Externally Carried Aircraft Stores, Technical Report Expected June 1973.

Burkhard, A., "Captive Flight Acoustic Test Criteria for Aircraft Stores," Shock and Vibration Bulletin No. 43, NRL, Wash, D.C., January 1973.

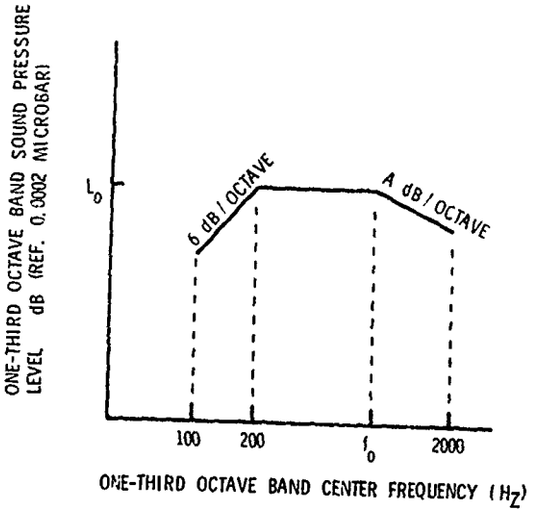

Fig. 515.1-3 - One-third octave band spectrum for acoustic testing of assembled externally carried aircraft stores

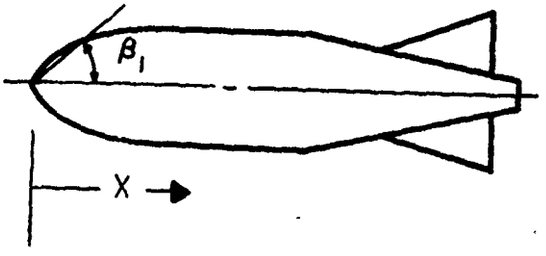

Fig. 515.1-4 - Typical store profile

TABLE 515.1-II Acoustic Test Levels for Assembled Externally Carried Aircraft Stores

Functional Test $L_o^{1,5,6,7} = 20\text{Log}(q_1) + 11\text{Log}(X) + 7\text{Log}(1-\cos\beta_1) + 72$

$f_o^{2,3} = 600\text{Log}(X/R) + C$

Endurance Test $L_o^{1,5,6,7} = 20\text{Log}(q_2/q_1) + 2.5\text{Log}(N/3T) +$ functional level

$f_o^{2,3} = 600\text{Log}(X/R) + C$

Definitions

q_1 = maximum captive flight dynamic pressure Lbs/Ft^2

q_2 = 1200 psf or maximum captive flight dynamic pressure (whichever is lower) Lbs/Ft^2

N = maximum number of anticipated service missions (minimum N = 3)

R[4] = local radius of store in inches

X = distance from nose of store along axis of store in inches

T = test time in hours (minimum T = 1 hour)

C = -200 locations within one D of aft end of store or aftward of re-entrant angle

C = 400 all other locations

A = -6 dB/octave $f_o > 400$ Hz

A = -2 dB/octave $f_o \leq 400$ Hz

D[4] = maximum store diameter in inches

β_1 = local nose cone angle at X equals 1 Tan β = (R/X)(ref Fig 515.1-4)

Representative Parametric Values to be used for Captive Flight when Specific Parameters are not Available

Store Type	Endurance	Local Nose Cone Angle Degrees	q max	f_o Nose Section	f_o Middle Section	f_o Aft Section
Air to Air Missile	100	69	1600	500	1000	500
Air to Ground Missile	3	12	1600	800	630	630
Instrument Pod	500	69	1800	500	1000	500
Reusable Dispenser	50	11	1200	630	1000	400
Demolition Bomb	3	24	1200	500	1000	630
Flat Nose Store	3	90	1200	400	630	315

Notes

1. Raise computed L_o level by 3 dB for a store carried in a TER cluster rack; by 6 dB for a MER cluster rack.
2. If calculated f_o is above 2000 Hz use upper frequency limit of 2000 Hz. If calculated f_o is below 200 Hz use 200 Hz.
3. Round off f_o upwards to a one-third octave band center frequency.
4. For stores which do not have circular cross-sections the radius used in the formulas shall be the radius of the circle which circumscribes the cross-section of the store.
5. For locations on flat nose stores ($80° \leq \beta_1 \leq 90°$) where $X < 100$
   Functional test $L_o = 20\text{Log}(q_1) - 6\text{Log}(X) + 96$
   Endurance test $L_o = 20\text{Log}(q_2) - 6\text{Log}(X) + 96 + 2.5\text{Log}(N/3T)$
6. For long cylindrical sections, $> 2D$, use for locations more than one D affward into the cylindrical section
   Functional test $L_o = 20\text{Log}(q_1) + 84$
   Endurance test $L_o = 20\text{Log}(q_2) + 84 + 2.5\text{Log}(N/3T)$
7. For changing radius section either aft of a long cylindrical section or when $X > 100$ on a flat Nose store, redefine X so that X = 1 at beginning of this section.
   Functional test $L_o = 20\text{Log}(q_1) + 11\text{Log}(X) + 84$
   Endurance test $L_o = 20\text{Log}(q_2) + 11\text{Log}(X) + 84 + 2.5\text{Log}(N/3T)$

DISCUSSION

Mr. Dickerson (Motorola): In our product line we are interested in protecting our circuits from the environment which was just discussed. Is there not another step that we have to take to get from the aerodynamic environment on the store to our circuits internally? Would that not be a strong function of the type of airframe on which that type of external store is carried?

Mr. Burkhard: That is true. This test criteria is for the complete store as a system. Are you talking about component testing?

Mr. Dickerson: Not necessarily a component, but a subsystem of a component.

Mr. Burkhard: I didn't present it here, but there is a new proposed random vibration component or subsystem test criteria for equipment installed in externally carried stores. This test criteria was based upon this same flight test I talked about, except that there are about 25 stores in this test criteria. The results and the criteria are discussed in a Flight Dynamics Laboratory technical report.

Mr. Kertesz (Lockheed Missiles & Space Company): Do you have any idea as to how the acoustic spectrum you derived compares with the pressure spectrum you measured in flight?

Mr. Burkhard: We did do comparisons. We had two to three microphones on the stores at various locations. We found in general that the measured captive flight acoustic environment as compared to the shaped one, the one before we enveloped it, had the same basic frequency content and relative amplitudes. However, our acoustic spectrum was generally less than the measured captive flight vibration acoustic spectrum. This was because these microphones were mainly put at locations where we might have shock or other phenomena at separation points.

Mr. Kertesz: Is the acoustic spectrum that you specified controlled in the chamber on the surface of the vehicle or at some microphone some distance away?

Mr. Burkhard: As the last two slides indicate, we define the acoustic environment by means of three microphones in each plane which are near the surface of the store. You are actually controlling then at each one of these three locations. You have to shape your required levels and spectrum around the store by means of those three locations.

Mr. Calkins(Naval Missile Center): What were your arguments for your upper boundary on the frequency? Why did you stop your roll-off at 2000 Hz?

Mr. Burkhard: We have not seen any real damage, equipment failures or structural failures, caused by frequencies above 2000 Hz. We don't say you have to cut your acoustic spectrum off at that point. It could go higher. We just say you have to control it to that point. We don't care what it is above that.

Mr. Calkins: What was your chamber?

Mr. Burkhard: It was a reverberation chamber.

Mr. Calkins: Did you do any investigation with progressive wave?

Mr. Burkhard: No, we were trying to make the test simple. We have the idea you could use, for example, a jet engine noise field with reverberent panels around it as your test facility. If you want to test live munitions, you wouldn't want to put these into an expensive chamber. They might explode.

Mr. Calkins: Do you contend that the best simulation for captive flight is to use a reverberation field? Is it more ideal than a progressive wave or is economy the major factor?

Mr. Burkhard: We did not investigate the progressive wave. I have no basis for a comparison.

AIRCRAFT EQUIPMENT RANDOM VIBRATION TEST CRITERIA BASED ON VIBRATIONS INDUCED BY TURBULENT AIRFLOW ACROSS AIRCRAFT EXTERNAL SURFACES

JOHN F. DREHER
Air Force Flight Dynamics Laboratory
Wright-Patterson AFB Ohio

The paper describes the development of random vibration test criteria for aircraft equipment whose prime source of vibration is turbulent airflow at the surface of the aircraft. Associated criteria for equipment vibration caused by jet engine noise or operation of aircraft guns can be found in references 15 and 16, respectively. The paper shows that the random vibration levels, as derived from the study of 4 jet aircraft, are generally less severe than existing applicable sinusoidal tests. The test levels are adaptable to a particular aircraft/equipment location and are based on the aircraft's aerodynamic pressure (q) and its surface geometry. The criteria contain both functional and fatigue test procedures. The paper stresses the importance of functional testing to alleviate operational malfunction. The fatigue test levels are adaptable from the standpoint that the level is based on the number of flights the equipment will be operational as well as the total qualification test time.

INTRODUCTION

Vibrations within jet aircraft are caused by a number of phenomena. The principal sources, generally, are: jet engine noise and turbulent airflow (pseudo-noise) which impinge on aircraft external surfaces; gust, landing, and takeoff loads; and on-board mechanical equipment such as engines and pumps. This paper describes the structural vibrations induced by turbulent airflow and generalizes the findings to develop pertinent, adaptable random vibration test criteria for aircraft equipment. These criteria are those recently proposed for inclusion in Method 514 of MIL-STD-810C, "Environmental Test Methods."

The results of the study are based on statistically significant quantities of measured flight vibration data from four distinct jet aircraft. Two of the aircraft used are fighter-bomber types and two are cargo types. Both fighter-bomber vehicles have engines which exhaust at or near the extreme aft fuselage such that most of the flight data measured could be considered as produced by turbulent surface airflow rather than from the jet engine noise. On the other hand, the cargo aircraft have wing mounted engines such that only the forward quarter fuselage data was considered applicable.

RELATIONSHIP BETWEEN VIBRATION & TURBULENT SURFACE AIRFLOW

The turbulent airflow impinging on an aircraft surface during high speed flight has sufficient oscillatory energy to cause significant vibrations in the surface structure [1]. This phenomena has caused extensive fatigue cracks in many military flight vehicles [2]. These surface vibrations are directly transferred, then, through the vehicle's internal structure and into the vehicle's equipment. Thus, the equipment vibration environment is a direct function of the surface airflow and the structure's dynamic transmissibility.

The characteristics of this turbulent airflow have been well established [3, 4, 5, 6]. Generally, it has a randomly oscillating amplitude and exhibits a frequency spectrum that varies continuously over a broad range. Its rms amplitude has been shown to be a function of the aircraft's aerodynamic pressure (q), Mach number (Mn), and local surface geometry. Generally, its magnitude increases with increasing q in a more or less linear fashion. Perturbations to this linear relationship occur at certain Mach numbers and are generally caused by local "shocks". These often occur in the transonic range (0.8 to 1.0 Mn) as well as at certain supersonic speeds. The flow over vehicle surfaces with irregular geometry is generally 15 to 25 decibels (5 to 20 times) more turbulent than flow over smooth surfaces. Such irregularities commonly found on aircraft are speed brakes, blade antennas, reentrant surface angles, engine boundary layer control

devices, open weapons bays, gun muzzles, and air conditioning exhaust ports.

Thus, we can expect equipment located in compartments adjacent to and immediately aft of surface irregularities to experience vibrations significantly higher than equipment in compartments adjacent to smooth external surfaces. Furthermore, since the aerodynamic source is random, the vibratory response is random [7]. The frequency characteristics of the input to the equipment is affected by the filtering (transmissibility) characteristics of the intermediate structure.

Over a broad range of flight vehicles, these structural filtering characteristics are reasonably similar. For example, most aircraft surfaces are principally monocoque consisting of light gage sheets riveted to stringers, frames, and longerons. Characteristically, these sheet metal surfaces, upon which the oscillating air directly impinges, have a sequence of natural vibration frequencies whose fundamental frequency is between 200 and 400 cps. While they vibrate at all of the forcing frequencies, they greatly amplify the vibrations at their natural frequencies. These frequencies, then, coupled with any significant resonances of the internal structure, are the dominant points on the frequency spectrum perceived by the aircraft's equipment. Figure 1 shows a typical spectrum of the structural vibration measured near an equipment mount.

DEVELOPMENT OF FUNCTIONAL TEST LEVELS

In the past two decades, and perhaps since the genesis of test specs, there has been considerable criticism that vibration test specifications are not realistic. The bulk of the criticism from industry, and recently from DOD equipment project officers, has been that test levels are too high. This criticism is especially intense when it has been discovered that an equipment item cannot pass its vibration test.

Environmental engineers have great difficulty in justifying the existing specifications, especially when they know that the environment is random while the test is sinusoidal, and when they know that the environmental levels vary appreciably from aircraft to aircraft and from point to point in the same aircraft while the existing specifications are relatively rigid. It is little wonder that reduction or complete waiving of test requirements has become more the rule rather than the exception in the last several years.

It follows that adaptable, random vibration tests are needed. Yet, since it is the usual custom that the equipment project engineer, rather than an environmental engineer, establishes the environmental test requirements for his equipment, any new adaptable test should be as easy to understand and apply as practicable. Thus, it is necessary to investigate the many parameters upon which test levels are dependent with a view toward simplifying the final criteria.

As discussed in the previous section, the aircraft equipment's environment is heavily dependent upon the characteristics of the turbulent flow at the vehicle's adjacent surfaces and the local structural dynamic transmissibility. As for this dynamic transmissibility, it is usually very difficult or impossible to determine. Perhaps the only practical approach is to statistically analyze measured flight vibration data from several flight vehicles and relate these, respectively, to the characteristics of the turbulent airflow at the vehicle surface adjacent to the vibration pickups, thus determining an average structural transfer function. Again, this is based on the assumption that most vehicles have similar construction.

As for the external flow, it can generally be parameterized in terms of the vehicle's surface geometry, aerodynamic pressure (q), and Mach number (Mn). As pointed out earlier, the vehicle's surface geometry causes a significant difference in the magnitude of the external flow turbulence for a given q. Thus, a practical approach in analysis is to break out the measured vibration data into various aircraft zones. These are characterized as zones adjacent to irregular surface geometry and zones adjacent to smooth surface geometry [6].

To include Mach number as a prediction parameter would also add a large degree of complication. Mach number effects are highly dependent upon local surface geometry and thus require too detailed a knowledge of the particular aircraft structure to be practical for use

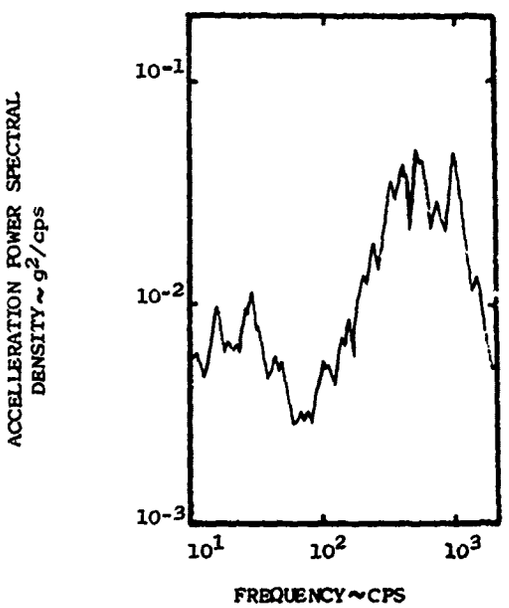

Fig. 1 Typical aircraft structural vibration spectrum measured near an equipment mount.

in such a document as MIL-STD-810.

Although Mach effects can occur at supersonic speeds, many occur at transonic speeds (0.8 to 0.95 Mn) at surface irregularities. The usual effect is a relatively abrupt increase in the magnitude of the local turbulence as the critical speed is approached, followed by a relative reduction in magnitude as this speed is exceeded. This phenomena is shown in Figure 2.

range. Furthermore, this linearity assumption is consistent with the relationship between vibration level and q in zones of smooth geometry.

Thus, the approach taken in this study was to assume that aircraft vibration levels are proportional to aerodynamic pressure (q), both in zones of smooth and irregular surface geometry, with the constant of proportionality, k, derived on the basis of a line that forms the

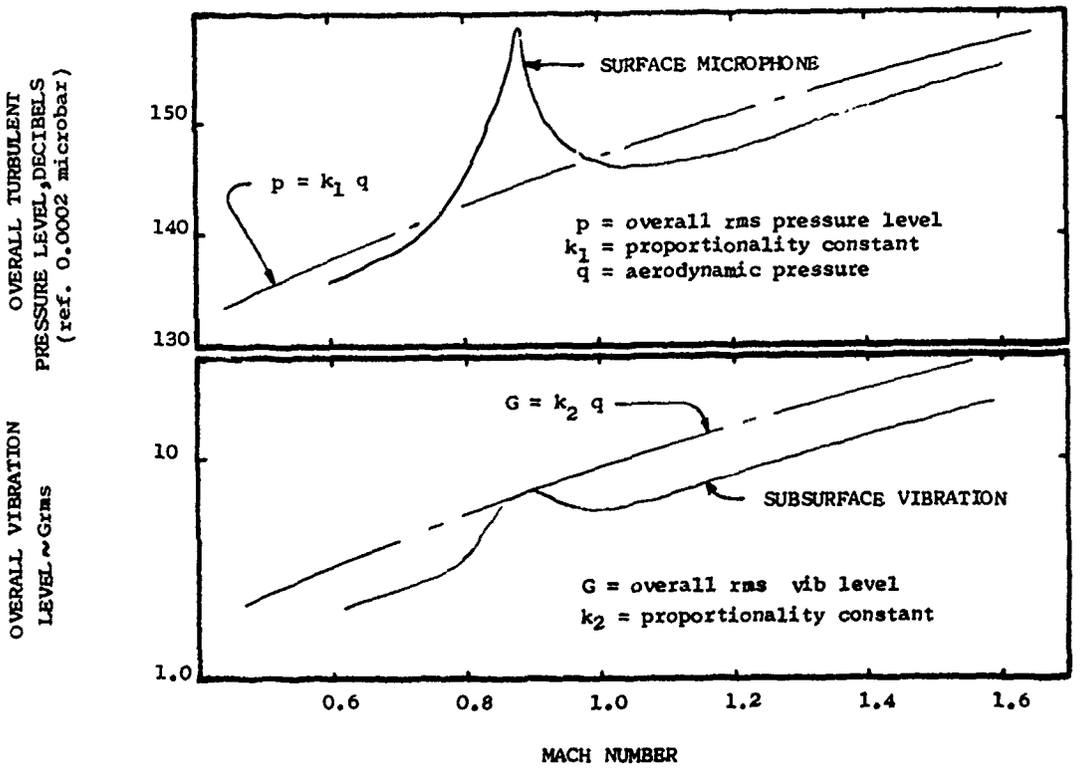

Fig. 2 Comparison of turbulent pressure and corresponding aircraft structural vibration as a function of Mach number (constant altitude).

Note in this figure that the turbulence level as well as the proximate vibration level tend generally to increase with increasing Mach number (and q), notwithstanding the perturbation at the critical Mach number. This suggests an approach which relates the vibration level directly as a linear function of q ($G = kq$) with the use of the vibration level at the critical Mach number to evaluate the coefficient k. Such a curve is also shown in Figure 2. This approach is described in more detail in references 8 and 9.

Admittedly, this relationship provides a conservative estimate of the vibration level at other Mach numbers. However, a significant percentage of the flight time of most vehicles is spent in this transonic range, and test levels are often based on measurements in this

upper tangent to the G vs q curve. As far as practicable, each vehicle used in the study was divided into zones of smooth and irregular surface geometry. When possible, the measurements in each zone were statistically analyzed (mean value, standard deviation σ) and the vibration level was established on the basis that 95% of the data in each zone was covered (mean value $+1.6\sigma$). The details of this process are shown in the next section.

ANALYSIS OF AIRCRAFT A

Aircraft A is a fighter-bomber type with extensive surface irregularities. The vibration data was separated into zones adjacent to smooth surfaces and zones adjacent to irregular surfaces. Although only small amounts of data were available from wing, stabilizer, and aft

fuselage (aft of wing trailing edge) zones, these zones were put in the irregular surface category. This step is considered reasonable because of high turbulences caused by external pylons and stores. Furthermore, equipment within wings and stabilizers are much closer to the source of vibration (i.e., less structural attenuation).

Figure 3 shows how the overall vibration levels vary with aerodynamic pressure. The curve representing each accelerometer is normalized based on its vibration level at 0.9 Mn. The curves shown were taken from flights at altitudes of 2000 feet and 30,000 feet. Note that a linear relationship between vibration level and q is not totally unrealistic.

the appropriate one-third octave bandwidth. Following this operation, all levels were increased by 4.5 decibels to insure enveloping the narrow band peaks [10]. This 4.5 decibel factor was determined by comparison of one-third octave band and narrow band plots of the same data. Figure 4 shows the results for both zones.

ANALYSIS OF AIRCRAFT B

Aircraft B is also a fighter-bomber. The analysis used was the same as used with Aircraft A. Unfortunately, no data was available to show the relationship between vibration level and q. However, vibration levels measured during takeoff and landing were available

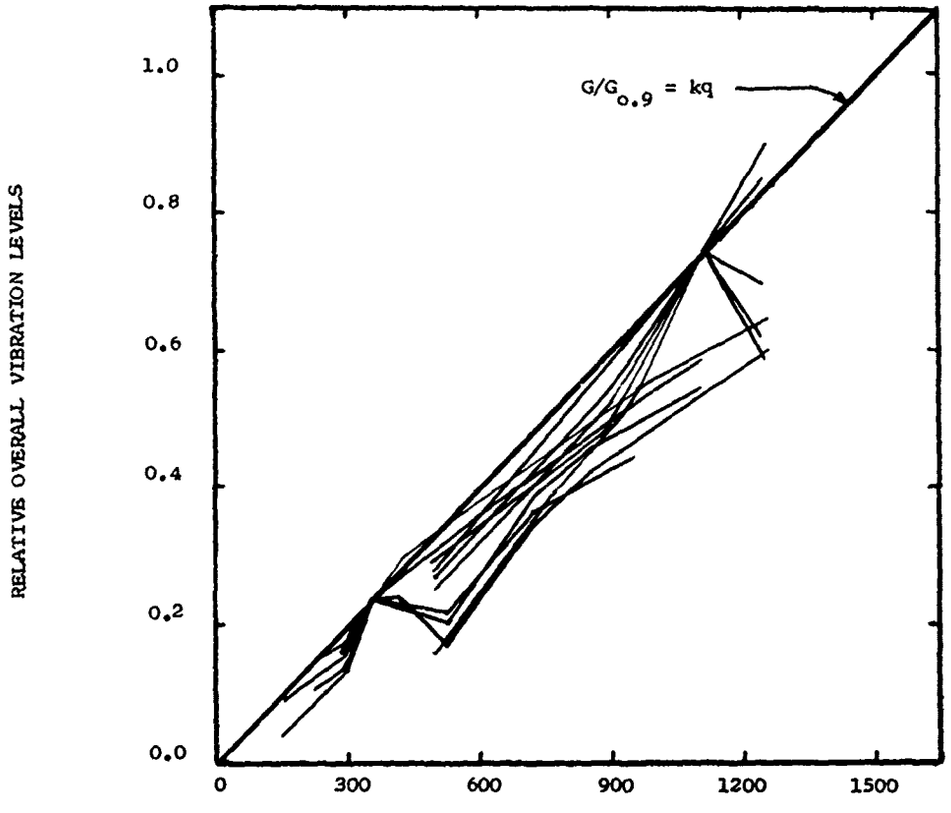

Fig. 3 Comparison of aircraft overall vibration level vs aerodynamic pressure. Data is taken from five accelerometers during flight at altitudes of 2000 feet and 30,000 feet. Vibration levels from each altitude have been normalized based on their levels at 0.9 Mach number.

To develop a test level, vibration data were used for flight conditions in the transonic range. One-third octave band frequency spectra were used to compute the mean level and standard deviation for each zone. These one-third octave band levels were then converted to power spectral density levels by squaring the one-third octave G_{rms} levels and dividing by

and are shown in Figure 5 along with the mean vibration levels and other parameters for transonic flight. Note how the takeoff and landing vibrations greatly exceed the flight vibration levels below 200 cps. This suggests that takeoff and landing should be considered in the development of the vibration test criteria. This subject is addressed further in the

Comparison of All Data section.

ANALYSIS OF AIRCRAFT C

Aircraft C is a four engine (wing mounted) jet cargo aircraft. Only data in the fuselage forward of the engines was used in the analysis

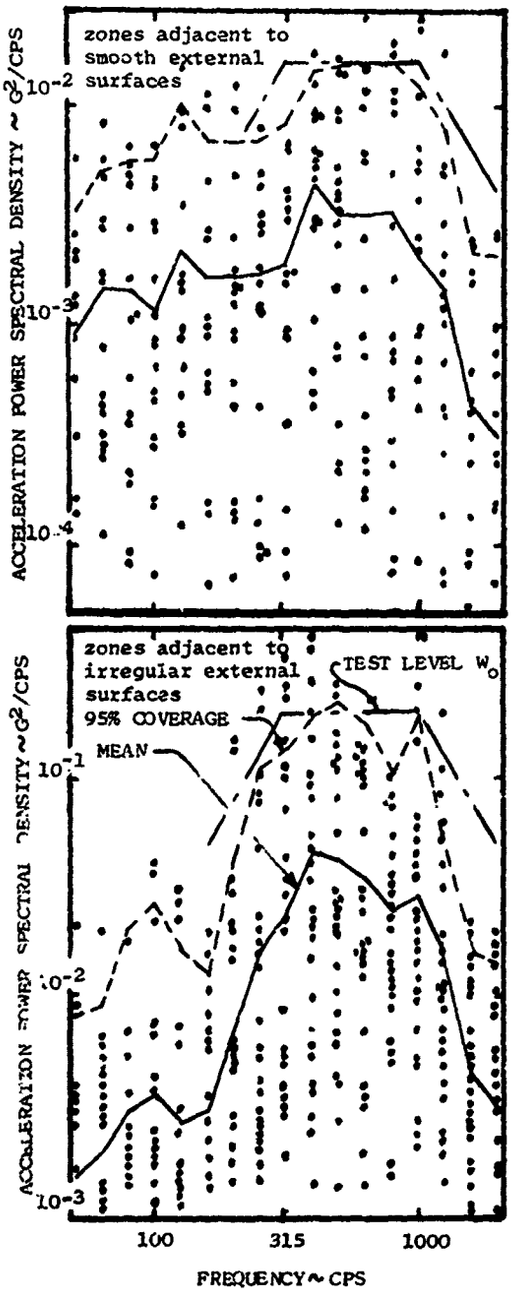

Fig. 4 Comparison of measured aircraft vibrations with qualification test levels for Aircraft A flying at 2000 feet and 0.9 Mach number (q = 1120 psf).

so as to eliminate the effects induced by jet engine noise. The data available for analysis was presented in terms of g^2/cps based on a 5 cps filter bandwidth analysis. Insufficient data was available to show the relationship between vibration level and q. Figure 6 shows the measured vibration levels and other parameters for q = 280 psf as well as during ground operations. In this case, the 95% qualification test level was obtained by constructing a line approximately 2 to 3 decibels below the maximum measured levels shown. This 2 to 3 decibel factor was derived from comparison of maximum levels and the 95% level from Aircraft A and B.

ANALYSIS OF AIRCRAFT D

Aircraft D is also a large four engine (wing mounted) jet aircraft. Again, only fuselage vibration data measured forward of the engines was used in the analysis.

Although a large number of accelerometers was used in this section of the fuselage, the available data was not sufficiently described so that mean zone levels and standard deviations could be computed. Rather, the available data was based on octave band filter analysis and only the upper 60% (two tail) confidence limits were shown. In an attempt to get at least ballpark results, these confidence limits were raised by a factor of 10 decibels and were used in that form as an estimate of the 95% data coverage curve. These are shown in Figure 7. The 10 decibel factor is the sum of a 7 decibel increase to insure enveloping the narrow band peaks [10, 5 (Page 25)] and a 3 decibel increase which the authors of reference 5 suggests will cover "most of the data" in the mid-frequency range (300 to 600 cps).

COMPARISON OF ALL DATA

Let us consider that a representative test curve can take the form shown in Figure 8. Then, Figure 9 shows the W_o test levels of Figures 4, 5, 6, and 7 plotted vs aerodynamic pressure. It can be seen that the relationship

$$W_o = 2.7 \times 10^{-8} \times q^2 \quad g^2/cps \qquad (1)$$

approximates the data for zones adjacent to smooth surfaces, and that the relationship

$$W_o = 14 \times 10^{-8} \times q^2 \quad g^2/cps \qquad (2)$$

approximates the data for zones adjacent to irregular surfaces.

With regard to the test level W_1 shown in Figure 8, it is sometimes more difficult to relate it to q. Vibrations in the low frequency range depend on the excitation of the bending and torsion modes of the vehicle's fuselage, wings, and empennage. While the higher frequency vibrations are almost totally dependent upon local surface flow and are thus highly repeatable from flight to flight [6, Page 97],

the lower frequency amplitudes are more dependent on transient exciting forces such as wind gusts, touchdown, and runway roughness, and are thus much less repeatable from flight to flight. Furthermore, the highest levels measured do not occur every mission, and perhaps occur only a few times over the life of the aircraft.

Since insufficient data is available to statistically characterize the vibration levels in this low frequency range, it was decided to use a test level that is based on sinusoidal test levels of approximately $\pm$ 1G to $\pm$ 2G which are commonly used in this frequency range (reference MIL-STD-810). Using a process similar to that described in a later section (comparison of Random and Sinusoidal Vibration Testing) for random/sine equivalence, the following test level was derived.

$$W_1 = 0.04 \quad g^2/cps \qquad (3)$$

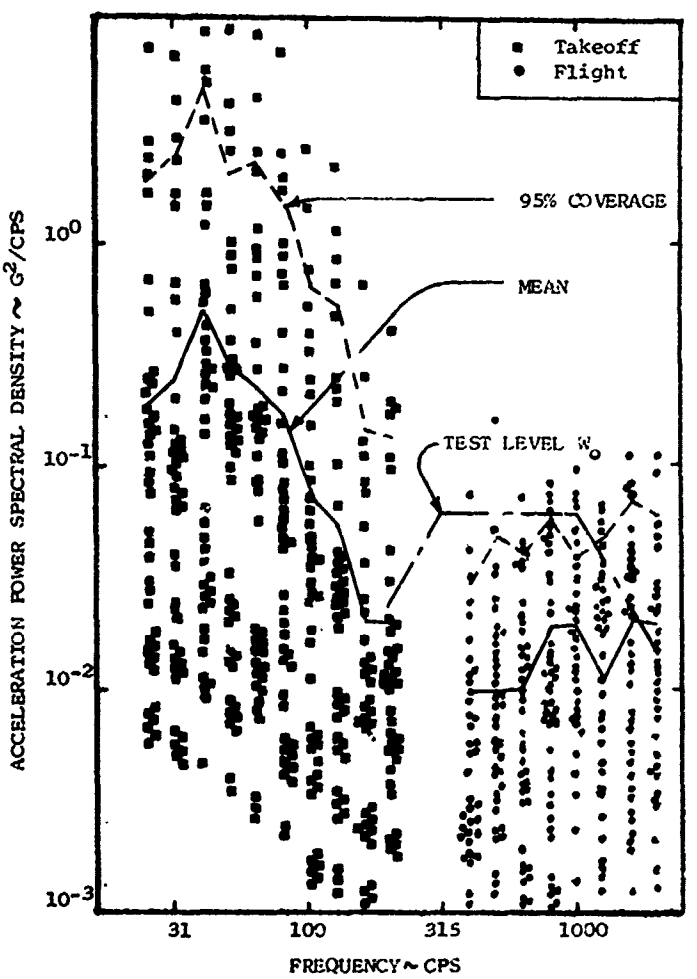

Fig. 5. Comparison of measured aircraft vibrations with qualification test levels for Aircraft B during ground operations and while in flight at 0.9 Mach number and 5,000 feet altitude (q = 1000)

As can be observed from Figures 4, 5, 6, and 7, this level is generally higher than flight measured data, but lower than some data measured during ground operations.

DEFINITION OF FUNCTIONAL TEST LEVELS

On this basis, the equipment functional qualification test levels shown in the Appendix were formulated. It is recommended that these functional test levels be computed using the maximum aircraft q. Such a practice will ensure that the equipment will function properly throughout the operating range of the flight vehicle.

Note that, unlike most conventional test specifications, the criteria in the Appendix contain both functional and fatigue tests. A separate functional test is deemed necessary so that the performance of an equipment item in the operational environment can be evaluated. Many instances of operational malfunction have been reported as caused by improper (or lacking) functional checks during laboratory vibration qualification [8, 11].

FATIGUE TEST LEVELS

Many operational equipment failures have also occurred because of material fatigue [11]. In developing qualification tests, it is a common practice to raise the test levels above the operational levels so that the test can simulate, in a relatively short time, the entire service life of the equipment.

In order to define an equivalent elevated fatigue test level, an equation of the form [12, 13]

$$G_f = G_o(T_o/T_f)^{\alpha} \qquad (4)$$

is often used, where G_f is the rms fatigue test level, G_o is the rms operational level, T_o is the operational time spent at vibration level G_o, T_f is the test time spent at level G_f, and α is a constant representing the slope of the curvalinear relationship between applied oscillatory stress and respective time (stress reversals) to fatigue failure of a given material. Although the reported values of α range considerably, values of 0.10 to 0.15 are often used for random vibration. In this case, the value of 0.125 is used because it appears to be a reasonable average. Thus, in terms of acceleration power spectral density (g^2/cps), we have, using equations of the forms (1) and (2) as an operational level and equation (4),

$$W_f = (W_c)(T_c/T_f)^{1/4} \; g^2/cps \qquad (5)$$

where W_f is the fatigue test level. Note that, when equation (4) is converted from terms of rms to terms of psd, the exponent becomes 2 α (i.e., 2x0.125 = 1/4).

Analysis of the mission profiles of several aircraft, including those in this study, shows that the flight time spent at maximum or near maximum q is approximately 20 minutes per flight. The exceptions to this are supersonic vehicles that obtain maximum q in the supersonic regime. They spend only a very small fraction of their time at maximum q, however, because of such factors as fuel economy and weapon delivery speed limitations. Their normal maximum q is usually about 1200 psf at which they usually spend a fatigue equivalent of 20 minutes per flight.

Thus, if we let N equal the total number

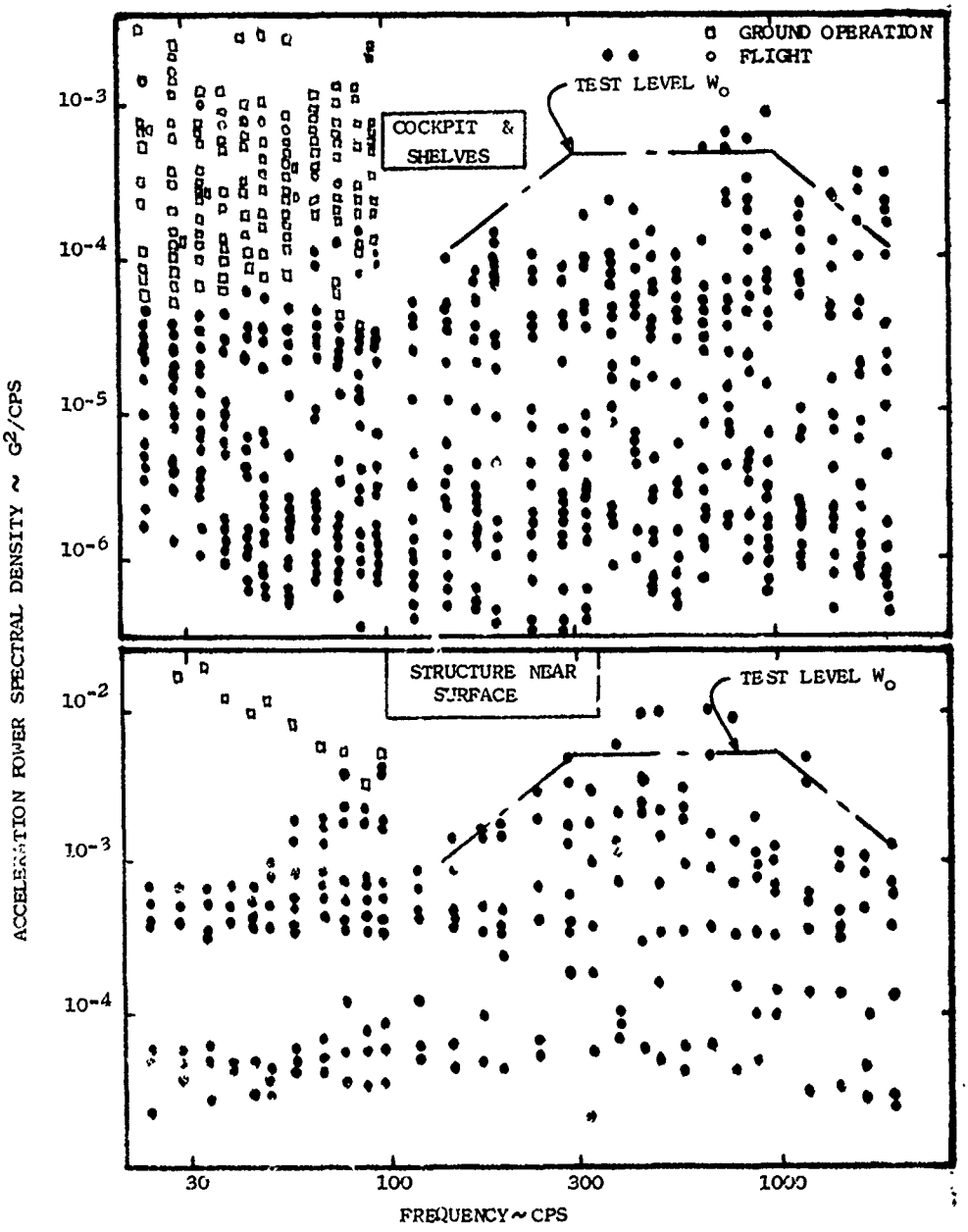

Fig. 6. Comparison of measured aircraft vibrations with qualification test levels for Aircraft C during ground operations and while in flight at 0.68 Mach number and 22,000 feet altitude (q = 280).

of missions a vehicle (or equipment) will fly over its lifetime, then

$$T_o = N/3 \text{ hours} \qquad (6)$$

and equation (5) becomes

$$W_f = (W_o)(N/3T)^{1/4} \qquad (7)$$

where T is the fatigue test time in hours and W_o is restricted by not allowing q to be larger than 1200 psf.

Equation (7) forms the basis for the fatigue (endurance) qualification tests shown in the Appendix. These fatigue tests are unique compared to most specifications since the test time is allowed to be variable and is left to the testing laboratory to decide. Permission to extend test time and thereby lower the fatigue test level is very practical in situations involving very heavy loads (relative to the shaker capacity) and in situations where high test levels may cause interference of equipment components (abrasion) which would normally not occur at operational (functional) vibration levels.

GENERAL PURPOSE EQUIPMENT

In many instances, an equipment item, such

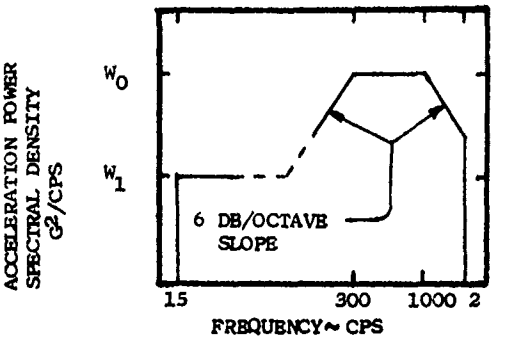

Fig. 8 Random vibration qualification test curve with undefined amplitude.

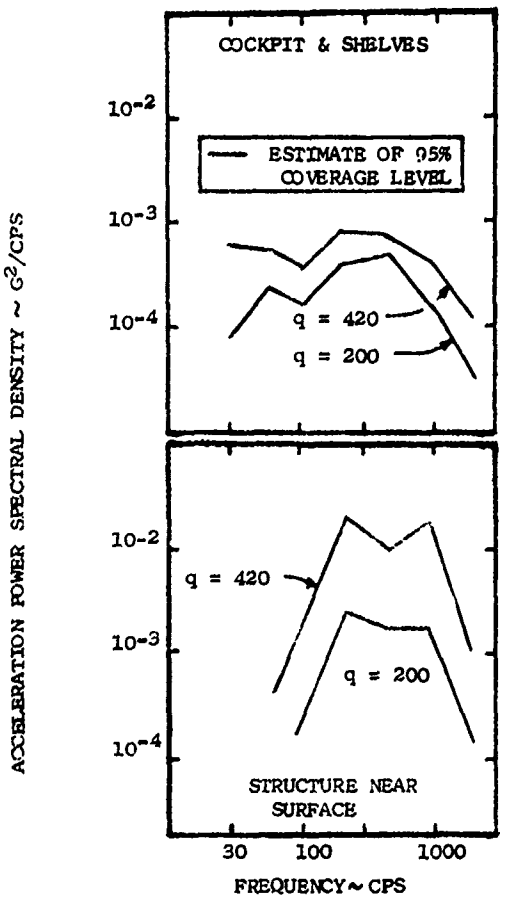

Fig. 7 Comparison of measured vibration levels and aerodynamic pressure, q, for Aircraft D.

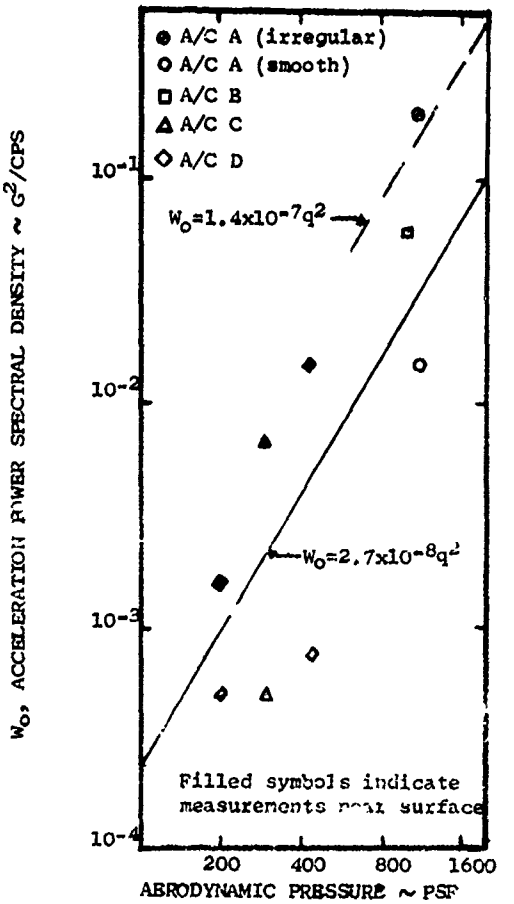

Fig. 9 Comparison of aerodynamic pressure q and W_o levels (ref Figure 8) for aircraft A, B, C, and D.

as a communication or navigation unit, is developed for use in a number of different aircraft types such that the project officer may not know all of its potential vehicle applications. In this case, the test criteria in the Appendix suggest a test suitable for a high performance fighter-bomber capable of flight at q = 1200 psf. Based on the assumption that these units may be placed in a compartment adjacent to an irregular surface, the test levels are

$$W_o = 0.20 \quad g^2/cps \quad (8)$$

$$W_f = (0.20)(1300/T)^{1/4} \quad g^2/cps$$

JUNK TESTS

In addition to the vibration and shock environments produced by aircraft, an equipment is also exposed to many dynamic environments produced by handling. As examples, consider removal and installation environments, accidental drops during transfer, and riding without its packing crate in the back of a jeep or field truck.

Equipment that could not survive this kind of environment has been labeled as junk. Of course, it is very difficult to determine exact amplitude and frequency statistics of this environment. However, our forebearers faced this problem by instituting a relatively simple sinusoidal test which is contained in a number of procedures in Method 514 of MIL-STD-810. In essence, the vibration level in this procedure is contained by the 0.10 inch double amplitude and ±2G curves and provides four ten-minute resonances and sweep on each of three mutually perpendicular axes. The test is in a "hard mounted" configuration and is applied to equipment that is isolated when installed in the aircraft. It was assumed that unisolated equipment would experience the standard ±10G test and, therefore, did not require this "extra" ±2G test.

In the test criteria in the Appendix, the ±2G test is also recommended for aircraft isolated equipment. To account for junk testing of equipment that are not aircraft isolated, however, a random junk test was developed. This is manifested by requiring a minimum fatigue (endurance) test level of 0.04 g^2/cps. Although the criteria in the Appendix states that this minimum level be applied to all equipment, it is relatively benign for isolated equipment.

This level was derived by equating the fatigue life expected when an equipment is exposed to a ten-minute, ±2G (or 0.10" DA) resonant environment and the fatigue life expected when exposed to a random level for one hour [13, 14]. This approach is explained in more detail in the next section.

COMPARISON OF RANDOM AND SINUSOIDAL VIBRATION TESTING

There are many who criticize random vibration tests as being much more severe than standard sine tests. Many people add up the total energy under the random curve (from 20 cps to 2000 cps) and exclaim that it is much greater than ±10G peak commonly found in sine tests. Yet the scientists tell us that it is not the total energy but only the energy near the resonance bandwidths that do the damage [13, 14].

On this scientific basis, let us compare the fatigue damage potential of the random tests herein and the standard ±10G peak test. References 12, 13, and 14 show us that the "fatigue equivalent" sinusoid G_f to the random power spectral density W_f is

$$G_f = \pm A\sqrt{\frac{\pi f_o W_f}{2Q}} \quad (9)$$

where A is an amplification factor relating the sinusoidal and random fatigue (S-N) failure curves for a given material, f_o is the resonance frequency, and Q is the amplification factor of the resonance.

If we can consider that the ratio f_o/Q = 10 in the 300 to 1000 cps frequency range and that A = 2 for a test time of 1/2 to one hour [14], then equation (9) becomes

$$G_f \cong 8\sqrt{W_f} \quad (10)$$

Applying equation (10) to a fatigue test level of $W_f = 0.10\ g^2/cps$, which is a typical level found in quiet aircraft zones, we find that the equivalent sinusoidal test level is only $G_f \cong \pm 2.5G$. In fact, it takes a level of $W_f \cong 1.6\ g^2/cps$ to be equivalent to a ±10G sinusoid. It is thus obvious that the test levels proposed in the Appendix are much less severe than most widely used sine tests.

Unfortunately, it is very difficult or impossible to draw "functional equivalences" between sine and random vibration. It is the author's judgment, however, that the random test is much more thorough. It has been observed that operational malfunctions were reproduced with random vibration which could not be reproduced by sine testing [8]. Sine testing is limited by the fact that only 4 (or a comparably small number) resonance dwells are run per axis while even the less complex equipments have many more resonances. While it is true that the associated sine sweeps do excite most of these other resonances, one must consider the short time period spent in any one resonance bandwidth and the fact that many of these resonances aren't excited long enough to peak out [12]. In contrast, the random test excites every resonance for the duration of the test.

It appears, then, that the random test proposed is a less severe but more thorough test.

SUMMARY

The paper describes the development of random vibration test criteria for aircraft equipment whose prime source of vibration is turbulent airflow at the surface of the aircraft. Associated criteria for equipment vibration caused by jet engine noise or operation of aircraft guns can be found in references 15 and 16, respectively.

The paper shows that the random vibration levels, as derived from the study of 4 jet aircraft, are generally less severe than existing applicable sinusoidal tests. The test levels are adaptable to a particular aircraft/equipment location and are based on the aircraft's aerodynamic pressure (q) and its surface geometry.

The criteria contain both functional and fatigue test procedures. The paper stresses the importance of functional testing to alleviate operational malfunction. The fatigue test levels are adaptable from the standpoint that the level is based on the number of flights the equipment will be operational as well as the total qualification test time.

REFERENCES

1. H. H. Hubbard, J. C. Houbolt, "Vibration Induced by Acoustic Waves," Ch. 48, Shock & Vibration Hdbk, McGraw-Hill, 1961.

2. Proceedings of the Symposium on Fatigue of Aircraft Structures, WADC Technical Report 59-507, Aug 1959.

3. K. M. Eldred, W. Roberts, R. White, "Structural Vibrations in Space Vehicles," WADD-TR-61-62, Mar 1961.

4. R. H. Lyon, "Random Noise and Vibration in Space Vehicles," Shock & Vibration Monograph SVM-1, U.S. Govt Printing Office, Wash DC 20402, 1967.

5. R. L. Barnoski, et al, "Summary of Random Vibration Prediction Procedures," NASA CR-1302, Apr 1969.

6. J. F. Dreher, W. D. Hinegardner, "RF-4C Vibration and Acoustic Environment Study," Shock & Vibration Bulletin 37, Supplement, Jan 1968.

7. S. H. Crandall, W. D. Mark, "Random Vibration in Mechanical Systems," Academic Press, 1963.

8. J. F. Dreher, E. D. Lakin, E. A. Tolle, "Vibracoustic Environment & Test Criteria for Aircraft Stores During Captive Flight," Shock & Vibration Bulletin 39, Supplement, Apr 1969.

9. J. F. Dreher, "The Effect of Tailfins on the Vibracoustic Environment of Externally Carried Aircraft stores," Shock & Vibration Bulletin 41, Supplement, Dec 1970.

10. D. L. Earls, J. F. Dreher, "Statistical Approach to Optimize Random Vibration Test Spectra," Shock & Vibration Bulletin 41, Supplement, page 30, Dec 1970.

11. A. Dantowitz, G. Hirschberger, D. Pravidlo, "Analysis of Aeronautical Equipment Environmental Failures," AFFDL-TR-71-32, May 1971.

12. M. Gertel, "Specification of Laboratory Tests," Chapter 24, Shock & Vibration Hdbk, McGraw-Hill, 1961.

13. J. W. Miles, "On Structural Fatigue Under Random Loading," Journal of Acoustic Society, Nov 1954.

14. G. Fitch, et al, "Establishment of the Approach to, and Development of, Interim Design Criteria for Sonic Fatigue," ASD-TDR-62-26, Jun 1962.

15. J. H. Wafford, J. F. Dreher, "Aircraft Equipment Random Vibration Test Criteria Based on Vibration Induced by Jet and Fan Engine Exhaust Noise," Shock & Vibration Bulletin No. 43, 1973.

16. R. Sevy, J. Clark, "Aircraft Gunfire Vibration," AFFDL-TR-70-131, Nov 1970 and Method 519, MIL-STD-810.

APPENDIX

PROPOSED TEST CRITERIA FOR METHOD 514
OF MIL-STD-810*

4.6.3 Procedure IA - Random vibration test for equipment installed in jet airplanes. (Not for turbo prop aircraft or jet powered helicopters.) The random vibration environment which occurs at equipment locations in jet aircraft stems from four principal sources:

a. Turbulent aerodynamic air flow along external surfaces of the aircraft structure.

b. Jet engine noise impinging on aircraft structure.

c. Gun blast pressure impinging on aircraft structure from high speed repetitive firing of installed guns.

d. General aircraft motions caused by such factors as runway roughness, landing, and gusts.

The tests outlined in the procedure consider all of these environments and require design to the most severe of these. These tests are preferred for use with equipment in jet aircraft in lieu of the sinusoidal tests of Procedure I, Table 514-II, Figure 514-2, except for jet engine mounted equipment. For equipment mounted directly to aircraft jet engines, use Procedure I. To determine an equipment specific random vibration test, compute functional and endurance test levels for aerodynamic induced and for jet engine induced vibration from Table 514-IIA and Figure 514-2A. Use the more severe of the two functional levels as the equipment's functional test, and the more severe of the two endurance levels (on an equal time, T, basis) for the equipment's endurance test. Gun blast tests shall be conducted in addition to this procedure, as applicable, in Method 519, if they are a higher level of severity.

4.6.3.1 Performance of Test. The individual equipment test item shall be subjected to broadband random vibration excitation. The power spectral density tolerances of applied vibration shall be according to para. 4.5.2. The test item shall be attached to the vibration exciter according to para. 4.2. Equipment hard mounted in service shall be hard mounted to the test fixture. Equipment isolated in service shall use service isolators when mounted on the test fixture. If service isolators cannot be made available during the qualification test, isolators shall be provided with characteristics such that the isolator/equipment resonant frequencies shall be between 20 hz and 45 hz with resonant amplification ratio between 3 and 5. Vibration shall be applied sequentially along each of the three orthogonal axes of the test item. Two test levels are required, a functional level and an endurance level. For each axis, one half of the functional test shall be conducted first, then the endurance test, followed by the second half of the functional test. The equipment shall perform according to the equipment specification operating requirements (ref. General Requirements, para. 3.2) during the functional testing. The acceleration power spectral density (G^2/Hz) of applied vibration, as measured on the test fixture at mounting points of the test item, shall be according to Table 514-IIA and Figure 514-2A. The functional and endurance test time durations and other test conditions shall be determined from the test level equations and other parameter values from Table 514-IIA.

4.6.3.2 Equipment with Isolators. Equipment designed for operational installation on vibration isolators shall also be subjected to a minimum rigidity endurance test with the isolators removed. This test shall be conducted according to para. 4.6.2, Table 514-II, and Curve AR of Figure 514-2. At the conclusion of this test the equipment shall provide specified performance. (Ref. General Requirements, para. 3.2.)

*Proposal also contains criteria for vibrations caused by jet engine noise.

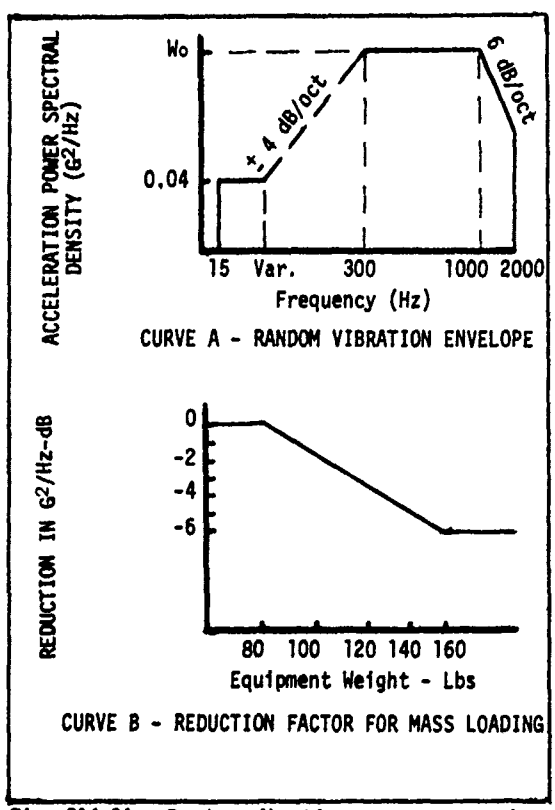

Fig. 514-2A. Random vibration test curve and mass loading reduction factor for jet aircraft equipment

TABLE 514-IIA

Random Vibration Test Criteria for Jet Aircraft Equipment

Criteria
Aerodynamic induced vibration (Curve A, Figure 514-2A)
Functional test level [1,5,6] $W_o = K(q_1)^2$
Endurance test level [2,3,5,6] $W_o = K(q_2)^2 (N/3T)^{1/4}$
Jet Engine noise induced vibration (Curve A, Figure 514-2A)
Functional test level [1,4,5,6,7,8] $W_o = (0.48 \cos^2\theta/R)[D_c(V_c/1850)^3+D_f(V_f/1850)^3]$
Endurance test level [2,3,4,5,6,7,8] $W_o = (0.48 \cos^2\theta/R)[D_c(V_c/1850)^3+D_f(V_f/1850)^3](N/10T)^{1/4}$
Gunblast induced vibration (See Method 519)

Definitions
K = 2.7×10^{-8} for cockpit panel equipment and equipment attached to structure in compartments adjacent to external surfaces that are smooth, free from discontinuities.
K = 14×10^{-8} for equipment attached to structure in compartments adjacent to or immediately aft of external surfaces having discontinuities (cavities, chins, blade antennas, speed brakes, etc.) and equipments in wings, pylons, stabilizers, and fuselage aft of trailing edge wing root.
q_1 = maximum aerodynamic pressure for carrying aircraft, psf.
q_2 = 1200 psf or maximum aircraft q, whichever is less.
N = maximum number of anticipated service missions for equipment or carrying aircraft. ($N \geq 3$)
T = test time per axis, hours ($T \geq 1$)
D_c = engine core exhaust diameter, feet (for engines without fans, use maximum exhaust diameter).
D_f = engine fan exhaust diameter, feet
R = minimum distance between center of engine aft exhaust plane and the center of gravity of installed equipment, feet.
V_c = engine core exhaust velocity, feet per sec. (for engines without fans, use maximum exhaust velocity without afterburner).
V_f = engine fan exhaust velocity, feet per sec.
θ = angle between R line and engine exhaust axis (aft vectored), degrees.

Notes
1. Functional test time shall be 1 hour per axis.
2. Use $W_o = 0.04$ g^2/hz if calculated endurance test level values are less than 0.04 g^2/hz, T = 1.
3. If one hour (T = 1) endurance test level is ≤ functional test level, no endurance test is required except according to Note 2.
4. If aircraft has more than one engine, W_o shall be the sum of the individually computed values for each engine.
5. If aircraft equipment location and/or using aircraft is unknown, use functional level, $W_o = 0.20$ g^2/hz and endurance level $W_o = (0.20) \times (1300/T)^{1/4}$.
6. For equipment weighing more than 80 pounds, the vibration test level may be reduced according to Curve B, Figure 514-2A.
7. For $70° \leq \theta \leq 180°$, use $\theta = 70°$ to compute W_o.
8. For engines with afterburner, use W_o which is 4 times larger than W_o computed using maximum V_c and V_f without afterburner.

DISCUSSION

Mr. Volin (Shock and Vibration Information Center): What do you consider to be a realistic percentage of aircraft life to use in design of equipment?

Mr. Dreher: What do you mean by realistic?

Mr. Volin: The percentage of the number of hours in the life of an aircraft.

Mr. Dreher: Well we kind of hedge that question and leave it up to the project engineer. I am the sort of a person who likes to see the equipment last for the life of the vehicle, like the radio in your automobile.

Mr. Volin: In short, you would like to see the radio outlast the airplane.

Mr. Dreher: Why don't we make it three or four lifetimes. We could use it in three or four airplanes.

Mr. Gertel (Kinetic Systems): Is there any variation of the test specification requirements made for different levels of equipment installation? In other words, are there any differences for components and sub-equipments within larger systems?

Mr. Dreher: No. These particular levels are for the black box type of assembled unit. It's not for an electronic unit that is part of a black box.

Mr. Gertel: Is any consideration being given to developing criteria for sub-structures or sub-components?

Mr. Dreher: Not right now, at least not by our organization. Rome Air Development Center does this kind of work. Perhaps they have some data.

AIRCRAFT EQUIPMENT RANDOM VIBRATION TEST CRITERIA BASED ON VIBRATION INDUCED BY JET & FAN ENGINE EXHAUST NOISE

J. H. Wafford
Aeronautical Systems Division
Wright-Patterson Air Force Base, Ohio

and

J. F. Dreher
Air Force Flight Dynamics Laboratory
Wright-Patterson Air Force Base, Ohio

This paper shows the development of a random vibration test criteria for aircraft equipment based on vibrations induced by jet engine noise. This criteria is to be used in conjunction with the criteria based on turbulent airflow currently proposed for inclusion into MIL-STD-810, "Environmental Test Method", and presented in another SVIC paper by Dr. J. F. Dreher. These criteria are developed in a unique formulation using existing prediction techniques for both noise and vibrations and are compared with measured data from a number of current engines and aircraft. The proposed criteria are a departure from the present rigidly established test curves and methods of military specifications and standards and allow the engineer to adjust or adapt the levels and durations depending on the equipment location relative to the acoustic source and the intensity and duration of exposure to the environment.

INTRODUCTION

Modern aircraft propulsion units are intense random noise generators. This random noise emanates from the complex turbulent pressure fields generated by the jet and fan engine exhaust. When the noise from this turbulent pressure field impinges on the aircraft structure, it induces structural vibrations which are transmitted to equipment locations within the airframe. This paper describes the prediction of random vibration levels induced at equipment locations by jet and fan engine exhaust noise.

This work is a follow on to that of the previous paper [1] by J. F. Dreher on vibrations induced by turbulent airflow and should be used in conjunction with that work to establish pertinent criteria for random vibration test of aircraft equipment. Both criteria have been recently proposed for inclusion into MIL-STD-810C, "Environmental Test Methods".

The philsophical approach taken was that any criteria or engineering method that is to be usable by the environmental test engineer or a specific equipment project engineer must be relatively simple and easy to apply. Therefore, in order to achieve this and present a somewhat conservative criteria, a number of approximations were made.

With these factors in mind, the test criteria shown in the Appendix of Reference 1 contained in this bulletin were formulated. The development of these criteria is accomplished in three major steps, namely

1. Prediction of surface noise levels.
2. Relationship between surface noise and internal vibration.
3. Formulation of the test criteria.

PREDICTION OF SURFACE NOISE LEVELS

The first step in the development of the random test levels is the prediction of the jet or fan engine near field noise levels on the surface of the aircraft. As a base, the jet noise prediction technique developed by

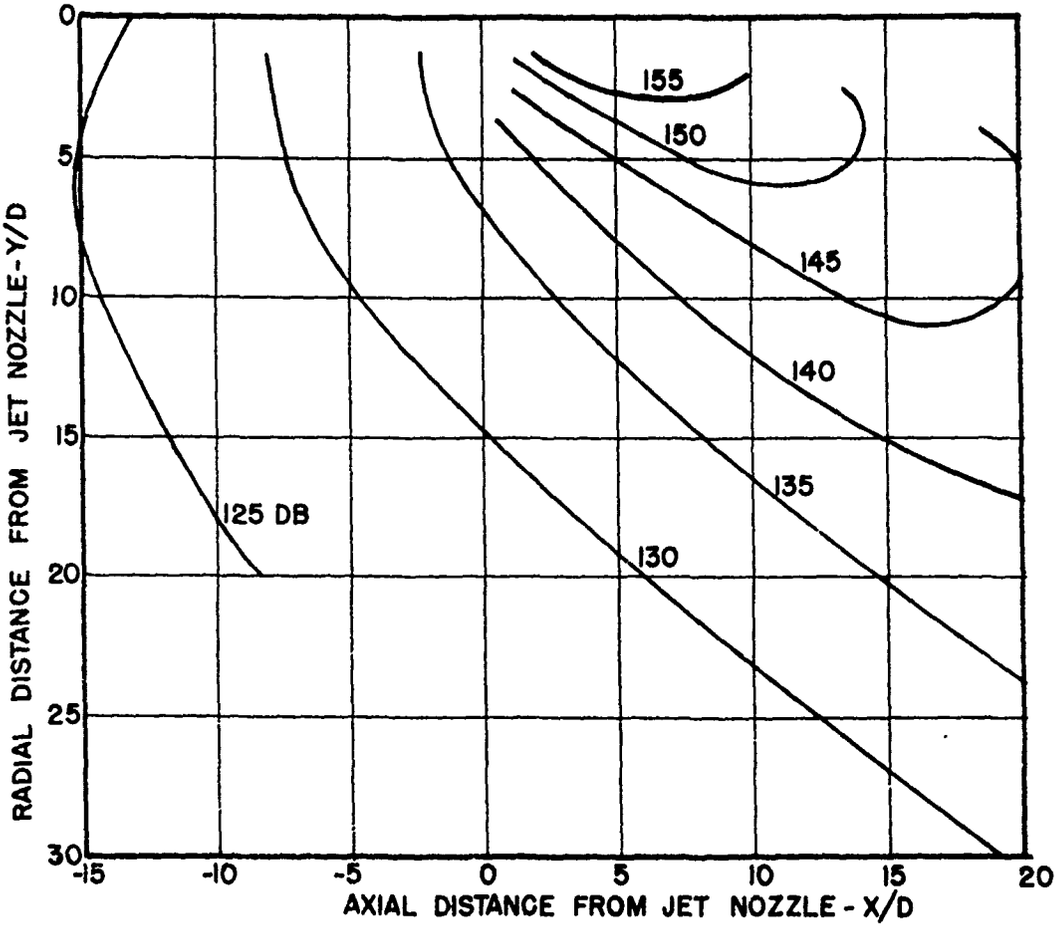

FIGURE 1 - NEAR SOUND FIELD OF A TURBOJET
REFERENCE CONTOURS OF OVERALL SOUND PRESSURE LEVEL [2]

Franken et al, and outlined in Reference 2 is used. The near field overall sound contours of Figure 1 are from Figure 16 of Reference 2 and are based on the J-57 engine data collected by Walton Howes [3].

A relatively simple mathematical expression was determined that approximates the contours of Figure 1. In its formulation, accuracy of the overall sound pressure levels above 145 dP was of prime concern, since noise-vibration correlations show rather negligible vibration power spectral densities below this level, as discussed in the next section [1, 4]. It was found that the following equation gives a reasonably close approximation for levels higher than 140 dB.

$$P_{oa} = 1.6(D/R)\cos^2\theta \qquad (1)$$

where P_{oa} is the overall rms oscillating pressure (psi), D is the engine exhaust diameter (ft.), R is the distance from the center of the engine exhaust plane to a given point in space (ft.) and θ is the angle between the engine thrust axis and the R line. The family of curves generated by this equation is shown in Figure 2. The curves in Figure 2, which are shown in terms of decibels, are related to the pressure levels, P_{oa}, in Equation 1 by the relationship

$$dB = 20 \log(P_{oa}/P_r)$$

where P_r is approximately 2.87×10^{-9}psi.

In order to adapt these curves to a particular installation, engine exhaust velocity changes, ground reflection and pressure doubling on the aircraft structure must be considered [2]. These corrections, in terms of decibels, are as follows:

Exhaust Velocity and Ground Reflection:

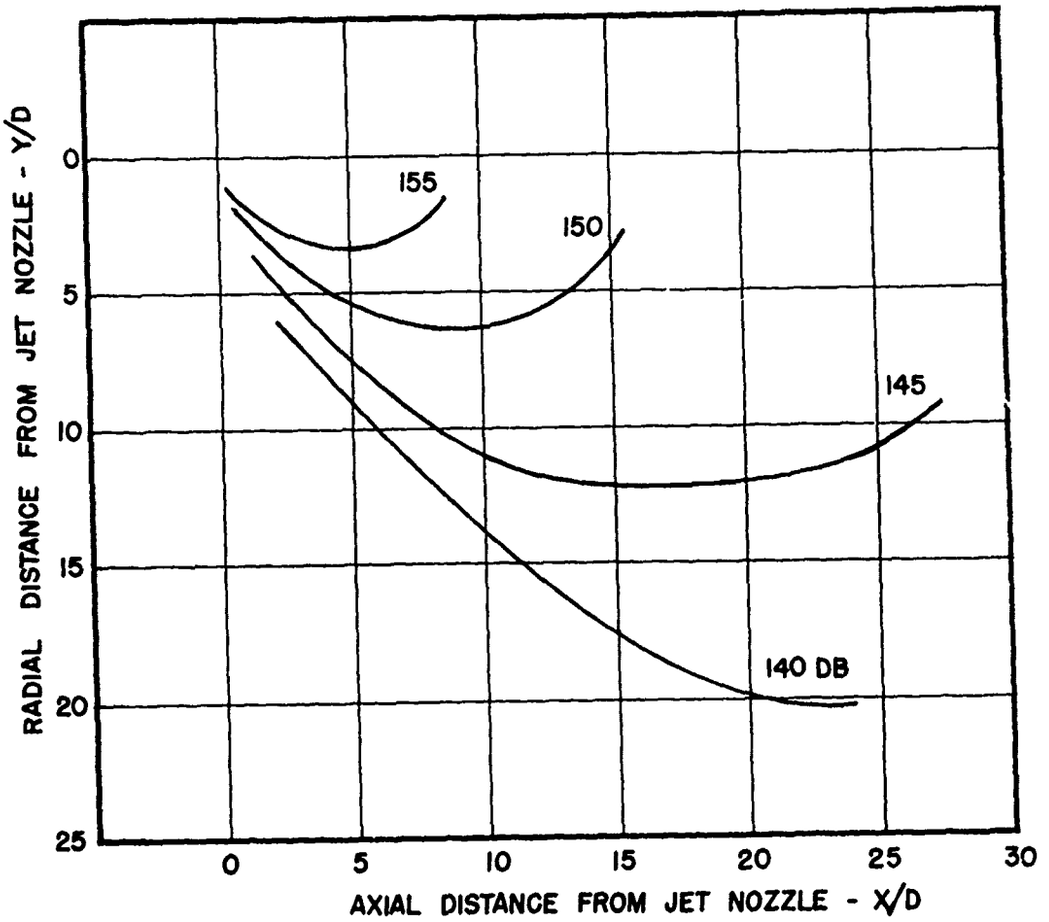

FIGURE 2 - PREDICTED SOUND PRESSURE LEVEL CONTOURS (EQ'N I)
REFERENCE CONTOURS OF OVERALL SOUND PRESSURE LEVEL

$$F = 65 \log_{10}(V/1850) \text{dB} \quad (2)$$

Aircraft Surface Reflection Correction:

$$+3 \text{ dB} \quad (3)$$

The velocity exponent used was 6.5 in lieu of the 8 from Equation 10 of Reference 2 based on the recommendation of Hermes and Smith [5] from their measurement and analysis of the near field of a J57-21 engine and consideration of ground reflection. The exhaust velocity of the engine used to establish the basic contours was 1850 ft./sec.

Since reflection of acoustically radiated noise on the surface of an aircraft causes pressure increases above free field levels ranging from 0 to 6 dB, 3 dB was chosen as an average level increase for the reflection correction value.

Based on Equations 1, 2, and the reflection correction, 3, the overall pressure level can be approximated by

$$P_{oa} = 2.26(D/R)(V/1850)^3 \cos^2\theta \quad (4)$$

The velocity exponent was changed from 3.25 to 3 for computational convenience on the slide rule.

Equation 1 has a shortcoming in that all contours go to the origin (X/D = Y/D = 0) when $\theta = 90°$. Therefore, for angles greater than 70°, the $\cos^2\theta$ term was made to remain constant, i.e. 0.12. The accuracy of this action is verified in the later section on Comparison of Predicted vs Measured levels.

If we consider afterburner (A/B) operations in accordance with Reference 2, an increase on the order of 8 dB will generally result over the maximum non-A/B operation of an

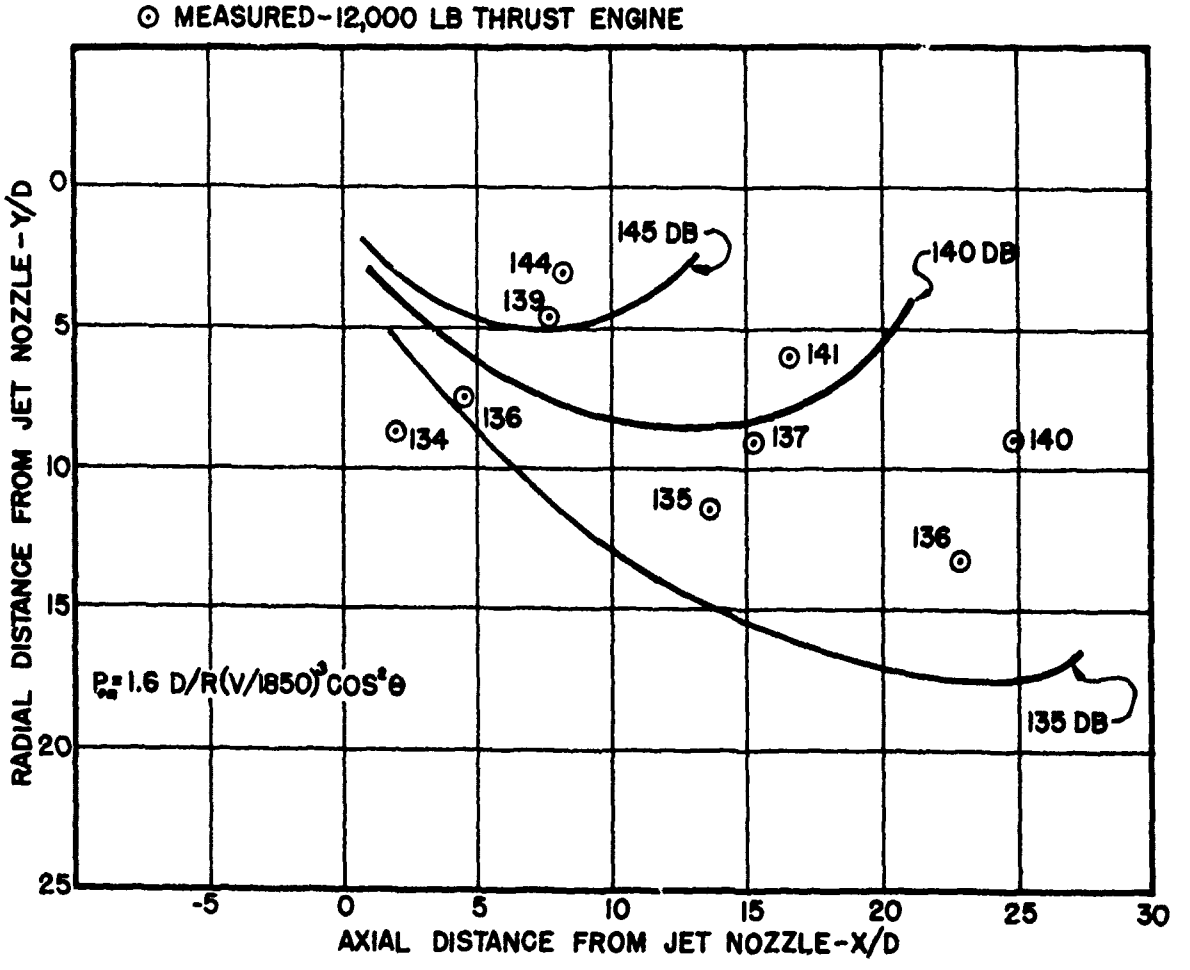

FIGURE 3 MEASURED VERSUS PREDICTED FREE FIELD OVER-ALL SOUND PRESSURE LEVELS FOR TURBOFAN ENGINE

engine. However, based on the authors' experience with measured data on aircraft with A/B, 6 dB should be added, instead, to Equation 4 using a V obtained for the maximum non-A/B power operation of the engine.

Although the basic method [2] used in predicting the surface noise is meant primarily for jet and not fan engines, the method does quite well when applied to fan engines. However, when using this equation to predict the fan engine exhaust noise, the fan and the core should be considered separately, i.e., velocity and diameter of each respectively, and the pressures added at the location of interest. For fan engines, Equation 4 takes the form

$$P_{oa} = 2.26\cos^2\theta/R[D_c(V_c/1850)^3+D_f(V_f/1850)^3] \quad (5)$$

where V_c and V_f and D_c and D_f are the velocities and diameters of the core and fan, respectively.

If we exclude the surface reflection correction of +3 dB we have a constant of 1.6 instead of 2.26 in Equation 4 and 5 and can then

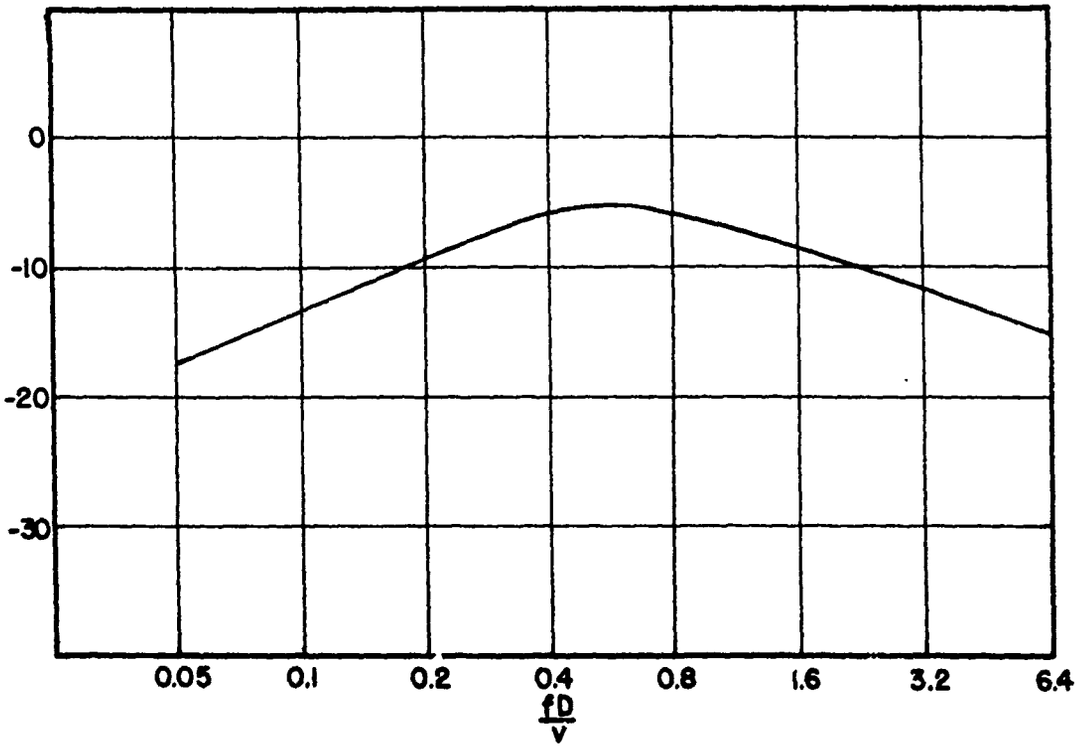

FIGURE 4 - SPECTRUM OF JET NOISE NEAR FIELD [2]

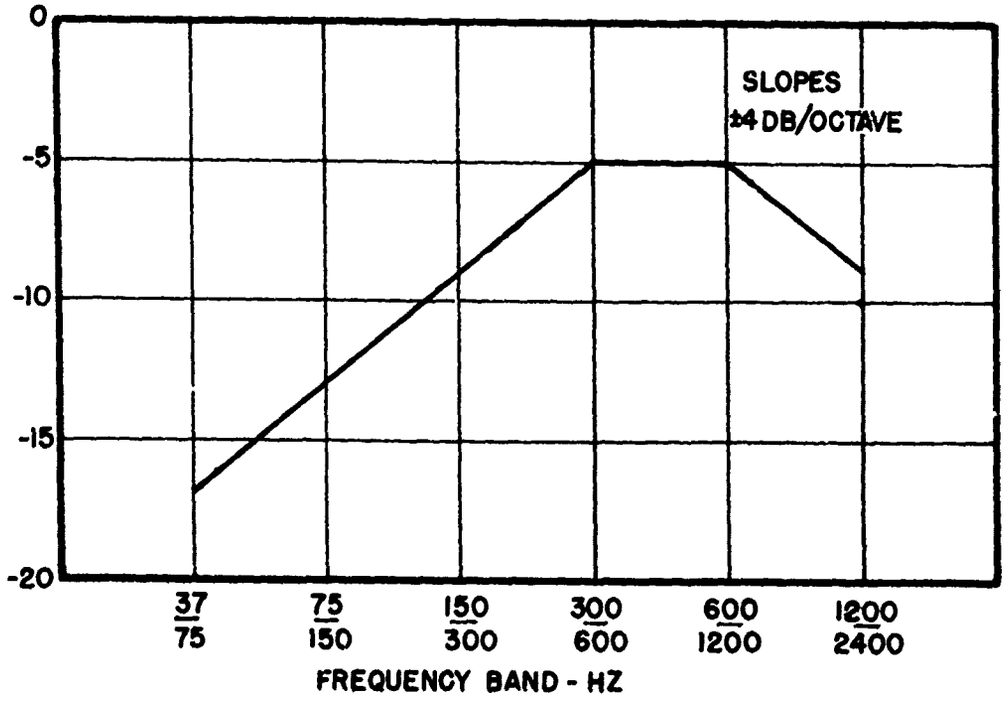

FIGURE 5 - SUGGESTED OCTAVE BAND SPECTRUM FOR
FOR NOISE FROM TYPICAL AIRCRAFT ENGINES

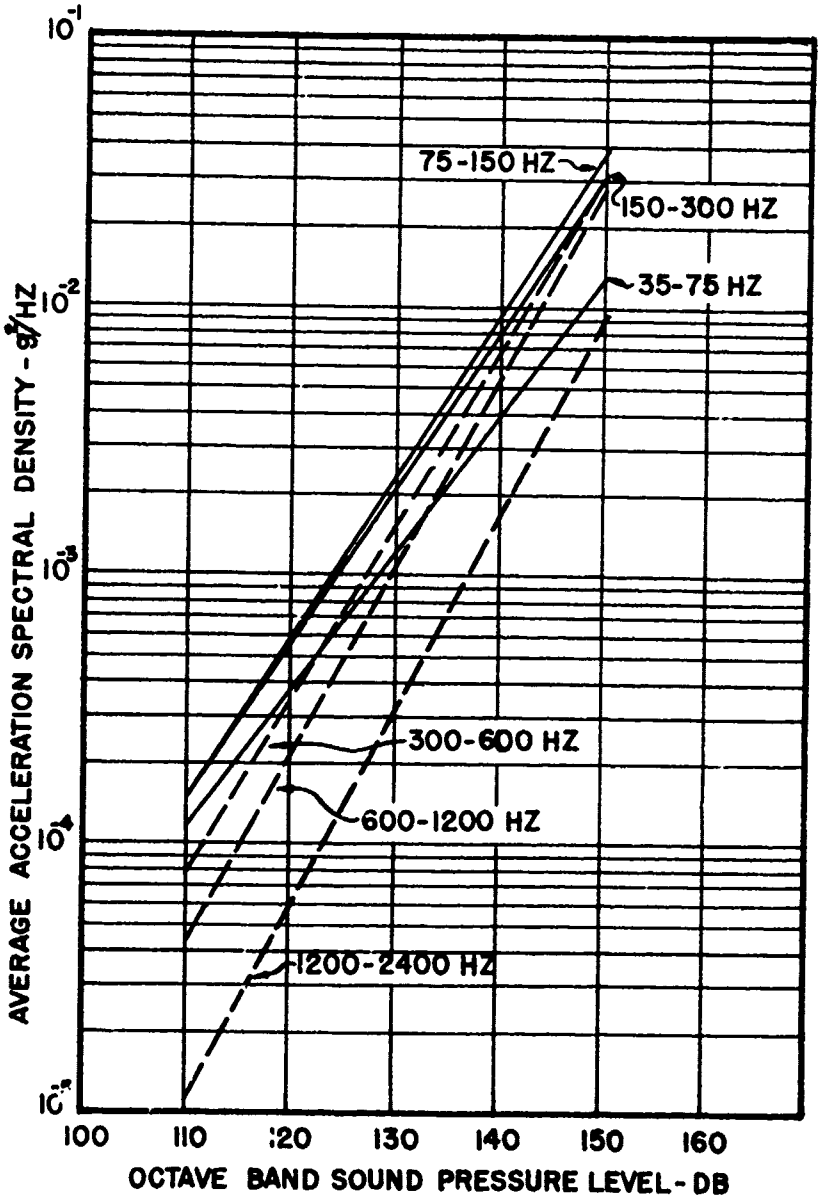

FIGURE 6 - RELATIONSHIP BETWEEN EXTERIOR SURFACE NOISE LEVEL AND CORRESPONDING INTERIOR VIBRATION LEVEL IN AIRCRAFT [7]

make comparison to engine test stand data [6]. Figure 3 shows a comparison with a fan engine. The measured data compares rather well with the predicted.

Most vibration-noise prediction criteria are based on octave band levels. Therefore, the pressure level in octave bands must be determined. Figure 4, which is taken from Figure 19 of Reference 2, shows the octave band spectrum for a jet engine exhaust.

Normally, engine diameters range from 12 inches to 24 inches and have exhaust velocities from 1000 to 2000 feet per second. This, therefore, from the octave band spectrum relation of Figure 4, would put the peak of the spectrum between 300 and 1000 Hz, and the suggested spectrum for octave bands would be as shown in Figure 5.

NOISE-VIBRATION RELATIONSHIP

TABLE I

Octave Band Vibration PSD Level Equations

Frequency Band (Hz)	Equation
75 - 150	$S_o = 0.153\ (D/R)(V/1850)^3\cos^2\theta$
150 - 300	$S_o = 0.267\ (D/R)(V/1850)^3\cos^2\theta$
300-600/600-1200	$S_o = 0.424\ (D/R)(V/1850)^3\cos^2\theta$
1200 - 2400	$S_o = 0.089\ (D/R)(V/1850)^3\cos^2\theta$

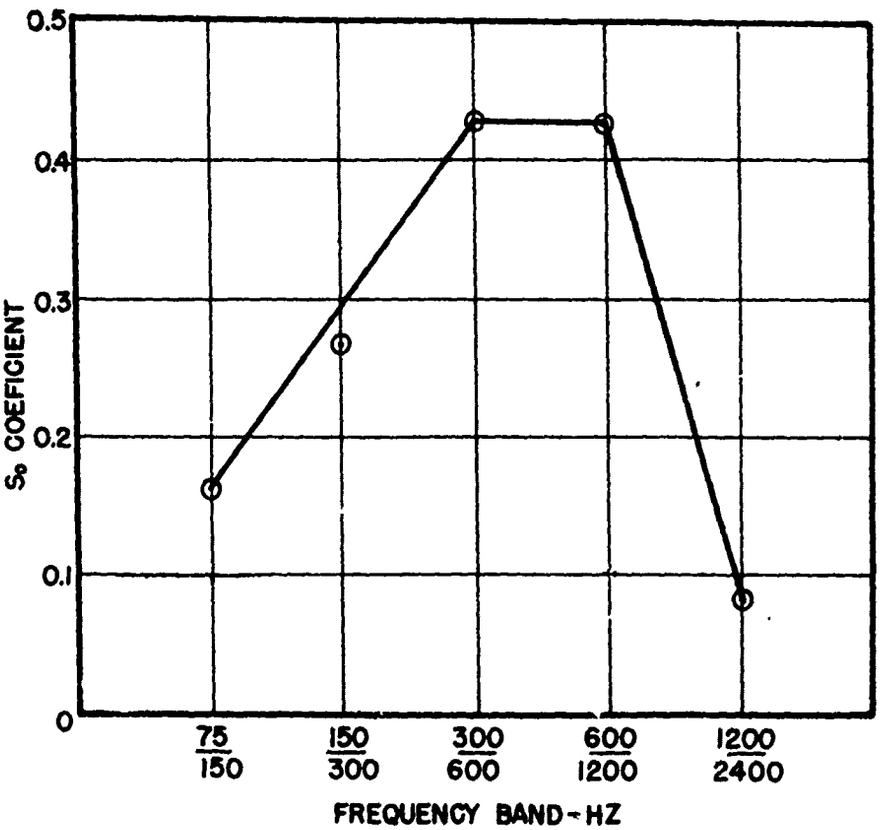

FIGURE 7 - AIRCRAFT VIBRATION SPECTRUM (REF. EQ'N. 7) PRODUCED BY JET ENGINE NOISE

The second step in the development of the random vibration test levels is to find a simple relationship between noise and vibration levels. The Brust-Himelblau (B-H) [7] adaptation of the Mahaffey-Smith [8] method provides an adequate relationship between octave band sound pressure levels and power spectral densities. These relationships are shown in Figure 6 (adapted from Reference 4).

From Figure 6, the relationships for various octave bands can be approximated by the following:

35-75 cps OB	$S_o = 1/7\ P_{OB}$	
75-1200 cps OB's	$S_o = 1/3\ P_{OB}$	(6)
1200-2400 cps OB	$S_o = 1/9\ P_{OB}$	

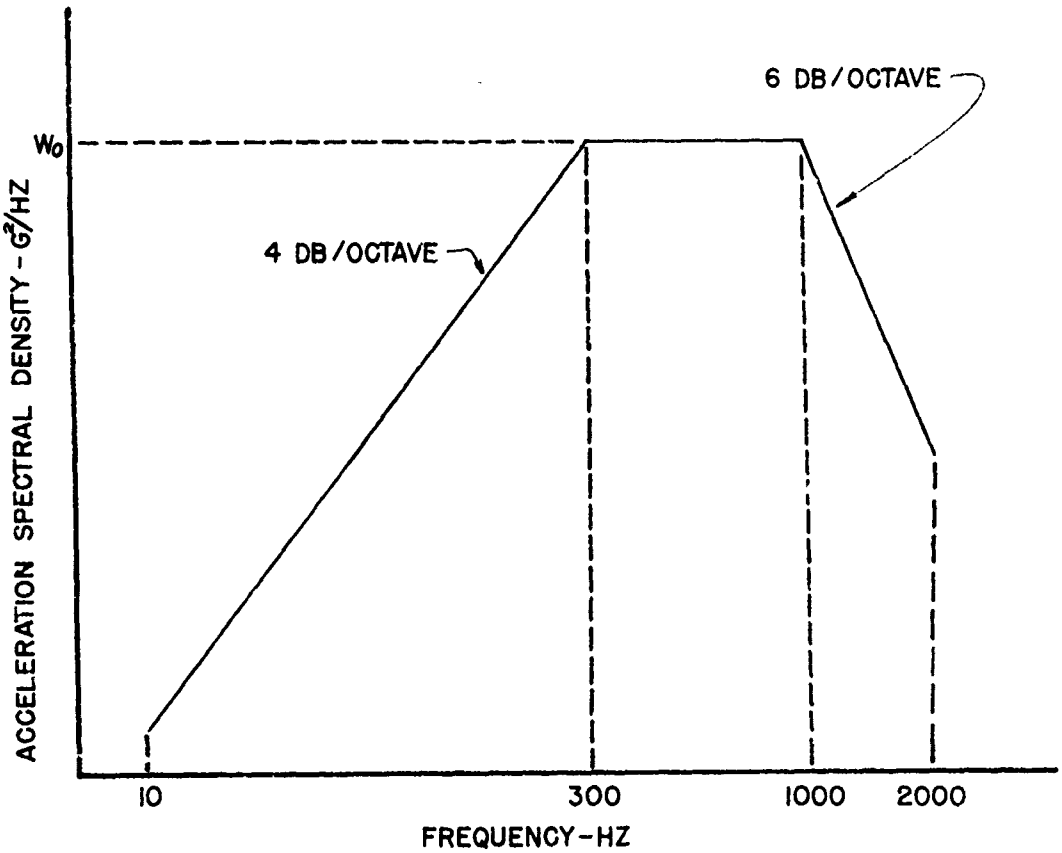

FIGURE 8 - ACCELERATION SPECTRAL DENSITY TEST SPECTRUM

where S_o is the psd level in g^2/Hz, and P_{OB} is the octave band pressure level. These approximations are accurate at P_{OB} = 150 dB and conservative by not more than 3 dB at P_{OB} = 130 dB. B-H [4] recommended that the random vibration (S_o) levels be increased by 7 dB to insure that PSD peaks are covered. This is consistent with the results of Earls and Dreher [9].

VIBRATION FUNCTIONAL TEST

Using Equation 4 and the octave band approximations of Equation 6 in conjunction with Figure 5, the vibration power spectral density level equations of Table I are obtained for the specific frequency band. Figure 7 shows S_o coefficient for the equations of Table I. Adding 7 dB to S_o to cover the spectral peaks [4] the functional test level becomes

$$W_o = 0.95\ (D/R)(V/1850)^3\cos^2\theta \qquad (7)$$

and the spectrum shape is shown in Figure 8. This functional test level is to be applied for one hour through each of 3 mutually perpendicular equipment axes. (See Appendix of Reference 1 for the vibration test.)

If more than one engine exists that could effect the equipment vibration environment, compute a W_o for each source and add the respective levels to determine the test level. Generally, this would be all the engines on the same side of the aircraft in question. To minimize the decision making requirements for the equipment project engineer, however, the criteria in the Appendix requires that all engines be considered in the computations. The Appendix test levels were thus reduced by 3 dB below Equation 7.

For simplification when computing R, the radial distance from the center of the engine exhaust plane to the c.g. of the equipment is used in the test method instead of the distance to the surface adjacent to the equipment. This is considered reasonable since Sevy's studies [10] show that vibration levels tend to reduce with depth within the structure.

FATIGUE TEST LEVELS

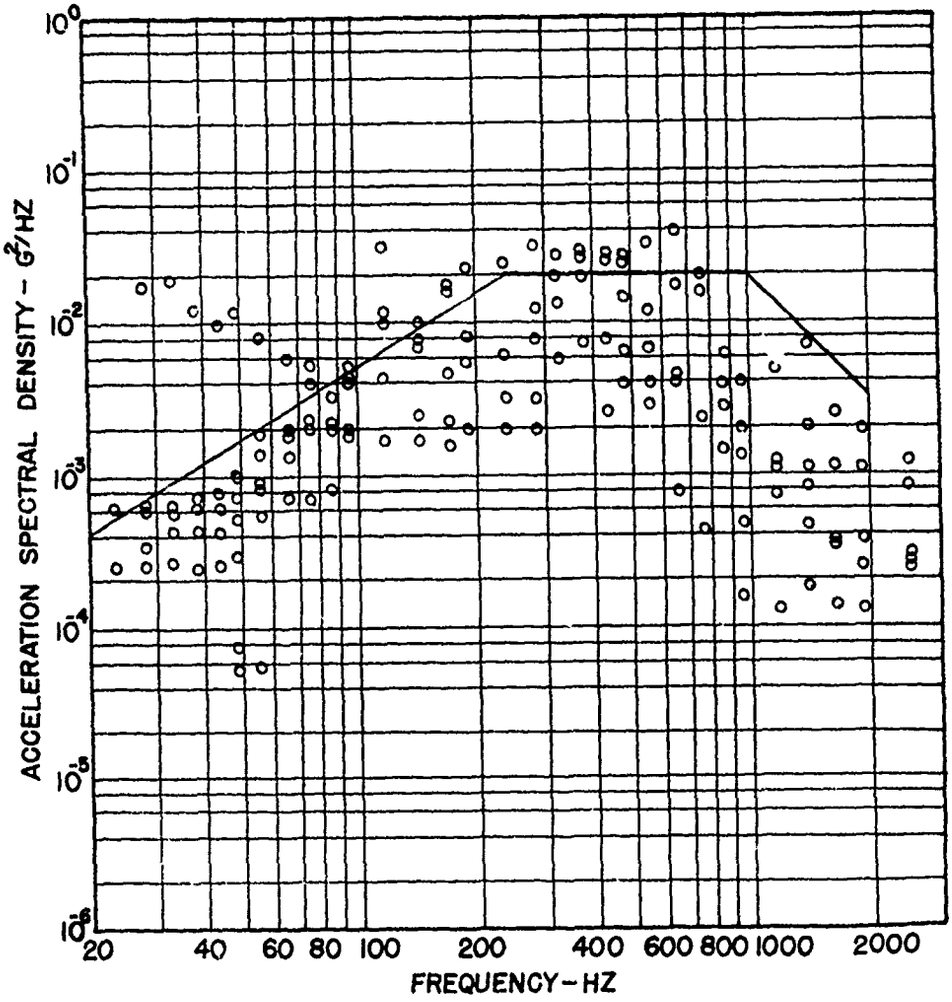

FIGURE 9 - COMPARISON OF PREDICTED AND MEASURED DATA IN THE FORWARD FUSELAGE OF A JET AIRCRAFT

Equipment in generally designed and expected to operate over the life of the aircraft without material failures. However, it is not practical to test for the corresponding long periods of time in the vibration laboratory. Generally, to shorten the fatigue or endurance test time, the test levels are increased above expected operational levels according to empirical laws relating stress levels and time to failure [1]. Thus, as in Reference 1, the functional level is raised by a factor of the form $(N/T)^{1/4}$ and the fatigue level becomes

$$W_o = W_f = 0.95(\cos^2\theta/R)(N/10T)^{1/4} \left[D_c(V_c/1850)^3 = D_f(V_f/1850)^3\right] \quad (8)$$

where T is test time per axis (hours) and N is the actual number of missions the equipment is expected to fly. The factor N/10 corresponds to engine ground operations at maximum power for one tenth of an hour per flight [11]. The 1/4 exponent is based on the slope of the random vibration S-N curve for equipment materials [1].

COMPARISON OF PREDICTED VS MEASURED LEVELS

The functional test levels were compared to extensive measurements in two cargo aircraft. The aircraft were zoned and although there were a significant number of accelerometers in each zone, there was no was to pinpoint the exact location. The zones compared were selected to include angles (θ) greater than 90° as well as less than 90°.

In Figures 9 and 10, the data from one

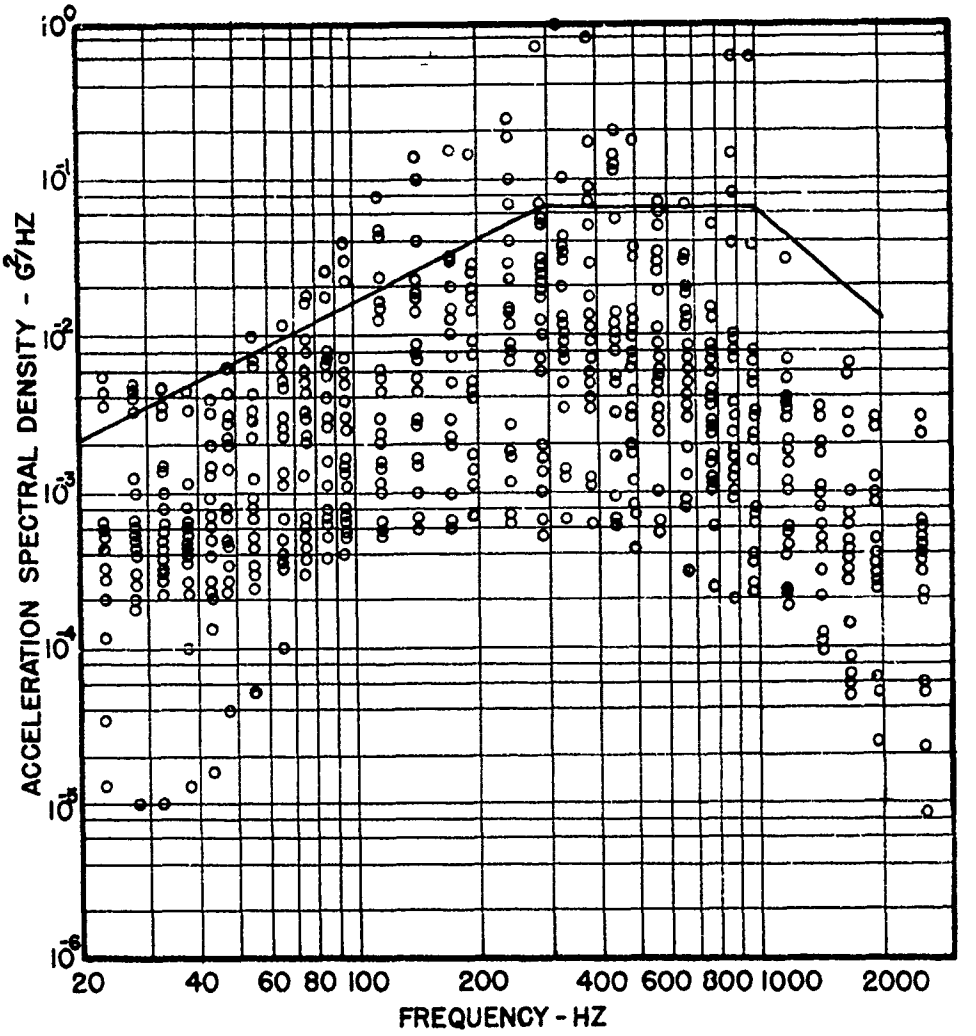

FIGURE 10 - COMPARISON OF PREDICTION AND MEASURED DATA IN THE AFT FUSELAGE OF A JET AIRCRAFT

aircraft are presented in pds's (g^2/Hz) based on a 5 cps filter band width analysis. The predicted curves shown are based on a point in the middle of each zone. It can be seen that the predicted curve covers most of the data in each zone.

Table II shows the relationship between the measured and predicted levels for the second aircraft. Only in Zone A are the levels significantly off. This zone is in the area of the cockpit where the measurements were made on isolated shelves. Thus, the overprediction is expected. The lower measured levels in Zone E are from the aft fuselage and were attenuated due to the masking effects of a wing flap-down condition. Thus, the agreement between measured and predicted levels is very reasonable.

SUMMARY

This study combines the results of existing noise and vibration prediction techniques into a unique formulation and provides a relatively simple tool for the equipment project engineer to use in developing a rational vibration test criteria in the design stages of new aircraft. The proposed criteria are a departure from the present rigidly established test curves and methods of military specifications and standards. They allow the engineer to adapt the test levels and test durations depending on the equipment location relative to the

TABLE II

Comparison of Predicted vs Measured Levels

TEST LEVEL - G^2/HZ			
ZONE	PREDICTED	MEASURED	RATIO P/M - DB
A	.003	.0005	+10
B	.0038	.006	-2
C	.0049	.005	0
D	.0143	.007	+3
E	.0170	.003	+7

acoustic source and the intensity and duration of exposure to the environment.

REFERENCES

1. J. F. Dreher, "Aircraft Equipment Random Vibration Test Criteria Based on Vibrations Induced by Turbulent Airflow Across Aircraft External Surfaces", Shock and Vibration Bulletin 43, December 1972.

2. Peter A. Franken, et al, "Method of Flight Vehicle Noise Prediction", WADC Technical Report 58-343, November 1958.

3. Walton L. Howes, et al, "Near Noise Field of a Jet Engine Exhaust", NACA Report 1338, 1958.

4. R. L. Barnoski, et al, "Summary of Random Vibration Prediction Procedures", NASA CR-1302, April 1969.

5. P. H. Hermes, D. L. Smith, "Measurement and Analyses of the J57-P21 Noise Field", AFFDL-TR-66-147, November 1966.

6. Unpublished noise measurements of 12,950 pound thrust aft fan engine.

7. J. M. Brust and H. Himelblau, "Comparison of Predicted and Measured Vibration Environments for Skybolt Guidance Equipment", Shock and Vibration Bulletin 33, March 1964.

8. P. T. Mahaffey and K. W. Smith, "A Method for Predicting Environmental Vibration Levels in Jet Powered Vehicles", Shock and Vibration Bulletin 28, August 1960.

9. David L. Earls and John F. Dreher, "Statistical Approach to Optimize Random Vibration Test Spectra", Shock and Vibration Bulletin 41, Supplement, December 1970.

10. R. Sevy, J. Clark, "Aircraft Gunfire Vibration", AFFDL-TR-70-131, November 1970.

11. G. Fitch, et al, "Establishment of the Approach to and Development of Interim Design Criteria for Sonic Fatigue", ASD-TDR-62-26, June 1962.

THEORETICAL AND PRACTICAL ASPECTS OF MULTIPLE-ACTUATOR SHAKER CONTROL†

Dennis K. Fisher
Lawrence Livermore Laboratory, University of California
Livermore, California 94550

An investigation into the dynamics of cross-coupled multiple-actuator shaker systems has led to the formulation of algorithms for the direct-digital control of swept-frequency sinusoidal, transient, and random-vibration tests. Digital simulation techniques have been used to demonstrate the validity of the algorithms. The inverse of the system transfer matrix is utilized as the mechanism for cross-coupling compensation. A direct-digital control system incorporating the use of the algorithms is under development.

NOMENCLATURE

[A]	M × M cross-coupling compensation matrix
[B]	M × M shaker-system input/output transfer matrix
[C]	M × 1 array of system responses
[C^D]	M × 1 array of desired system responses
[~D_]	M × M diagonal array of transfer elements
D(Z)	Digital controller, expressed in Z transforms
FFT [ ]	Indicates Fast Fourier Transform operation
FFT^{-1}[ ]	Indicates Inverse Fast Fourier Transform operation
[G]	M × M forward-loop transfer matrix of multivariable control system
[~H_]	M × M diagonal feedback transfer matrix of multivariable control system
[~I_]	M × M identity matrix
Im	Indicates "imaginary part of"
K_I	Integral control gain
M	Number of actuators in control system
N	Number of data values in FFT operations
[P]	M × M cross-coupling transfer matrix of multivariable control system
{R}	M × 1 array of shaker system command inputs
{R'}	M × 1 array of compensator command inputs
Re	Indicates "real part of"
s	Laplace variable
{S(ω)}	M × 1 array of autospectral densities
ω	Frequency, rad/sec
*	Designates sampled variable

INTRODUCTION

Multiple-actuator shakers are often employed in the shock and vibration testing of large rigid objects. When resonances are excited in the test package, substantial inter-actuator forces can be generated. This interaction, referred to as dynamic cross-coupling, generally leads to deviations from the vibration-test specification and often to control instability.

The first multiple-actuator-shaker control systems combined conventional single-actuator equipment and special multiple-channel phase controllers [1, 2, 3]. Cross-coupling was acknowledged as a problem but was not dealt with directly. More recently, Helmuth and Hunter [4] reported on a manually tuned cross-coupling compensator for swept-frequency sinusoidal testing. The principal of operation of the Helmuth-Hunter device has been related to modern system theory by Wyman [5]. Trubert [6] suggested a random-vibration control method that involves the use of the inverse of the system transfer matrix to calculate the required autospectral density of the input function. In a further development of this approach, Trubert [7] used an analog representation of the shaker system to synthesize inputs

†This work was performed under the auspices of the U.S. Atomic Energy Commission.

suitable for swept-frequency-sinusoidal, transient, and random-vibration testing. Although shown to be effective, the practical problems of mechanizing such an approach were noted.

Direct-digital control (DDC) is the most recent development in shaker control technology. In DDC systems, a digital computer is used to close the feedback loop. With but few exceptions, efforts in this area have been confined to single-actuator systems [8-15]. Wyman [5] has described the hardware necessary to implement the Helmuth-Hunter approach to sinusoidal testing for a multiple-actuator DDC system. Auslander and Kohli [16] used a simulation of a two-actuator shaker system to study different algorithms for swept-frequency sinusoidal DDC. Finally, the hardware necessary to implement an ideal cross-coupling compensator in a DDC system has been discussed by Fisher [17].

This paper presents the results of an investigation into the theoretical and practical aspects of digitally controlling a multiple-actuator shaker in the presence of cross-coupling. The ideal cross-coupling compensator is shown to be related to the inverse of the system transfer matrix. Different control algorithms, constrained by the limitations of practical hardware and software, are presented for swept-frequency sinusoidal, transient, and random-vibration control. The paper is concluded by a description of the hardware being developed to implement DDC of the multiple-actuator electrohydraulic shaker system at the Lawrence Livermore Laboratory (LLL).

FORMULATION OF THE IDEAL CROSS-COUPLING COMPENSATOR

The most concise formulation of an ideal cross-coupling compensator is obtained with the use of modern system theory. A generalized linear M-actuator cross-coupled shaker system and compensator are depicted in Fig. 1. The shaker system [B] has M inputs {R} and M responses {C}. Because of cross-coupling, each input R_i causes responses at every output C_j, j=1, 2, . . . , M. The principal of cross-coupling compensation is to insert a device [A] that will result in decoupled responses between the compensator inputs $\{R'\}$ and shaker response {C}; i.e., each R'_i causes a response at C_i only. The compensator is an open-loop element; it contains no response-feedback paths. Stability of the compensated system is therefore solely dependent on the stability of the shaker system [B]. In the following paragraphs we will establish the requirement for the stability of [B] and then use the resulting system formulation to arrive at the characteristics of the cross-coupling compensator [A].

Shaker System Stability

The requisite conditions for stability will be derived first for the linear, time-invariant two-actuator shaker system shown in Fig. 2. The results will then be generalized so as to apply to an M-actuator system.

The system in Fig. 2 consists of two closed-loop actuator controllers that have been cross-coupled by a "load" comprised of the elements $P_{ij}(s)$. The response equations for each actuator, expressed in terms of Laplace transformed variables, are:

Actuator 1

$$C_1(s) = P_{11}(s)D_1(s)E_1(s) + P_{12}(s)D_2(s)E_2(s) \quad (1)$$

and

$$E_1(s) = R_1(s) - H_1(s)C_1(s). \quad (2)$$

Actuator 2

$$C_2(s) = P_{22}(s)D_2(s)E_2(s) + P_{21}(s)D_1(s)E_1(s) \quad (3)$$

and

$$E_2(s) = R_2(s) - H_2(s)C_2(s). \quad (4)$$

Equations (1) and (3) may be combined into the matrix equation†

$$\{C\} = [G]\{E\}, \quad (5)$$

where

$$\{C\} = \begin{Bmatrix} C_1 \\ C_2 \end{Bmatrix} \quad (6)$$

$$[G] = \begin{bmatrix} P_{11} & P_{12} \\ P_{21} & P_{22} \end{bmatrix} \begin{bmatrix} D_1 & 0 \\ 0 & D_2 \end{bmatrix}, \quad (7)$$

and

$$\{E\} = \begin{Bmatrix} E_1 \\ E_2 \end{Bmatrix} \quad (8)$$

Similarly, for Eqs. (2) and (4),

$$\{E\} = \{R\} - [H]\{C\}, \quad (9)$$

where

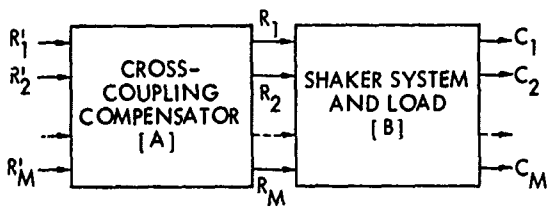

Fig. 1 - Block diagram of multiple-actuator shaker system with cross-coupling compensator

†For the sake of simplicity, the notation (s) is dropped at this point.

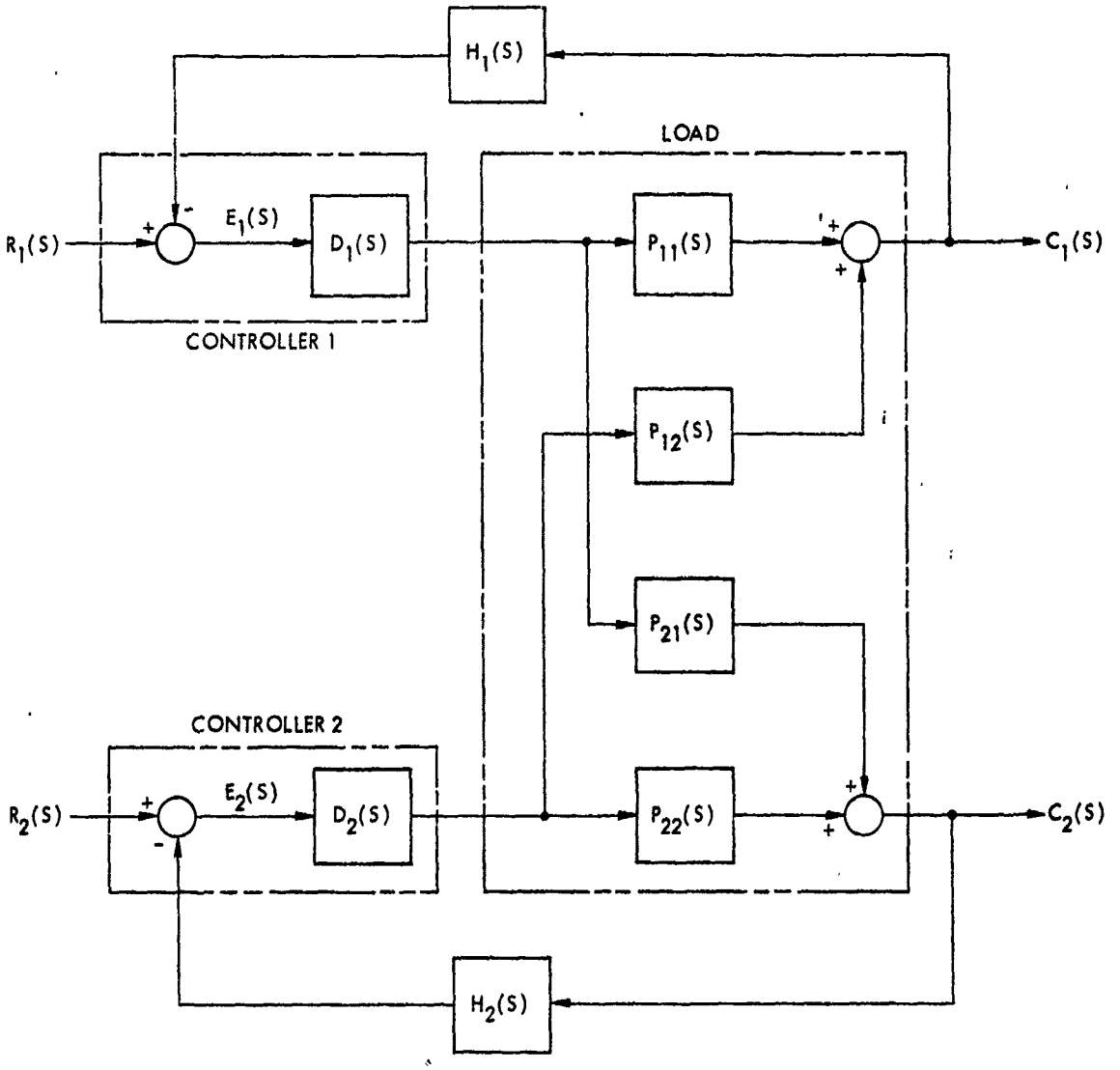

Fig. 2 - Cross-coupled two-actuator shaker system

$$\{R\} = \begin{Bmatrix} R_1 \\ R_2 \end{Bmatrix} \tag{10}$$

$$[\sim H_\sim] = \begin{bmatrix} H_1 & 0 \\ 0 & H_2 \end{bmatrix}. \tag{11}$$

The total system response is obtained by substituting Eq. (9) into Eq. (5) and solving for $\{C\}$:

$$\{C\} = \left[[\sim I_\sim] + [G][\sim H_\sim]\right]^{-1}[G]\{R\}, \tag{12}$$

where $[\sim I_\sim]$ is an identity matrix. Since the inverse of any nonsingular square matrix $[Z]$ is

$$[Z]^{-1} = \frac{\text{Adj}\,[Z]}{|Z|}, \tag{13}$$

Eq. (12) can be written

$$\{C\} = \frac{\text{Adj}\left[[\sim I_\sim] + [G][\sim H_\sim]\right]}{\left|[\sim I_\sim] + [G][\sim H_\sim]\right|}[G]\{R\}. \tag{14}$$

The similarity between Eqs. (5), (9), and (14) and their counterparts in the classical formulation of a single-input/single-output control system should be noted at this point [18].

For $\{C\}$ to be finite, the determinant in the denominator of Eq. (14) must be nonzero. Hence, the characteristic equation for the system is:

$$|[\sim I_\sim] + [G][\sim H_\sim]| = 0. \tag{15}$$

If all the roots of Eq. (15) are located in the left-half s-plane, the shaker system is stable.

For an array of desired system responses $\{C^D\}$, Eq. (12) can be arranged into the form

$$\{R\} = [G]^{-1}\left[\left[[\sim I_\sim] + [G][\sim H_\sim]\right]\right]\{C^D\}. \tag{16}$$

From Eq. (16) we can see that, given the conditions of linearity, stability, and known system dynamic response characteristics, it is theoretically possible to derive the array of shaker system inputs $\{R\}$ required to produce the desired responses $\{C^D\}$.

The preceding analysis pertains to the two-actuator system of Fig. 2. The concluding equation may be made to apply to an M-input/M-output system by generalizing the definition of the system matrices as follows:

$$\{R\} = \begin{Bmatrix} R_1 \\ \cdot \\ \cdot \\ R_M \end{Bmatrix}, \qquad \{E\} = \begin{Bmatrix} E_1 \\ \cdot \\ \cdot \\ E_M \end{Bmatrix}, \qquad \{C\} = \begin{Bmatrix} C_1 \\ \cdot \\ \cdot \\ C_M \end{Bmatrix}$$

$$[G] = \begin{bmatrix} P_{11} \cdots P_{1M} \\ \cdot \\ P_{M1} \cdots P_{MM} \end{bmatrix}\begin{bmatrix} D_1 & & 0 \\ & \ddots & \\ 0 & & D_M \end{bmatrix}, \quad [H] = \begin{bmatrix} H_1 & & 0 \\ & \ddots & \\ 0 & & H_M \end{bmatrix}. \tag{17}$$

Cross-Coupling Compensation

Equation (12) may be written as

$$\{C\} = [B]\{R\}, \tag{18}$$

where

$$[B] = \left[[\sim I_\sim] + [G][\sim H_\sim]\right]^{-1}[G]. \tag{19}$$

This is the formulation of the generalized cross-coupled M-actuator shaker shown in Fig. 1.† The response of the compensated system may be written

$$\{C\} = [B][A]\{R'\}, \tag{20}$$

where the characteristics of $[A]$ are momentarily undefined. Ideally, we would like the system to behave according to the equation

$$\{C\} = [\sim G^\circ_\sim]\{R'\}, \tag{21}$$

where $[\sim G^\circ_\sim]$ is a diagonal matrix in which each element G°_{ii} is the desired transfer function between input R_i and response C_i. By comparing Eqs. (20) and (21) we see that the compensation matrix $[A]$ must have the property that

$$[B][A] = [\sim G^\circ_\sim] \tag{22}$$

or

$$[A] = [B]^{-1}[\sim G^\circ_\sim].$$

Equation (22) is the generalized formulation of the ideal open-loop cross-coupling compensator for stable time-invariant linear systems. Equation (20) says that to get decoupled responses to the inputs $\{R'\}$, the shaker system must be driven with the derived inputs $\{R\}$ where

$$\{R\} = [A]\{R'\}. \tag{23}$$

This formulation is general within the given constraints and applies in principle to swept-frequency sinusoidal, transient, and random-vibration testing.

CONTROL OF SWEPT-FREQUENCY SINUSOIDAL TESTS

In swept-frequency sinusoidal testing the objective is to control the amplitudes and relative phases of the sinusoidal actuator responses as the frequency is swept over a specified range. In this section a control algorithm capable of being implemented on a small-scale digital computer will be developed for swept-frequency sinusoidal testing.

The idealized cross-coupling compensation matrix [Eq. (22)] was derived in terms of Laplace-transformed variables for a linear time-invariant system. To make practical use of the compensator for swept-frequency sinusoidal testing, three steps are necessary:

- Equation (20) must be interpreted in the frequency domain,
- An experimental method must be developed for identifying the system transfer matrix from which the cross-coupling compensation matrix is calculated,
- An outer feedback-loop must be added to correct response errors resulting from system nonlinearities or identification errors.

Frequency Domain Formulation

The conversion to the frequency domain is relatively straightforward. The Laplace variable s consists of real and imaginary parts where

†See Appendix A for a comparison between this formulation and the Cross-Coupling Factor formulation used in Ref. [4].

$$
\begin{aligned}
s &= \sigma + j\omega, \\
\sigma &= \text{real part}, \\
\omega &= \text{imaginary part}, \\
j &= \sqrt{-1}.
\end{aligned} \tag{24}
$$

In the frequency domain, $\sigma = 0$ so that

$$s = j\omega \tag{25}$$

and $j\omega$ is referred to as the complex frequency. Equations (18) and (20) may then be written

$$\{C(j\omega)\} = [B(j\omega)]\{R(j\omega)\} \tag{26}$$

and

$$\{R(j\omega)\} = [A(j\omega)]\{R'(j\omega)\}. \tag{27}$$

To bypass the direct use of complex arithmetic operations,† the variables of Eqs. (26) and (27) must be separated into their real and imaginary parts. First we define

$$C_i(j\omega) = CR_i(\omega) + j\,CI_i(\omega), \tag{28}$$

$$B_{ik}(j\omega) = BR_{ik}(\omega) + j\,BI_{ik}(\omega), \tag{29}$$

$$R_i(j\omega) = RR_i(\omega) + j\,RI_i(\omega), \tag{30}$$

$$A_{ik}(j\omega) = AR_{ik}(\omega) + j\,AI_{ik}(\omega), \tag{31}$$

and

$$R'_i(j\omega) = RR'_i(\omega) + j\,RI'_i(\omega). \tag{32}$$

It should be noted that each of the terms on the right-hand side of Eqs. (28) through (32) is a function of frequency only. By direct substitution of these definitions, Eqs. (26) and (27) become the partitioned-matrix equations

$$\begin{Bmatrix} CR \\ CI \end{Bmatrix} = \begin{bmatrix} BR & -BI \\ BI & BR \end{bmatrix} \begin{Bmatrix} RR \\ RI \end{Bmatrix} \tag{33}$$

and

$$\begin{Bmatrix} RR \\ RI \end{Bmatrix} = \begin{bmatrix} AR & -AI \\ AI & AR \end{bmatrix} \begin{Bmatrix} RR' \\ RI' \end{Bmatrix}. \tag{34}$$

Equations (33) and (34) constitute the frequency domain formulation of the system equations.

Determination of the Compensation Matrix

The elements of the partitioned transfer matrix [B] and compensation matrix [A] of Eqs. (33) and (34) are continuous functions of frequency. The finite storage capacity of a digital computer and the sampled-data nature of a DDC system dictate that the compensation matrix must be discretized; that is, the frequency range of interest must be divided into frequency intervals and a fixed compensation submatrix used for each interval. This results in the three-dimensional compensation matrix (Fig. 3).

†Arithmetic operations involving complex variables directly are generally inconvenient for implementation on small-scale computers.

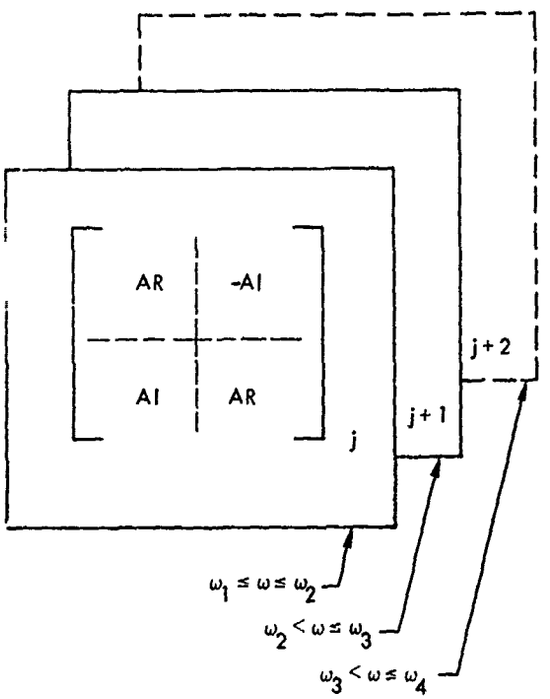

Fig. 3 - Three-dimensional discretized compensation matrix

The compensation submatrix for each interval is obtained from the system transfer matrix obtained experimentally at the center frequency of that interval. The transfer matrix is determined column by column by exciting the system sinusoidally one channel at a time. By expanding Eq. (33) and setting all inputs except RR_j to zero, we obtain

$$\begin{bmatrix} CR_1 \\ \vdots \\ CR_j \\ \vdots \\ CR_M \\ \hline CI_1 \\ \vdots \\ CI_j \\ \vdots \\ CI_M \end{bmatrix} = \left[\begin{array}{ccc|ccc} BR_{11} & \cdots & BR_{1M} & -BI_{11} & \cdots & -BI_{1M} \\ \vdots & & \vdots & \vdots & & \vdots \\ BR_{j1} & & BR_{jM} & -BI_{j1} & & -BI_{jM} \\ \vdots & & \vdots & \vdots & & \vdots \\ BR_{M1} & \cdots & BR_{MM} & -BI_{M1} & \cdots & -BI_{MM} \\ \hline BI_{11} & \cdots & BI_{1M} & BR_{11} & \cdots & BR_{1M} \\ \vdots & & \vdots & \vdots & & \vdots \\ BI_{j1} & & BI_{jM} & BR_{j1} & & BR_{jM} \\ \vdots & & \vdots & \vdots & & \vdots \\ BI_{M1} & \cdots & BI_{MM} & BR_{M1} & \cdots & BR_{MM} \end{array}\right] \begin{bmatrix} 0 \\ \vdots \\ RR_j \\ \vdots \\ 0 \\ \hline 0 \\ \vdots \\ 0 \\ \vdots \\ 0 \end{bmatrix} \tag{35}$$

At any channel k the responses due to input RR_j are then

$$CR_k = BR_{kj}\,RR_j \tag{36}$$

and

$$CI_k = BI_{kj}\, RR_j. \tag{37}$$

The terms CR_k and CI_k correspond to the coherent and quadrature components of the phasor response at channel k with respect to the reference sinusoidal input R_j. These components are readily measured by commercial CO/QUAD analyzers. Therefore, excitation of channel j permits column j of the transfer matrix to be calculated as

$$\left.\begin{aligned} BR_{kj} &= \frac{CR_k}{RR_j} \\ BI_{kj} &= \frac{CI_k}{RR_j} \end{aligned}\right\} \quad k = 1, 2, \ldots, M. \tag{38}$$

Once the transfer matrix at a given frequency has been fully determined, the corresponding compensation submatrix is obtained via Eq. (22). In swept-frequency sinusoidal testing, a flat system frequency-response characteristic is generally desirable. This is obtained by equating $[\sim G^{\circ}\_]$ to an identity matrix. The compensation submatrix at the specified frequency is then simply the inverse of the system transfer matrix:

$$\left[\begin{array}{c|c} AR & -AI \\ \hline AI & AR \end{array}\right] = \left[\begin{array}{c|c} BR & -BI \\ \hline BI & BR \end{array}\right]^{-1}. \tag{39}$$

By partitioning the matrices intc real and imaginary parts, the subject of the matrix inversion is changed from an M × M complex matrix to a 2M × 2M partitioned real matrix. Numerical procedures for calculating the inverse of a partitioned real matrix have been described elsewhere [19].

The spacing of the compensation submatrices over the frequency range of interest is arbitrary. Thus, several submatrices can be grouped near a frequency at which the system dynamics are rapidly changing. Simulation studies have indicated that five or more submatrices may be required to pass through a single sharp resonance. The compensation matrix can be established by low-level pretesting at selected frequencies, or it can be built up "on-the-run" during the first frequency sweep of the actual test by stopping the sweep momentarily at intervals and perturbing the amplitude and phase of each input. It can be shown that perturbation of RR_j permits the elements of column j of the transfer matrix to be calculated as

$$\left.\begin{aligned} BR_{kj} &= \frac{\Delta CR_k}{\Delta RR_j} \\ BI_{kj} &= \frac{\Delta CI_k}{\Delta RR_j} \end{aligned}\right\} \quad k = 1, 2, \ldots, M, \tag{40}$$

where

ΔRR_j = perturbation of input RR_j,

ΔCR_k, ΔCI_k = resulting perturbations of CO and QUAD responses of channel k.

Both amplitude and velocity-dependent nonlinearities are encountered in electrohydraulic and electrodynamic shaker systems. The determination of the compensation matrix at full test level has the advantage of minimizing the effects of amplitude-dependent nonlinearities. Velocity effects become a frequency consideration in sinusoidal testing and are inherently accounted for by the use of the frequency-dependent compensation matrix. Both the pretest and perturbation techniques are being studied further with regard to their ability to cope with system nonlinearities.

The procedures for swept-frequency sinusoidal testing discussed thus far have been validated by means of a frequency domain simulation of the four-actuator shaker system shown in Fig. 4. The mathematical model of the actuator controllers for each channel are simplified representations of the electrohydraulic actuators in the LLL system. The load, consisting of a rigid table and a spring-damper coupled test mass, is fictitious and was chosen to provide a high degree of actuator cross coupling. The actuator-piston accelerations were considered to be the system responses {C} to input command voltages {R}. The amplitude of a typical transfer element is shown in Fig. 5; the corresponding cross-coupling compensation element is shown in Fig. 6.†

DDC Algorithm for Swept-Frequency Sinusoidal Testing

In practice, the open-loop cross-coupling compensation procedure is imperfect because of amplitude or velocity-dependent nonlinearities. It is therefore necessary to introduce an outer feedback loop that continually corrects the responses as the frequency is swept. The sampled-data system for accomplishing this is shown in Fig. 7. Amplitude and phase control are achieved indirectly by controlling the coherent and quadrature components of response for each actuator.

The functions isolated by samplers are performed by the hardware and software of the digital computer system. The time domain coherent and quadrature responses of the system are sampled‡ by S_1 at time t_n, digitized, and subtracted from the sampled command inputs to give the error array

†The associated cross-coupling factor as defined in Ref. [14] is plotted in Appendix A.

‡The symbol * is used to designate sampled variables.

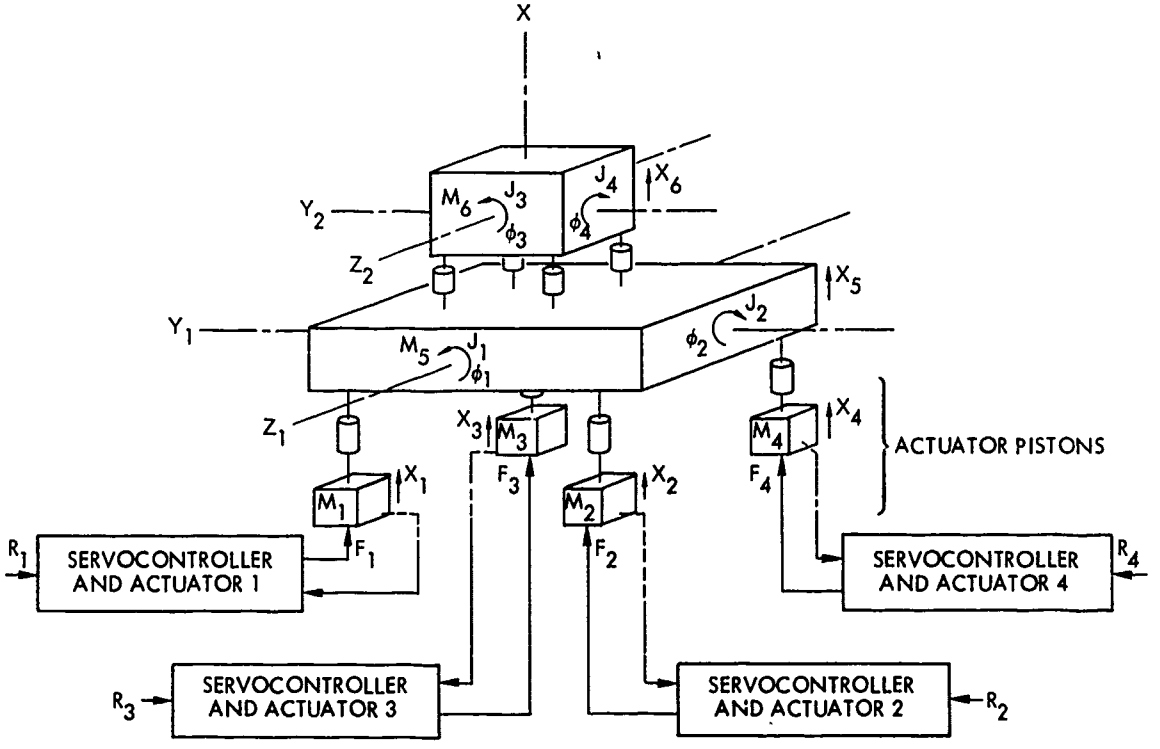

Fig. 4 - Mathematical model of shaker system used in validation of cross-coupling compensation procedure

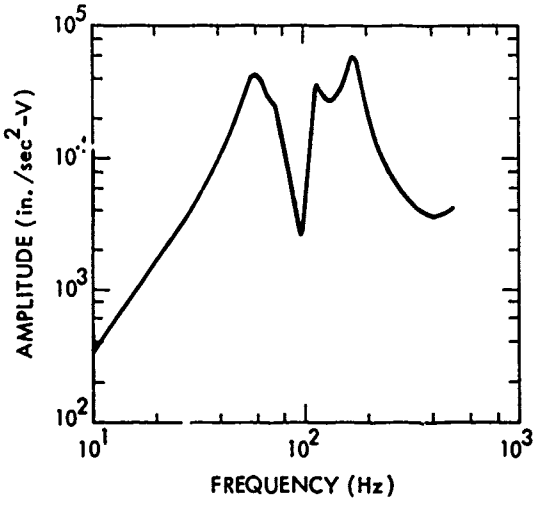

Fig. 5 - Transfer matrix element $B_{12}(j\omega)$

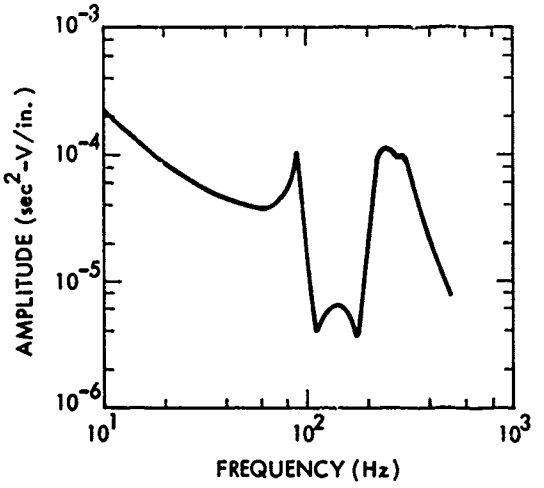

Fig. 6 - Cross-coupling compensation element $A_{12}(j\omega)$

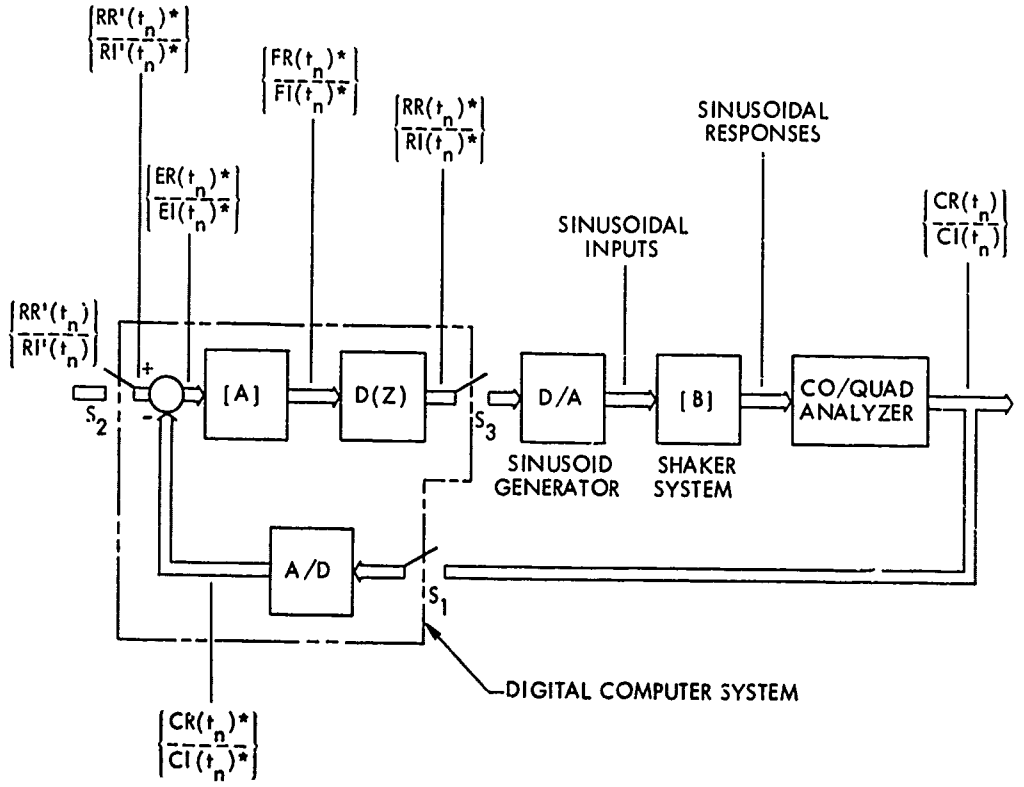

Fig. 7 - Block diagram of DDC system for swept-frequency sinusoidal testing.

$$\begin{Bmatrix} ER(t_n)^* \\ \hline EI(t_n)^* \end{Bmatrix} = \begin{Bmatrix} RR'(t_n)^* \\ \hline RI'(t_n)^* \end{Bmatrix} - \begin{Bmatrix} CR(t_n)^* \\ \hline CI(t_n)^* \end{Bmatrix} \qquad (41)$$

The error array is then premultiplied by the appropriate compensation submatrix to get the decoupled error array

$$\begin{Bmatrix} FR(t_n)^* \\ \hline FI(t_n)^* \end{Bmatrix} = \left[\begin{array}{c|c} AR & -AI \\ \hline AI & AR \end{array}\right] \begin{Bmatrix} ER(t_n)^* \\ \hline EI(t_n)^* \end{Bmatrix}. \qquad (42)$$

The function of the digital controller D(Z) is to introduce such classical control algorithms as integral or derivative control. In general, the digital controller can be expressed in Z transforms as [20]:

$$D(Z) = \frac{a_0 + a_1 Z^{-1} + \ldots a_L Z^{-L}}{b_0 + b_1 Z^{-1} + \ldots b_K Z^{-K}}, \quad K \geq L. \qquad (43)$$

For the particular case of integral control,

$$D(Z) = \frac{K_I}{1 - Z^{-1}} \qquad (44)$$

where

K_I = integral control gain.

The application of D(Z) to the decoupled error array results in outputs

$$\begin{Bmatrix} RR(t_n)^* \\ \hline RI(t_n)^* \end{Bmatrix} = \underbrace{\begin{Bmatrix} RR(t_{n-1})^* \\ \hline RI(t_{n-1})^* \end{Bmatrix}}_{\text{previously calculated output array.}} + K_I \begin{Bmatrix} FR(t_n)^* \\ \hline FI(t_n)^* \end{Bmatrix} \qquad (45)$$

The digital controller outputs are sampled at S_3 and used to generate analog sinusoids of appropriate amplitude and phase to drive each channel of the shaker system. A means of synthesizing these sinusoids using an analog sine/cosine signal generator, two multipliers, and a summer is illustrated in Fig. 8.

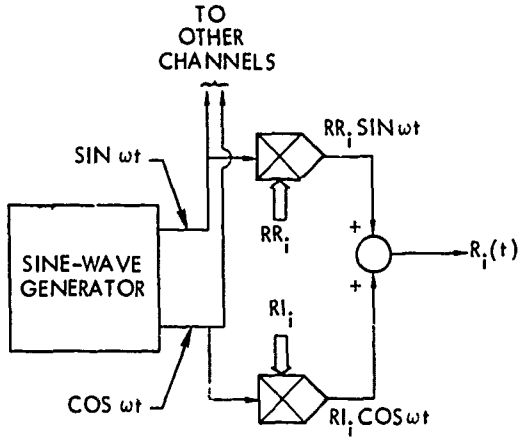

$$R_i(t) = |R_i| \sin(\omega t + \phi_i)$$

$$= |R_i| \sin \omega t \cos \phi_i + |R_i| \cos \omega t \sin \phi_i$$

$$= \underbrace{|R_i| \cos \phi_i}_{RR_i} \sin \omega t + \underbrace{|R_i| \sin \phi_i}_{RI_i} \cos \omega t$$

$$= RR_i \sin \omega t + RI_i \cos \omega t$$

Fig. 8 - Algorithm for synthesizing sinusoidal command $R_i(t)$ from calculated RR_i and RI_i values

The interval between sequential samples affects both the stability and accuracy of the closed-loop process. Both analytical and digital simulation techniques have been used to investigate this situation. For the LLL electrohydraulic shaker system and typical test objects, optimum transient response (in the sense of minimum integral squared error for a step change in sinusoidal amplitude) is expected for a sample period of 30 ms. For system resonances as sharp as Q = 50 and sweep rates up to 5 octaves/min, the predicted response errors are less than 5%, exclusive of instrumentation error.

TRANSIENT RESPONSE CONTROL

In transient response control, the objective is to generate independently specified time domain responses simultaneously at each actuator. A preliminary study indicated that a dedicated computer capable of performing direct-digital transient response control would be economically impractical with current technology. Therefore the technique described here is open loop in nature and similar to that used for single-actuator transient-response control [8]. The theoretical analysis assumes that the shaker system is linear and time invariant.

Synthesis Procedure

Referring to Eq. (16), the inputs required to obtain an array of desired responses $\{C^D(s)\}$ are

$$\{R(s)\} = [B(s)]^{-1}\{C^D(s)\} \tag{46}$$

or

$$\{R(s)\} = [A(s)]\{C^D(s)\}, \tag{47}$$

where $[A(s)]$ is the cross-coupling compensation matrix with $[\sim G_c^{\sim}]$ equated to an identity matrix. If analtyical expressions could be obtained for each $C_i^D(s)$ and $A_{ij}(s)$, Eq. (47) could be used directly. This is not the case, however, so once again we resort to the frequency domain. The fast Fourier transform† (FFT) equivalent of Eq. (47) is written

$$\left\{\begin{matrix} RR(\omega) \\ \hline RI(\omega) \end{matrix}\right\} = \left[\begin{matrix} AR(\omega) & -AI(\omega) \\ \hline AI(\omega) & AR(\omega) \end{matrix}\right] \left\{\begin{matrix} CR^D(\omega) \\ \hline CI^D(\omega) \end{matrix}\right\}, \tag{48}$$

where

$RR_i(\omega)$, $RI_i(\omega)$ = real and imaginary (M×1) partitions of FFT of $R_i(t)$,

$CR_i^D(\omega)$, $CI_i^D(\omega)$ = real and imaginary (M×1) partitions of FFT of $C_i^D(t)$,

$AR_{ik}(\omega)$, $AI_{ik}(\omega)$ = real and imaginary (M×M) partitions of compensation matrix.

Equation (48) is the mathematical basis for the transient response synthesis procedure discussed in the following paragraphs. It should be noted that this equation has an implied third dimension corresponding to the N frequency values of the FFT. Wherever arithmetic operations between transformed variables are used, that operation is assumed to apply to all N terms in the series representations.

The procedure for determining the required time domain input array $\{R(t)^*\}$ is diagramed in Fig. 9. The transfer matrix is determined by exciting the shaker one channel at a time with a deterministic test pulse P(t). For each input pulse the transient response of every actuator is sampled. The sampling rate, of course, must be sufficiently high to avoid aliasing. The transfer matrix elements are calculated as the complex ratio of the FFT's of the response and input transients.‡ That is, for a calibration pulse P(t) into channel j, the real and imaginary elements of column j of the transfer matrix are

†See Appendix B for a definition and properties of the FFT.

‡Alternately, each transfer element can be calculated as the ratio of the cross- and auto-spectral densities [19,21 and 22]. More sophisticated methods offering greater statistical confidence at the expense of increased computational complexity are also available [15].

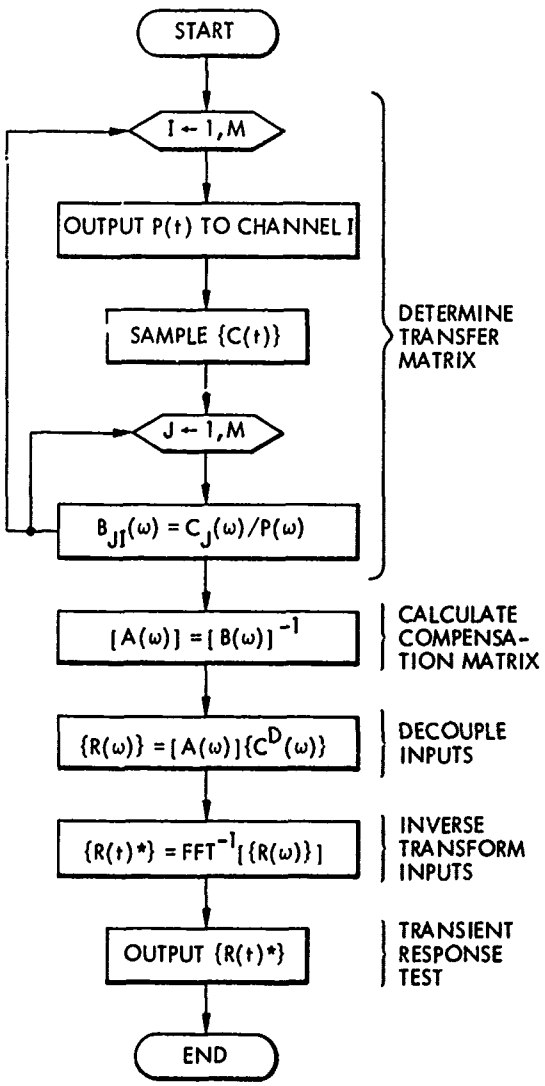

Fig. 9 - Algorithm for transient response synthesis

$$BR_{ij}(\omega) = \mathrm{Re}\left(\frac{C_i(\omega)}{P(\omega)}\right) \quad (49)$$

$$BI_{ij}(\omega) = \mathrm{Im}\left(\frac{C_i(\omega)}{P(\omega)}\right) \quad (50)$$

$i = 1, 2, \ldots, M,$

where

$C_i(\omega)$ = complex FFT of sampled response $C_i(t)$,

$P(\omega)$ = complex FFT of sampled input $P(t)$,

M = number of actuators.

When the transfer matrix has been completely determined, the compensation matrix is calculated according to Eq. (39).† The transform of the required inputs is obtained by premultiplying the transformed array of desired responses by the compensation matrix. Finally, the inverse FFT is used to get the time domain inputs.

The transient response synthesis procedure has been validated via a digital simulation using the mathematical model of the shaker system shown in Fig. 10. For a given mathematical model, the simulation of time domain responses are computationally much more time consuming than frequency domain. Therefore, to keep computation times within reason, the model used in the transient-response simulation is much simpler than that used for swept-frequency sinusoidal testing. The parameters of the model were adjusted to give peak values of cross-coupling comparable to those illustrated in Fig. 5. Typical results are shown in Fig. 11. The synthesis procedure was found to give acceptable results as long as the desired waveform was within the capabilities of the simulated system.

Limitations of the Synthesis Procedure

The mathematics of the transient response synthesis process give one, at first, a feeling of omnipotence. That is, it appears possible to generate any transient waveform on any shaker system. Unfortunately, this is not the case. What follows is a discussion of some of the limitations of the waveform synthesis process. These comments apply to single- as well as multiple-actuator systems.

The first limitation is mathematical in nature and has to do with the relationship between the specific transient waveform to be synthesized and the dynamics of the shaker system. Consider the single-input, single-output system of Fig. 12. The input necessary to generate the desired response $Y^D(s)$ is

$$X(s) = \frac{Y^D(s)}{H(s)}, \quad (51)$$

where

†This would at first appear to require N matrix inversions. It can be shown, however, that the N complex FFT coefficients $A_{ij}(k)$, $k = 0, 1, \ldots, N-1$, have the property that

$$A_{ij}(k) = \overline{A_{ij}}(N - k), \quad k = 1, 2, \ldots, \frac{N}{2},$$

where

$\overline{A_{ij}}(N - k)$ is the complex conjugate of $A_{ij}(N - k)$.

Therefore, with the inclusion of zero frequency terms, only N/2 + 1 submatrices need be calculated directly.

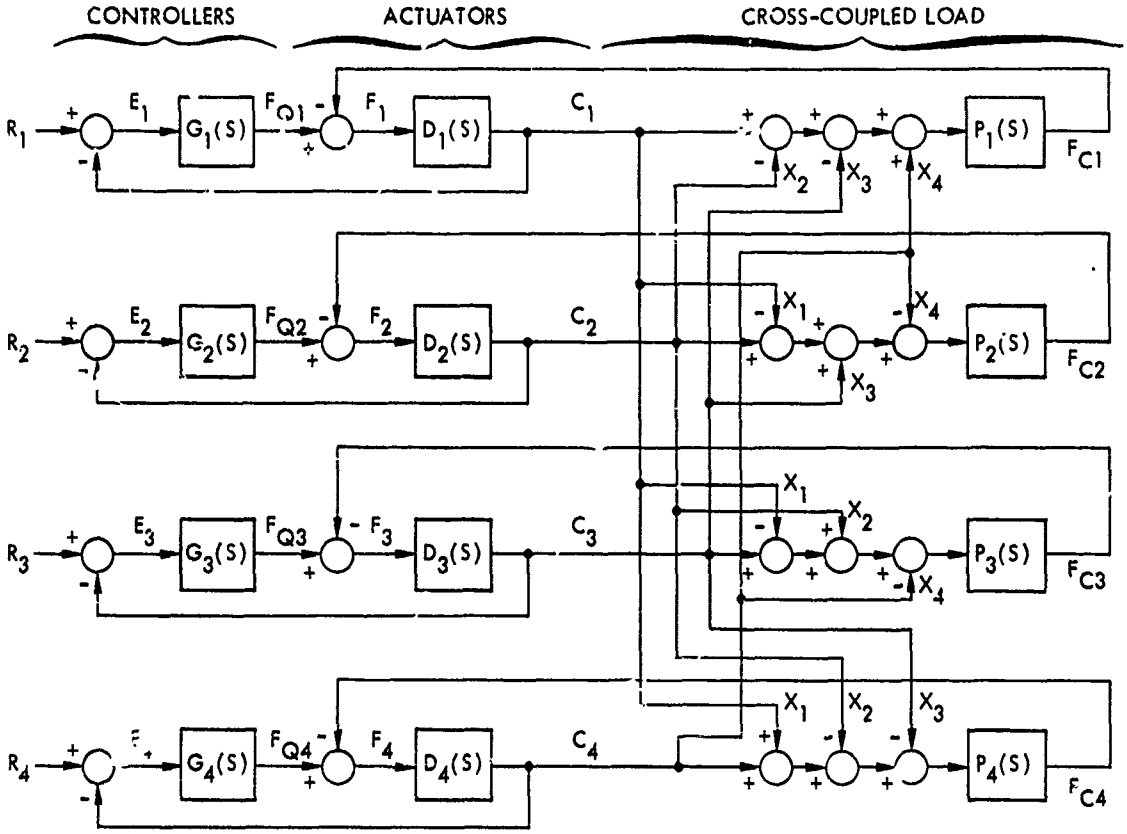

Fig. 10 - Mathematical model of shaker system used in simulation of transient response synthesis procedure

$X(s)$ = Laplace transform of input,

$Y^D(s)$ = Laplace transform of desired response,

$H(s)$ = transfer function of system.

If we assume $Y^D(s)$ and $H(s)$ can be represented as

$$Y^D(s) = \frac{s^J}{b_0 + b_1 s \ldots + b_k s^K} \tag{52}$$

and

$$H(s) = \frac{s^L}{a_0 + a_1 s + \ldots + a_M s^M} \tag{53}$$

over the frequency range of interest, then

$$X(s) = \frac{s^{J-L}\,[a_0 + a_1 s + \ldots a_M s^M]}{[b_0 + b_1 s + \ldots b_k s^K]}. \tag{54}$$

By applying the initial- and final-value theorems of Laplace transforms [22], we find that

$$\lim_{t \to 0} X(t) = \lim_{s \to \infty} sX(s)$$

$$= \infty, \quad (J-L+1+M) > K \tag{55}$$

$$= \text{finite}, \quad (J-L+1+M) = K \tag{56}$$

$$= 0, \quad (J-L+1+M) < K \tag{57}$$

and

$$\lim_{t \to \infty} X(t) = \lim_{s \to 0} sX(s)$$

$$= 0, \quad J \geq L-1 \tag{58}$$

$$= \text{finite}, \quad J = L-1 \tag{59}$$

$$= \infty, \quad J < L-1. \tag{60}$$

The conditions specified by Eqs. (57) and (58) are most desirable, while the remaining conditions risk or assure saturation of the physical system.

The preceding type of limit analysis can be extended to the frequency domain to give

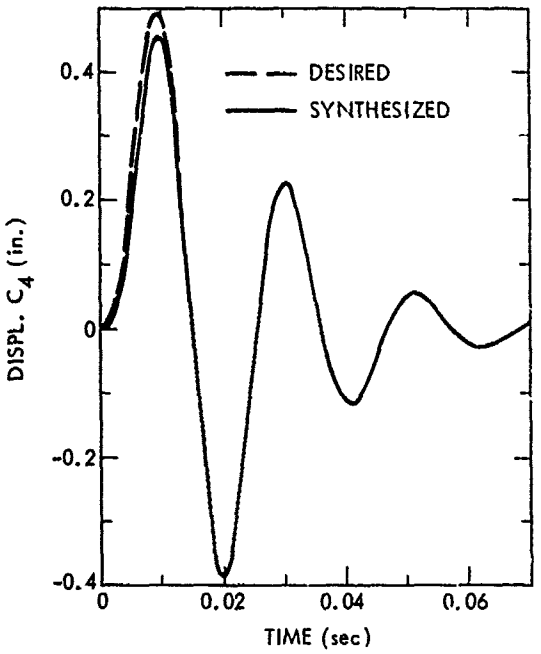

Fig. 11 - Typical simulated results of waveform synthesis procedure

information on the behavior of the Fourier coefficients of X:

$$\lim_{\omega \to 0} X(\omega) = \lim_{s = j\omega \to 0} X(s)$$

$$= 0, \quad J > L \tag{61}$$

$$= \text{finite}, \quad J = L \tag{62}$$

$$= \infty, \quad J < L \tag{63}$$

$$\lim_{\omega \to \infty} X(\omega) = \lim_{s = j\omega \to \infty} X(s)$$

$$= \infty, \quad (J-L+M) > K \tag{64}$$

$$= \text{finite}, \quad (J-L+M) = K \tag{65}$$

$$= 0, \quad (J-L+M) < K \tag{66}$$

Equations (61), (62), and (63) are important since they apply to the low-frequency coefficients of X(ω). The implications of Eqs. (64), (65), and (66) can be dealt with by limiting the frequency range of the FFT analysis.

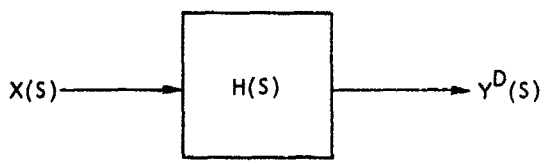

Fig. 12 - Single-input single-output system

Equations (55), (60), (63), and (64) define the mathematical limits of the waveform synthesis procedure. Whenever these boundaries are approached, saturation of the physical system becomes a possibility and compromises in the fidelity of the synthesized waveform must be accepted.

The second limitation of the transient-response synthesis procedure has to do with nonlinearities. Both amplitude- and velocity-dependent nonlinearities will cause inaccuracies in the synthesized waveforms. Iterative techniques have reportedly been used successfully in single-actuator systems to overcome nonlinear effects. In the iterative procedure, successive system identifications are performed using the synthesized input from one iteration as the calibration pulse for the next until, finally, the response converges to the desired waveform. This technique also appears promising for use in multiple-actuator systems.

RANDOM VIBRATION CONTROL

The algorithm for random vibration control is a logical extension of the procedures developed for transient response control. The flow diagram of Fig. 13 is for the general problem of controlling the autospectral density responses of M actuators in accordance with M independent desired spectral densities. Slight modifications to the procedure, to be discussed later, are required to obtain amplitude and phase-coherent actuator responses.

The random vibration control algorithm begins with the pretest determination of the cross-coupling compensation matrix using the method previously described for transient response control. At the beginning of the DDC loop, an FFT processor transforms the buffered frame of N data points for each of the M actuators to form a partitioned matrix:

$$\left\{\begin{matrix} CR(\omega) \\ \hline CI(\omega) \end{matrix}\right\}_n = \left\{\begin{matrix} \text{Re}[\text{FFT}(\{C(t)^*\})] \\ \hline \text{Im}[\text{FFT}(\{C(t)^*\})] \end{matrix}\right\}_n, \tag{67}$$

where

$\{C(t)^*\}_n$ = current array of sampled responses,

n = frame index.

The N/2 + 1 autospectral density lines of each actuator response are then calculated as

$$S_i^C(k) = \frac{2\Delta T}{N}\left[CR_i(k)^2 + CI_i(k)^2\right], \quad k = 0, 1, \ldots, \frac{N}{2}, \tag{68}$$

where

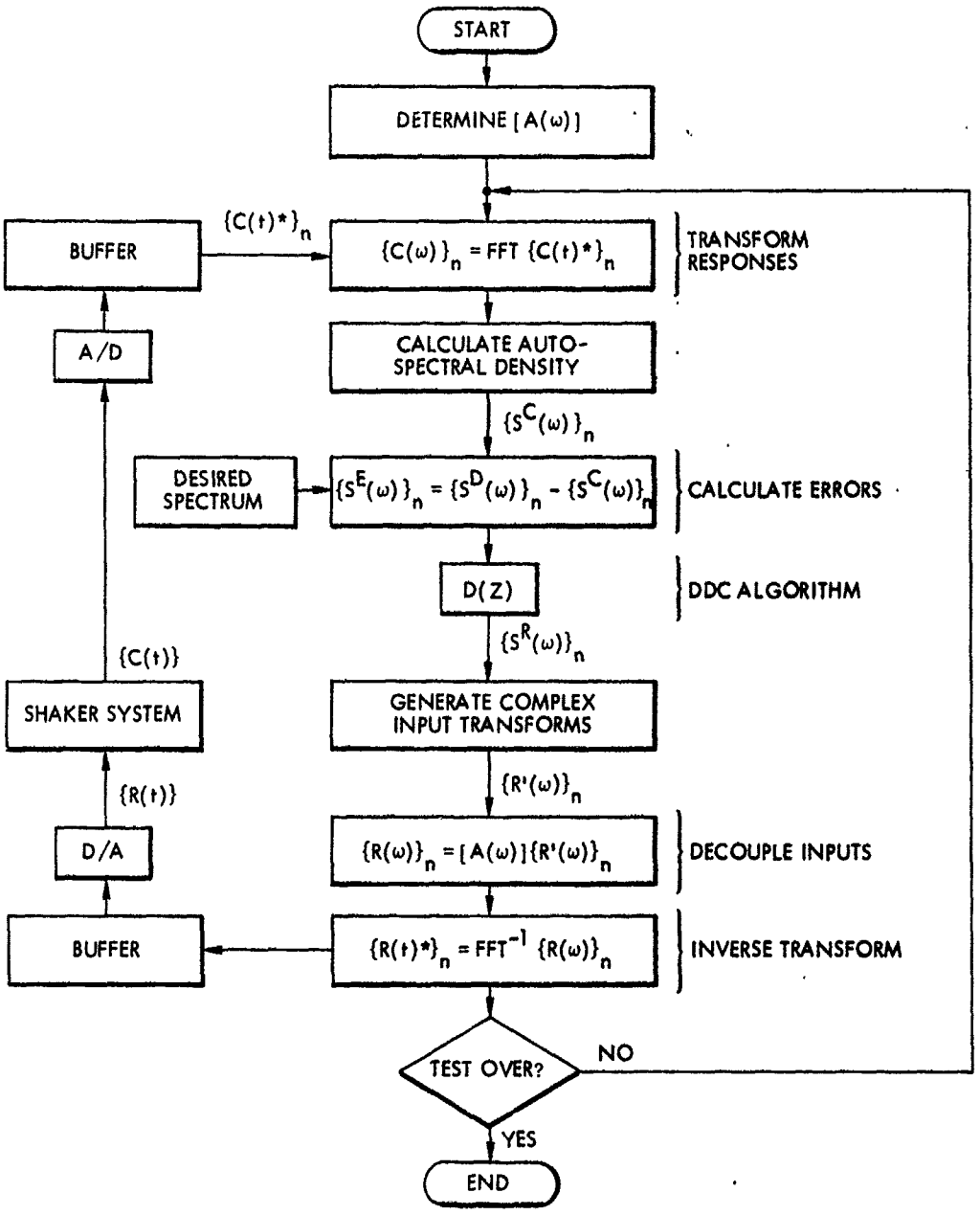

Fig. 13 - Algorithm for DDC of random vibration

$CR_i(k)$, $CI_i(k)$ = real and imaginary parts of kth complex coefficient of $C_i(\omega)$.

The measured autospectral density array is subtracted from the stored array of desired spectral densities $\{S^D(\omega)\}_n$ to obtain the error array

$$\{S^E(\omega)\}_n = \{S^D(\omega)\}_n - \{S^C(\omega)\}_n. \quad (69)$$

A DDC algorithm of the form of Eq. (43) is applied to the error array to get a new array of command spectral densities $\{S^R(\omega)\}_n$. For the case of integral control,

$$\{S^R(\omega)\} = \{S^R(\omega)_{n-1} + K_I\{S^E(\omega)\}_n. \quad (70)$$

where

$\{S^R(\omega)\}_{n-1}$ = previous command spectral density array.

We must now work backward from the command spectral density of Eq. (70) to an array of time-domain inputs. Since all phase information has been lost at this point, it must be introduced artificially. More importantly, it must be done in such a manner as to produce a Gaussian amplitude probability density distribution in the resultant time-domain waveform. This is achieved if the coefficients of the real and imaginary parts of the Fourier transform of each $R_i(\omega)$ have independent Gaussian distributions and

$$RR_i'(k)^2 + RI_i'(k)^2 = \frac{N}{2\Delta T} S_i^R(k), \quad k = 0, 1, \ldots, \frac{N}{2}, \tag{71}$$

where

$RR_i'(k)$, $RI_i'(k)$ = real and imaginary parts of kth complex coefficient of $R_i'(\omega)$

i = actuator index

Equation (71) defines only the first N/2 + 1 terms. To yield real time-domain transients, the remainder of the coefficients are defined to be complex conjugates of the first N/2 + 1 as follows:

$$\left.\begin{aligned} RR_i'(N-k) &= RR_i'(k) \\ RI_i'(N-k) &= -RI_i'(k) \end{aligned}\right\} \quad k = 1, 2, \ldots, \frac{N}{2}. \tag{72}$$

Several approximate methods for satisfying Eq. (71) have been discussed in the literature [9, 10].

Having arrived at the array of synthesized commands, the decoupled input transforms are calculated as

$$\left\{\begin{array}{c} RR(\omega) \\ \hline RI(\omega) \end{array}\right\}_n = \left[\begin{array}{c|c} AR & -AI \\ \hline AI & AR \end{array}\right] \left\{\begin{array}{c} RR'(\omega) \\ \hline RI'(\omega) \end{array}\right\}_n. \tag{73}$$

The inputs are then inverse transformed and placed in a buffer area from which they are continuously retrieved and transmitted in analog form to the shaker.

To obtain phase- and amplitude-coherent responses within one or more groups of actuators, the above procedure must be slightly modified. For each group, one frame of sampled data points is obtained by time-division multiplexing the responses of the actuators within that group. Each group is handled as though it was a single actuator up to the time the complex input transforms are generated. At this point the calculated input transforms are replicated for each actuator within a group. In this way the process will attempt to generate identical waveforms at each actuator of a coherent group, regardless of cross-coupling.

The stability of the random vibration DDC algorithm hinges on the execution time of the digital calculations. Although no specific estimates have been made, it appears likely that at least one hardware FFT processor and possibly array multiplication hardware will be required to provide the speed necessary to give satisfactory control system response.

A DEVELOPMENTAL MULTIPLE-ACTUATOR DDC SYSTEM

The configuration of the four-actuator DDC system currently under development at LLL is illustrated in Fig. 14. This system consists of four groups of hardware: (a) a general purpose digital computer, (b) unique hybrid data acquisition and signal generation equipment, (c) four individual actuators and their associated controllers, and (d) supervisory hardware.

The system operates in a closed-loop manner. The computer obtains digitized load response information from the data acquisition unit (DAU), calculates new commands based on this information, and outputs appropriate data to the digital waveform synthesizer (DWS) and command generation unit (CGU). The DWS and CGU function together under the control of the central processor to generate the dynamic and setpoint analog command signals required by each of the four electrohydraulic actuators of the shaker system. Each actuator controller operates to produce, ideally, an actuator displacement proportional to the sum of its dynamic and setpoint commands. The supervisory hardware is basically analog in nature and monitors the system for out-of-range operating conditions.

The items of interest here are the computer system and the LLL-designed hybrid interface equipment. These items are discussed in the following sections.

Computer System

The computer system, Fig. 15, is configured about a 16-bit word size central processor having 32 k of 800 nsec core memory, floating-point hardware, 120 Hz real-time clock, and an interval time. Peripherals include a 500-line/min electrostatic printer/plotter, a 1.2-million word disk, industry-compatible magnetic tape, a 300-card/min reader, a high-speed paper tape reader/punch, a storage-type CRT with keyboard and a teletype. It is anticipated that the hardware FFT processor shown will be added to the system in the near future.

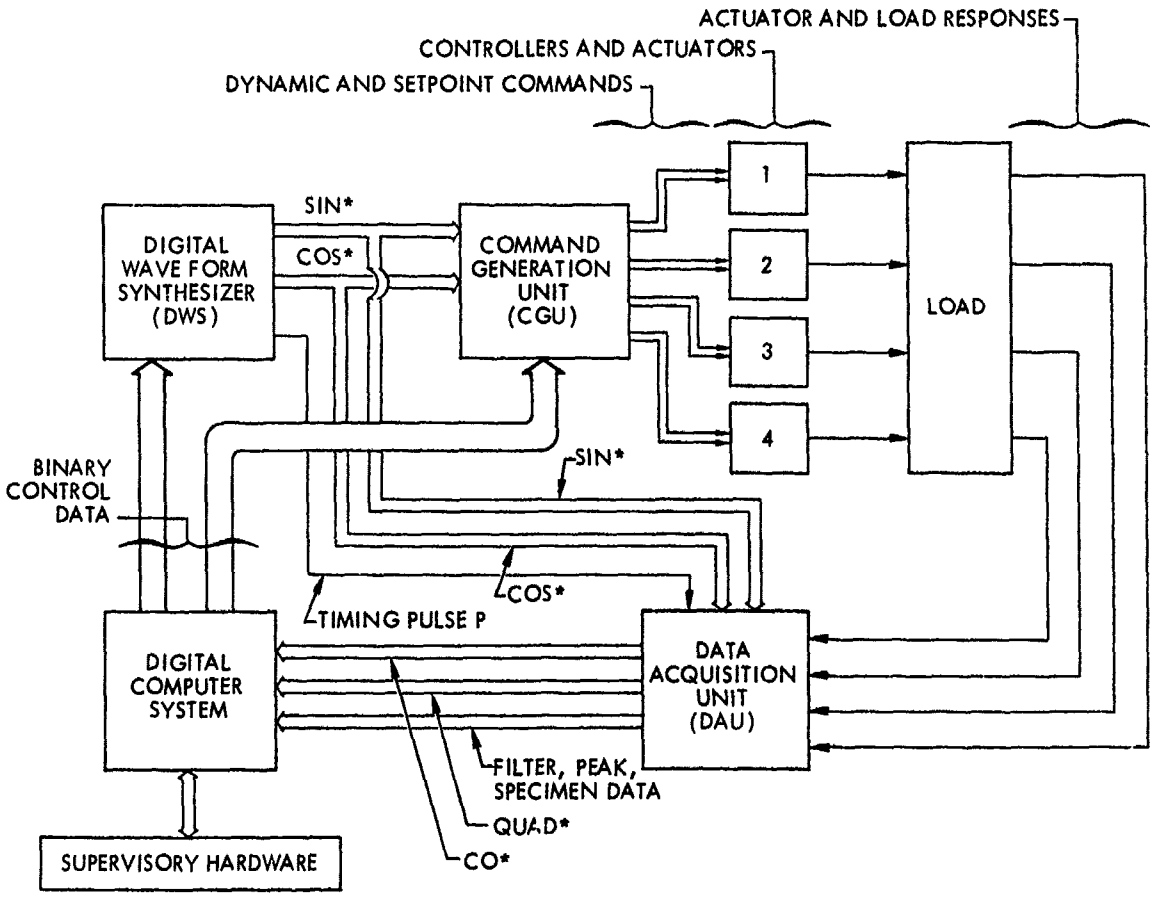

Fig. 14 - Configuration of DDC system

Digital Waveform Synthesizer

The DWS is used to generate a time series of digital values corresponding to sequential points on any desired periodic or transient waveform. For periodic waveforms, the device is designed to operate over a fundamental frequency range of 0.1 Hz to 1 kHz with a frequency resolution of 0.1% of the nominal frequency setpoint.

The hardware (Fig. 16) is composed of two sections, a timing circuit and a shift register. The timing section receives frequency commands from the central processor in a binary floating-point format. The frequency data are decoded and used to generate two output pulse trains. One of these provides timing information to the DAU; the other steps the shift register.

The shift register is a 12-bit wide by 512-position semiconductor component which is loaded by the central processor with the desired sequence of digital values. Under clocked control of the timing section, one value at a time is shifted into the output buffer register and simultaneously back into the beginning of the shift register. In this manner the shift register appears to rotate when pulsed repeatedly. A second output buffer register is located one quarter of the length of the shift register ahead of the first. Thus, if the stored values define a sinusoidal waveform, both sine and cosine functions can be generated simultaneously.

Command Generation Unit

The purpose of the CGU is to output independent dynamic and setpoint analog commands to the four actuator controllers. Figure 17 depicts the first channel of the CGU. The remaining three channels are similar but not identical.

There are five dynamic-command signal sources which may be selected individually or in any combination. In swept-sinusoid testing the first two inputs are the digital sine and cosine values from the DWS. These inputs are passed serially through conventional digital/

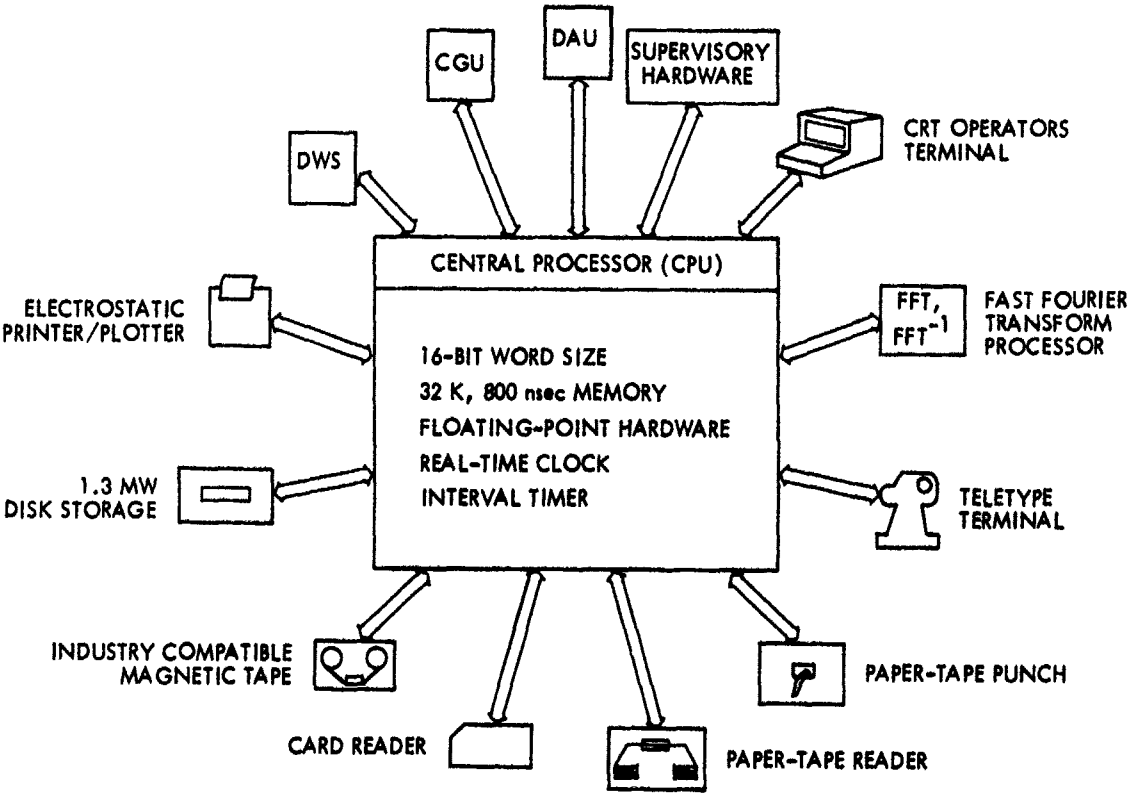

Fig. 15 - Digital computer system

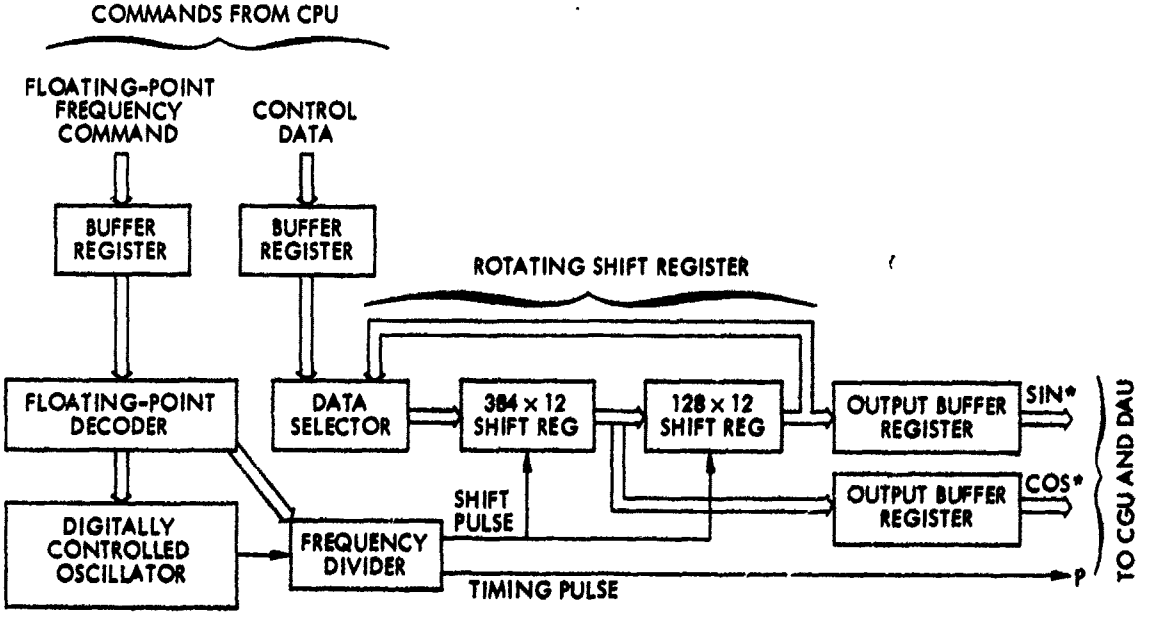

Fig. 16 - Digital waveform synthesizer

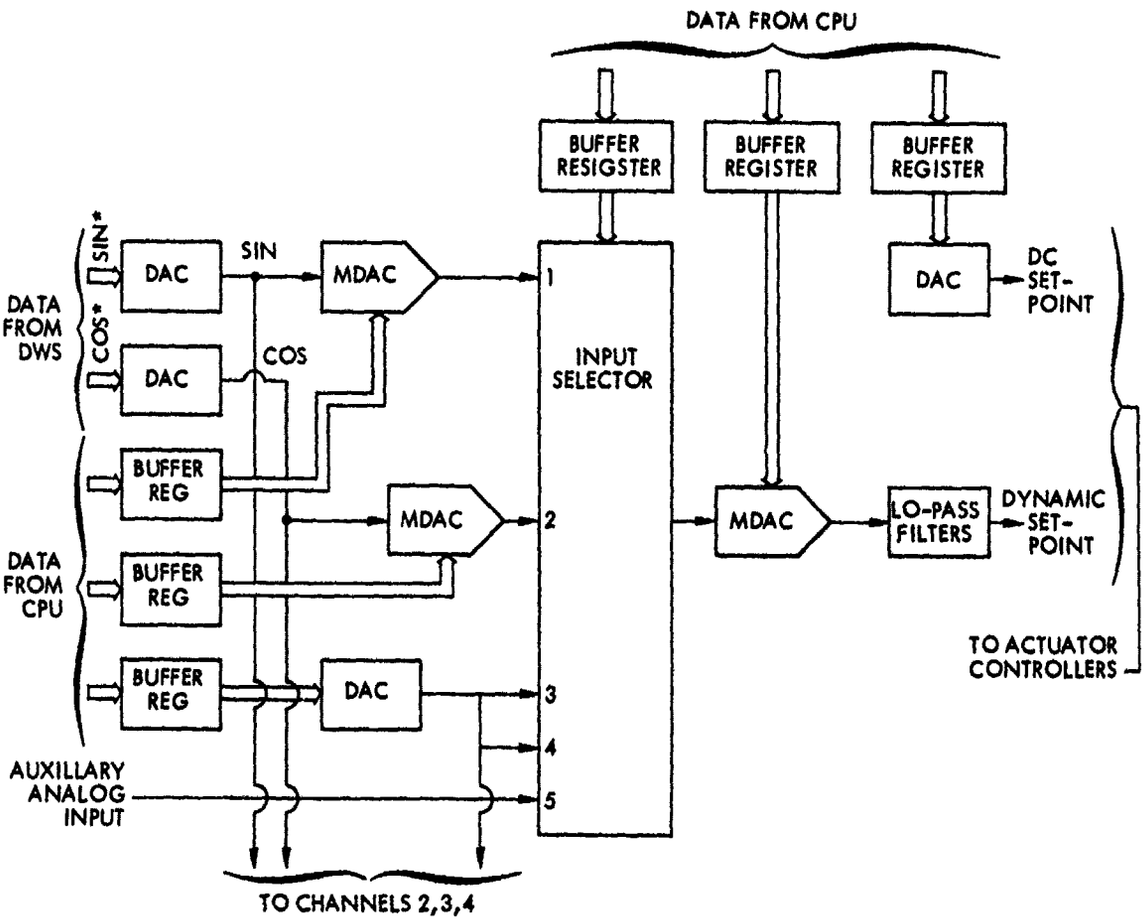

Fig. 17 - Command generation unit

analog converters (DAC's) and then multiplying digital/analog converters (MDAC's). The coefficients in the MDAC's are set directly by the central processor. By selecting inputs 1 and 2 in combination, it is possible to define a sinusoid of arbitrary amplitude and phase relative to the output of the DWS in the manner described by Fig. 8. The third dynamic input is from a DAC driven directly by the central processor. It provides the capability to generate transient and random excitation waveforms. Input 4 is common to all four channels and is also tied to input 3 of channel 1 (only). In this way up to four channels may be driven identically by a single DAC. A fifth input is provided for external command requirements.

The selected command inputs are summed and passed through an MDAC that provides amplitude scaling for the combined inputs. Finally, low-pass filters are used to remove any noise generated by the D/A process.

The setpoint command is necessary to establish the DC operating position of the electrohydraulic actuators. This quantity is set independently for each channel by DAC's driven directly by the central processor.

Data Acquisition Unit

The DAU consists of four channels of functionally identical analog and digital data processing hardware (Fig. 18). Each channel performs a number of selection, detection, and digitizing tasks generally related to data acquisition.

The inputs to each channel consist of the acceleration, displacement and force response data from the load as well as the dynamic and set-point commands of the corresponding actuator. The command inputs are solely for the purpose of system checkout and calibration. During a typical control task, the selected variable is passed through a variable-gain amplifier, anti-aliasing filters, and if a swept-sinusoid test is underway, through a CO/QUAD analyzer. The CO/QUAD analyzer uses the timing and digital waveform outputs of the DWS

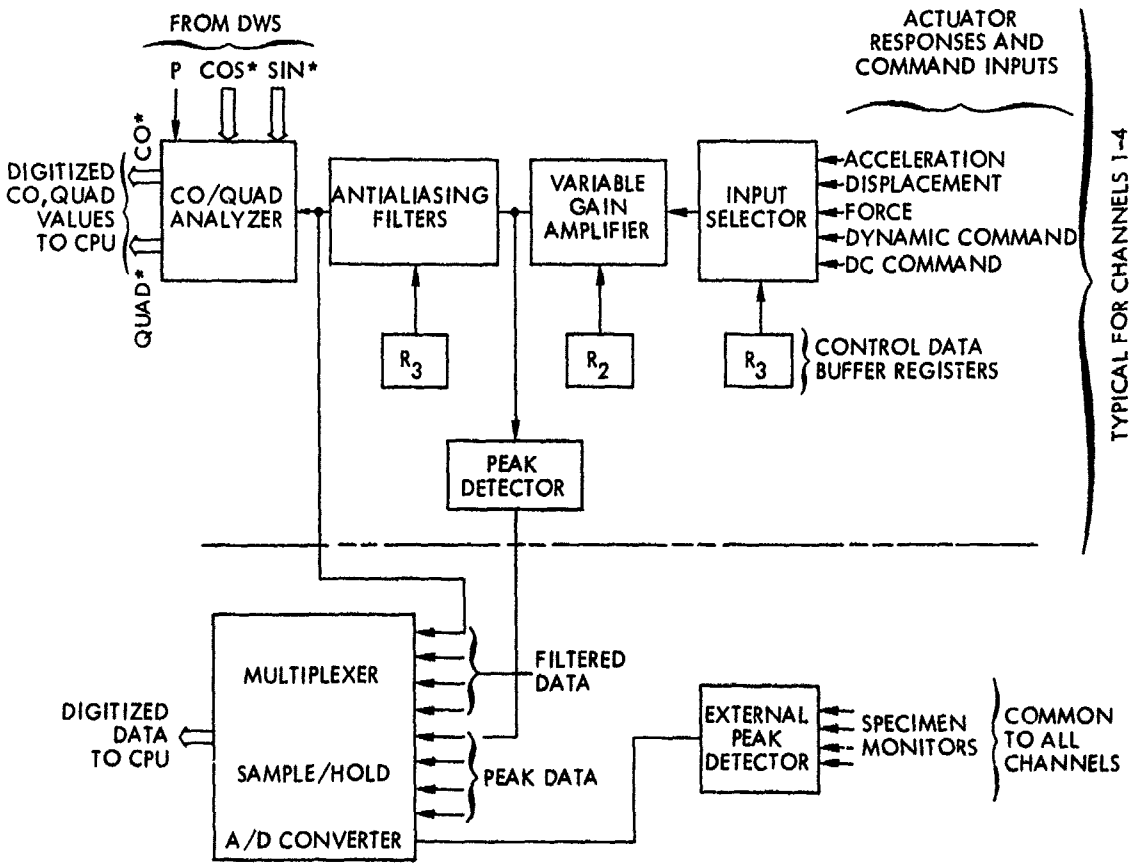

Fig. 18 - Data acquisition unit

to perform a first-term Fourier analysis. It outputs digitized coherent and quadrature values of the fundamental component of the feedback variable directly to the central processor.

The output of the variable gain amplifier is also passed through a peak detector. The peak response of each actuator, along with the outputs of the anti-aliasing filters, is multiplexed and passed through a high-speed A/D converter. The availability of the peak raw data values permits any large harmonic responses (the CO/QUAD analyzer detects only the fundamental) to be detected.

Specimen-monitoring transducers are often used during a test to protect the payload from large, unforeseen resonant conditions. The DAU provides for as many as six specimen monitors. The peak response of the monitors, along with an arbitrary number (up to 16) of general-purpose data acquisition channels, are also multiplexed, digitized, and sent to the central processor.

CONCLUSION

An investigation has been made into the theoretical and practical aspects of controlling multiple-actuator shakers. The ideal cross-coupling compensation matrix for stable, linear, time-invariant systems has been shown to be related to the inverse of the system transfer matrix. Practical algorithms incorporating cross-coupling compensation have been developed for the direct-digital-control of swept-frequency sinusoidal, transient, and random vibration testing. Hardware and software to implement the algorithms on an existing four-actuator electrohydraulic shaker system are under development.

REFERENCES

1. J. D. Newton, "Methods of Control of Multiple Shaker Testing Systems," Shock and Vibration Bull. 35, Pt 2, pp. 85-96, Jan. 1966.

2. R. A. Arone and P. A. Brock, "Control Techniques for Multiple-Shaker Vibration Systems," Shock and Vibration Bull. 36, Pt 3, pp. 147-55, Jan. 1967.

3. D. F. Redford, "Shock and Vibration Testing Using Four Shaker System," Shock and Vibration Bull. 36, Pt 3, pp. 91-9, Jan. 1967.

4. W. E. Hunter and J. S. Helmuth, "Control Stabilization for Multiple Shaker Tests," Shock and Vibration Bull. 37, Pt 3, pp. 155-62, Jan. 1968.

5. R. H. Wyman, "Control of Multiple-Head Shaker Systems: An Application of Linear Algebra," 1970 Proceedings, Institute of Environmental Sciences, pp. 277-281, April 1970.

6. M. R. Trubert, "Structural Electromechanical Interaction in the Multiple Exciter Technique for Random Vibration," J. Acoust. Soc. Amer., Vol. 41, No. 5, pp. 1185-92, May 1967.

7. M. R. Trubert, "An Analog Technique for the Equalization of Multiple Electromagnetic Shakers for Vibration Testing," J. Spacecr. Rockets, Vol. 5, No. 12, pp. 1438-43, Dec. 1968.

8. J. D. Favour and J. M. Lebrun, "Transient Waveform Control of Electromagnetic Test Equipment," Shock and Vibration Bull. 40, Pt 2, pp. 157-71, Dec. 1969.

9. C. P. Chapman, J. Shipley, and C. L. Heizman, "A Digitally Controlled Vibration or Acoustic Testing System, Parts I, II, and III," 1969 Proceedings, Institute of Environmental Sciences, pp. 387-409, April 1969.

10. A. G. Ratz, "Random Vibration Test Systems Using Digital Equalizers," 1970 Proceedings, Institute of Environmental Sciences, pp. 75-91, April 1970.

11. F. C. Bosso, "Sine Test Electrodynamic Vibration System Using Digital Control," 1970 Proceedings, Institute of Environmental Sciences, pp. 61-69, April 1970.

12. A. G. Ratz, "The Development of Digital Control Systems for Electrodynamic Vibration Exciters," 1971 Proceedings, Institute of Environmental Sciences, pp. 178-86, April 1971.

13. C. P. Chapman, "Hardware Implementation for Direct Digital Control of Random Excitation Environmental Testing," 1971 Proceedings, Institute of Environmental Sciences, pp. 156-62, April 1971.

14. C. L. Heizman, "A High Performance Digital Vibration Control and Analysis System," 1972 Proceedings, Institute of Environmental Sciences, April 1972.

15. E. A. Sloan, "Optimum Random Vibration Control Using Transfer Function Analysis," 1972 Proceedings, Institute of Environmental Sciences, April 1972.

16. D. M. Auslander and J. C. Kohli, "Direct Digital Control of Multiple-Head Shakers," Lawrence Livermore Laboratory Rept. UCRL-13558, p. 139, June 1972.

17. D. K. Fisher, "Implementation of a Direct-Digital Multiple-Actuator-Shaker Control System," Lawrence Livermore Laboratory Rept. UCID-16016, p. 21, April 1972.

18. J. J. D'Azzo and C. H. Houpis, Feedback Control System Analysis and Synthesis 2nd ed., p. 824, McGraw-Hill, New York, 1966.

19. L. D. Enochson and R. K. Otnes, "Programming and Analysis for Digital Time Series Data," Shock and Vibration Information Center, p. 277, 1968.

20. B. C. Kuo, Analysis and Synthesis of Sampled Data Control Systems, p. 528, Prentice-Hall, Englewood Cliffs, N. J., 1963.

21. J. S. Bendat and A. G. Piersol, Measurement and Analysis of Random Data, p. 390, Wiley, New York, 1966.

22. W. Kaplan, Operational Methods for Linear Systems, p. 577, Addison-Wesley, Reading, Mass., 1962.

23. H. A. Gaberson and D. Pal, "Digital Fourier Analysis of Mechanical Shock Data," Shock and Vibration Bull. 41, Pt 5, pp. 39-52, Dec. 1970.

24. H. J. Weaver, "An Introduction to Discrete Fourier Analysis," Lawrence Livermore Laboratory Rept. UCRL-73113, p. 133.

APPENDIX A: RELATIONSHIP OF TRANSFER MATRIX FORMULATION TO CROSS-COUPLING FACTORS

In this Appendix the cross-coupling factors (CCF) of Ref. [4] are related to the transfer matrix formulation of Eq. (18).

Using CCF's, the responses of the M-actuator system of Fig. 1 are:

$$\left.\begin{aligned} C_1 &= Z_{11}\,R_1 + Z_{12}\,C_2 + Z_{13}\,C_3 \\ &\quad + \ldots + Z_{1M}\,C_{M'} \\ C_2 &= Z_{21}\,C_1 + Z_{22}\,R_2 + Z_{23}\,C_3 \\ &\quad + \ldots + Z_{2M}\,C_{M'} \\ &\cdots \\ C_M &= Z_{M1}\,C_1 + Z_{M2}\,C_2 + Z_{M3}\,C_3 \\ &\quad + \ldots + Z_{MM}\,R_{M'} \end{aligned}\right\} \quad (A\text{-}1)$$

where

$R_i = R_i(s)$ = Laplace transform of input i,

$C_i = C_i(s)$ = Laplace transform of response i,

$Z_{ij} = Z_{ij}(s)$ = cross coupling factor.

By solving for the actuator inputs, Eq. (A-1) can be placed into matrix form:

$$\{R\} = [W]\,\{C\}, \quad (A\text{-}2)$$

where

$$[W] = \begin{bmatrix} \frac{1}{Z_{11}} & \frac{Z_{12}}{Z_{11}} & \frac{Z_{13}}{Z_{11}} & \cdots & \frac{Z_{1M}}{Z_{11}} \\ \frac{Z_{21}}{Z_{22}} & \frac{1}{Z_{22}} & \frac{Z_{23}}{Z_{22}} & \cdots & \frac{Z_{2M}}{Z_{22}} \\ \cdots & & & & \\ \frac{Z_{M1}}{Z_{MM}} & \frac{Z_{M2}}{Z_{MM}} & \frac{Z_{M3}}{Z_{MM}} & \cdots & \frac{1}{Z_{MM}} \end{bmatrix} \quad (A\text{-}3)$$

By comparing Eqs. (A-2) and (18), we conclude that

$$[W] = [B]^{-1}; \quad (A\text{-}4)$$

i.e., the inverse of the system transfer matrix is directly related to the cross-coupling factors for that system.

For comparison purposes, the frequency response of the CCF corresponding to the transfer matrix element of Fig. 5 is plotted in Fig. A-1.

APPENDIX B: BASIC PROPERTIES OF FAST FOURIER TRANSFORM

In this Appendix the basic properties of the Fast Fourier Transform (FFT) are defined. No attempt has been made to present proofs of these properties and the reader is referred elsewhere for more rigorous treatments of the subject [19, 23, 24].

The FFT, as used in the analysis of shock and vibration data, is the discrete Fourier transform of time series data. The available algorithms are generally based on the complex summation

$$A_k = \sum_{i=0}^{N-1} X_i\, e^{j(2\pi ik/N)}, \quad k=0, 1, \ldots, N-1 \quad (B\text{-}1)$$

where

A_k = kth of N complex Fourier coefficients

$= AR_k + j\,AI_k$

X_i = ith of N complex data points

$= XR_i + j\,XI_i$

$j = \sqrt{-1}$

N = number of data points.

The number of data points, N, is generally restricted to powers of two:

$$N = 2^L, \quad (B\text{-}2)$$

where L is referred to as the order of the transform.

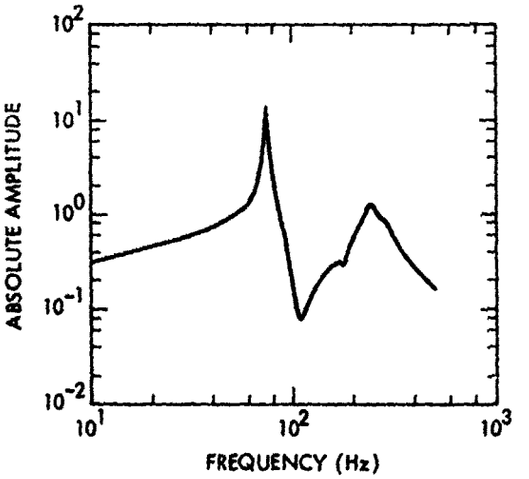

Fig. A-1 - Cross coupling factor $Z_{12}(j\omega)$

The inverse FFT operation is defined as

$$X(i) = \frac{1}{N} \sum_{k=0}^{N-1} A(k)\, e^{-j(2\pi ik/N)},$$

$$i = 0, 1, \ldots, N-1 \qquad \text{(B-3)}$$

and may be performed by executing a forward FFT on the series $\overline{A(k)}/N$:

$$X(i) = \overline{\sum_{k=0}^{N-1} \frac{\overline{A(k)}}{N}\, e^{j(2\pi ik/N)}},$$

$$i = 0, 1, \ldots, N-1, \qquad \text{(B-4)}$$

where the horizontal bars indicate conjugation.

A sequence of data points, when operated on by an FFT, are transformed from the time domain to the frequency domain. The results of the transform of N real data points are shown in Table B-1. For data points sampled at intervals ΔT, the spacing of the frequency points is

$$B = \frac{1}{N\Delta T} = \frac{1}{T} \text{ (HZ)}. \qquad \text{(B-5)}$$

For real (as opposed to complex) sequences of data, the transform coefficients have the property that

$$A(k) = \overline{A(N-k)},\ k = 1, 2, \ldots, \frac{N}{2}, \qquad \text{(B-6)}$$

where

$\overline{A(N-k)}$ is the complex conjugate of A(N-k),

and

$$\text{Im}\,[A(0)] = \text{Im}\,[A(N/2)] = 0.0.$$

TABLE B-1

Transformation of a Sequence of N Real Data Points

Time (sec)	X(i)		Index	A(k)		Frequency (Hz)
	XR(i)	XI(i)		AR(k)	AI(k)	
0	XR(0)	0.0	0	AR(0)	0.0	0
t_1	XR(1)	0.0	1	AR(1)	AI(1)	$-f_1$
.	.	.	.	.	.	.
.	.	.	.	.	.	.
$t_{\frac{N}{2}-1}$	$XR\left(\frac{N}{2}-1\right)$	0.0	$\frac{N}{2}-1$	$AR\left(\frac{N}{2}-1\right)$	$AI\left(\frac{N}{2}-1\right)$	$-f_{\frac{N}{2}-1}$
$t_{\frac{N}{2}}$	$XR\left(\frac{N}{2}\right)$	0.0	$\frac{N}{2}$	$AR\left(\frac{N}{2}\right)$	0.0	$-f_{\frac{N}{2}}$
$t_{\frac{N}{2}+1}$	$XR\left(\frac{N}{2}+1\right)$	0.0	$\frac{N}{2}+1$	$AR\left(\frac{N}{2}-1\right)$	$-AI\left(\frac{N}{2}-1\right)$	$+f_{\frac{N}{2}-1}$
.	.	.	.	.	.	.
.	.	.	.	.	.	.
.	.	.	.	.	.	.
t_{N-1}	XR(N-1)	0.0	N - 1	AR(1)	-AI(1)	$+f_1$

$$t_k = k\Delta T,\ k = 0, 1, \ldots, N-1$$

$$f_k = -k\left(\frac{1}{N\Delta T}\right),\quad k = 0, 1, \ldots, \frac{N}{2}$$

$$= (N + 1 - k)\left(\frac{1}{N\Delta T}\right),\quad k = \frac{N}{2}+1, \frac{N}{2}+2, \ldots, N-1$$

Thus, only N/2 + 1 different spectral lines are obtained for an analysis of N data points and the effective analysis bandwidth is

$$F = \left(\frac{N}{2}\right) B = \frac{1}{2\Delta T} . \qquad \text{(B-7)}$$

Since the sample rate is

$$S = \frac{1}{\Delta T} , \qquad \text{(B-8)}$$

the Nyquist frequency is identically equal to F. To avoid aliasing, the sampled data must therefore be bandwidth-limited to the frequency F.

As a final note, it is possible to transform two sets of real data Y(i) and Z(i) simultaneously by setting

$$X(i) = Y(i) + jZ(i).$$

Then the FFT coefficients of Y(i) are

$$B(k) = \frac{[A(k) + \overline{A}(N-k)]}{2}, \quad k = 0, 1, \ldots, N-1$$

and for Z(i)

$$C(k) = \frac{[A(k) - \overline{A}(N-k)]}{j2}, \quad k = 0, 1, \ldots, N-1,$$

where A(k) are the complex coefficients resulting from the FFT transformation of X(i).

GROUND VIBRATION SURVEY AS A MEANS OF ELIMINATING POTENTIAL IN-FLIGHT COMPONENT FAILURES

J. A. Hutchinson and R. N. Hancock
Vought Aeronautics Company
Dallas, Texas

ABSTRACT

Vought Aeronautics Company has subjected two complete aircraft, XC-142A and A-7E, to ground vibration tests and surveys up to 300 Hz. This procedure was aimed at empirically resolving potential environmental vibration problems of complex installation not amenable to design analysis. Two hundred five and one hundred thirty-three design changes resulted on the respective aircraft. Marked improvements were noted in maintainability and reliability. Hydraulic leaks and intermittent electrical connector failures were virtually eliminated. The paper discusses the test philosophy, describes the survey procedures and comments on the test results and benefits which were derived.

INTRODUCTION

In the development of any new military aircraft, with its many varied components and its complex electrical and hydraulic systems, there are many design details which are not amenable to vibration design analysis but which can be resolved through vibration testing.

For years various aircraft dynamicists have advocated the use of a ground vibration test, on an early production aircraft, to correct the design analysis inadequacies and to forestall later flight problems. During a test of this type, all component mountings, hydraulic lines, electrical wire bundles, and their assorted bracketry can be observed in order to obtain their response to a given vibrational environment. When the response of a particular item is considered excessive, a redesign of that installation can be incorporated early in the production phase rather than after customer complaint.

The Vought Aeronautics Company (VAC) has utilized this type of ground vibration survey during the development of both the XC-142A tilt-wing V/STOL transport aircraft and the A-7E Corsair II light-attack aircraft. In both of these programs the specific objectives for performing the test were twofold: (1) To determine the aircraft components with a resonance in the high amplitude frequency range below about 300 Hz, particularly those components with any resonance frequency coinciding with known discrete forcing function frequencies; and (2) to alter or attenuate the response of those components with resonances below 300 Hz that were considered a potential problem.

In its early operation the XC-142A experienced repeated hydraulic and fuel connector leaks, component mounting problems, minor electrical malfunctions, etc. The down time between flights was excessive. Loss of one of the aircraft because of a control linkage vibration failure finally precipitated a ground vibration survey on an entire vehicle. Completion of the survey and installation of 205 recommended design changes resulted in an almost unbelievable reduction of approximately 60% in the maintenance-to-flight-hour ratio, and, it might be added, improved relations between engineering and the pilot staff and ground crews. Because of the dramatic improvements shown on the XC-142A, VAC decided to subject the A-7 to a similar ground vibration survey.

The A-7 test was conducted at the time of model change between A/B and D/E. Several hundred A & B models were in operation at the time so that a gross assessment of improvements could be made, even though the model changes were significant. Table I compares the number of components surveyed to the number of changes made as a result of the vibration survey. A similar comparison is shown for the XC-142. The hydraulic systems are similar enough between the A-7 models to assess effectiveness of the survey. As given in Table I, 133 design changes were made on the A-7E. A comparison of hydraulic system failures between models with and without

Table I
Number of Components Investigated During Ground Vibration Survey

TYPE OF AIRCRAFT	TOTAL NUMBER SURVEYED	NO MODIFICATION NEED	FURTHER INVESTIGATION NEED	NUMBER OF MODIFICATIONS INCORPORATED
XC-142A	574	355	14	205
A-7E	549	356	60	133

changes showed an improvement of 21% in mean-times-between-failures (MTBF). Granted, methods of comparison are always subject to question, and reliability numbers are difficult to define exactly. However, as with the XC-142, hydraulic leaks due to vibrational induced motion at the connectors were practically eliminated through better application of restraints, and these greatly affect maintenance time. Even if credit is only taken for a 5% increase in MTBF as a direct result of the survey, systems and cost effectiveness quite handily justify its use.

A secondary benefit from the survey is accrued in the dynamics education experienced by the designers and others associated with the test. Most of those not working directly in dynamics tend to regard the structure from the static viewpoint and as being rigid. Generally speaking, a large part of the vibration problem can be regarded as cured if the designer can be taught to think "vibration." The "wet spaghetti" appearance of installations when excited at resonance is a memorable experience for most designers which will carry over to future programs.

The test methods and procedures used during both the XC-142A and A-7E ground vibration surveys were essentially the same. Therefore, only the A-7E will be described. Since the details of vibration testing are general knowledge, no attempt will be made to describe the test in great detail. Only the unusual or unique aspects relating to the test will be reported so that the original purpose of this paper will not be obscured, i.e. the reporting of a method that has proven to be an extremely reliable tool in eliminating potential in-flight vibration problems.

TEST ARTICLE

To attain the primary objectives of the ground vibration survey, the most desirable test article was a production, fully equipped, flight-ready A-7E Corsair II aircraft as shown in Figure 1. Because of the short supply of certain major avionics components and the tight delivery schedule of the aircraft to the Navy, it was impossible to maintain a complete, unaltered aircraft during the entire test period. A compromise was established between Engineering and Manufacturing so that only the portion of the aircraft that was being surveyed at a particular time would be kept in production configuration. This arrangement worked satisfactorily, since only local structural response was desired. To simulate flight operations as much as possible, a full load of fuel and the aircraft's hydraulic system pressure were maintained throughout the test, so that fluid pressure in the fuel and hydraulic lines would add the appropriate mass, damping and stiffness to those installations during the vibration survey.

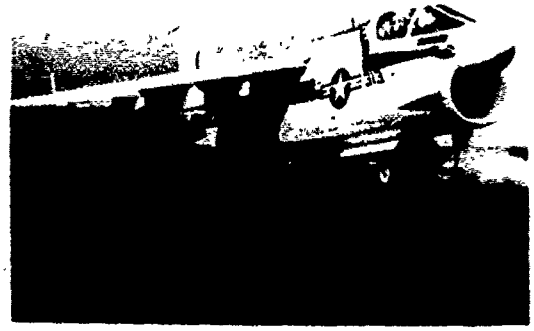

Figure 1. A-7E Corsair II Light-Attack Aircraft

TEST SETUP

The aircraft was divided into several zones, such as those given in MIL-A-8892, for purposes of studying local response with a minimum number of shakers. The major zones where the majority of the investigation was accomplished are shown pictorially in Figure 2. Other areas outside the major zones were investigated if the nature of equipment warranted it, e.g. control system connecting rods and bell cranks, hydraulic lines and connections, antenna installation, etc.

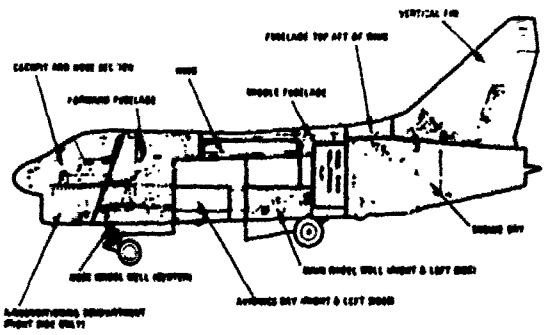

Figure 2. Major Test Zones Utilized During Ground Vibration Survey on A-7E Aircraft

The test equipment comprised a low-frequency oscillator, electro-magnetic shakers and stroboscopic equipment. The oscillator was capable of exciting twelve 150 pound force electromagnetic shakers simultaneously with controlled phasing. The stroboscopic equipment, which was tuned by the oscillator, provided a visual display of component vibration. A frequency lag between the oscillator and the stroboscopic lamps provided the illusion of slow motion which permitted the test personnel to view an item's vibratory motion in detail and thus determine the natural frequency of a particular component and define the requirements for a design change, if necessary. A typical test setup is shown in Figure 3. The shakers are arranged for a survey of the cockpit and nose section.

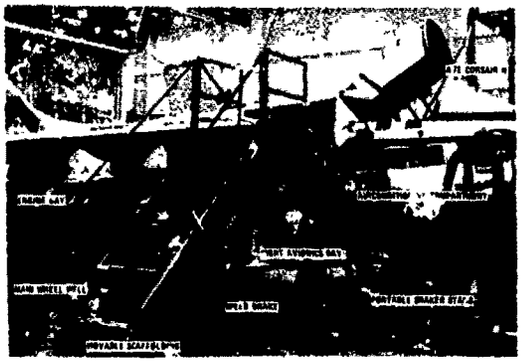

Figure 3. Typical Test Arrangement During Ground Vibration Survey on A-7E Aircraft

The movable scaffolding provided easy access to all areas of the zone. As can be seen from this figure, all aircraft access panels have been removed to permit visual observation of all components during the vibration survey. Some of the equipment from the right avionics bay has been removed since that area was not under invetigation at the time this photograph was taken.

To provide the necessary energy to excite and sustain component resonances so local structural modes could be identified visually with stroboscopic lamps, it was necessary to drive the aircraft structure along the path of minimum impedance. This was accomplished by geometrically arranging the shakers to excite either the local panel modes or the local surface modes. By placing the shakers symmetrically on both sides of the airplane and applying in-phase or out-of-phase excitation the desired modes were obtained. Figure 4 illustrates the manner in which the shakers were attached to the structure. This was accomplished by cementing blocks to the aircraft and attaching the shakers to those blocks by means of force rods. Shear bolts were used to attach the force rods to the shaker armature to prevent side loads from damaging the armature. In order to inject the necessary force into the aircraft structure as many as seven shakers were utilized at one time, depending upon which zone of the aircraft was being investigated and in what axis the vibration was being applied.

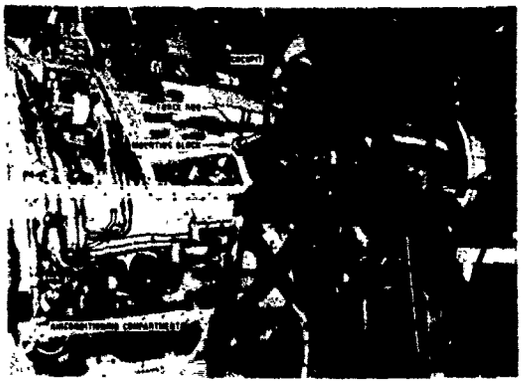

Figure 4. Typical Shaker Arrangement to Fuselage Structure

PROCEDURE

Prior to the start of this test, a review board was established. This board was comprised of representatives from all cognizant engineering and manufacturing groups. The participants on this board had the responsibility and the authority to make design change decisions when required, and to incorporate these design changes into the manufacturing process. These decisions were made at the test site when the problems were encountered, thus eliminating any misunderstanding in the requirements for the design change and affording each member of the board the opportunity to examine the problem area and observe the results of the proposed fix. VAC found this to be an extremely workable procedure which increased the efficiency of the design process by eliminating time consuming debriefing of the dynamics engineers by the design personnel. This board reviewed all systems throughout the aircraft and categorized components into the following four groups:

- Safety-of-flight
- High Maintainability
- Low Reliability
- No Problem

Prior to the start of any vibration testing, each component was tagged with a circular tag as specified in Table II.

Table II
Pre-Test Identification Tags

CIRCULAR TAGS	DENOTE
Red	Safety-of-Flight Items
Yellow	High Maintainability Items
Green	Low Reliability Items

These tags aided the dynamics engineer in selecting the components which he would investigate during the vibration sweep. However, he was not limited to the tagged components, but would investigate any installation that responded in an adverse manner to the applied vibration.

Once the shakers were located and attached to the aircraft, for a particular zone investigation, the dynamics engineers holding stroboscopic lamps positioned themselves so the entire test zone could be observed. Each observer was equipped with a head-set which kept him in constant communication with the test conductor and all other observers. A vibration survey from 10 Hz to 300 Hz was conducted. The test controller announced the vibration frequencies as the sweep was continued, dwelling when necessary to allow each observer to tag those items which were responding to the input vibration and to record on white rectangular tags the approximate frequency at which the maximum excursion occurred. This procedure was continued until all the components in the particular zone being surveyed were investigated. Once this was accomplished, observers would request the test conductor to dwell at the resonance frequency of each component which they had tagged during the sweeps. The test conductor dwelled at these frequencies, one at a time, starting with the lowest. The motion of each resonating component was studied to determine the severity of the resonance to define the requirements for a design change, if deemed necessary. Colored rectangular tags, as specified in Table III, were attached to each component as it was surveyed. These tags illustrated by their color whether the component had a vibration problem, the severity of that problem, and if a redesign was needed or further study was recommended.

Table III
Component Response Classification Tags

RECTANGULAR TAGS	DENOTE
Red	Major response below 300 Hz – Modification required
Yellow	Major response below 300 Hz – modification required but cannot be incorporated – Further investigation needed
Blue	No major response below 300 Hz – No action required
Green	Modification incorporated – Redesign acceptable

If a design change was required, the necessary modification to the aircraft was installed; the component was then resurveyed to see whether the change was effective or if more modification was needed. Design engineers were available at the test site to "red line" installation drawings on the spot, thus decreasing the time required to incorporate the test modifications into the production drawing. If the recommended design change could not be incorporated into the aircraft without major rework of the local structure, then the installation was presented to the review board for its consideration. It was the board's responsibility to decide whether the installation was a potential maintenance problem; and if it was, what course of action would be taken. If the installation was classified as noncritical, then it was accepted as designed. However, if the item represented a potential maintenance problem, then it was selected for further investigation during future flight test programs where the flight vibration environment and component response would be measured. If the flight data verified the ground survey findings, the recommended change was incorporated. On the other hand, if the flight data indicated the component installation was satisfactory, no further action was taken.

The tabulation of all tagged components and the scheduling of each recommended redesign was kept in order by maintaining large bulletin boards next to the test site. These boards listed the items investigated, the result of the investigation, and the recommended modification. They also indicated whether review board action was required and what action was taken.

The airconditioning compartment which is shown in Figure 4 is a good example of the contrast involved in analytically predicting the response of some component installations versus determining the response during a vibration test. Because of the complexity of this installation, analytical prediction of the response of the many varied component installations is highly impractical. On the other hand, it is a relatively simple task to probe the area with a stroboscopic lamp during a vibration survey. Each component resonance frequency can be determined and equated to known forcing function frequencies. A failure to deal with this problem can reduce the aircraft's reliability through increased maintenance, cause aborted combat missions, ground the aircraft until design changes could be installed.

Aside from the normal problems encountered in the vibration test, one unique to this methodology is associated with the length of time that engineering personnel can use high intensity stroboscopic lamps. A resonance type phenomena is encountered involving the optic nerves and alpha brain wave between 8 and 14 cps. After a short period of time, disorientation and nausea were induced in some personnel. A few individuals were restricted from participating in the test because of this phenomena. All were limited in the amount of time they were continuously exposed to the strobe lamp. The procedure used by VAC was to have the engineers who were using the stroboscopic lamps to alternate their test coverage in two hour shifts, with a two hour rest period between shifts.

TEST RESULTS

A combined total of 549 components and installations were investigated within the A-7E aircraft. Out of this total, 356 of these items, which had either a small amplification factor at resonance or a resonance frequency in a noncritical range, were left as designed, i.e. no modification needed. Of the remaining 193 items, 60 of these had large vibration amplitudes at resonance but could not be readily reworked; so they were selected for further investigation

during future flight tests. The remaining 133 items were corrected, either by changing their natural frequencies, introducing high damping or otherwise restricting motion to attenuate their response to a negligible amplitude. The modifications generally consisted of marriage clamps to adjacent lines or tubes, additions of component attachments to adjacent structure or the alteration of localized structure to change the mounting stiffness characteristics of the items. Some of these typical modifications can be seen in Figure 5, which is a photograph of a portion of the inside wall of the engine bay. There are three different types of test modifications shown in this figure: a structural strap connecting several fuselage ribs together to increase their stiffness; a support clamp on a hydraulic line to increase its resonance frequency; and the modification of a component mounting support bracket. All of these

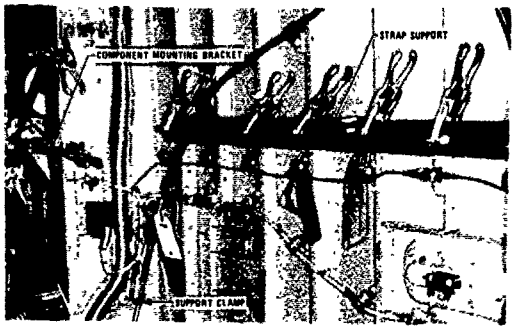

Figure 5. Typical Component and Structural Modification Used During Survey

test modifications were resurveyed to determine their effectiveness. If they proved to be acceptable, then a formal design change was initiated and incorporated into the manufacturing process for the A-7E.

PROGRAM EFFECTIVENESS

Estimated cost effectiveness is a key consideration prior to the initiation of any program. Experience with the XC-142A had shown some of the benefits to be expected prior to the A-7E program, and a reasonably good estimate could be made of the costs. Completion of the survey finally required approximately 20 engineering and test personnel for a one-month time period. Tests were run on a 12-hour day, 6 days per week basis, in order to hold the aircraft for a minimum time period. This minimum required diversion of a production aircraft from the line for 20 days. Costs following the survey, for drawing change, production order changes, etc., are not considered a part of the procedure cost, since they would have been incurred later on some other basis.

Based on experience with the XC-142A, a primary motivation in the vibration test was to survey all control system components and linkages that might result in a critical flight failure. No unusual problems were found in the survey and none have been experienced in flight. It is at best difficult to quantitize effectiveness of a program of this type; however, a review of the reliability and maintainability of two systems, hydraulic and electrical, grossly exemplifies this elusive quantity. The A-7A/B had presented a history of leakage in hydraulic connectors and trombone type extension units as well as problems with loose electrical connectors. The survey resulted in additional hydraulic line attachments and changes in the connector seals. Minor changes were made at the time of the survey on the extension unit seals. Flight test follow-up later resulted in a change to flexible lines for the two major extension units between airframe and engine mounted hydraulic pump.

In reviewing reliability and maintainability, at the weapon systems level, a comparison of similar aircraft with and without the changes showed an improvement of 21% in the mean-time-between-failures (MTBF) for hydraulics on changed aircraft, averaged over a one-year period. For the same time period (and in different terms) the electrical system showed a 14% decrease in direct-maintenance manhours-per-flight-hour (DMMH/FH). Of course, total credit cannot be given to the vibration survey for these improvements since system improvements were being made on other bases; however, flight acceptance of the A-7E was greatly aided due to solution of the hydraulic leakage problem, which did directly result. If only 25% of the indicated improvement is credited to the survey, it is easily seen that the costs are amortized over just a short time period for a few aircraft.

CONCLUSIONS

The ground vibrabiton survey on a production complete aircraft, up to 300 Hz, has proved a very effective tool in preventing environmental vibration problems on two aircraft programs. The procedure is particularly effective for complex installations, tubing and wiring runs, and components that do not lend themselves to practical theoretical analysis. Direct benefits have been improved systems reliability and maintainability; virtual elimination of repeated hydraulic joint leaks, improving ground crew performance; improved confidence in critical control system performance; a better weapon system. Peripheral benefits were derived from the test procedure through education of lead designers in component dynamic response. In short, experience has shown the benefits to far outweigh the costs in the two vehicles tested to date. The test procedures used on these programs have worked quite well, and can be easily varied to suit other vehicles. VAC plans to use this type survey on all future programs and can highly recommend it to others

DISCUSSION

Mr. Koen (Bell Laboratories): Why pick 300 Hz; why not higher frequency or lower?

Mr. Hutchinson: Strobe lights are not much good over 500 Hz and our shaker was only capable of going to 300 Hz.

Mr. Koen: How were you able to detect resonance in the neighborhood of 100 to 300 Hz? Was it by visual means alone?

Mr. Hutchinson: Yes, it was strictly visual using strobe lamps, watching displacement and then determining if we had excessive amplitudes. It is the judgement of the individual holding the strobe lights. If he considers the motions to be excessive with respect to the low vibration inputs, then he marked it for further investigation.

Mr. Koen: It would seem difficult because of the low displacements.

Mr. Hutchinson: Well, of course, if it is a low displacement it won't produce much stress in the design. You are really only worried about the large displacements. If you get large displacements with small inputs you will probably have a problem when you fly.

PROBABILITY DENSITY FUNCTIONS OF MEASURED DATA

Robert G. Merkle and Roger E. Thaller
Air Force Flight Dynamics Laboratory
Wright-Patterson Air Force Base, Ohio

In structural systems subject to complex distributions of randomly varying external excitation forces, continuous measurements of system response are made at a number of points. Statistical measures of average, dispersion, skewness, and kurtosis are defined and used to identify the mathematical form of the probability density functions associated with such measured data. A careful examination is made to determine the extent to which variations in the shape of the probability density function were associated with variation in sensor location and flight condition.

INTRODUCTION

Vibration surveys of aircraft and other complex structural systems are commonly taken by recording instantaneous acceleration time history data for a fixed interval of time from sensing devices at a large number of structural locations under the full range of flight or test conditions of interest (airspeeds, altitudes, etc.). The resulting three dimensional block of measurements, flight condition versus sensor location versus time, constitutes the input data for statistical analysis.

The purpose of this paper is to discuss a statistical analysis technique in which these recorded data can be utilized to test hypotheses concerning:

a. The probability density functions associated with the time measurements for a single location at a single flight condition.

b. The extent to which such probability density functions depend on sensor location and on parameters specifying flight conditions.

By comparing the statistics of the time series histograms with the corresponding parameters associated with theoretical probability density functions (pdf), the form of the pdf will be determined. As an example of this procedure, comparison of the statistics of a set of actual time histories with parameters of theoretical probability density functions will test the hypothesis that the time history data follows one of these probability densities [1, 2]. Further analysis will determine whether this form of probability density function is independent of flight condition and sensor location.

The probability density functions provide the basis for estimating the rate of occurrence of extreme values of acceleration and sound pressure level. These extreme values may cause catastrophic failure or greatly accelerate fatigue damage. If the form of the probability density function is independent of sensor location and flight condition, then estimating the rate of occurrence of extreme values of vibration is simpler and less expensive.

Knowledge of the probability density function of the input time history data is useful in establishing the density function associated with important measures of vibration and acoustic intensity such as overall mean square values and estimates of power spectral density [2, 3]. Statistical theory indicates how one can obtain the probability density of data derived by taking a mathematical function of other data having a known pdf. Since vibration and acoustic data analyzers operate by performing known sequences of mathematical operations on the input data, the pdf of the analyzer output depends solely on the pdf of the data input.

STATISTICAL MEASURES

A set of observations for any variable can be characterized by an overall average value as well as some measure of dispersion or scatter in the data. In addition, whenever such a distribution of observed values is arranged in the bar graph form, characteristics related to the symmetry and shape of the distribution become evident. These concepts are quantified in the next few paragraphs.

Let x_i, $i = 1 \ldots N$ denote a sample of N observations of the variable x. If the range of x is subdivided into a series of m adjacent

intervals by the ordered sequence of values x_k, k = 0...m, m<<N, then the function $y_k=f(x_k)$ can be defined to mean the number of observations that fall in the interval $x_{k-1}<x<x_k$. An example of such a function is plotted as a histogram in Figure 1a.

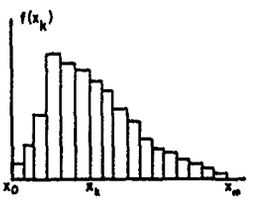

Fig. 1a - Histogram

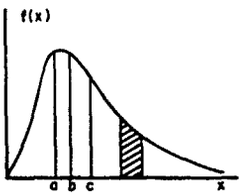

Fig. 1b - Frequency Distribution Function

For large numbers of observations and more refined subdivisions, such histograms approximate continuous mathematical functions illustrated in Figure 1b. Here the total area under the curve f(x) represents the total number of observations and the shaded area between the curve and any fixed interval on the x axis represents the number of observations expected to fall in that interval. If the area under the curve in Figure 1b is normalized to one by dividing f(x) by the total number of observations, the shaded area then represents the probability that a randomly selected observation x_i will fall in the underlying x interval. The probability density, p(x), the value of the ordinate in such a normalized curve, is defined as the limit of the ratio of the probability associated with a given interval to the length of the interval as the latter approaches zero.

Statistics characterizing histograms and probability density functions can be defined in terms of the observation x and the continuous x variate of the probability density function. The most useful measure of average value is given by the arithmetic mean defined respectively as follows:

$$\bar{x} = \sum_{i=1}^{N} \frac{x_i}{N}$$

and

$$\mu = \int_{-\infty}^{\infty} xp(x)dx \qquad (1)$$

The mean value illustrated at x=c in Figure 1b is the x coordinate of the centroid (or balance point) of the area enclosed by the curve and the x axis. The median or middle value illustrated at x=b in Figure 1b is the x coordinate of the vertical line dividing the enclosed area in half. The mode illustrated at x=a in Figure 1b is the most frequently occurring value of x.

Another attribute of interest for measured data or probability density functions is some measure of the scatter or variability in the data. The mean square deviation from the mean value is called the variance and its square root is called the standard deviation. Expressing the variance mathematically for both observed data and probability density functions gives:

$$s^2 = \sum_{i=1}^{N} \frac{(x_i-\bar{x})^2}{N-1}$$

and

$$\sigma^2 = \int_{-\infty}^{\infty}(x-\mu)^2\, p(x)dx \qquad (2)$$

where $\bar{x}$ and μ are as defined previously in Equation 1.

Both the mean and variance are related to a more general set of statistics called the moments of a probability density function. Moments are useful in specifying the shape of a pdf. The j th moment about point a is defined as follows for observed data and probability density functions respectively:

$$\sum_{i=1}^{N} \frac{(x_i-a)^j}{N}$$

and

$$\int_{-\infty}^{\infty}(x-a)^j p(x)dx \quad j=1, 2, \ldots \qquad (3)$$

The first moment about zero is simply the arithmetic mean given in Equation 1 and the second moment about the mean is the variance given in Equation 2. Higher moments are related to other characteristics of statistical data that govern the shape of the probability density function.

In order to specify the higher moments in a more useful form the effect of uniform changes in the observations on their mean value and standard deviation should be noted. Adding or subtracting a constant to each observation will add or subtract the same amount to the mean value but leave the standard deviation unchanged. On the other hand multiplying or dividing each observation by constant value will multiply or divide both the mean value and the standard deviation by the same constant. In either kind of uniform change the relative magnitudes of the deviations from the mean and consequently the shape of the histogram of frequency distribution function remains

unchanged. A special case of uniform changes is of interest: first subtracting the mean value from each observation and then dividing the result by the standard deviation to form a new set of standardized data having a mean value of zero and a standard deviation of one. Standardized data are quite useful in studying characteristics of statistical data related to the shape of the probability density function and in measuring the correlation between two variables.

The first four moments of the standardized value of x are as follows:

$$\frac{\sum_{i=1}^{N}\left(\frac{x_i-\bar{x}}{s}\right)}{N} = \frac{1}{s}\,\frac{\sum_{i=1}^{N}(x_i-\bar{x})}{N} = 0$$

$$\int_{-\infty}^{\infty}\left(\frac{x-\mu}{\sigma}\right)p(x)dx = \frac{1}{\sigma}\int_{-\infty}^{\infty}(x-\mu)p(x)dx = 0$$

$$\frac{\sum_{i=1}^{N}\left(\frac{x_i-\bar{x}}{s}\right)^2}{N} = \frac{1}{s^2}\,\frac{\sum_{i=1}^{N}(x_i-\bar{x})^2}{N} = 1$$

$$\int_{-\infty}^{\infty}\left(\frac{x-\mu}{\sigma}\right)^2 p(x)dx = \frac{1}{\sigma^2}\int_{-\infty}^{\infty}(x-\mu)^2p(x)dx = 1$$

$$\frac{\sum_{i=1}^{N}\left(\frac{x_i-\bar{x}}{s}\right)^3}{N} = \frac{1}{s^3}\,\frac{\sum_{i=1}^{N}(x_i-\bar{x})^3}{N} = b_1$$

$$\int_{-\infty}^{\infty}\left(\frac{x-\mu}{\sigma}\right)^3 p(x)dx = \frac{1}{\sigma^3}\int_{-\infty}^{\infty}(x-\mu)^3p(x)dx = \sqrt{\beta_1}$$

$$\frac{\sum_{i=1}^{N}\left(\frac{x_i-\bar{x}}{s}\right)^4}{N} = \frac{1}{s^4}\,\frac{\sum_{i=1}^{N}(x_i-\bar{x})^4}{N} = b_2$$

$$\int_{-\infty}^{\infty}\left(\frac{x-\mu}{\sigma}\right)^4 p(x)dx = \frac{1}{\sigma^4}\int_{-\infty}^{\infty}(x-\mu)^4p(x)dx = \beta_2$$

The standardized third moment $\sqrt{\beta_1}$ called the coefficient of skewness is necessarily zero for symmetric probability density functions in which $p(x) = p(-x)$. (Sufficient conditions for symmetry require that all odd moments equal zero.) For probability density functions skewed to the right as in Figure 1b, $\sqrt{\beta_1} > 0$, for those skewed to the left $\sqrt{\beta_1} < 0$. The standardized fourth moment β_2 called the kurtosis is associated with the varying degree of concentration about the mean that is possible for probability density functions having the same mean and standard deviation as shown in Figure 2.

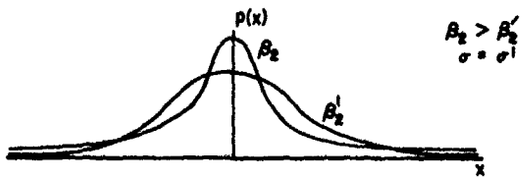

Fig. 2 - Kurtosis Variations In Probability Density Functions

Values of the skewness $\sqrt{\beta_1}$ and the kurtosis β_2 for several probability densities of theoretical and practical interest are given in the next section.

PROBABILITY DENSITY FUNCTIONS

Square, sinusoidal, and triangular waves commonly used in instrumentation laboratories are each associated with probability density functions of theoretical interest. In each case shown in Figure 3 the mean value μ is set equal to zero, the root mean square value (or standard deviation) is set equal to σ by choosing the appropriate wave amplitude, and the coefficient of skewness $\sqrt{\beta_1}$ is zero due to the symmetry with respect to positive and negative values. Illustrations of the kurtosis β_2 values indicated in Figure 3 are, therefore, those associated with the corresponding pdf shapes.

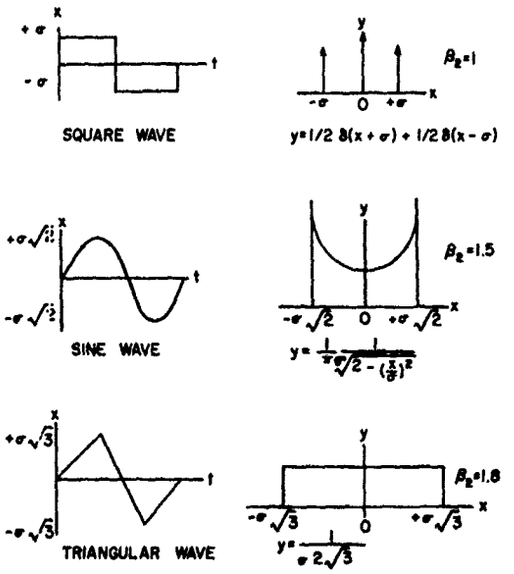

Fig. 3 - Wave Form Probability Densities

The normal or Gaussian probability density function shown in Figure 4 is the most important in statistics for randomly varying quantities.

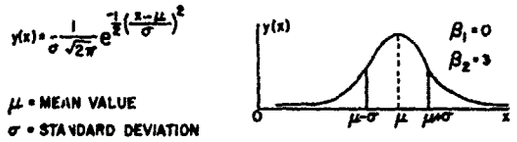

Fig. 4 - Normal Probability Density Function

For the normal probability density function the mean, median, and mode all coincide and have the value of the parameter μ. The standard deviation given by the second parameter σ is always the difference between the x-coordinates of the mode and the point of inflection or maximum slope on either side. Since the normal pdf is symmetric the coefficient of skewness $\sqrt{\beta_1}$ is zero. The coefficient of kurtosis has a value of 3 for all values of the parameters μ and σ.

The normal pdf is not only the basic distribution law for many stochastic processes but also plays a vital role in statistics. If samples of size n are repeatedly drawn from a normal population and mean values are computed, these means themselves constitute a new normal distribution with a mean value equal to the mean of the parent population, $\mu_{\bar{x}}=\mu$, and a standard deviation equal to the standard deviation of the parent population divided by the sample size, $\sigma_{\bar{x}}=\sigma/n^{1/2}$. Therefore, a mean value computed from one sample is, in reality, a single observation from this sampling distribution of the mean and $\sigma/n^{1/2}$, called the standard error, is it's measure of variability. Even when the parent population is not normally distributed the distribution of sample means still approaches the normal distribution as the sample size increases. It is this property that gives the normal probability density function its position of importance in statistics.

TIME-HISTORY MEASUREMENTS

Analysis of a set of time histories was performed as an example of procedures for determining the characteristics of probability density functions of test data. The time histories are measurements of vibration of the QRC-335 electronic equipment carried as an external store mounted under the wing of a jet aircraft, the RF-4C. Figure 5 is a sketch of the QRC-335. The boxes and lines depict the locations of four accelerometers and four microphones mounted parallel to the structure. The first two accelerometers were mounted in the vertical direction; the second pair of accelerometers were in the lateral direction. According to their direction and their location on the QRC-335, the accelerometers were classified in contrasting groups for regression analysis. The microphones were also classified into contrasting groups, based upon their location on the store. The classifications of accelerometers and microphones are illustrated in Table 1. Table 2 is a summary of the twenty-one conditions under which tests were conducted.

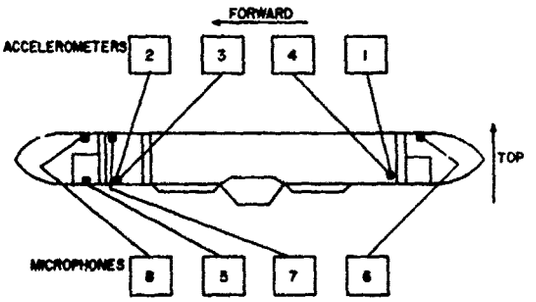

Fig. 5 - Location of Sensors

TABLE 1

ACCELEROMETER AND MICROPHONE CHARACTERISTICS

ACCELEROMETER	DIRECTION	HORIZONTAL POSITION	MICROPHONE	TOP OR BOTTOM	HORIZONTAL POSITION
1	VERTICAL	AFT	5	BOTTOM	FORWARD
2	VERTICAL	FORWARD	6	TOP	AFT
3	LATERAL	FORWARD	7	TOP	FORWARD
4	LATERAL	AFT	8	TOP	FORWARD

The data measured by the instruments during flight tests were in part due to boundary layer turbulence and, in part, due to jet engine noise, even though the QRC-335 was not located directly in the jet stream.

TABLE 2

AIRCRAFT FLIGHT CONDITION CODES

CODE	MACH	ALT	CODE	MACH	ALT	CODE	MACH	ALT
1	.60	2000	8	.95	2000	15	.65	31,000
2	.65	2000	9	1.00	2000	16	.70	31,000
3	.70	2000	10	1.05	2000	17	.75	31,000
4	.75	2000	11	1.10	2000	18	.80	31,000
5	.80	2000	12	1.15	2000	19	.85	31,000
6	.85	2000	13	.95	2000	20	.90	31,000
7	.90	2000	14	.60	31000	21	.95	31,000

Table 2 is a summary of the twenty-one conditions under which the test was conducted. A sample of 250 points was taken from an analog time history from each accelerometer and microphone at each flight condition. A computer program was used to calculate the skewness and kurtosis for each distribution of 250 points. Figure 6 is a plot of the skewness and kurtosis for each distribution of acceleration data and Figure 7 is a plot of the skewness and kurtosis of acoustic data. Plots of the skewness and kurtosis of various theoretical distributions are also indicated on the same figures. These figures show that almost all the skewness and kurtosis points are clustered very close to the point $\beta_1 = 0$ and $\beta_2 = 3$.

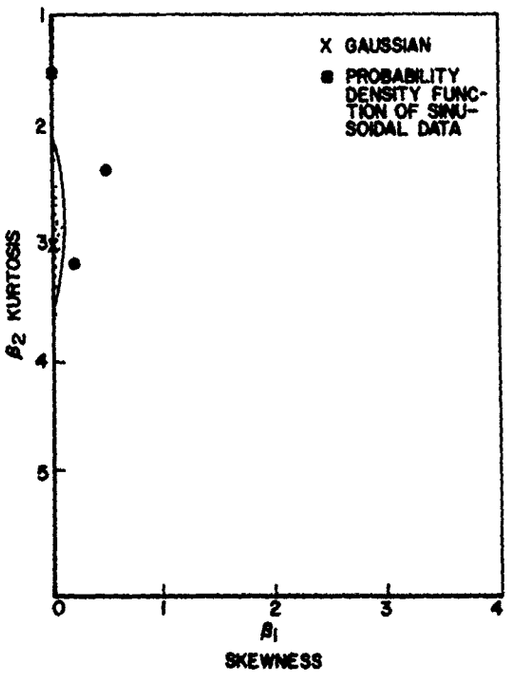

Fig. 6 - Amplitude Probability Density Fc Acceleration Data

QRC Time History

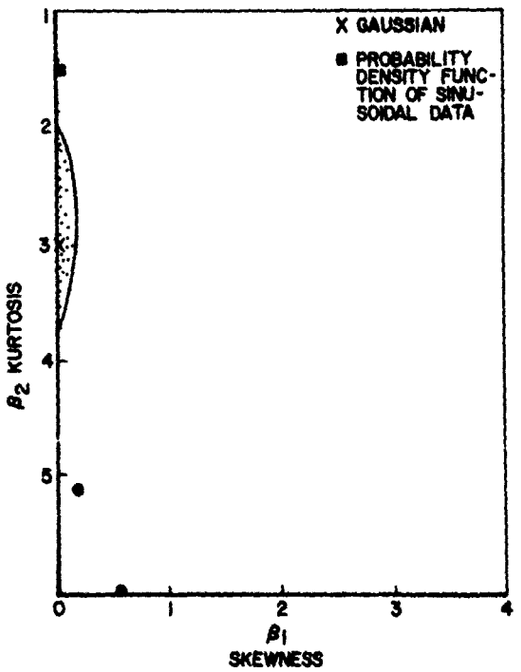

Fig. 7 - Amplitude Probability Density Of Acoustic Data

QRC Time History

Table 3 shows the ranges of the skewness ($\sqrt{\beta_1}$) and kurtosis (β_2) for both accelerometers and microphones. The extreme values of the two statistics are given, along with the associated sensor identification and flight condition information.

TABLE 3

[illegible] STATISTICS

	[illegible]	SENSOR	MACH	ALT
ACCELEROMETER				
MINIMUM SKEWNESS	[illegible]	#3	0.95	2000
MAXIMUM SKEWNESS	.26	#1	1.00	2000
MINIMUM KURTOSIS	2.03	#3	1.05	2000
MAXIMUM KURTOSIS	3.61	#3	.70	31000
MICROPHONE				
MINIMUM SKEWNESS	-.770	#8	.95	31000
MAXIMUM SKEWNESS	+.402	#5	.85	31000
MINIMUM KURTOSIS	1.99	#7	.70	31000
MAXIMUM KURTOSIS	6.16	#8	.95	31000

The question arises as to whether the range of variation in skewness and kurtosis indicated in this table are the result of sampling error or whether they are related to sensor location, mach, and altitude. This matter is treated next.

PROBABILITY DENSITY OF MEASURED DATA

One might hypothesize that the basic form or type of probability density function associated with the vibration time history data will remain the same even though the overall rms value of the time history will vary significantly from one sensor to another and from one flight condition to another. If this is so then the coefficients of skewness and kurtosis which are statistical measures of the symmetry and peakedness of the probability density should remain the same for all sensors and test conditions. To test this conjecture we assume for both vibration and acoustic statistics a general linear hypothesis model of the form:

$$\bar{a}_{ji} = \bar{a}_j + b(x_i - \bar{x}) + c(y_i - \bar{y}) \quad j = 1....8 \quad (4)$$

where

$\bar{a}_{ji}$ is the expected skewness or kurtosis for sensor j at flight condition i,

$\bar{a}_j$ is the mean skewness or kurtosis of sensor j over all flight conditions,

x_i and $\bar{x}$ are respectively altitude codes ($x_i = 0$ at 31,000 feet and $x_i = 1$ at 2,000 feet) and the corresponding mean value,

y_i and $\bar{y}$ are respectively the mach number of flight condition i and the mean mach number, and

b and c are regression coefficients having values which minimize the rms value of the difference between the measured and computed values of the $\bar{a}_{ji}$.

Actual computations were carried out using Program 06V, "General Linear Hypothesis with Contrasts," from Biomedical Programs, Ref. [4]. Estimates and standard errors for the a, b, and c coefficients in Equation 4 were computed for four different cases: skewness and kurtosis for vibration data shown in Table 4 and skewness and kurtosis for acoustic data shown in Table 5.

TABLE 4

ACCELERATION STATISTICS

ACCELEROMETER SYMBOL	POSITION	SKEWNESS ESTIMATE	SKEWNESS STD DEV	KURTOSIS ESTIMATE	KURTOSIS STD DEV
$\bar{a}_1$	VERT, AFT	-.040	.039	2.91	.466
$\bar{a}_2$	VERT, FWD.	.023	.039	2.65	.466
$\bar{a}_3$	LATERAL, FWD	.001	.039	2.67	.466
$\bar{a}_4$	LATERAL, AFT	-.016	.039	2.97	.466
b	ALTITUDE	-.027	.030	.019	.348
c	MACH Nr	.045	.092	.215	1.104

TABLE 5

ACOUSTIC STATISTICS

MICROPHONE SYMBOL	MICROPHONE POSITION	SKEWNESS ESTIMATE	SKEWNESS STD DEV	KURTOSIS ESTIMATE	KURTOSIS STD DEV
a_5	BOTTOM, FWD	023	.038	2.76	.451
a_6	TOP, AFT	.060	.038	3.24	451
a_7	TOP, FWD	.009	.038	2.54	451
a_8	TOP, FWD	.076	.038	3.00	.451
b	ALTITUDE	.027	.030	019	348
c	MACH Nr	.045	091	215	1.069

In Table 1 accelerometers and microphones were identified according to their direction and location. The contrasts of Table 6 and 7 indicate whether these differences result in significantly different values of skewness and kurtosis. For example, Table 1 indicates sensors 1 and 2 are vertically oriented and sensors 3 and 4 laterally directed. If skewness is not related to direction, then the average value of skewness for 1 and 2 should be about the same as for 3 and 4, and their difference should be about zero. In symbols

$$\frac{a_1+a_2}{2} - \frac{a_3+a_4}{2} = \frac{a_1+a_2-a_3-a_4}{2} \approx 0$$

This is the difference shown in the first line, third column, of Table 6 for the vertical-lateral skewness contract. The actual difference from measured data is given in the fourth column and its associated standard error in the last column. A similar line of reasoning applies to the remaining lines of Tables 6 and 7. These results all come from the same computer program cited for Tables 4 and 5.

TABLE 6

CONTRASTS FOR ACCELEROMETERS

CONTRAST	STATISTIC	DIFFERENCE	ESTIMATE	STD ERROR
VERT.–LAT	SKEWNESS	$(a_1+a_2-a_3-a_4)/2$	-.001	0.039
FWD–AFT	SKEWNESS	$(a_2+a_3-a_1-a_4)/2$	.040	0.039
VERT.–LAT	KURTOSIS	$(a_1+a_2-a_3-a_4)/2$	-.041	0.466
FWD–AFT	KURTOSIS	$(a_2+a_3-a_1-a_4)/2$	-.278	0.466

TABLE 7

CONTRASTS FOR MICROPHONES

CONTRAST	STATISTIC	DIFFERENCE	ESTIMATE	STD ERROR
AFT–FWD	SKEWNESS	$a_6-(a_5+a_7+a_8)/3$	-.024	.044
BOTTOM–TOP	SKEWNESS	$a_5-(a_6+a_7+a_8)/3$	+.025	.044
AFT–FWD	KURTOSIS	$a_6-(a_5+a_7+a_8)/3$	+.466	0.521
BOTTOM–TOP	KURTOSIS	$a_5-(a_6+a_7+a_8)/3$	-.164	0.521

Examining the last two tables first, one notes that none of the contrast estimates differ from zero by more than the value of its standard error except for one case where the estimate and error are approximately equal. Thus, no reference to statistical tables is necessary to conclude that these data are consistent with the hypothesis that variation in the direction and location of measurement points are not associated with statistically significant variations in either the skewness or kurtosis statistics of vibration and acoustic time history data. This, in turn, is entirely consistent with the original conjecture that the form of the probability density is independent of the location and direction of the measurements.

Examining next the b and c regression coefficients in the last two lines of Tables 4 and 5 one again notes that in all four cases the estimate differs from its standard deviation by less than the value of its standard error. Again this leads directly to the conclusion that variations in altitude and mach number are not associated with statistically significant variations in either the skewness or kurtosis statistics of vibration and acoustic time history data. This in turn, is entirely consistent with the original conjecture that the form of the probability density function is independent of the flight conditions at which the measurements were taken.

Finally the skewness and kurtosis estimates in Tables 4 and 5 are examined in the light of similar values for the theoretical pdf's given previously. Since contrasts of the kind shown in Table 6 indicate no statistically significant differences in skewness or kurtosis estimates between any pair of measurements, a single estimate of a may be obtained by taking the mean value of the four estimates in each group shown in Tables 4 and 5. Since the standard deviation of the four estimates in each group is the same, dividing it by the square root of the group size, $\sqrt{4} = 2$, gives the standard deviation associated with the single mean value estimate for each group. These results are indicated in Table 8.

TABLE 8

SKEWNESS AND KURTOSIS ESTIMATES

	SKEWNESS		KURTOSIS	
	ESTIMATE	STD DEV	ESTIMATE	STD DEV
VIBRATION DATA	-.008	.020	2.80	.253
ACOUSTIC DATA	-.042	.019	2.61	.226

These estimates may be compared with the known values of 0 and 3 for the skewness and kurtosis of the normal probability density function. For vibration data both the skewness and kurtosis estimates fall within one standard deviation of the 0 and 3 values respectively. Therefore, these data provide no statistically significant evidence for rejecting a normal pdf assumption for vibration time history data. For acoustic data the kurtosis falls within one standard deviation of 3 but the skewness estimate is 2.21 standard deviations below zero. A 99 percent confidence interval for each of these four tests separately would be required to have about 96 percent confidence for all four simultaneously. This, in turn, implies a confidence interval of 2.58 standard deviations on either side of the estimates, a range which includes 0. Therefore, these data provide no statistically significant evidence for rejecting a normal pdf assumption for acoustic time history data. Of course the more powerful chi-square test could have been used for this purpose but this test provides no information at all about what the pdf should be if the assumed form is not consistent with the measured data. With computed values of skewness and kurtosis, on the other hand, one simply selects mathematical probability density forms which exhibit similar values of these parameters. Having selected such a form one can still go on and perform the chi-square test. In the present case the data provided so little evidence of non-normality that further testing was considered unnecessary.

Sinusoidal vibration is generated from imperfections in engine turbine shaft balance and transmitted throughout the structure. Since the pdf associated with sinusoidal data has a kurtosis of 1.5 (Figure 3), its presence might be expected to reduce the kurtosis of observed data somewhat below the value of 3 expected from sources of random vibration. In a laboratory test sinusoidal and random vibration having the same rms value were summed, and the kurtosis of the resulting data was found to be 2.62. The 2.8 values shown in Table 8 thus suggest a predominance of random vibration with some sinusoidal present. This conforms to what might be expected from engineering judgments.

CONCLUSIONS

Based on the comparison of the statistics of the time series histograms with the parameters of the Gaussian probability density function, the hypothesis that the time data follows a Gaussian pdf cannot be rejected. According to the results of the tests performed with the BMD06V, the hypothesis that the pdf is independent of sensor location and flight condition also cannot be rejected.

The form of the probability density function can also be used to obtain the frequency of occurrence of extreme values. These extreme values may severely damage aircraft. As noted in the introduction, knowledge of the shape of the pdf of the time history data may also be used to obtain the pdf of other important measures of vibration data which are functions of the time history.

Once the form of the time history pdf is determined to be independent of changes in flight condition and sensor location, the skewness and kurtosis can be calculated once for all the data collected during the test. It remains necessary to calculate the mean and variance for the sets of data associated with each combination of sensor location and flight condition.

REFERENCES

1. Norman Johnson and Samuel Kotz, "Continuous Univariate Distributions," Volumes I and II, John Wiley & Sons, 1969

2. Gerald J. Hahn and Samuel S. Shapiro, "Statistical Models in Engineering," John Wiley & Sons, 1967

3. Gwilym M. Jenkins and Donald G. Watts, "Spectral Analysis and Its Applications," Holden-Day, 1969

4. W. J. Dixon, Editor, "BMD: Biomedical Computer Programs," University of California Press, 1970

*U.S. GOVERNMENT PRINTING OFFICE: 1973 542-164/2-45 1-3